Summer 8-13-2010

Integrating Theoretical and Experimental Methods for Multi-Scale Tissue Engineering of the Annulus Fibrosus of the Intervertebral Disc

Nandan L. Nerurkar
University of Pennsylvania, nlnerurkar@gmail.com

Integrating Theoretical and Experimental Methods for Multi-Scale Tissue Engineering of the Annulus Fibrosus of the Intervertebral Disc

Abstract
There is a critical need for tissue engineered replacements for diseased and degenerated intervertebral discs in order to assuage low back pain while restoring function to the spine. Despite progress by many research groups, it remains a challenge to engineer a replacement tissue that can withstand the complex, demanding loading environment of the spine. Due to the hierarchical organization of the intervertebral disc, successful recapitulation of its functional behavior requires replication of anatomic form and physiologic function over a wide range of length scales. In this work, the technology of electrospinning has been employed for tissue engineering of the annulus fibrosus (AF) of the intervertebral disc using a multi-scale approach. The mechanics of electrospun nanofibrous assemblies was first characterized, focusing on how microscopic organization translates to macroscopic mechanical function. Next, engineered tissues were formed by culturing cells on nanofibrous scaffolds, generating aligned, dense collagenous tissues that replicate the single lamellar organization of the AF. This technology was then expanded to engineer angle-ply laminates that replicated both the anatomic form and mechanical function of the native AF. Finally, these results were further extended to engineer an angle-ply fiber-reinforced hydrogel composite that parallels the macroscopic structural organization of the intervertebral disc. Throughout, mechanical testing and mathematical modeling was used to understand material behavior, quantify functional growth, and guide comparison between engineered AF constructs and native tissue benchmarks. Emphasis has been placed on reconciling compositional and structural observations with their macroscopic mechanical implications, utilizing theoretical models to understand these relationships, and using engineered tissues to improve our understanding of structure-function relations within native fiber-reinforced soft tissues.

Degree Type
Dissertation

Degree Name
Doctor of Philosophy (PhD)

Graduate Group
Mechanical Engineering & Applied Mechanics

First Advisor
Dawn M. Elliott

Second Advisor
Robert L. Mauck

Keywords
mesenchymal stem cells, tissue engineering, electrospinning, laminate, orthopaedics

INTEGRATING THEORETICAL AND EXPERIMENTAL METHODS FOR MULTI-SCALE TISSUE ENGINEERING OF THE ANNULUS FIBROSUS OF THE INTERVERTEBRAL DISC

Nandan Nerurkar

A DISSERTATION

in

Mechanical Engineering and Applied Mechanics

Presented to the Faculties of the University of Pennsylvania

in

Partial Fulfillment of the Requirements for the

Degree of Doctor of Philosophy

2010

Supervisors of Dissertation

_____
Dawn M. Elliott, Ph.D.
Associate Professor of Orthopaedic Surgery and Bioengineering

_____
Robert L. Mauck, Ph.D.
Assistant Professor of Orthopaedic Surgery and Bioengineering

Graduate Group Chairperson

_____
Jennifer R. Lukes, Ph.D.
Associate Professor of Mechanical Engineering and Applied Mechanics

Dissertation Committee
John L. Bassani, Ph.D. (Committee Chair)
Mechanical Engineering and Applied Mechanics, University of Pennsylvania
Irving M. Shapiro, Ph.D.
Orthopaedic Surgery, Thomas Jefferson University
Gerard A. Ateshian, Ph.D.
Mechanical Engineering and Biomedical Engineering, Columbia University

INTEGRATING THEORETICAL AND EXPERIMENTAL METHODS FOR MULTI-SCALE TISSUE ENGINEERING OF THE ANNULUS FIBROSUS OF THE INTERVERTEBRAL DISC

Nandan Nerurkar

ACKNOWLEDGEMENTS

I would like to first acknowledge my advisors Robert L. Mauck and Dawn M. Elliott. They have provided great support and guidance during the past several years, allowing me to develop as a student of science. Many of the proudest accomplishments during my Ph.D. were born from their confidence in me, and their urging (if not sometimes dragging me kicking and screaming) me to aim high. In addition to the great deal I have learned from them, both have been tremendous friends throughout my Ph.D. It is certainly a rare occurrence that students get along so well with their advisor, and I am grateful for it.

I also thank the other members of my thesis committee, John L. Bassani, Irving M. Shapiro, and Gerard A. Ateshian for their valuable input and willingness to offer help and guidance. I would also like to thank Lou Soslowsky for his guidance and useful discussions, and Barbara Gibson in the front office, for everything from reprimanding Penn facilities on my behalf to doing just about anything she could to make my life easier. She's also been a great friend and I have truly enjoyed working with her for the past several years.

The work contained here would not have been possible without the help of many graduate and undergraduate students. In particular I would like to acknowledge Sounok Sen for working with me on so many of the projects with a dedication that matched (and perhaps at times exceeded) my own. He has been a great coworker, and an exceptional friend. He also knows what DAPS actually stands for. I would also like to acknowledge Emily Wible and An Nguyen for

working with me as undergraduates, and contributing numerous hours of hard work to our projects together. Many of the members of the McKay Orthopaedic Research Lab have contributed to this work, either directly or through valuable discussions: Lachlan J Smith, Daniel Cortes, John Martin, Grace O'Connell, John Boxburger, Amy Orlansky, Megan Farrell, Isaac Erickson, Minwook Kim, Su-jin Heo, Albert Gee, Ashwin Nathan, Norm Gibson, David Beason, Nelly Andarawis, and Spencer Lake. Finally, I would like to acknowledge my two close friends and office mates, Brendon Baker and Alice Huang. They have contributed directly to the work presented here, have always been eager to discuss science and results, and most importantly, they've let me complain until my mouth goes dry. Their friendship has been a most valuable part of my graduate experience. Would I have enjoyed my time in lab without them? *Probably not. I don't think so.*

This work would not have been possible without the support of my family. I would like to thank my brother, Neelesh Nerurkar for always supporting my interest in science and research. I also thank my parents, Mangal and Laxmikant Nerurkar for their support and for impressing upon me that "if you want a hot naan, you've got to burn your hand a little." I was also fortunate to acquire a whole new family during my Ph.D., and would like to thank my brother-in-law, Rupesh Shah, and sister-in-law, Ajita Shah, along with my parents-in-law, Asmita and Rajani Shah, for their support and encouragement. Finally, I would like to acknowledge my wife, Rishita. Even the hardest struggles of the last few years have been surmountable for the knowledge I was going home to her at the end of the day.

ABSTRACT

INTEGRATING THEORETICAL AND EXPERIMENTAL METHODS FOR MULTI-SCALE TISSUE ENGINEERING OF THE ANNULUS FIBROSUS OF THE INTERVERTEBRAL DISC

Nandan L. Nerurkar

Robert L. Mauck and Dawn M. Elliott

There is a critical need for tissue engineered replacements for diseased and degenerated intervertebral discs in order to assuage low back pain while restoring function to the spine. Despite progress by many research groups, it remains a challenge to engineer a replacement tissue that can withstand the complex, demanding loading environment of the spine. Due to the hierarchical organization of the intervertebral disc, successful recapitulation of its functional behavior requires replication of anatomic form and physiologic function over a wide range of length scales. In this work, the technology of electrospinning has been employed for tissue engineering of the annulus fibrosus (AF) of the intervertebral disc using a multi-scale approach. The mechanics of electrospun nanofibrous assemblies was first characterized, focusing on how microscopic organization translates to macroscopic mechanical function. Next, engineered tissues were formed by culturing cells on nanofibrous scaffolds, generating aligned, dense collagenous tissues that replicate the single lamellar organization

of the AF. This technology was then expanded to engineer angle-ply laminates that replicated both the anatomic form and mechanical function of the native AF. Finally, these results were further extended to engineer an angle-ply fiber-reinforced hydrogel composite that parallels the macroscopic structural organization of the intervertebral disc. Throughout, mechanical testing and mathematical modeling was used to understand material behavior, quantify functional growth, and guide comparison between engineered AF constructs and native tissue benchmarks. Emphasis has been placed on reconciling compositional and structural observations with their macroscopic mechanical implications, utilizing theoretical models to understand these relationships, and using engineered tissues to improve our understanding of structure-function relations within native fiber-reinforced soft tissues.

TABLE OF CONTENTS

TABLE OF FIGURES

CHAPTER 1: INTRODUCTION

The spine is comprised of a series of repeating elements formed from two vertebral bodies separated by an intervertebral disc. The disc is a heterogeneous structure that transmits loads across the joint and permits motion of the spine. Degeneration of the disc, which afflicts up to 97% of the population by 50 years of age, is thought to play a dominant role in the development of low back pain (Miller, Schmatz et al. 1988; Bogduk 1991). Back pain is the most common cause of activity limitations in adults younger than 45 years, permanently disables more than 5 million Americans, and results in annual costs of over $100 billion in the United States (Deyo and Tsui-Wu 1987; Frymoyer 1988; Andersson 1999; Luo, Pietrobon et al. 2004). Clinical treatments for discogenic back pain and disc degeneration are focused primarily on alleviation of the symptoms associated with these pathologies, while restoration of function remains largely unaddressed. The gold-standard for clinical treatment, intervertebral fusion, is highly invasive and, despite its frequency, often fails to permanently alleviate low back pain. In fact, fusion can result in degenerative changes in adjacent discs (Levin, Hale et al. 2007). While total disc replacements have recently garnered more clinical attention, the long term efficacy of artificial implants has not been established and mechanical wear over several years may reduce this treatment to nothing more than a temporary fix. It is apparent, given the current state of clinical treatment for degenerative disc disease and low back pain, that there is

great need for a tissue engineering strategy that aims to alleviate low back pain while restoring function and range of motion to the spine.

The overarching goal of the present work is to develop an approach for tissue engineering of the intervertebral disc, with emphasis on one critical component of the disc: the annulus fibrosus. The annulus fibrosus is a multi-lamellar fibrocartilage that surrounds the central gelatinous nucleus pulposus. These two functionally and compositionally disparate tissues work in concert to provide the appropriate gross mechanical behaviors of the intervertebral disc. A successfully engineered replacement for the annulus must be functionally equivalent to the native tissue. Due to the intimate relation between form and function, the current work was conducted under the paradigm that replication of anatomic form is a necessary condition for engineering a tissue that mimics physiologic mechanical function.

The specific objective of the proposed work, therefore, is to employ a multi-tiered approach to fabricate engineered tissue that replicates the multi-scale form and function of the native annulus fibrosus. At each level, constitutive modeling will be employed to characterize functional growth and to describe evolving structure-function relationships. Chapter 2 presents the background of intervertebral disc tissue engineering, emphasizing functional hallmarks the native tissue and assessing the progress of engineered tissues in replicating these behaviors. In Chapter 3, the mechanics of acellular electrospun poly-(ε-caprolactone) (PCL) scaffolds are investigated by uniaxial tensile testing to provide a basic understanding of the behavior of the scaffold material that will be

used in each of the chapters that follow. The focus is on relating macroscopic function to microstructural organization. In the chapters that follow, cell-seeded constructs are fabricated and grown with increasing structural complexity, from a single lamella in Chapters 4 and 5, to a bi-lamellar construct with two fiber-populations in Chapters 6 and 7, and concluding with a fully formed, three-dimensional tissue engineered disc containing anatomic annulus fibrosus and nucleus pulposus regions in Chapter 8. Finally, Chapter 9 will conclude this work with a discussion of the remaining challenges to tissue engineering of the annulus fibrosus and the intervertebral disc, and future work that may help to overcome these challenges so that tissue engineering may ascend to the level of clinical implementation for the treatment of low back pain and disc degeneration.

CHAPTER 2: BACKGROUND

2.1 An Introduction to the Intervertebral Disc

2.1.1 Multi-scale composition and structure of the intervertebral disc

The intervertebral disc is a fibrocartilage that lies between bony vertebral bodies, conferring flexibility, load transfer, and energy dissipation to the spine. It is comprised of the central gelatinous nucleus pulposus (NP) surrounded circumferentially by the annulus fibrosus (AF) (Figure 2.1). The hyaline cartilage endplate forms an interface between the disc and adjacent vertebral bodies. The NP is structurally and mechanically isotropic and contains a network of type II collagen interspersed with proteoglycans, resulting in a high water content within

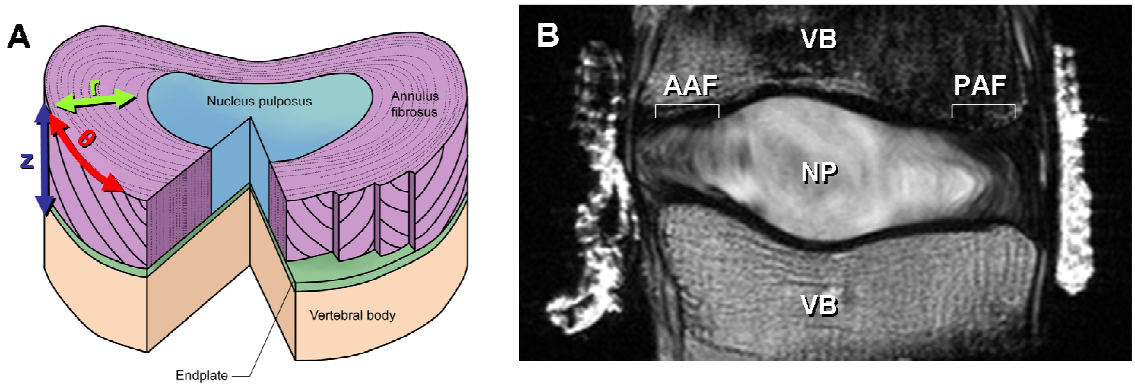

Figure 2.1 A) Schematic representation of the multi-scale architecture of the intervertebral disc indicates the primary geometric axes that are regularly referred to in the text: r = radial direction (from the nucleus pulposus outward), z = axial direction (the spinal long axis), and θ = circumferential direction (parallel to the lamellae as they wrap around the disc). Image modified from (Guerin and Elliott 2006). B) MRI of a human motion segment, with disc substructures as labeled: AAF = anterior annulus fibrosus, PAF = posterior annulus fibrosus, NP = nucleus pulposus, VB = vertebral body. MRI image courtesy of Grace D O'Connell.

the tissue. As discussed below, the associated osmotic swelling is a defining feature of NP mechanics.

Each lamella of the multi-lamellar AF consists of highly aligned type I and type II collagen fibers whose orientation alternates above and below the transverse axis of the spine by approximately 30^{o} in adjacent lamellae (Figure 2.1A) (Cassidy, Hiltner et al. 1989; Marchand and Ahmed 1990). While the AF can be approximated as an angle-ply laminate ring, its true architecture is more complex: lamellae are circumferentially discontinuous and traversed by fibrous elements that run radially outward (Pezowicz, Robertson et al. 2005; Schollum, Robertson et al. 2008).

2.1.2 Development and cell biology of the intervertebral disc

Morphogenesis of tissues is, in a manner of speaking, an idealization of the tissue engineering process. As such, understanding the developmental cues that guide disc formation could provide insight for engineering constructs that more closely approximate the form and function of the disc. While little is known about disc development, the process is clearly distinct from tissues of similar composition or function, such as tendon and cartilage (Peacock 1951; O'Rahilly and Mueller 1994; Rufai, Benjamin et al. 1995; Hayes, Benjamin et al. 1999; Benjamin and Ralphs 2000; Hayes, Benjamin et al. 2001; Zhu, McAlinden et al. 2001). The disc is formed from cells of two disparate developmental origins: the NP cells descended from notochordal cells (Figure 2.2A), and the AF and vertebrae form from the surrounding mesenchyme (Walmsley 1953; O'Rahilly

and Mueller 1994; Choi, Cohn et al. 2008). During endochondral ossification of the vertebrae, notochordal cells migrate from the forming vertebral bodies into the developing NP. Currently, it is unknown what signals drive the differentiation of notochordal cells into NP cells that elaborate the specialized extracellular matrix of this tissue. The inner AF appears to develop from cells that migrate into the disc space from the neighboring pre-vertebral cartilage bodies, while the outer AF forms directly from cells in the surrounding mesenchyme, a region of somitic mesenchyme known as the sclerotome (Rufai, Benjamin et al. 1995; Zhu, McAlinden et al. 2001). Within the developing AF, signals of unknown provenance direct the organization of AF-precursor cells into an elongated shape, forming sheets with opposing orientations that presages the mature AF collagen architecture(Figure 2.2B) (Peacock 1951; Hayes, Benjamin et al. 1999). This occurs prior to the deposition of organized extracellular matrix, suggesting that cellular alignment precedes, and is compulsory for, ordered matrix deposition (Figure 2.2C). A better understanding of these developmental phenomena may generate new avenues for disc tissue engineering.

Consistent with their distinct origins during disc development, cells of the mature disc are also phenotypically distinct, reflecting regional differences in the heterogeneous tissue in which they reside. Although at birth the NP consists of both NP and notochord cells, in humans, the large, vacuolated notochordal cells disappear during adolescence (Trout, Buckwalter et al. 1982). Mature NP cells

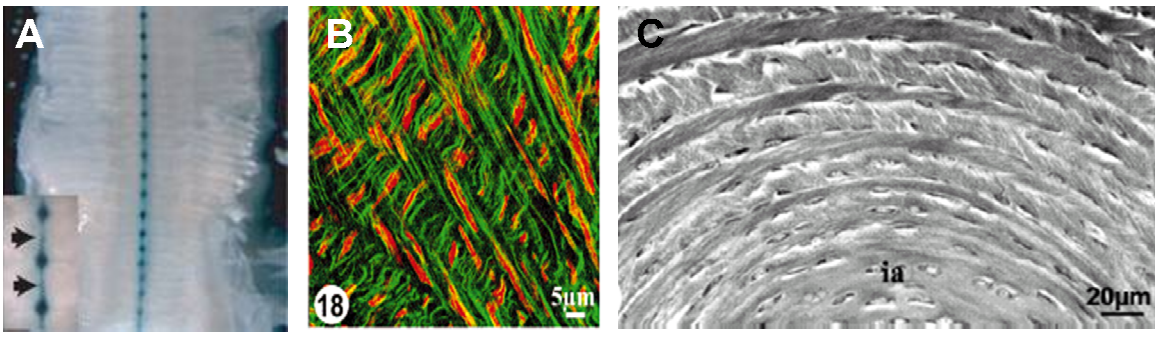

Figure 2.2 Intervertebral disc development. A) Fate-mapping of Shh-expressing notochordal cells reveals forming NP tissue is of notochordal origin (Choi et. al 2008). B) Actin staining of embryonic AF precursor cells indicates angle-ply alignment prior to the formation of an organized matrix (Hayes and Ralphs 1999). C) Neonatal rat disc illustrates full formation of the multi-lamellar angle-ply AF prior to birth (Hayes and Ralphs 1999).

have a rounded morphology *in vivo* and express chondrogenic markers such as Sox-9, type II collagen, and aggrecan (Sive, Baird et al. 2002). However, NP cells are distinct from chondrocytes; they harbor specific phenotypic traits suited for survival in the unique microenvironment of the NP, which includes lower pH, oxygen, and glucose levels, and higher osmolarity than what is physiologic for most tissues (Maroudas, Stockwell et al. 1975; Boyd, Richardson et al. 2005; Risbud, Guttapalli et al. 2006; Tsai, Guttapalli et al. 2007; Uchiyama, Guttapalli et al. 2008). Work to better understand these adaptations is important for the determination of NP-specific phenotypic markers and to distinguish between notochordal and NP cells. Considerably less work has been performed on the biology of AF cells, which are most frequently discussed as fibrochondrocytes, due to their expression of markers typical of both fibroblasts (e.g. type I collagen) and chondrocytes (type II collagen, aggrecan). An advanced understanding of the *in vivo* function of AF and NP cells will be instrumental in developing stem

cell-based tissue engineering strategies where differentiation into a disc-like phenotype is necessary.

2.1.3 Degeneration of the intervertebral disc

Disc degeneration is an aberrant, cell-mediated response to progressive structural failure, whereby changes in structure and composition give rise to mechanical dysfunction (Miller, Schmatz et al. 1988; Adams and Roughley 2006). Degeneration is also thought to play a dominant role in the development of low back pain (Miller, Schmatz et al. 1988; Bogduk 1991). Clinical treatments for discogenic back pain and disc degeneration are focused on the alleviation of symptoms, while restoration of function remains largely unaddressed. Fusion is the surgical standard for the treatment of axial low back pain (Deyo, Gray et al. 2005). This treatment is highly invasive and is intended to stop pain by eliminating motion across the joint space. Despite the frequency of its practice, fusion often fails to alleviate pain and may accelerate degenerative changes in adjacent discs (Levin, Hale et al. 2007; Harrop, Youssef et al. 2008). Total disc arthroplasty is a recently approved surgical option that aims to maintain segmental motion; however, its long term efficacy has not been established and mechanical wear may challenge its the long-term success (Resnick and Watters 2007; van Ooij, Kurtz et al. 2007). NP partial disc implants are under development; however, while they may restore disc height and mechanical support, they do not aim to repair AF damage incurred during implantation or due to degeneration (Di Martino, Vaccaro et al. 2005). Given the current treatment

options, there is tremendous need for a tissue engineering strategy that alleviates pain and restores spine function. Therefore, it will be of great importance that engineered replacement tissues overcome the harsh mechanical challenges of an extended lifetime in the intervertebral joint space. An advantage of this approach over arthroplasty is that living tissues, both native and engineered, retain their capacity for adaptive remodeling.

2.2 Functional Benchmarks for Tissue Engineering of the Intervertebral Disc

The disc is mechanically quite complex. Therefore, successful engineering of replacements for the disc and its component tissues, the AF and NP, is contingent upon replication of native tissue mechanical function. In order to establish design criteria for engineered replacement tissues, we must first establish the functional properties of their native counterparts. In this section, we will discuss the complex mechanical behaviors of the AF, NP, and motion segment. In doing so, we will use published data to generate quantitative functional benchmarks for disc tissue engineering (Table 2.1). Brief discussion of testing modalities and their relative importance is also included (Figure 2.3). These properties will be referred to throughout the remaining chapters, in order to draw quantitative and qualitative comparisons between the mechanical behavior of engineered and native intervertebral disc tissues.

Given the inherent complexity of the disc and the variability in most mechanical measures, it is nearly impossible to establish discrete, “hard and fast” benchmark values. Therefore the values reported here are culled from various studies in the literature and provide a range of standards against which engineered constructs can be compared. Because different animal models are employed in the study of disc mechanics, benchmarks are further obfuscated by inter-species variability (O'Connell, Vresilovic et al. 2007; Beckstein, Sen et al. 2008). Here, we will discuss results obtained for human tissue (when available). Also, this section will focus the discussion to overall tissue properties of the NP, AF, and disc, without explicit reference to local variations that are present within each. Nonetheless, it is important to note that these properties vary with region, and functional heterogeneity is quite relevant to discussions of both disc pathogenesis and certain specific applications in disc tissue engineering.

Discussion of mechanical properties is limited to elastic and some viscoelastic measures. Much of the tissue engineering literature has emphasized failure properties such as ultimate stress and percent elongation at failure. These properties are instructive for material characterization, but have limited relevance for *in vivo* function. Deformations that occur after the yield stress/strain but prior to failure are irrecoverable, meaning that when the external loads are removed, the initial geometry does not return. Naturally, this is problematic for *in vivo* implantation, where the engineered tissue would be loaded repeatedly. Moreover, many materials become weaker after yielding, making further damage

probable. Therefore, measures characterizing the post-yield behavior of materials and engineered tissue constructs are omitted here.

2.2.1 Mechanics of the annulus fibrosus

AF architecture and composition combine to produce an anisotropic, nonlinear, and viscoelastic tissue, uniquely suited to withstand the complex mechanical loading experienced *in vivo*. Consequently, extensive studies have been performed on the AF using multiple loading modalities and spanning many length scales, and studies are still ongoing to fully characterize its behavior.

2.2.1.1 Uniaxial tension

The AF is subjected to large tensile stresses along the circumferential direction of the disc. In uniaxial tensile testing, loads are applied along a single axis while all surfaces parallel to the loading axis are stress-free (Figure 2.3). Due largely to the technical difficulty associated with isolation of single lamellae, only a handful of studies have investigated mechanics at this level (Skaggs, Weidenbaum et al. 1994; Holzapfel, Schulze-Bauer et al. 2005) (Table 2.1). The single lamella presents two important functional behaviors that are mirrored by the AF at larger length-scales: anisotropy and stress-strain nonlinearity. Tensile nonlinearity is a common feature of many fiber-reinforced soft tissues, and is often characterized by a small-strain or toe-region modulus, a linear region modulus, and a transition strain at which the transition from toe to linear region occurs (Figure 2.3). While often overlooked, transition strain is important to tissue

function: implanting an engineered tissue with too high a transition strain would result in laxity and instability, while too low a transition strain will limit motion and overload the surrounding tissues. The AF undergoes large elastic deformations during physiologic function (Miller, Schmatz et al. 1988; Bogduk 1991). It is therefore important that replacement tissues also deform elastically over a large range before yielding (ε_{yield}, Table 2.1).

Due to AF anisotropy, it is necessary to consider how tensile behavior varies with orientation within the AF. The uniaxial tensile modulus of the AF is one to two orders higher along the circumferential direction than in the axial and radial directions (Table 2.1, Figure 2.1). This level of anisotropy should be preserved by an engineered tissue in order to avoid failure under multi-axial loading *in vivo*.

The high water content and intrinsic material composition of the AF introduce viscoelastic, strain-rate dependent behavior to its tensile properties (Kasra, Parnianpour et al. 2004); however, these have received considerably less attention than compressive and torsional rate dependence. *In vivo* deformations of the disc can range from slow or quasi-static loads (body weight) to high frequency deformations such as those experienced during running or the operation of large machinery (Virtanen, Karppinen et al. 2007). Consequently, it is important to understand the relation between loading rate and mechanics for engineered tissues and how this relation compares to the native AF. It is possible that an engineered tissue that replicates the static tensile modulus of AF may still prove inferior when loaded at physiologic rates, limiting its *in vivo* function.

Because of its physiologic relevance and ease of implementation/analysis, uniaxial tensile testing is used extensively in Chapters 3 – 7 in order to characterize the mechanics of acellular scaffolds and cell-seeded, engineered AF tissues. It is only in Chapter 8, when the engineered AF is coupled with engineered NP tissue to form a composite macroscopic disc that tensile testing is omitted in favor of compression testing (below).

2.2.1.2 Biaxial tension

While uniaxial extension is a simple and valuable testing modality, the AF has no free boundaries *in vivo*. Biaxial testing permits rigorous mechanical testing in a format that replicates the constrained boundaries encountered *in vivo* (Figure 2.3) (Sacks and Sun 2003). By simultaneously loading along two orthogonal directions, an abundance of data can be generated from a single test. This also poses a drawback, however, in that it is not straightforward to determine what subset of this information is most relevant for tissue characterization or comparison of engineered and native AF. Multiple combinations of strain ratios can be applied, ranging from fixed boundary tests to equibiaxial tension. While it remains unclear what combination of strain ratios most closely approximates *in vivo* deformations of the AF, two commonly considered scenarios are circumferential extension with fixed axial boundaries and equibiaxial tension (O'Connell, Sen et al. 2007). Although these two special cases are useful as benchmarks of biaxial function, constitutive modeling may be necessary to process complex datasets in a fashion that enables meaningful

comparisons between engineered and native tissue (Humphrey, Strumpf et al. 1990; Billiar and Sacks 2000; Bass, Ashford et al. 2004; O'Connell, Guerin et al. 2009).

2.2.1.3 Compression

Compressive loading of the disc simultaneously produces narrowing of the disc height and outward bulging of the NP, placing axial and radial compressive stresses on the AF. For this reason, the AF has been well characterized in compression (Best, Guilak et al. 1994; Drost, Willems et al. 1995; Iatridis, Setton et al. 1998; Klisch and Lotz 2000; Yao, Justiz et al. 2002; Perie, Korda et al. 2005; Perie, Iatridis et al. 2006). While properties can be probed in unconfined compression, confined compression is more amenable to theoretical analyses, and more closely approximates *in vivo* loading. In confined compression, the compressive load is applied via a porous (water permeable) platen to samples that are confined so as to prevent lateral expansion of the solid phase and to restrict fluid flow to the loading axis (Figure 2.3). While the mechanical properties discussed thus far have treated the AF as an elastic solid, the high water content of the AF strongly influences its behavior in compression. As such, many of these studies have described AF compressive properties in a biphasic framework. Under small strains, biphasic materials are described by an aggregate modulus (H_A) and a fluid permeability (k). Biphasic theory has been generalized to include large deformations such as those experienced by the AF *in vivo* by the use of additional properties describing the strain dependence (nonlinearity) of the

modulus (β) and permeability (*M*) (Ateshian, Warden et al. 1997). Analyses of AF nonlinear biphasic properties (Iatridis, Setton et al. 1998; Perie, Korda et al. 2005) provide similar values of H_A and k_o to the linear case (Best, Guilak et al. 1994), although the nonlinearity parameters *M* and *β* are nonzero, indicating that under large deformations the AF behaves nonlinearly (Table 2.1). Despite the

Nanoindentation: AF
Sub-lamellar

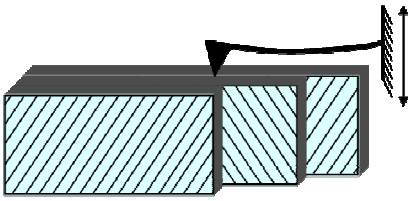

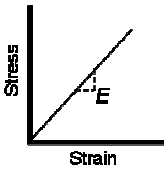

Uniaxial tension: AF
Single/Multi-lamellar

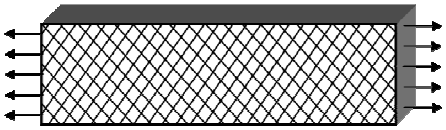

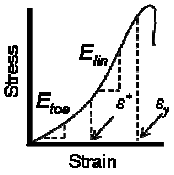

Biaxial tension: AF
Single/Multi-lamellar

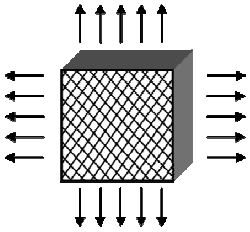

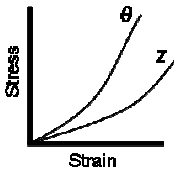

Shear: AF
Single/Multi-lamellar

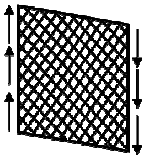

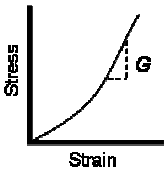

Lap testing: AF
Multi-lamellar

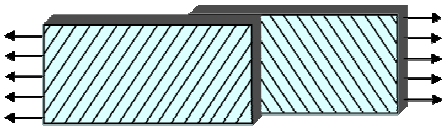

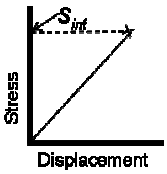

Confined
compression:AF/NP
Multi-lamellar

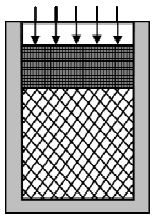

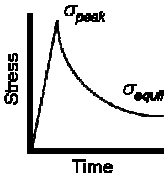

Torsional Shear:
AF/NP/Motion
segment

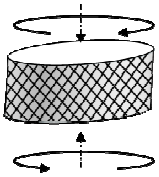

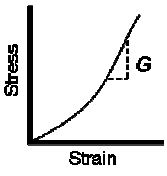

Figure 2.3 Schematic representations are shown for the testing modalities discussed (Left), along with typical stress-strain profiles associated with each (Right). E = modulus; toe/lin = toe region/linear region; ε* = transition strain; ε_y = yield strain; G = shear modulus; S_{int} = interfacial/lap strength; $\sigma_{peak/equil}$ = peak/equilibrium stress.

strong tensile anisotropy of the AF, confined compression indicates no variation in properties with orientation, suggesting that the fibrous components of the AF have little to no contribution to compressive properties in the absence of tensile strains (Iatridis, Setton et al. 1998). Although swelling is typically a behavior reserved for discussions of NP mechanics, confined compression experiments have measured considerable swelling pressures in the AF, and have found this propensity for tissue swelling to play an important role in the compressive properties (Yao, Justiz et al. 2002; Perie, Korda et al. 2005). While less has been done to characterize the role of swelling pressure in tensile mechanics of the AF, there is evidence that hydration plays an important role in tension as well (Hirsch and Galante 1967). Despite its role in native AF mechanics, swelling has remained largely unaddressed by tissue engineering.

TISSUE *Scale*	**Testing Modality**	**Benchmark**	**Native Value**	**Reference**
Annulus Fibrosus *Sub-lamella*	Nanoindentation	E	0.6 – 1.2 MPa	Lewis et al. 2008 (Lewis, Hussain et al. 2008)
Annulus Fibrosus *Single Lamella*	Uniaxial Tension	E $(\varphi=0^o)$	80 – 120 MPa	Skaggs et al. 1994 (Skaggs, Weidenbaum et al. 1994) Holzapfel et al. 2005 (Holzapfel, Schulze-Bauer et al. 2005)
		E $(\varphi=90^o)$	0.22 MPa	
		v $(\varphi=0^o, 90^o)$	N/A	
Annulus Fibrosus *Multiple Lamellae*	Lap Testing	S_{int}	N/A	N/A
	Uniaxial Tension	E_θ (toe/linear)	2.5/18-45 MPa	Acaroglu et al. 1995 (Acaroglu, Iatridis et al. 1995) Ebara et al. 1996 (Ebara, Iatridis et al. 1996) Fujita et al. 1997 (Fujita, Duncan et al. 1997) Guerin et al. 2006(Guerin and Elliott 2006) Elliott et al. 2001 (Elliott and Setton 2001) Kasra et al. 2004 (Kasra, Parnianpour et al. 2004) (Guerin and Elliott 2007)
		ε_θ^*	0.06	
		E_z (toe/linear)	0.27/0.82 MPa	
		E_r (toe/linear)	0.19/0.45 MPa	
		$v_{\theta z}$	1.77	
		$v_{\theta r}$	0.33	
		ε_{yield}	20% - 30%	
	Biaxial Tension	Axial Fixed E (toe/linear)	9.8/27.2 MPa	(O'Connell, Sen et al. 2010)
		Equibiaxial E (toe/linear)	Circumferential 16.5/43.3 MPa Axial 10.7/ 26.8 MPa	
	Planar/Torsional Shear	$G_{z\theta}$	20 – 125 kPa	(Iatridis, Kumar et al. 1999) (Fujita, Wagner et al. 2000) (Jacobs, Morelli et al. 2010)
		$\lvert G^* \rvert$	75 – 200 kPa	
		δ	17^o – 20^o	
	Confined Compression	P_{swell}	110 - 130 kPa	(Best, Guilak et al. 1994) (Iatridis, Setton et al. 1998) (Perie, Korda et al. 2005)
		H_{Ao}	440 - 750 kPa	
		β	2.7	
		k_o	1.6 – 2.3 (x 10^{-16} $m^4 N^{-1} s^{-1}$)	
		M	1.5	
NUCLEUS PULPOSUS	Confined Compression	P_{swell}	0.138 MPa	(Johannessen and Elliott 2005)
		H_A^{eff}	1.0 MPa	
		k_o	9.0 (x 10^{-16} $m^4 N^{-1} s^{-1}$)	

TISSUE *Scale*	**Testing Modality**	**Benchmark**	**Native Value**	**Reference**
NUCLEUS PULPOSUS	Torsional shear	$\|G^*\|$	7.4 – 19.8 kPa	(Iatridis, Setton et al. 1997)
		δ	23^o – 30^o	
MOTION SEGMENT	Axial Compression	Stiffness	1.73 kN/mm	(Nachemson, Schultz et al. 1979) (Shea, Takeuchi et al. 1994) (Beckstein, Sen et al. 2008)
		E	3 – 10 MPa	
	Torsion	G_{app}	2 – 9 MPa	(Elliott and Sarver 2004) (Abumi, Panjabi et al. 1990) (Haughton, Schmidt et al. 2000) (Beckstein, Espinoza Orias et al. 2007)
	Static Viscoelasticity	Various multi-parameter rheological models; see referenced literature for details.		(Keller, Spengler et al. 1987) (Beckstein, Sen et al. 2008)
	Dynamic Viscoelasticity	Dynamic Stiffness	3.5 – 5.1 kN/mm (0.001 – 1 Hz, respectively)	(Costi, Stokes et al. 2008)

Table 2.1 Summary of native tissue benchmarks related to mechanics of the AF, NP, and motion segment. E = modulus; φ indicates angle relative to the prevailing collagen orientation; S_{int} = interfacial strength; toe/lin = toe region/linear region of stress-strain curve; θ,z, and r indicate the loading axes along the disc circumferential, axial, and radial directions as indicated in Figure 2.1A; ε* = transition strain indicating the transition from toe to linear region of the stress-strain curve; v = Poisson's ratio; ε_{yield} = yield strain; G = shear modulus; $\|G^*\|$ = complex shear modulus; δ = phase shift; P_{swell} = swelling pressure; H_{Ao} = aggregate modulus; β = modulus nonlinearity parameter; k_o = permeability; M = permeability nonlinearity parameter; G_{app} = apparent shear modulus; $\tau_{1/2}$ = time constants describing short/long term creep response.

2.2.1.4 Shear and torsion

The AF experiences considerable shear stresses during torsion and bending of the spine. Because application of pure shear is often difficult, AF

shear tests have been performed on cylindrical, cuboidal, or planar samples under compressive or tensile preloads (Figure 2.3). In shear, the AF is anisotropic (Fujita, Wagner et al. 2000; Yoder, Henninger et al. 2009; Jacobs, Morelli et al. 2010) and viscoelastic (Iatridis, Kumar et al. 1999). Under tensile pre-stress representing physiological AF loading, shearing in the lamellar plane is resisted by stretching of the collagen fibers, resulting in larger shear moduli than measured in the absence of this preload (Yoder, Henninger et al. 2009). Torsional shear studies have been used to measure dynamic viscoelastic behavior, resulting in estimates of complex shear modulus ($|G^*|$) and phase shift (δ), which characterize dynamic stiffness and energy dissipation, respectively (Iatridis, Kumar et al. 1999). Because torsion of the spine produces prominent shearing of the AF in the radial plane, circumferential shear properties (Figure 2.3, Table 2.1) may be most crucial for replication in engineered tissues.

2.2.1.5 Inter-lamellar and sub-lamellar mechanics

The macroscopic response of the AF is a unique product of its microscopic organization and associated mechanical properties. As such, assessment of the functional viability of engineered replacement tissues necessitates an understanding of how AF function evolves over a broadening length scale. Relatively little work has been done at the sub-lamellar scale to characterize nano-scopic mechanics of the disc. In the only such study to date, AFM indentation tests revealed isotropic and heterogeneous behavior (Figure 2.3, Table 2.1) (Lewis, Hussain et al. 2008). Much work remains to investigate

sub-lamellar mechanics and how they relate to the aggregate behavior of a single lamella.

Although very little is known about the functional role of the inter-lamellar matrix, theoretical models predict large inter-lamellar shear stresses (Iatridis and ap Gwynn 2004). Moreover, recent work suggests that interlamellar properties may be important to macroscopic AF mechanics (Michalek, Buckley et al. 2009). The potential role of interlamellar shearing in reinforcing the tensile properties of the AF will be discussed in detail in Chapters 6 and 7. Direct measurement of interfacial strength at the interlamellar surface via lap or peel tests (Figure 2.3) would provide an improved understanding of how single lamellar mechanics relate to the overall behavior of the AF. No such data are currently available in the native AF.

2.2.2 Mechanics of the nucleus pulposus

NP mechanics are central to disc function and the overall flexibility and stability of the spine. Mechanical function of the NP is largely dictated by its composition: an extracellular matrix comprised primarily of type II collagen and proteoglycans. A high fixed charge density provided by sulfated glycosaminoglycans generates considerable osmotic pressure and causes the NP to imbibe water. Swelling of the NP is constrained by the AF and endplates, establishing a hydrostatic pressure in the absence of external loads. As a result, mechanical properties of the NP share physical traits of both a solid and a fluid (Iatridis, Weidenbaum et al. 1996).The NP is isotropic and subject primarily to

compressive and shear stresses *in vivo*. Consequently, studies of NP mechanics have focused on these properties, accounting for the importance of the fluid-based effects through either a multi-phasic or lumped-parameter viscoelastic framework.

2.2.2.1 Compression

Compressive properties of the NP have been investigated via local indentation (Umehara, Tadano et al. 1996; Causa, Manto et al. 2002) and unconfined (Cloyd, Malhotra et al. 2007) or confined (Best, Guilak et al. 1994; Johannessen and Elliott 2005) compression. Indentation methods are instructive in obtaining information about mechanical heterogeneity; however, indentation produces tensile stresses transverse to the loading axis, resulting in a complex loading scheme not experienced by the NP *in vivo*. Likewise, compression-induced fluid flow and lateral expansion of the NP are restricted *in vivo* by the surrounding AF and endplate cartilage, resulting in an increase in intra-discal pressure that is necessary to support axial spine loads. As a result, it is difficult to reconcile unconfined compression testing with physiologic function. Therefore, confined compression is the key functional benchmark for tissue engineering of the NP. While it is quite soft in unconfined compression, results in confined compression show the NP to withstand much larger loads, attributed directly to the considerable role of fluid pressurization in NP mechanics (Johannessen and Elliott 2005). Linear biphasic material parameters for the NP are provided in Table 2.1.

2.2.2.1 Shear and torsion

In vivo, torsion of the spine generates shearing about the axial direction of the disc. Because this is superimposed upon compressive stresses, NP torsional shear properties have been investigated under axial compression (Figure 2.3). Because there are very pronounced rate-dependent effects in shear (Iatridis, Weidenbaum et al. 1996), studies of torsional shear have primarily focused on viscoelastic behavior (Iatridis, Setton et al. 1997) (Table 2.1). One important observation is that under constant shear deformation, the shear stress of NP relaxes almost completely, similar to its behavior in unconfined compression (Johannessen and Elliott 2005). This unique, fluid-like behavior poses an interesting hurdle for NP tissue engineering.

2.2.3 Mechanics of the motion segment

A motion segment consists of the intact disc along with its adjacent vertebral bodies (Figure 2.1). Typically the term "motion segment" may or may not include other surrounding substructures (e.g., facet joints, longitudinal ligaments). Each paper should be evaluated for its definition. For studies related to disc tissue engineering, the interactions between the engineered constructs and the bony interface are of great interest; therefore, motion segment studies that introduce the additional complexity of facet joints are not as relevant to establish structural benchmarks. Because functional analyses at this level can be easily considered in the context of physiologic loading, motion segment

mechanics have been well studied for many decades. Due to our focus on benchmarks for disc tissue engineering, many details of this complex mechanical system are not discussed here; the reader is directed to the referenced work for detailed accounts of motion segment mechanics.

The spine is compressed axially due not only to body weight and daily activity, but also due to loads from the musculature that surrounds the spine. The macroscopic response of the motion segment relies on the properties of both AF and NP substructures. Similarly, torsional properties of the motion segment are important for stability and flexibility of the spine for a broad range of daily activities. Compressive and torsional properties of the human motion segment are provided (Table 2.1). These measures define perhaps the most important benchmarks in disc tissue engineering, as they represent the macroscopic response that must be obtained by an engineered disc, or by a segment of remnant disc when coupled with an engineered replacement such as an annular patch. Replicating of the properties of isolated AF and NP does not ensure replication of motion segment mechanics when the two are combined; therefore it is important to consider the overall response of engineered AF and NP in concert. If the resulting material does not compare favorably with motion segment benchmarks, the material may fail regardless of constituent properties.

Like the AF and NP, the motion segment also has rate dependent behavior. There are many approaches for analyzing creep and stress relaxation experiments, and consequently there is no one established method or metric to describe this complex behavior (Keller, Spengler et al. 1987; Beckstein, Sen et

al. 2008). Therefore, while such studies are undeniably important for understanding disc function, an in depth analysis of multi-parameter rheological models is beyond the scope of the current work. Dynamic compressive stiffness of the motion segment has also been measured, and depends significantly on the frequency of loading (Costi, Stokes et al. 2008). This rate-dependence is dominated by fluid-solid interactions (poroelastic effects) rather than the intrinsic rate dependence of the solid extracellular matrix (viscoelasticity).

2.2.4 Theoretical Modeling of Intervertebral Disc Mechanics

Theoretical models have a long-standing history of application in disc research (Wu and Yao 1976; Hickey and Hukins 1980; Spilker 1980). Constitutive models, mathematical relationships between tissue deformation and stress, have been developed to better understand and characterize the structure-function behaviors of the AF (Klisch and Lotz 1999; Eberline, Holzapfel et al. 2001; Elliott and Setton 2001; Sun and Leong 2004; Wagner and Lotz 2004; Yin and Elliott 2005; Guo, Peng et al. 2006; Guerin and Elliott 2007; O'Connell, Guerin et al. 2009). Constitutive models provide insight into the structure-function relationships of native tissues, and can thereby guide tissue engineering approaches, providing quantitative benchmarks that unify multiple testing modalities. Moreover, while linear measures such as modulus are sufficient for characterizing conventional engineering materials such as steel and concrete, a single slope cannot sufficiently characterize the nonlinear stress-strain behavior of biological tissues like the AF. Hyperelastic constitutive models allow for

characterization of both the small and large strain behaviors of biological tissues, and therefore provide a more robust material definition. Hyperelastic models will be discussed in greater detail in Chapters 5 and 7 of this work.

Accurate constitutive models can be incorporated into finite element analyses to perform simulations of mechanical function that account for the complex loading and geometry of the tissue that comprise the disc. These can then provide insight into the stress distributions and concentrations that result from a range of physiologic motions (Shirazi-Adl, Shrivastava et al. 1984; Shirazi-Adl 1994; Martinez, Oloyede et al. 1997) and have been used to assess the ability of total disc replacements and injectable NP reinforcements to dissipate stresses within the spine (Denoziere and Ku 2006; Rohlmann, Zander et al. 2008). For tissue engineering, these models can predict the local stress-strain environment that the construct will encounter upon implantation. Finally, through the use of poroelastic, viscoelastic, and biphasic constitutive laws, finite element models can be used to characterize complex behaviors such as dynamic mechanics of the motion segment under combined loading conditions like compression, bending and torsion (Laible, Pflaster et al. 1993; Ferguson, Ito et al. 2004; Williams, Natarajan et al. 2007).

2.3 Tissue Engineering of Fiber-reinforced Soft Tissues

2.3.1 Directing alignment of cells in vitro

The annulus fibrosus of the intervertebral disc, along with tendon, ligament, muscle, and the knee meniscus is an example of a fiber-reinforced load bearing tissue. These tissues are varied in their exact functions, but each is subject to tensile loading during physiologic motions. The ability to resist large tensile stresses in these tissues is due in large part to the presence of organized collagen networks in the extracellular matrix (and in the case of muscular tissues, intracellular networks of contractile filaments as well). In order to engineer replacements for such tissues, it is important to develop ways in which cells can be instructed to form tissues uni-directionally, with the resulting tissue possessing anisotropic properties. Groups studying a range of cell-types have developed *in vitro* systems to guide cell alignment and elongation (Figure 2.4). For instance, cells cultured in narrow troughs track along the edges and elongate parallel to

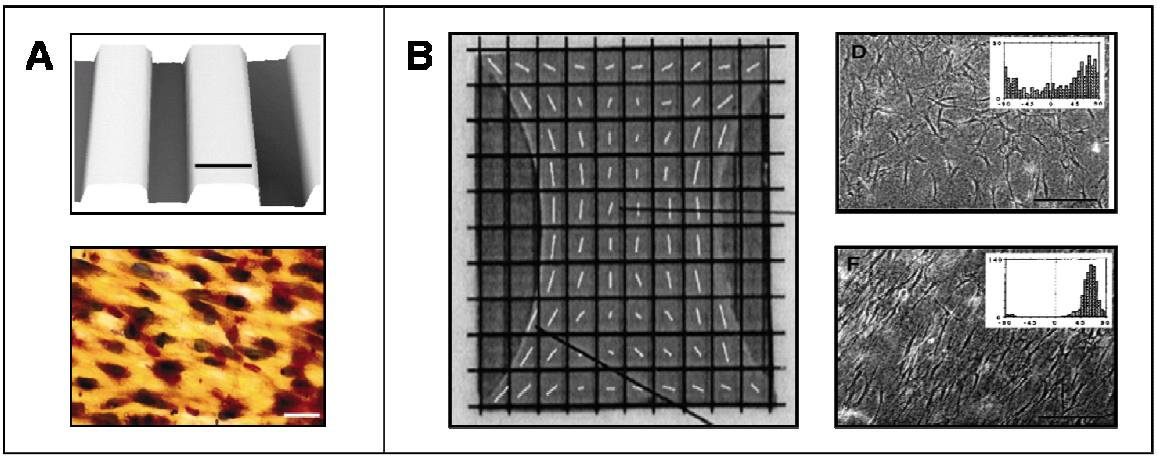

Figure 2.4 Aligning cells in vitro. A) micro-patterned grooves (above) direct cell and subcellular alignment (bottom)(Wang, Jia et al. 2003). B) Cells constrained at two boundaries contract, deforming free edges and aligning themselves along the boundaries (Costa, Lee et al. 2003).

their boundaries (Figure 2.4A) (Wang, Jia et al. 2003). Alternatively, cells within a soft collagen will compact their matrix via cell mediated contractions, resulting

in deformations that align cells along free gel boundaries (Figure 2.4B) (Barocas and Tranquillo 1997; Costa, Lee et al. 2003). While it is conceivable that deposition of aligned extracellular matrix would require cell alignment as a pre-requisite, evidence that aligned cells deposit aligned collagenous extracellular matrix is limited.

2.3.2 Electrospinning for tissue engineering

Electrospinning is a method by which large electrostatic forces are used to deform polymeric droplets into nanofibers, a transformation that results from charge repulsive forces overcoming surface tension to initiate the formation of a nanofibrous jet (Mauck, Baker et al. 2009). This jet whips and twists as it transits through the air, and evaporation of the organic solvent results in polymeric nanofibers that deposit on the grounded surface near by (Figure 2.5). If the grounded surface is static, the accumulation of nanofibers over time results in a random, disorganized mesh of fibers ranging between 300 nm – 1 μm in diameter. If the fibers are instead collected onto a moving surface, such as a rotating mandrel (Figure 2.5), the fibers are drawn into alignment along the direction of rotation, resulting in an array of highly aligned nanofibers. Cells on aligned nanofibrous scaffolds align with the underlying fiber direction, and represent a promising approach for engineering fibrous soft tissues. In the work presented in this thesis, electrospinning is utilized to generate aligned

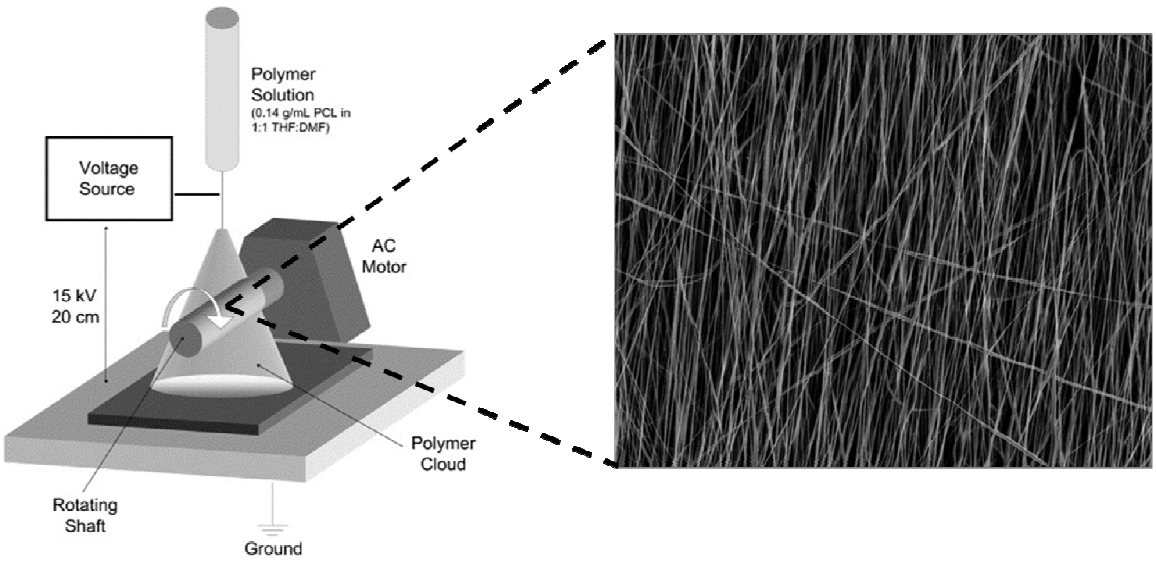

Figure 2.5 Electrospinning for nanofiber formation. Polymer is extruded from a needle via syringe pump, and a voltage source used to statically charge the polymer. Deposition of fibers onto a rotating shaft (>10 m/s) results in accumulation of aligned nanofibers, as shown via SEM (right) (Li, Mauck et al. 2007)

nanofibrous scaffolds, which are then used to direct the extracellular matrix deposition by resident cells in order to create tissues that replicate the form and function of the annulus fibrosus at multiple length scales of its hierarchical organization.

2.4 Tissue Engineering of the Intervertebral Disc

While the study of disc mechanics has spanned several decades, tissue engineering of the disc is a relatively new field of research. As such, while many promising approaches have been developed using various biomaterials and cell sources, little has been done to evaluate their functional equivalence with native tissue (Butler, Goldstein et al. 2000; 2008). Recent reviews are available that

summarize progress in disc tissue engineering from a cellular and biomaterials perspective (O'Halloran and Pandit 2007; Kandel, Roberts et al. 2008). Therefore, here we will focus on landmark disc tissue engineering studies and emphasize, whenever possible, the measurement of mechanical properties of engineered constructs (Table 2.2). A central aim of this discussion is to identify in the literature where well-crafted pursuits have produced viable disc-like tissue, but mechanical properties have yet to be assessed and/or functional benchmarks have not yet been met. Additionally, pursuits in the following chapters, where we will engineer AF and disc tissues will attempt to fill in the voids identified by the present discussion.

Early disc-related tissue engineering work was concerned primarily with establishing culture systems in which the phenotypes of AF and NP cells could be preserved. One early study probed the effect of various combinations of growth factors on the fibrocartilagenous phenotype of AF and NP cells seeded in a cross-linked type I collagen/hyaluronan scaffold (Alini, Li et al. 2003). Proteoglycan and collagen synthesis were maintained by various combinations of growth factors, with TGF-β1 yielding the most pronounced anabolic response by both cell types. Although native tissue composition was not achieved and mechanics were not assessed, this study first indicated that tissue engineering may indeed hold some potential for the treatment of disc degeneration. In the years following this work, AF and NP cells have been successfully cultured on a wide array of synthetic and natural polymers (Rong, Sugumaran et al. 2002; Sato, Asazuma et al. 2003; Sato, Kikuchi et al. 2003; Mizuno, Roy et al. 2006;

Chang, Kim et al. 2007; Shao and Hunter 2007; Wan, Feng et al. 2007; Chang, Kim et al. 2009; Gruber, Hoelscher et al. 2009).

2.4.1 Tissue engineering of the annulus fibrosus

Numerous groups have demonstrated the capacity for AF cells to attach to and proliferate on a range of scaffolding materials. In many such studies, AF cells retained phenotypic stability and elaborated an extracellular matrix that compositionally resembled native AF (Sato, Asazuma et al. 2003; Wilda and Gough 2006; Chang, Kim et al. 2007; Chou, Reza et al. 2008; Nesti, Li et al. 2008; Yang, Kandel et al. 2008; Gruber, Hoelscher et al. 2009). A particular challenge for AF tissue engineering has been to replicate the multi-scale architecture that distinguishes the AF from other soft tissues. In one recent study, unidirectionally aligned alginate/chitosan fibers (Figure 2.6A, Table 2.2) were synthesized to mimic the collagen alignment within a single lamella of AF and seeded with AF cells (Shao and Hunter 2007). Although cells adhered to these fibers and deposited fibrocartilagenous extracellular matrix, mechanical properties and extracellular matrix organization were not investigated, and due to the large size of scaffold fibers, cells maintained a rounded morphology.

Others have synthesized a novel biodegradable polymer for AF tissue engineering, and demonstrated maintenance of fibrocartilagenous phenotype by rat AF cells seeded onto the material (Wan, Feng et al. 2007). Although a compressive modulus was measured (Table 2.2), it was several orders of magnitude lower than native AF. Some studies have also successfully replicated

the multi-lamellar organization of the AF. Recently, one such study developed a biphasic scaffold, where an inner AF region was constructed from a concentrically wrapped bio-polymer sheet seeded with chondrocytes, and an outer AF was fashioned from demineralized bone matrix (Figure 2.6D) (Wan, Feng et al. 2008). Compressive and tensile tests of the engineered AF constructs were performed at fabrication; however, only failure properties were reported. Additionally, while this study mimicked the multi-lamellar architecture of the AF, intra-lamellar collagen synthesis and organization was not reported.

While these and other studies demonstrate clear progress of the field of annulus fibrosus tissue engineering, no study has yet been able to re-create the +/-30^{o} angle-ply organization of the AF. Consequently, of the few studies to investigate mechanics of engineered AF tissues, none have yet reached functional parity with the native AF. The focus of research presented in the chapters that follow is to employ electrospinning in order to engineer tissues that replicate anatomic form of the AF at multiple length scales, and at each to observe the functional consequences of extracellular matrix deposition. The mechanical benchmarks outlined above will be referred to wherever possible to assess the equivalence of engineered and native AF tissues.

2.4.2 Tissue engineering of the nucleus pulposus

Gene expression and extracellular matrix production by NP cells has been characterized under a number of culture conditions (Yang and Li 2009). From these studies, it is evident that, like chondrocytes, extracellular matrix production

and phenotypic stability of NP cells requires culture in a three-dimensional format, where rounded cell morphology can be maintained (Gruber, Stasky et al. 1997; Wang, Baer et al. 2001; Gruber, Ingram et al. 2003; Chou, Bansal et al. 2006; Roughley, Hoemann et al. 2006; Chou and Nicoll 2008; Chou, Reza et al. 2008; Reza and Nicoll 2009). Similar to the AF, mechanics have not been widely investigated for engineered NP tissue, and often times such measures are only made at the time of scaffold fabrication. Therefore, functional changes due to extracellular matrix deposition are generally not examined. While to our knowledge, confined compression properties of engineered NP have not yet been reported, a number of studies have reported findings in unconfined compression for various hydrogel-based constructs (Baer, Wang et al. 2001; Cloyd, Malhotra et al. 2007; Chou, Akintoye et al. 2009; Reza and Nicoll 2009). Because in unconfined compression the NP is quite soft (~ 5 kPa), many of these studies report comparable properties to native NP prior to any matrix deposition (Table 2.2). However, the critical role of swelling pressure and the biphasic properties that define the time-varying behavior of NP may be more challenging to achieve.

One noteworthy study examined the compressive and torsional shear properties of alginate hydrogels seeded with porcine inner AF cells and cultured for up to 16 weeks *in vitro* (Baer, Wang et al. 2001). Although the NP-like phenotype of cells was preserved, dynamic shear modulus declined with culture duration, and remained an order of magnitude below native NP. Additionally, the

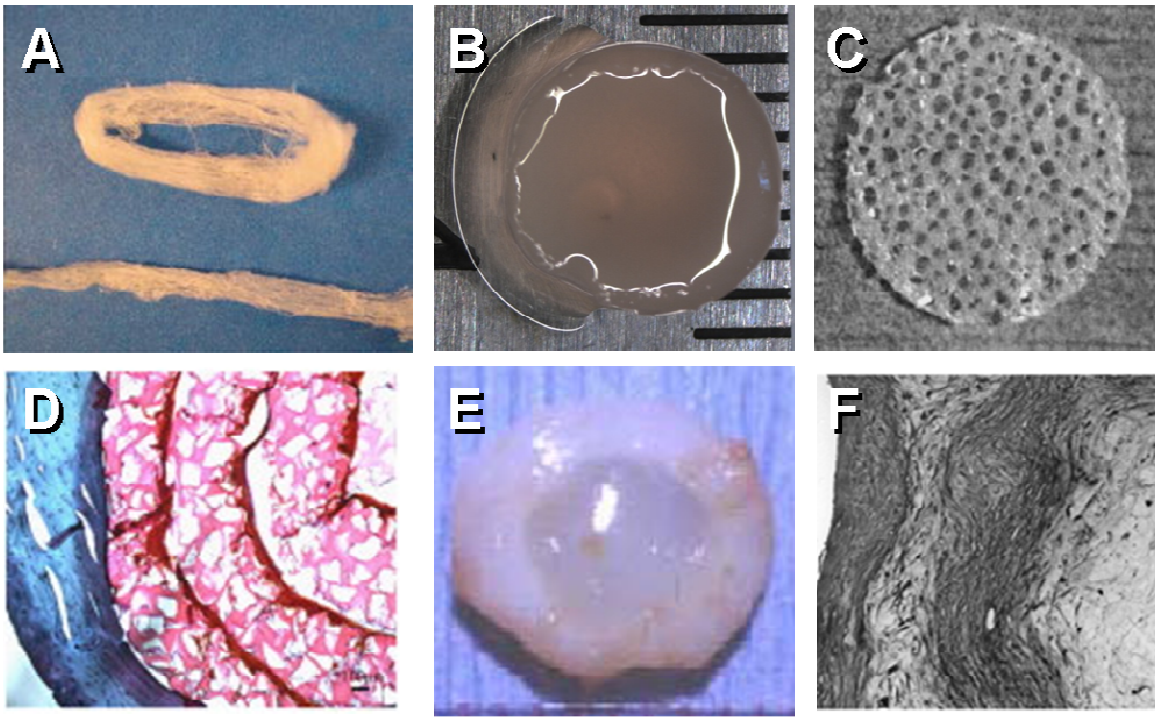

Figure 2.6 An array of strategies for disc tissue engineering. A) hybrid alginate/chitosan fibers synthesized for AF tissue engineering (Shao and Hunter 2007). B) Carboxymethylcellulose gel seeded with NP cells (Reza and Nicoll 2009). C) Atelocollagen honeycomb scaffolds engineered from natural extracellular matrix (Sato, Asazuma et al. 2003; Sato, Asazuma et al. 2003). D) Engineered multi-lamellar AF constructed from poly(polycaprolactone-triol-malate) seeded with chondrocytes, and surrounded with a demineralized bone matrix (Wan, Feng et al. 2008). E) Composte whole-discs constructed from an NP cell-encapsulated alginate hydrogel surrounded by an AF cell-seeded PGA mesh (Mizuno, Roy et al. 2006). F) Disc formed from a composite hyaluronic acid/nanofibrous scaffold seeded with human mesenchymal stem cells (Nesti, Li et al. 2008).

phase angle increased to within 5^{o} of native. While these values demonstrate a gap between engineered and native tissue mechanics, this work is among the few to exhaustively measure mechanics for engineered NP. One recent study measured the dynamic shear properties of type I collagen gels for NP tissue engineering, and while phase angle was lower than native NP, the dynamic shear modulus compared quite favorably (Table 2.2) (Bron, Koenderink et al. 2009).

	Cell Source	Scaffold Material	Major Finding	Mechanics Measured		Native Benchmark	Reference
AF	AF cells (lapine)	Atelocollagen honeycomb (Figure 3C)	AF cells retained fibrocartilage phenotype and produced more extracellular matrix in 3-D culture than in monolayer	N/A		N/A	Sato et al. 2003 (Sato, Asazuma et al. 2003)
	AF cells (canine)	Alginate/chitosan hybrid fibers (Figure 3A)	AF cells attached to fibers and deposited extracellular matrix containing types I and II collagen and aggrecan	N/A		N/A	Shao et al. 2007 (Shao and Hunter 2007)
	AF cells (rat)	Poly(1,8-octanediol malate)	AF cells proliferated and expressed type II collagen; constructs were nonimmunogenic upon subcutaneous implantation	Compressive modulus	0.12 – 0.25 kPa	440 – 750 kPa	Wan et al. 2007 (Wan, Feng et al. 2007)
				Ultimate tensile stress	7-15 MPa	N/A	
	Chondrocytes (lapine)	Bone matrix gelatin and poly(polycaprolactone triol malate) (Figure 3E)	Cells survived within multi-lamellar constructs, deposited disc-like extracellular matrix, and constructs survived 100 cycles of compression without permanent deformation	Ultimate tensile stress	1.3 MPa	N/A	Wan et al. 2008 (Wan, Feng et al. 2008)
				Ultimate compressive stress	3.5 MPa	N/A	
NP	Inner AF (bovine)	Alginate	Cells survived and expressed fibrocartilage markers, but compressive and torsional properties declined with culture duration despite matrix accumulation	Comrpession and torsion	$\delta = 6^o – 14^o$	$23 - 30^o$	Baer et al. 2001 (Baer, Wang et al. 2001)
					$\lvert G^* \rvert = 0.2 – 0.6$ kPa	7.4 – 19 kPa	
	NP cells (bovine)	Calcium polyphosphate substrate	Cells deposited extracellular matrix that matched native proteoglycan content but not collagen content, resulting in improved properties in unconfined compression	Unconfined compression	$E_{eq} = 8.3$ kPa	5.4 kPa	Séguin et al. 2004 (Seguin, Grynpas et al. 2004)

	Cell Source	Scaffold Material	Major Finding	Mechanics Measured		Native Benchmark	Reference
NP	N/A	Type I collagen gel	Gel formation was tailored to replicate mechanical function of the NP in dynamic shear	Torsional shear	$\delta = 6.5^o – 8.5^o$	23 -30^o	Bron et al. 2009 (Bron, Koenderink et al. 2009)
					$\|G^*\| = 2 – 10$ kPa	7.4 – 19 kPa	
	NP cells (bovine)	Photo-crosslinked carboxymethylcellulose (Figure 3B)	Hydrogel processing produced tunable mechanical properties; NP cells survive when encapsulated	Unconfined compression	$E_{eq} = 4.3$ kPa	5.4 kPa	Reza et al. 2009 (Reza and Nicoll 2009)
	NP cells (bovine)	Photo-crosslinked alginate	Photocrosslinking improved proteoglycan accumulation by NP cells, resulting in increased compressive properties with culture duration	Unconfined compression	$E_{eq} = 4.3$ kPa	5.4 kPa	Chou et al. 2009 (Chou, Akintoye et al. 2009)
IVD	AF and NP cells (ovine)	PGA (AF) and Alginate (NP) (Figure 3F)	Successfully formed AF-NP composites with extracellular matrix accumulation and increased compressive properties after subcutaneous implantation	Unconfined compression	$H_A = 50$ kPa $k = 5$ (x10^{-14}m^2/Pa s)	3 – 10 MPa	Mizuno et al. 2004 (Mizuno, Roy et al. 2004), 2006 (Mizuno, Roy et al. 2006)
	MSCs (human)	Electrospun PLLA (AF) and hyaluronic acid (NP) (Figure 3G)	Human MSCs adopted AF and NP like phenotypes and accumulated disc-like extracellular matrix	N/A	N/A	N/A	Nesti et al. 2008 (Nesti, Li et al. 2008)

Table 2.2. Summary of recent advances in functional tissue engineering of the AF, NP, and intervertebral disc.

2.4.3 Tissue engineering of the intervertebral disc

While many groups have sought to engineer replacements for either the NP or AF, replacement of only one or the other may prove insufficient for cases beyond mild degeneration when both tissues are compromised. However, few groups have focused on engineering an entire intervertebral disc. The union of two tissues as disparate as the fibrous AF and gelatinous NP poses formidable challenges in tissue engineering, and will likely require a combination of biomaterials, cell types, and chemical and mechanical factors. Additionally, diffusion limitations in free swelling culture may preclude the growth and vitality of cells within large, dense tissues. This is problematic for engineering discs that have the appropriate geometries for implantation both clinically and in translational studies using large animal models.

Despite these challenges, in an elegant recent study, a full disc was formed by seeding NP and AF cells into a composite formed from a central alginate gel surrounded by a fibrous PGA mesh (Figure 2.3E) (Mizuno, Roy et al. 2006). To address diffusion limitations associated with *in vitro* free swelling culture, engineered discs were implanted subcutaneously in athymic mice. Cells within the construct proliferated and deposited extracellular matrix. Most notably, extracellular matrix deposition resulted in measurable changes in mechanical function: compressive equilibrium modulus increased by nearly four-fold over 16 weeks while hydraulic permeability decreased. However, the magnitude of equilibrium modulus obtained in this work (~kPa) remained below the axial compressive modulus of the motion segment (~MPa) and the engineered AF

region within the construct lacked the angle-ply organization of native AF. Nonetheless, this work represents a landmark achievement in disc tissue engineering. Further, it emphasizes the importance of functional metrics - and not simply histologic or biochemical assessment - as indicators of success.

Another recent study coupled hyaluronic acid (HA) hydrogels with electrospun nanofibrous scaffolds to form engineered discs seeded with human mesenchymal stem cells (MSCs) (Nesti, Li et al. 2008). MSCs were encapsulated in HA and injected into the center of nonaligned nanofibrous meshes that had also been seeded with MSCs. This method produced distinct NP and AF zones (Figure 2.3F). Cells residing within these regions appropriately achieved chondrogenic and fibrous phenotypes, respectively. Nonetheless, mechanical function was not assessed and the microstructural details of native AF organization were not achieved. However, this work demonstrates the ability to generate disc-like tissue from MSCs obtained from human donors, representing an important clinical advancement of the field.

2.4.4 Other regenerative approaches

It is important to note that tissue engineering is not the only treatment for disc disease that is being actively researched. Although disc allografts have had moderate success in canine and nonhuman primate models (Matsuzaki, Wakabayashi et al. 1996; Luk, Ruan et al. 2003), availability of healthy human disc tissue is very limited. Moreover, differences in mechanics, composition, geometry, and immunoreactivity preclude interspecies allografts from being a

viable alternative (Sakai, Mochida et al. 2003; Crevensten, Walsh et al. 2004). While MSC delivery by bolus injection has reduced degenerative changes such as GAG depletion and loss of disc-height, these studies are typically carried out in animal models where degeneration (which normally progresses pathologically over several years) is emulated rather abruptly by injury, injection of some agent, or mechanical stimulation (Boxberger, Sen et al. 2006; Hoogendoorn, Wuisman et al. 2007; Imai, Okuma et al. 2007; Elliott, Yerramalli et al. 2008; Hsieh, Hwang et al. 2009; Wuertz, Godburn et al. 2009). Injection of growth factors and anabolic agents into the disc has also been considered, with promising results observed for molecules such as OP-1 and BMP-2 (Masuda, Takegami et al. 2003; Li, Yoon et al. 2004; Masuda, Imai et al. 2006). Alternatively, some groups have sought to revive cells within the ailing disc via gene therapy. This is a promising approach, that could potentially induce disc cells to generate protective or anabolic signals themselves, eliminating the need for repeated injections of growth factors or other therapeutics (Nishida, Kang et al. 1998).

These minimally invasive, injection-based therapies - be they cells, proteins, or gene therapy - will likely be most effective when implemented early in degeneration, before structural breakdown of the AF has occurred. However, because discogenic low back pain develops quite late during the degenerative process, these therapies might not be a substitute for structural tissue engineered replacements. However, it is possible that the success of tissue engineering treatments may require commingling with one or a combination of these other regenerative techniques.

2.5 Conclusions

The intervertebral disc is a particularly illustrative example of the intimate relationship between form and function. The highly ordered disc is uniquely organized to resist the complex, multi-directional loads endured during normal physiologic movements of the spine. Because of this correlation of form with function, engineering tissues that behave mechanically like the native disc will likely require replication of anatomic form. This defines a challenge that has thus far been unaddressed in tissue engineering of the disc: how can cells be instructed to form a specialized extracellular matrix that possesses a high degree of organization spanning multiple length scales? Motivated by this concept, the work presented in this thesis is aimed at replicating anatomic form at scales spanning from sub-lamellar alignment of collagen to the formation of angle-ply laminates, and ultimately to the incorporation of such laminates into whole-disc constructs that possess both an NP and AF.

CHAPTER 3: MECHANICS OF ORIENTED, ELECTROSPUN NANOFIBROUS SCAFFOLDS FOR ANNULUS FIBROSUS TISSUE ENGINEERING

3.1 Introduction

Fiber reinforced musculoskeletal tissues, such as the annulus fibrosus (AF) of the intervertebral disc (IVD), tendons, ligaments, and the knee meniscus, rely on highly organized collagen fibers embedded in a hydrated, proteoglycan-rich matrix to bear large multi-axial loads *in vivo*. The AF is a laminated fibrocartilagenous ring forming concentric layers around a gelatinous core, the nucleus pulposus (NP). Each layer of the AF possesses an oriented collagen architecture (Hickey and Hukins 1980), with adjacent lamellae alternating in fiber angles from ± 28^{o} (outer AF) to 44^{o} (inner AF) with respect to the transverse axis of the spine (Cassidy, Hiltner et al. 1989; Marchand and Ahmed 1990). These unique structural characteristics of the AF enable its function in the context of the large and multi-axial physiologic loads. Type I collagen accounts for nearly 70% of the dry weight of outer AF, with type II collagen increasing from outer to inner AF (Eyre 1979; Oegema 1993). The oriented collagen fibers of the AF are embedded in a proteoglycan rich matrix. The cells of the IVD exist as a continuum of phenotypes, ranging from chondrocyte-like in the NP to fibrochondrocyte-like and fibroblastic in the inner and outer AF (Chelberg, Banks et al. 1995; Bruehlmann, Rattner et al. 2002; Johnson and Roberts 2003).

The architecture and composition of the AF results in a complex mechanical behavior that is nonlinear, anisotropic (direction dependent), and viscoelastic (rate dependent). AF mechanical behavior has been widely characterized in uniaxial tension (Acaroglu, Iatridis et al. 1995; Ebara, Iatridis et al. 1996; Elliott and Setton 2000; Elliott and Setton 2001), and to a lesser extent in compression, shear and biaxial loading (Iatridis, Kumar et al. 1999; Bass, Ashford et al. 2004; Bruehlmann, Hulme et al. 2004; Perie, Korda et al. 2005) (see Chapter 2). Guerin and Elliott (Guerin and Elliott 2006) measured a 60-fold increase in Young's modulus from the radial (0.4 MPa) to the circumferential direction (26 MPa), demonstrating the considerable anisotropy of the AF. Tensile properties of a single lamella of the AF have also been measured (Skaggs, Weidenbaum et al. 1994; Holzapfel, Schulze-Bauer et al. 2005). In these studies, lamellar modulus varied with radial and circumferential position, ranging from 59 MPa (inner AF) to 130 MPa (outer AF) in the fiber direction. Hyperelastic constitutive models have been widely used to study the structure-function relationship of the AF in tension (Wu and Yao 1976; Eberline, Holzapfel et al. 2001; Wagner and Lotz 2004; Guerin and Elliott 2006). Such models are useful in understanding the mechanical effects of disc degeneration and the design criteria for creating tissue engineered analogues to the AF.

Disc degeneration cascades from an unknown origin, in which the soft, hydrated nucleus pulposus progressivey becomes stiffer and more fibrous. Concomitant with this transformation in the nucleus pulposus, structural organization and biochemical composition of the AF are compromised, coincident

with mechanical degradation (Marchand and Ahmed 1990) . The sequelae of these alterations include tears and fissures of the AF, along with disc height loss, herniation, low back pain, and spinal stenosis. No treatment is available to restore the degenerated AF or nucleus pulposus. Current surgical treatments, such as discectomy, fusion, and total disc arthroplasty may alleviate pain, but fail to restore the function to the disc and may lack long term efficacy. There is a recognized need for an engineered replacement tissue for degenerate AF to both assuage low back pain and restore disc function (Richardson, Mobasheri et al. 2007).

A number of AF tissue engineering strategies have emerged over the last decade. In most cases, cells have been seeded in a three-dimensional tissue engineering scaffold or hydrogel and their ability to reconstitute the histological structure and composition of native tissue examined (Chiba, Andersson et al. 1997; Baer, Wang et al. 2001; Wang, Baer et al. 2001; Gruber, Hoelscher et al. 2006). Scaffolds have included alginate and agarose hydrogels, collagen gels, collagen/glycosaminoglycan gels, collagen/hyaluronic acid scaffolds and collagen sponges (Horner, Roberts et al. 2002; Alini, Li et al. 2003; Sato, Kikuchi et al. 2003; Saad and Spector 2004). Some studies have applied mechanical preconditioning (deformation and/or hydrostatic pressure) to modulate AF biosynthetic activities in 3D culture (Gokorsch, Weber et al. 2005). These and other studies have established that AF cells can be maintained in 3D culture, that they produce plentiful extracellular matrix with time, and that certain mechanical, biologic and structural cues, such as porous/fibrous scaffolds, may foster construct maturation (Gruber, Leslie et al. 2004). While these studies have

demonstrated the potential to generate AF-like neo-tissue, only a few recent studies have considered the *functional* mechanical properties of engineered constructs (Mizuno, Roy et al. 2006), and none have achieved native tissue organization or properties.

In this study, we propose a new paradigm for AF tissue engineering that focuses on the functional mechanical properties of the AF through reconstitution of the anatomic fiber architecture of the native AF tissue. This aim is realized via electrospinning, a scaffold fabrication technology increasingly employed in musculoskeletal tissue engineering (Li, Mauck et al. 2005; Mauck, Baker et al. 2009). We and others have recently shown that by depositing electrospun nanofibers onto a rotating mandrel, one can dictate fiber alignment, as well as structural and mechanical anisotropy of these scaffolds (Courtney, Sacks et al. 2006; Li, Mauck et al. 2006). As a first step toward engineering of the IVD, we focus on reproducing the primary functional unit of the AF, the single fiber-aligned lamella (Holzapfel, Schulze-Bauer et al. 2005). As such, the objectives of this study were as follows: (1) mechanically evaluate aligned electrospun scaffolds in a manner that highlights physiologic and anatomic details of the native AF, (2) using a constitutive model previously used to describe AF behavior (Yin and Elliott 2005), predict the anisotropic tensile mechanics of electrospun scaffolds in order to the identify key design criteria for AF tissue engineering, and (3) use this model to quantitatively describe time dependent deposition of functional extracellular matrix on AF cell-seeded scaffolds.

3.2 Materials and Methods

3.2.1 Electrospinning biodegradable nanofibrous scaffolds

Nanofibrous polymer scaffolds were formed through the process of electrospinning as described previously (Li, Cooper et al. 2006; Li, Mauck et al. 2006). Briefly, 2 grams poly-(ε-caprolactone) (PCL) was dissolved in 7 mL each of tetrahydrofuran and N, N-dimethylformamide. After vortexing for 48 hours to dissolve the PCL, the solution was loaded into a 10 mL syringe attached to an 18 gauge stainless steel needle. The needle was positioned 20 cm above a grounded aluminum shaft (1" diameter) attached to an AC motor, with rotation speed regulated by rheostat. Using a high voltage generator, the needle was charged to 12kV, initiating a polymer nanofibrous jet. To generate fiber alignment, the grounded shaft was rotated at 7,500 rpm (~10 m/s) while polymer fibers collected on the grounded surface, creating alignment along the tangential direction of the shaft (Li, Mauck et al. 2007). Nanofiber production over 12-14 hours resulted in a fibrous sheet ~1 mm in thickness. After formation, scaffolds were stored in a vacuum desiccator until use. As we have shown previously (Li, Mauck et al. 2006), and confirm here via SEM (Figure 3.1, 3.2 inset), this fabrication process results in nanometer-scale fiber diameters (ranging from 300 to 750 nm) with a high degree of fiber alignment. To create samples with discrete fiber orientations, rectangular samples (5 mm × 30 mm) were excised from the nanofibrous sheet with the long axis of the sample rotated by an angle, φ, with respect to the prevailing fiber direction (Figure 3.2, inset).

3.2.2 Uniaxial tensile testing of electrospun scaffolds and AF cell-seeded scaffolds

Characterization of acellular scaffold mechanics was carried out for the following fiber angle groups: $\varphi = 0^{o}$ (n = 17), 15^{o}, (n = 12), 30^{o} (n = 14), 45^{o} (n = 9), and 90^{o} (n = 17). Samples were culled from four electrospun sheets to account for batch-to-batch variability. Prior to mechanical testing, scaffold thickness was determined from calibrated images using a Leica MZ6 dissecting microscope, and measured using ImageJ. Specimen gage length and width were determined by digital caliper. Testing in uniaxial tension was performed using an Instron 5542. All samples were placed into customized grips and hydrated in a phosphate buffered saline (PBS) bath during the following testing protocol: (1) a nominal tare load of 0.1N was applied at a strain rate of 0.1% strain/sec, and held constant for 5 minutes (2) 15 preconditioning cycles to 0.1% strain were applied at a rate of 0.05% strain/sec, and (3) a quasi-static constant elongation was applied until failure, at a rate of 0.1% strain/sec. Tensile modulus was calculated by fitting a linear regression to the linear region of the stress-strain plot for each sample.

3.2.3 Homogenization modeling of acellular scaffold mechanics

An established two-dimensional homogenization model for linear elastic fiber-reinforced soft tissues (Yin and Elliott 2005) was adapted to characterize the mechanical behavior of fiber aligned scaffolds. Briefly, homogenization is a

method by which composite materials are characterized by mathematically averaging the heterogeneous material properties of the constituents while incorporating their special organization as well. The present model consisted of a 'fiber' component embedded in a 'matrix' (see Yin and Elliott for details). It is assumed that these constituents are themselves isotropic, but their anisotropic microstructural arrangement results in macroscopic mechanical anisotropy. Therefore, such a model allows for the determination of a homogenized (e.g. averaged) elasticity tensor, **C**, and thereby the homogenized composite modulus, using five inputs: fiber volume fraction (ρ), matrix modulus (E_m), matrix Poisson's ratio (v_m), fiber modulus (E_f), and fiber Poisson's ratio (v_f). A detailed explanation of the homogenization theory, formulation, and implementation is provided in Yin and Elliott (Yin and Elliott 2005); the resulting nonzero components of the homogenized elasticity tensor are given below:

$$C_{1111} = \frac{\rho E_f}{1-\upsilon_f^2} + \frac{(1-\rho)E_m}{1-\upsilon_m^2} - \frac{\rho E_f \upsilon_f^2}{1-\upsilon_f^2} - \frac{(1-\rho)E_m \upsilon_m^2}{1-\upsilon_m^2} + \frac{(\rho\upsilon_f + (1-\rho)\upsilon_m)^2 E_m E_f}{\rho E_m(1-\upsilon_f^2) + (1-\rho)(1-\upsilon_m^2)E_f}$$

$$C_{1122} = \frac{(\rho\upsilon_f + (1-\rho)\upsilon_m)E_m E_f}{\rho E_m(1-\upsilon_f^2) + (1-\rho)(1-\upsilon_m^2)E_f}$$

$$C_{2222} = \frac{E_m E_f}{\rho E_m(1-\upsilon_f^2) + (1-\rho)(1-\upsilon_m^2)E_f}$$

$$C_{1212} = \frac{1}{2}\frac{E_m E_f}{\rho E_m(1+\upsilon_f) + (1-\rho)(1+\upsilon_m)E_f}.$$

By applying a rigid rotation (φ) to **C**, the elasticity tensor can be determined for any fiber angle with respect to the direction of applied load. Finally, the average composite material properties (E, v) are determined by inverting **C**. The model

was used to predict the composite modulus as a function of fiber orientation, $E(\varphi)$, for φ ranging from 0^o - 90^o.

Input properties were applied as follows: Tan, et. al., measured the tensile modulus of a single electrospun PCL fiber as 120 MPa; this was used as the input value for the parameter E_f (Tan, Ng et al. 2005); PCL was assumed incompressible (v_f = 0.49). Preliminary parametric analyses showed little dependence of the computed $E(\varphi)$ on v_m, and so v_m = 0.25 was chosen. ρ and E_m were reserved as free parameters, determined by least squares fit to measured E data as a function of fiber orientation φ. For acellular scaffolds, the model 'matrix' terms refer to frictional interactions, connectivity of fibers, and void space within the scaffold (discussed below). Parametric analyses were performed based on variations of the following baseline properties: E_f = 120 MPa, v_f = 0.49, E_m = 1.0 MPa, v_m = 0.25, and ρ = 0.15. In order to compare cell-seeded constructs to native tissue, the model was used to generate $E(\varphi)$ for a single lamella from the native outer and inner AF. Parameter values for AF tissue were taken from Yin and Elliott (Yin and Elliott 2005): E_f = 500 MPa, v_f = 0.35, E_m = 0.8 MPa, v_m = 0.45, ρ_{IA} = 0.05, and ρ_{OA} = 0.23, where ρ_{IA} and ρ_{OA} are the inner and outer AF fiber volume fractions.

3.2.4 Isolation of bovine AF cells

To assess the ability to grow functional AF-like tissue on oriented fiber aligned scaffolds, AF cells were isolated from skeletally mature bovine caudal discs within 12 hours of slaughter. After gross dissection to remove musculature

and ligaments from the tail, IVDs were dissected free of surrounding vertebral bodies. AF tissue was separated from the NP, and diced under sterile conditions. AF pieces were then transferred to tissue culture treated polystyrene, and incubated in basal culture media consisting of DMEM, 10% fetal bovine serum, and 1% PSF. After two weeks, cells that had migrated from the tissue were trypsinized and replated, expanding to passage 2.

3.2.5 Seeding and culture of AF cells on electrospun nanofibrous scaffolds

Fiber aligned scaffolds ($\varphi = 0^o, 30^o, 90^o$) were sterilized for 1 hour in 100% ethanol, and rehydrated through a series of decreasing concentration ethanol washes(70%, 50%, 30%, PBS, PBS) of 1 hour each, and incubated overnight at room temperature in 20 μg/mL fibronectin. After washing in PBS, 1×10^6 AF cells were seeded onto each scaffold in four 30 min applications (two 50μL applications per side). Cell seeded scaffolds were cultured in 3 mL of a chemically defined medium in non-tissue culture treated 6 well plates for up to 4 weeks. Chemically defined growth media consisted of DMEM, 0.1μM dexamethasone, 40 μg/mL L-Proline, 100 μg/mL Sodium Pyruvate, 1% ITS/Premix, and 1% PSF supplemented with 10 ng/mL Transforming Growth Factor β-3 (Mauck, Yuan et al. 2006). At 1 day, 2 weeks, and 4 weeks samples were harvested for mechanical testing as described above, followed by biochemical analyses (below, $n = 5$ per group). Additional samples were fixed in 4% paraformaldehyde, dried, sputter-coated with AuPd, and imaged with a JEOL 6400 SEM at an accelerating voltage of 10kV and magnifications ranging from

100×-2500×. SEM was performed at day 3 to visualize cell borders prior to their obfuscation by cell confluence and newly deposited extracellular matrix, which occurs by 1 week.

3.2.6 Biochemical Analyses

To determine matrix production and cellularity of cell seeded scaffolds, assays were performed to determine sulfated glycosaminoglycan (GAG), total collagen, and DNA content as described previously (Mauck, Yuan et al. 2006). Briefly, mechanical test samples were digested for 16 hours in papain at 60^{o}C. Aliquots of digest were analyzed for GAG content using the 1,9-dimethylmethylene blue dye-binding assay, for DNA content using the PicoGreen dsDNA Quantification kit, and for orthohydroxyproline (OHP) content (after acid hydrolysis) by reaction with chloramine T and dimethylaminobenzaldehyde. OHP was converted to collagen content using a 1:10 ratio of OHP:collagen.

3.2.7 Statistics

Statistical analysis was carried out using Systat Software with one or two-way ANOVA for independent variables time and/or fiber angle and dependent variables modulus, DNA, GAG, and collagen contents. A Fisher's post hoc comparison was used to establish significance ($p < 0.05$).

3.3 Results

Uniaxial tensile testing revealed anisotropic and nonlinear mechanical behaviors for samples tested in the fiber ($\varphi = 0^o$) and transverse to the fiber ($\varphi = 90^o$) directions (Fig 3.1), similar to fiber-reinforced soft tissues like the AF (Chapter 2). For $\varphi = 0^o$, a nonlinear elastic domain was observed up to approximately 20-30% strain, followed by failure. Conversely, samples loaded at $\varphi = 90^o$ demonstrated a small linear elastic region followed by a clear transition to plastic deformation, which for many samples continued up to 100% strain, but at stresses an order of magnitude lower than that of $\varphi = 0^o$ samples (Fig 3.1, inset). We next determined how the modulus of electrospun scaffolds varied with specific deviations from the predominant fiber direction. Tensile testing revealed a nonlinear decrease in modulus with increasing fiber angle (Fig 3.2). Modulus declined significantly between $\varphi = 15^o$ and $\varphi = 30^o$ ($p < 0.05$), with little additional decrease up to $\varphi = 90^o$.

The homogenization model was fit to these experimental results to determine the values of ρ and E_m that would best recreate the dependence of modulus on fiber angle (Figure 3.2) by a least squares fit. The fit was optimized to within one standard deviation of each data point ($R^2 = 0.98$), yielding $\rho = 0.157$, and $E_m = 0.58$ MPa (Figure 3.2). A parametric study was next performed within a physiologically relevant range of parameters. Computed modulus, $E(\varphi)$, showed little sensitivity to changes in Poisson's ratio of the fibers or matrix (Figure 3.3A, B). This has two implications for our model formulation: (1) the assumption of material incompressibility ($v_f = 0.49$) did not affect the model

results and (2) the chosen matrix Poisson's ratio (v_m = 0.25) also had little bearing on computed modulus. E(φ) was strongly dependent upon E_m (Figure

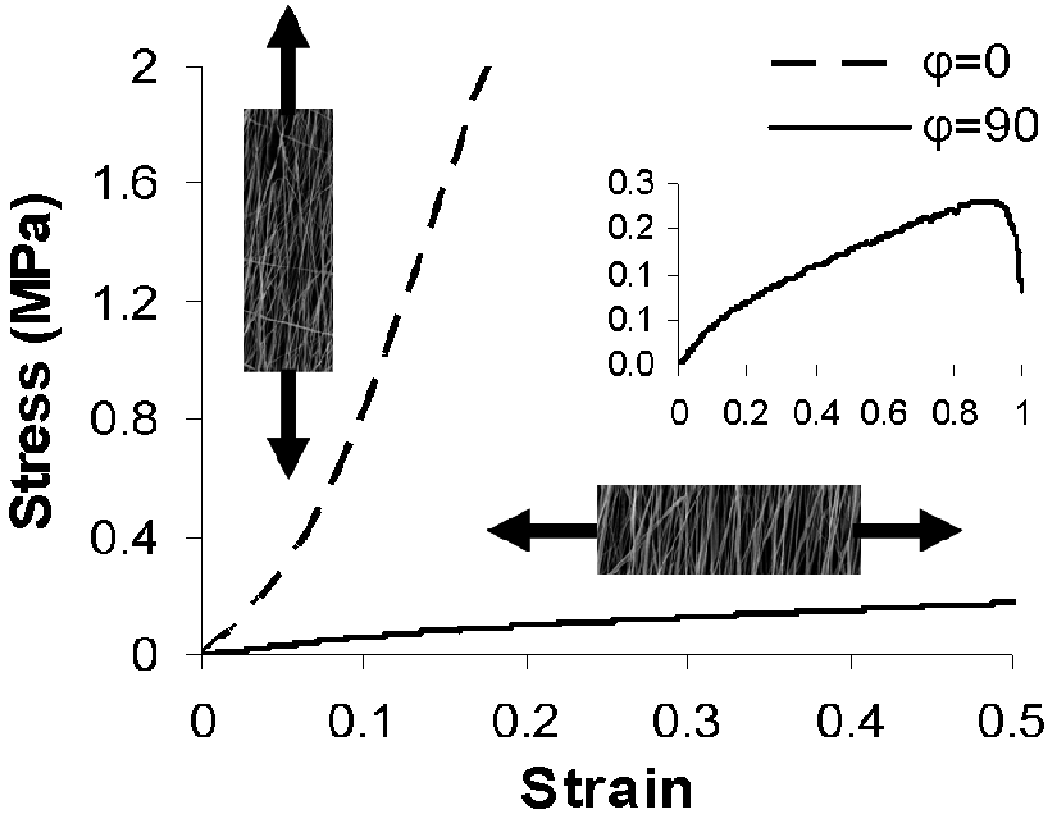

Figure 3.1 Mechanics of acellular nanofibrous scaffolds. Sample stress-strain plot for aligned electrospun PCL scaffolds tested in the fiber direction (φ = 0°) and transverse to the fiber direction (φ = 90°). Scaffolds exhibit distinct fiber orientation dependent qualitative and quantitative mechanical behaviors. At φ = 0° the material exhibits a nonlinear elastic deformation for moderate to large strains, while at φ = 90° a small linear elastic region precedes a large region of plastic deformation (inset).

3.3C) for all φ (particularly above φ = 15°). In contrast, changing fiber properties E_f and ρ affected E(φ) only at small φ (Fig 3.3D,E insets), with all curves converging near φ = 40° (Figure 3.3D, E). Having established the ability to effectively model the mechanical behavior of scaffolds, we next determined their capacity for fostering AF cell proliferation and synthesis of extracellular matrix compositionally similar to native AF. Scaffolds with prescribed fiber angles (φ =

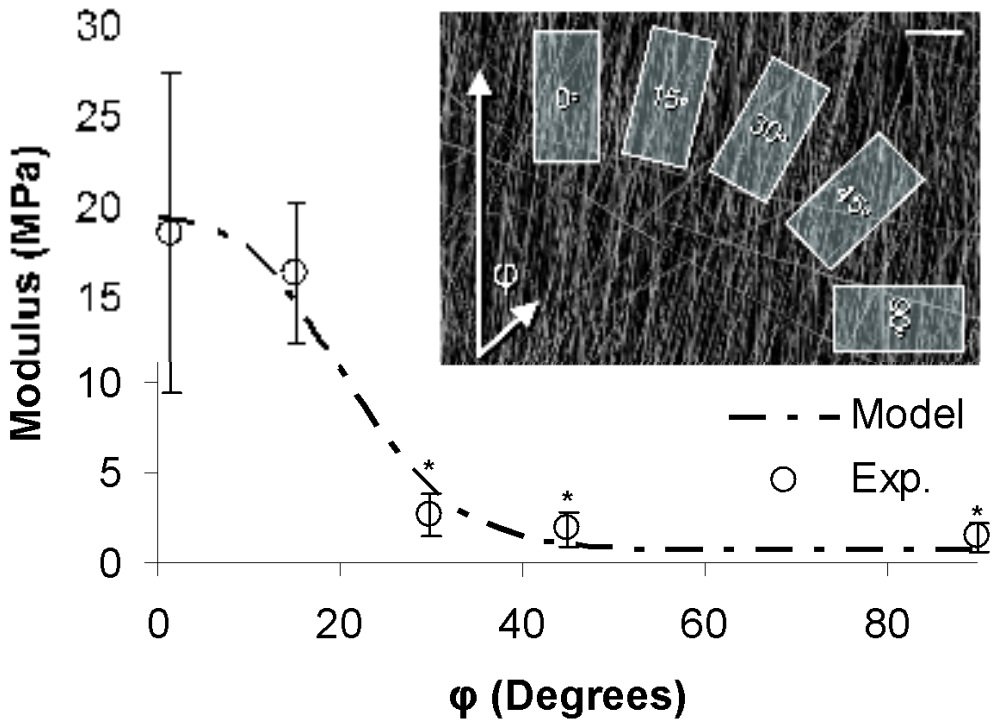

Figure 3.2. Experimental results and homogenization model predictions for the dependence of scaffold modulus on φ. Tensile testing revealed nonlinear loss of modulus with increasing φ. Homogenization model predicted modulus as a function of fiber angle to within one standard deviation at each data point. Inset: schematic showing how fiber orientations were prescribed in rectangular test samples by rotating from the direction of nanofiber alignment, scale: 25 μm. * = p<0.05 compared to φ = 0°.

0°, 30°, 90°) were seeded with AF cells and cultured up to 4 weeks. Mechanical testing revealed no significant changes with time at either φ = 0° or φ = 90° (Fig 3.4A). The modulus at φ = 30°, however, doubled over four weeks of culture, reaching 5.8 ± 3.1 MPa ($p < 0.05$ vs. day 1). As early as 3 days in culture, adherent cells were found colonizing the surface of the scaffold (Fig 3.4B). Importantly, the underlying fiber alignment dictated AF cell morphology, with elongated cells extending processes along the predominant fiber direction. DNA content increased initially for each fiber orientation ($p < 0.05$), stabilizing by 4

weeks (Figure 3.4C). GAG and collagen content increased with time in culture ($p < 0.05$, Fig. 3.4 D,E). Notably, no differences between fiber angle groups were observed for DNA ($p = 0.3$), GAG ($p = 0.5$), or collagen ($p = 0.4$).

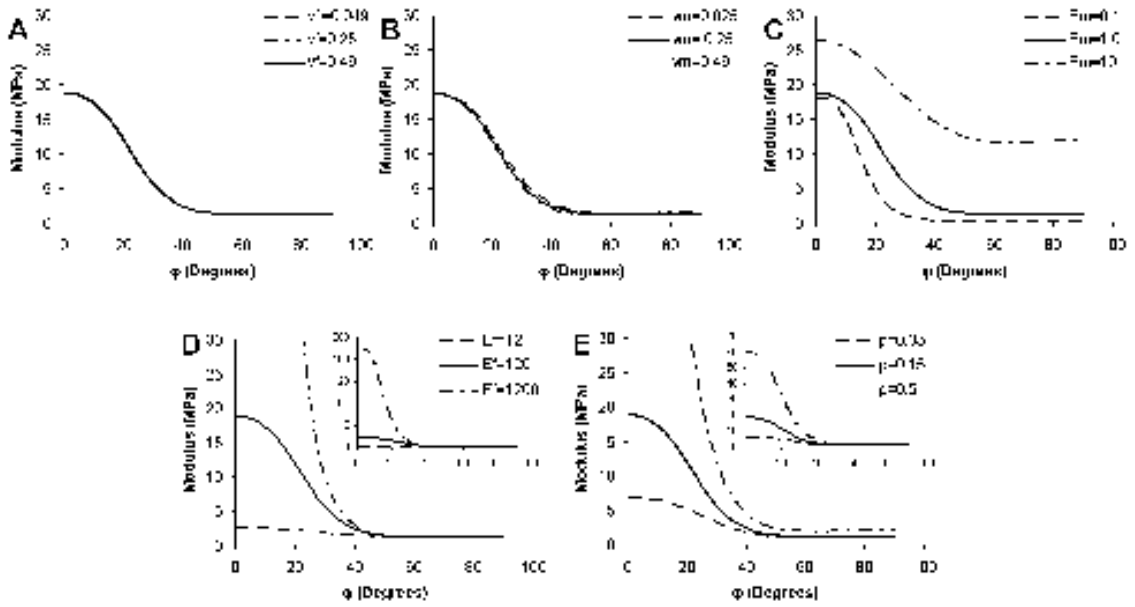

Figure 3.3 Parametric study for the homogenization model of PCL scaffolds reveals little dependence of E(φ) on v_f (A) and vm (B). Variations in E_m (C) greatly affect E(φ), particularly between φ = 25^o and φ = 45^o. Ef (D) and ρ (E) strongly influence E(φ) at low φ (insets), but the curves converge as E(φ) decays for larger φ. Baseline properties used in the analysis are: E_f = 120 MPa, v_f = 0.49, E_m = 1.0 MPa, v_m = 0.25, and ρ = 0.15.

The homogenization model was applied to uniaxial test data (Figure 3.4A) to provide a quantitative measure of functional matrix deposition by AF cells over time in culture. For day 1 data, the homogenization model was used to generate an E(φ) that matched the full dataset (φ = 0^o, 30 ^{o}, 90 ^{o}), creating a plot similar to the one shown for acellular scaffolds in Figure 3.2. As above, the least squares fitting of E(φ) to the experimental dataset resulted in an estimate for E_m and ρ that was similar at 1 day to that obtained for acellular scaffolds. This was

repeated for the full datasets at 2 weeks, and again at 4 weeks. E_m and ρ values determined for each time point revealed a 3.5-fold increase (from 0.4 to 1.4 MPa) in E_m over four weeks (Fig 3.5A), while ρ decreased only slightly (Figure 3.5B). Finally, the model was used to compare the engineered AF construct to single lamellae of the native inner and outer AF. The resulting E(φ) for the cell-seeded construct and single lamellae of native inner and outer AF are shown in Figure 3.5C (inset). Although the three tissues have disparate moduli at low φ, in the range of anatomic relevance (28^o – 44^o) the three curves were similar in shape and magnitude (Figure 3.5C).

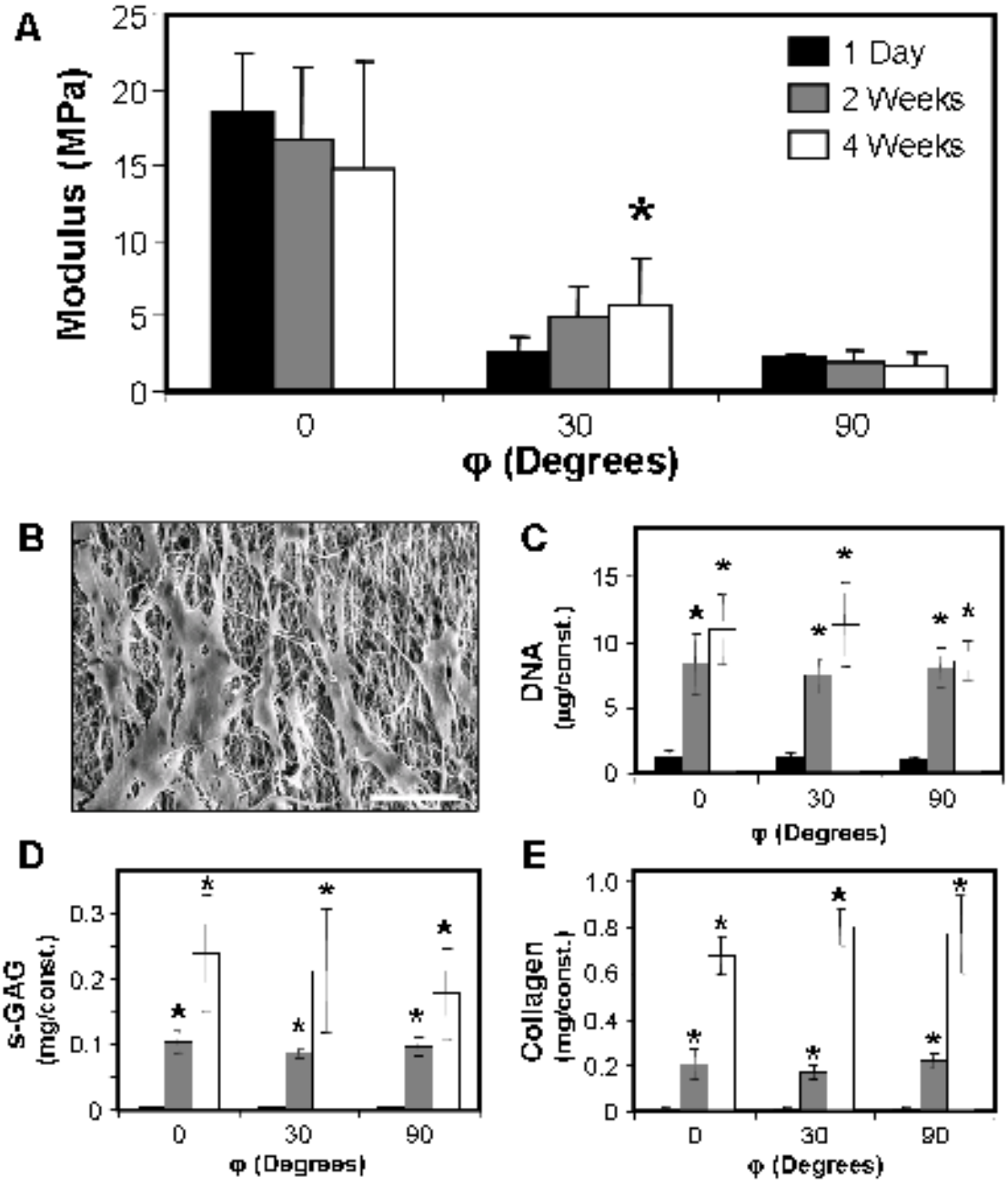

Figure 3.4 AF cells proliferate and secrete extracellular matrix proteins when seeded on oriented electrospun scaffolds, improving properties of oblique 30^o constructs. A) Tensile testing revealed that cell seeded construct increased in modulus for φ = 30^o, doubling in value by 4 weeks; modulus did not change significantly for φ = 0^o or φ = 90^o. B) SEM of AF cell seeded scaffolds at 3 days of culture demonstrates the alignment of cells along the predominant fiber direction. Scale = 100 µm. C) DNA content increased initially and then plateaued by 4 weeks. GAG (D) and

collagen (E) increased over 4 weeks of culture. * = p < 0.05 compared to day 1.

3.4 Discussion

In the engineering of fiber-reinforced orthopaedic soft tissues, special consideration must be made of the unique architectural features that underlie and dictate the mechanical behavior of the native tissue. A challenge particular to the native AF is that the direction of maximum applied stress is not parallel to the predominant fiber direction of the tissue. This distinction motivated our approach to AF tissue engineering using fiber-aligned nanofibrous scaffolds. In this study, we demonstrate that such scaffolds mimic both the anisotropy and nonlinearity of the basic functional unit of the AF, the single fiber-aligned lamella. Further, we demonstrated that orienting fiber-aligned scaffolds with respect to the prevailing fiber direction generates vastly different mechanical behaviors, and demonstrated the ability to predict this phenomenon with a model previously applied to native AF tissue. Finally, we established that AF cells attach to these aligned nanofibrous scaffolds and deposit fibrocartilagenous extracellular matrix that contributes to the mechanical behavior of the construct under loading conditions relevant to the *in vivo* environment.

For acellular scaffolds excised at varying angles with respect to the prevailing fiber direction, modulus varied nonlinearly with fiber angle (Figure 3.2).

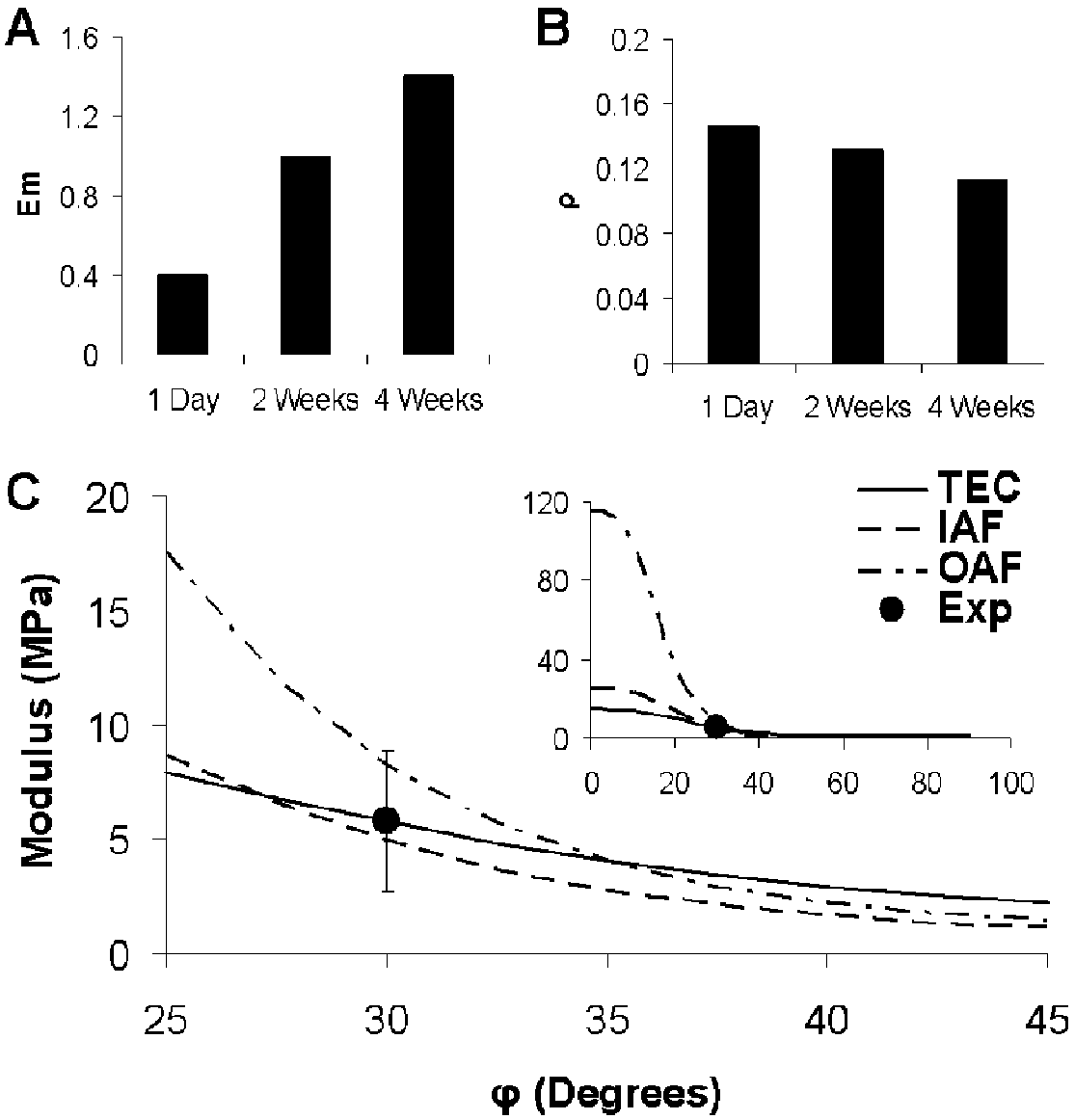

Figure 3.5 A) The homogenization model was fit to experimental E(φ) data for cell-seeded scaffolds at 1 day, 2 weeks, and 4 weeks, revealing an increase in matrix modulus (E_m) at each time point. B) Model predicted fiber volume fraction, ρ, decreased nominally with time in culture. C) The homogenization model was used to generate E(φ) for single lamellae of the native inner (IAF) and outer (OAF) annulus fibrosus, and compared to E(φ) as predicted by the model for AF cell-seeded tissue engineered constructs (TEC). Despite divergent behavior at small φ (inset), in the range of anatomic fiber angle (φ = 28° – 44°), AF construct modulus ranged between IAF and OAF. Exp = Experimentally measured modulus of cell seeded construct at 4 weeks in culture.

The sharp drop from $\varphi = 15^o$ to $\varphi = 30^o$ suggests that fibers pulled obliquely may slide past one another without rotating toward the loading direction or transmitting tensile load. This finding is supported by recent work by Li, et. al., where a simple structural model was used to illustrate the effects of fiber scatter on scaffold properties (Li, Mauck et al. 2006). Sliding of collagen fibers has been observed in ligaments (Wood, Lester et al. 1998), and recent work by Bruehlmann, et. al., showed that flexion of bovine caudal discs results in sliding of collagen fibrils in the AF (Bruehlmann, Matyas et al. 2004). This sliding may contribute to material nonlinearity in both aligned electrospun scaffolds and the native AF.

The mechanical response of scaffolds was successfully modeled using a fiber-reinforced homogenization model originally developed to describe native AF behavior (Yin and Elliott 2005). The homogenization model captured the full nonlinearity of the modulus-fiber angle relationship, $E(\varphi)$. For acellular scaffolds, E_m lacks a physically straightforward meaning, due to the lack of a proper matrix; instead, E_m quantifies interfibrillar forces, such as frictional interactions between sliding fibers and interfibrillar connectivity. Despite this limitation, the model produced a strikingly accurate prediction for the scaffold fiber volume fraction: $\rho = 0.157$, compared to $\rho = 0.15$ as measured by Li, et. al., (Li, Mauck et al. 2006). Model predicted E_m (0.58 MPa) was also similar to E_m for the AF (0.4 MPa), determined by tensile testing AF in the radial direction (Guerin and Elliott 2006).

The sensitivity of model output to the parameters E_f, E_m, and ρ was strictly fiber angle dependent. Because for the AF, anatomic fiber angle ranges from $\varphi = 28^o$ to $\varphi = 44^o$, this range is of particular interest. For low φ, E_f and ρ altered the

magnitude of the predicted modulus, while in the anatomic range of φ neither parameter had a great effect (Figure 3.3D,E). Conversely, E_m altered E(φ) in the anatomic range (Figure 3.3C), suggesting that matrix modulus is a key parameter to be considered in AF tissue engineering. These results have explicit implications for scaffold design in orthopaedic tissue engineering applications. For instance, modulation of fiber density or modulus by polymer selection or changing fiber diameter (Tan, Ng et al. 2005; Li, Cooper et al. 2006) may be critical for tendon and ligament engineering, where the predominant fiber and loading directions coincide. For AF tissue engineering, however, emphasis should be placed on fiber-fiber interactions and extra-fibrillar matrix material. This is consistent with constitutive models of the AF that have illustrated that fiber-matrix interactions are essential to AF mechanical behavior (Elliott and Setton 2001; Wagner and Lotz 2004; Guerin and Elliott 2006). Using the same homogenization model for AF tissue, Yin and Elliott similarly concluded that matrix properties are important for multi-lamellar AF behavior (Yin and Elliott 2005).

In addition to producing a mechanical behavior similar to the native tissue, we also demonstrated that aligned nanofibrous scaffolds serve as a suitable substrate for AF cell proliferation and extracellular matrix production. The underlying scaffold geometry served as a 3D micro-pattern, directing AF cell alignment along the predominant fiber direction. During AF development, organized extracellular matrix forms after precursor cells have been organized into concentrically layered sheets with discrete cellular orientations above and below the transverse axis (Rufai, Benjamin et al. 1995; Hayes, Benjamin et al. 1999).

Development of the disc suggests that this AF cell orientation is an essential prerequisite to oriented extracellular matrix deposition. Instilling cell alignment in monolayer has been shown to direct oriented extracellular matrix deposition by fibroblasts and newly differentiated osteoblast-like cells (Wang, Jia et al. 2003; Zhu, Lu et al. 2005). The maturation of a tissue engineered AF construct that reproduces the anisotropy and nonlinearity of the native tissue, particularly after polymer degradation, may likewise depend on the provision of the appropriate 3D micropattern for directing matrix deposition.

AF cells colonized electrospun scaffolds and produced two major constituents of the AF, collagen and proteoglycan (GAG). While no change was observed in the fiber ($\varphi = 0^o$) or transverse ($\varphi = 90^o$) directions, modulus at $\varphi = 30^o$ doubled during the four week culture period, suggests that extracellular matrix production did have functional value for this anatomically relevant fiber architecture. Based on the results of the parametric study, it is likely that this orientation-dependent change is the result of altered matrix properties; e.g., moderate changes in E_m alters $E(\varphi)$ significantly within this anatomic range, but have a negligibile effects at $\varphi = 0^o$ or $\varphi = 90^o$ (Figure 3.3C). At 4 weeks, constructs tested at $\varphi = 30^o$ ($E = 5.8$ MPa) closely matched experimentally measured modulus of the native inner AF tested in the circumferential direction, $E = 5.6$ MPa (Elliott and Setton 2001). Interestingly, cell-laden constructs at each of the three fiber orientations were compositionally similar but yielded very different mechanical behaviors. Again, as indicated by the homogenization model, equivalent changes in composition can result in unexpected changes in mechanical behavior (Figure

3.3C), based on whether this newly deposited extracellular matrix contributes to changes the matrix or the fiber components. To quantify load transmission between fibers by cell-deposited matrix, the homogenization model was simultaneously fit to cell-seeded scaffold modulus data at each orientation ($\varphi = 0^o$, 30^o, 90^o) to generate the parameters E_m and ρ at each time point (1 day, 2 weeks, ad 4 weeks). The 3.5-fold increase in E_m with time suggests that extrafibrillar matrix deposition contributes to the mechanical response of these constructs. Thus the model provides quantitative parameters of functional matrix production that are not discernable from modulus data alone, or from biochemical composition. Specifically, the evolution of functional matrix and interfibrillar interactions can be extrapolated from uniaxial tensile testing data. Validation of the model provides a powerful tool as the same mathematical framework may now be applied to engineered AF neo-tissue and native AF tissue alike, highlighting key mechanical design criteria for AF tissue engineering.

The homogenization model demonstrated that fiber reinforced tissues such as native and engineered AF behave very differently when tested in the fiber direction compared to at oblique angles from the fiber direction. *In vivo* the AF is subject to large stresses oriented at an angle from the fiber direction. Thus an appropriate design criteria for AF tissue engineering is to match the native tensile modulus for loads applied obliquely with respect to the predominant fiber direction ($\varphi = 28^o - 45^o$). Using literature values for the input parameters of native AF (Yin and Elliott 2005), the homogenization model was used to predict $E(\varphi)$ for a single inner and outer AF lamella, and these results compared to $E(\varphi)$ for cell seeded

scaffolds at 4 weeks. Model predictions for native AF agreed with values reported in the literature for testing of single lamellae in the fiber direction (Skaggs, Weidenbaum et al. 1994; Holzapfel, Schulze-Bauer et al. 2005). At lower values of φ the engineered "AF" underperformed native inner and outer AF (Fig 3.5C, inset). However, at the anatomic fiber angles of the native AF, the engineered material behaved very much like the native tissue, suggesting that the tissue engineered construct closely replicates the physiologic mechanical behavior of the single AF lamella (Fig 3.5C).

3.5 Conclusion

In this study, we deployed aligned electrospun nanofibrous scaffolds for AF tissue engineering. We characterized the mechanical behavior of these scaffolds, and illustrated a strong dependence of material properties on fiber orientation. We also applied a constitutive model to characterize this orientation dependent behavior as a function of fiber and interfibrillar properties. The model demonstrated that extrafibrillar matrix and fiber-fiber interactions dictate both scaffold and neo-tissue behavior at fiber orientations observed in native AF. When these scaffolds were seeded with AF cells the scaffold instilled an *a priori* oriented micropattern, providing a template for anisotropic tissue growth. Long-term culture of these cell-laden scaffolds resulted in the accumulation of abundant proteoglycan and collagen, the two predominant structural elements of the intervertebral disc. Functionality of newly deposited matrix was confirmed by mechanical tests that

revealed a two-fold increase in modulus for constructs with anatomic fiber orientations. Although increasing moduli were not observed in the fiber direction, these data demonstrate the potential of time-dependent maturation of engineered AF constructs and suggest several routes by which this growth may be optimized, including extended culture durations. In the next chapter, longer culture durations will be considered to examine the role of GAG and collagen in the mechanical function of cell-seeded electrospun scaffolds.

The homogenization model demonstrated the evolution of key parameters with cell-seeded construct maturation, and demonstrated (by direct comparison to single lamella of inner and outer AF) that the engineered AF may recapitulate the physiologic mechanical behavior of the primary functional unit of the AF, the single lamella. These findings represent an important step in the engineering of AF tissue, and define key principles that may be extended to the engineering of other fiber-reinforced orthopaedic soft tissues, such as tendon, ligament, articular cartilage, and the meniscus of the knee. Because the homogenization model is linear while mechanical function of these materials is nonlinear, in the chapters that follow a hyperelastic model will be used to extend the characterization of scaffold and engineered tissue mechanics, such that the entire curve, and not just the slope of the linear region can be studied.

In the study presented here, 1 mm thick scaffolds were used due to the ease of handling. However, because the lamellar thickness of AF layers is ~250 μm, the studies that follow in subsequent chapters will be carried out with thinner scaffolds. This is beneficial, as in the present study cell infiltration and extracellular

matrix deposition were restricted to the periphery of the scaffold. Nonetheless, the present study provides an important foundation by characterizing the mechanical behaviors of aligned electrospun nanofibrous scaffolds formed from PCL. This understanding is essential for studies that will follow in chapters 4 – 8, where the purpose is to discern the functional contribution of cell mediated extracellular matrix deposition to the overall mechanics of cell-seeded scaffold constructs.

CHAPTER 4: SELECTIVE REMOVAL OF EXTRACELLULAR MATRIX COMPONENTS REVEALS HOMOLOGOUS STRUCTURE-FUNCTION RELATIONSHIPS BETWEEN ENGINEERED AND NATIVE FIBROCARTILAGES

4.1 Introduction

The overarching goal of tissue engineering is to develop ways in which cells can be coaxed into forming new tissues to replace damaged, diseased, or ailing ones. This task is quite challenging for the engineering of load-bearing soft tissues of the musculoskeletal system, however many groups have published on a wide array of promising strategies for engineering such tissues in recent years, with great advances made in tissues such as meniscus (Baker, Nathan et al. 2009; Ballyns, Cohen et al. 2009), tendon and ligament (Cooper, Sahota et al. 2007; Juncosa-Melvin, Matlin et al. 2007; Nirmalanandhan, Rao et al. 2007; Moffat, Kwei et al. 2009), cartilage (Mauck, Soltz et al. 2000; Moutos, Freed et al. 2007), and the particular tissue of interest in the present work, the annulus fibrosus of the intervertebral disc (Bowles, Williams et al. ; Mizuno, Roy et al. 2006; Shao and Hunter 2007). Typical outcome measures in such studies, including the results presented in Chapter 3, include compositional analyses to determine the amount of collagen and GAG present, organizational analyses to determine how these constituents are put together, and ultimately how the engineered tissues function mechanically with respect to their respective native

counterparts. While many testing modalities are available and germain to native tissue function (Chapter 2), the two most commonly used methods are uniaxial tension (Chapters 3 – 7) and unconfined compression (Chapter 8).

A number of load-bearing tissues exemplify the interrelation between these three traits: composition, structure, and function. For instance, it is conventionally thought that tissues subject to large tensile stresses, such as the annulus fibrosus, ligament and tendon, and the knee meniscus, contain a large proportion of collagen while tissues subject primarily to compressive loading such as the nucleus pulposus and articular cartilage, contain large amounts of GAG (Figure 4.1).

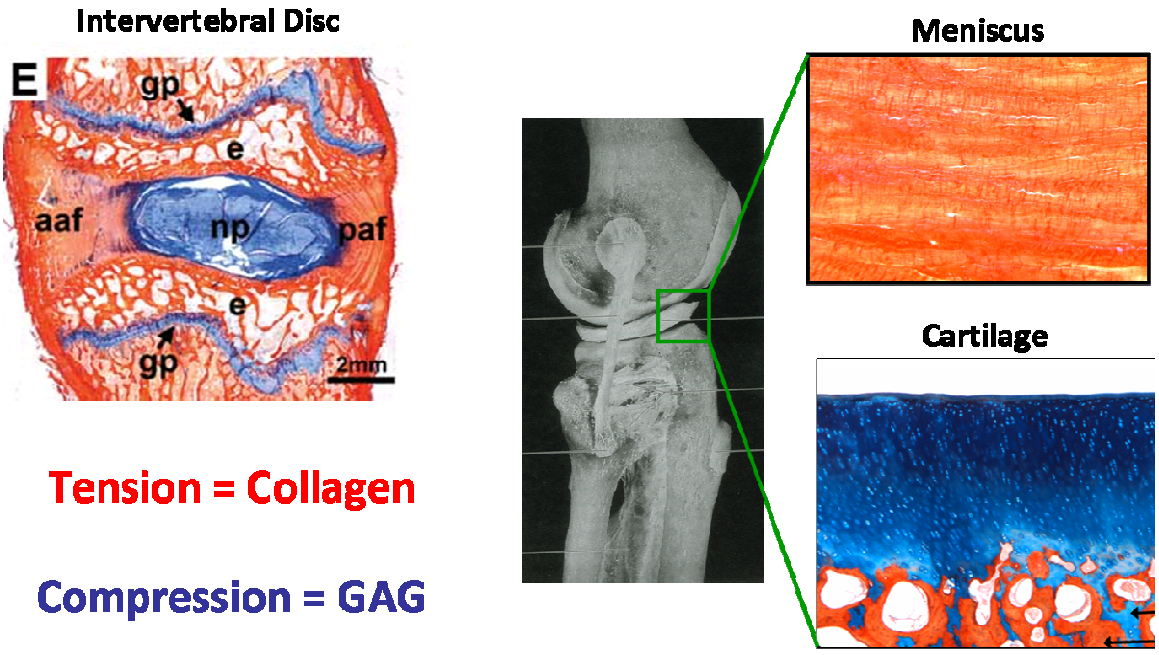

Figure 4.1 Tissue function is strongly related to tissue composition, as demonstrated by the intervertebral disc and its sub-strucures, the knee meniscus, and articular cartilage. In each histology section, collagen is stained (red) with Picrosirius Red and GAG is stained (blue) with Alician Blue (Buma, Ramrattan et al. 2004; Smith, Martin et al. 2009). Articular cartilage histology courtesy of Albert Gee.

To arrive at function from composition, it is necessary to consider structural organization. Fibrocartilages like the annulus fibrosus and knee meniscus are highly ordered structures, densely packed with collagen fibers that are highly aligned and in the case of the annulus fibrosus, hierarchical in nature. This combination of structure and composition results in complex mechanical behaviors including stress-strain nonlinearity, mechanical anisotropy, and finite elastic deformations (Chapter 2). We showed in the previous chapter that electrospun PCL scaffolds replicate each of these features qualitatively, and that they support cell attachment, elongation and alignment, and extracellular matrix deposition. Specifically cells deposited GAG and collagen. Concomitant with extracellular matrix deposition it was observed here and in related studies that mechanical properties improved (Chapter 3)(Baker and Mauck 2007). While clearly matrix deposition and mechanical properties are related in these engineered tissues, the nature of this relationship, and how it compares to native tissue, is unknown. Therefore the objective of this chapter is to determine the functional role of GAG and collagen in engineered fibrocartilage formed from aligned electrospun nanofibrous PCL scaffolds seeded with cells.

4.2 Materials and Methods

4.2.1 Scaffold fabrication

Nanofibrous PCL scaffolds were electrospun as described in Chapter 3, with some modifications. Briefly, 8 g poly(ε-caprolactone) (PCL, Sigma Aldritch, batch # 00702CE) was dissolved at 37^{o}C overnight in 56 mL of equal parts tetrahydrofuran and N, N-dimethylformamide. The PCL solution was ejected via syringe pump at 2.5 mL/h through a spinneret charged to +13 kV, generating a nanofibrous jet that was collected on a grounded mandrel rotating at 10 m/s at a distance of 20 cm from the spinneret tip. The spinneret was fanned axially along the mandrel to ensure uniform fiber deposition. Aluminum shields on either side of the spinneret were charged to +9 kV in order to focus the jet toward the mandrel, while the spinneret was fanned back and forth axially to ensure uniform deposition along the mandrel (Baker, Gee et al. 2008). Fibers were collected onto the mandrel for 6 to 8 hours, resulting in an aligned nanofibrous mesh of approximately 1 mm thickness. Rectangular samples (5 mm x 30 mm) were excised from the mesh with the long axis parallel to the prevailing fiber direction.

4.2.2 Isolation of bovine mesenchymal stem cells (MSCs)

MSCs were isolated from bone marrow obtained from juvenile (3 – 6 month old) bovine knee joints. Joints were first rinsed in soapy warm water, then soaked for five minutes in 70% ethanol to sterilize. Gross dissection was performed to remove surrounding musculature, skin, fat and other connective tissues, while keeping the synovial capsule intact for sterility. When sufficient tissue was removed, the synovial capsule was breached, exposing marrow. The saw was then used to cut away lateral cortical bone to further expose marrow

rich trabecular bone. Finally, marrow rich bone was cubed and collected into 50 mL conical tubes containing DMEM supplemented with 1X PSF and 2 mg/mL heparin. Tubes were capped and shaken to rinse marrow from trabecular space, and decanted into fresh tubes. Tubes were centrifuged to collect marrow, and resuspended in basal media containing DMEM with 10% FBS and 1% PSF. Marrow was then plated, and colony formation observed within 1-2 weeks. Bone debris were removed with subsequent media changes. Cells were filtered at first passage, and expanded to passage 2 as described in the previous chapter for AF cells.

4.2.3 Seeding and culture of Nanofibrous Scaffolds with MSCs

As in Chapter 3, scaffolds were hydrated by sequential washes in 100%, 70%, 50% and 30% ethanol and finally Phosphate Buffered Saline (PBS). Before seeding, scaffolds were incubated overnight in 20 µg/mL fibronectin, then rinsed with PBS. 50 µL of cell solution (1 x 10^7 cells/mL) were applied to one side, followed by incubation at 37^{o}C for one hour. Scaffolds were then turned and an additional 50 µL of cell solution applied to the other side. After two hours further incubation, samples were transferred to chemically defined media (DMEM, 0.1µM dexamethasone, 40 µg/mL L-Proline, 100 µg/mL Sodium Pyruvate, 1% Insulin, Transferrin, Selenium/Premix, and 1% penicillin, streptomycin and fungizone supplemented with 10 ng/mL Transforming Growth Factor β3) (Mauck, Yuan et al. 2006). Media was replaced twice weekly for the duration of the study. Additional acellular scaffolds were maintained in culture under identical

conditions but without cells in order to establish a functional baseline (see below).

4.2.3 Enzymatic digestion of matured fibrocartilage constructs

In order to assess the roles of GAG and collagen, enzymatic digestions were performed on MSC-seeded electrospun PCL scaffolds after 120 days of culture. This long culture duration was chosen to ensure formation of a mature tissue with abundant extracellular matrix, so that GAG and collagen could be enzymatically perturbed to examine the effect on mechanical function. All digestions were performed in PBS at 37^{o}C for 36 hours. GAG depletion was achieved by digestion with Chondroitinase ABC (ChABC, 0.125 U/mL) and collagen depletion was achieved by digestion with collagenase (COL-ASE, 10 U/mL). A control group was subject to the digestion protocol, but without any enzymes (PBS). Finally, a fourth group was tested directly from culture (fresh) in order to determine whether the digestion protocol alone (PBS) had any effects on the mechanics of these engineered fibrocartilages. The acellular scaffold only group will be referred to as SCAF.

4.2.4 Mechanical, histologic, and biochemical analyses

Samples were either subject to uniaxial tensile testing followed by biochemical analyses (n = 5), compression testing (n = 3), or histologic examination (n = 2). Uniaxial tensile testing was performed similarly to Chapter 3, with some modifications. Cross-sectional area was measured using a custom

laser device that provided accurate, noncontact measurements of thickness and width (Peltz, Perry et al. 2009). Samples were lightly airbrushed with black enamel paint to generate texture for strain analysis (below). Testing in uniaxial tension was performed using an Instron 5542. All samples were placed into customized serrated grips and maintained in a phosphate buffered saline bath during the testing protocol described in the previous chapter. Briefly, following a 5 minute preload and 15 cycles of preconditioning, a quasi-static constant elongation test was performed until failure at a rate of 0.1% strain/sec. During the test, strain control was performed via crosshead displacement and images of the sample midsubstance were collected per 0.5% strain increments. Images were analyzed by texture correlation to determine the local surface deformations, and two-dimensional components of Lagrangian strain (**E**) were calculated (Vic-2D, Correlated Solutions Inc.). To calculate strain, a region of interest spanning approximately 50% of the sample width was selected within the mid-length of the sample, in order to collect strain information sufficiently far from the grips and associated boundary effects. Two dimenionsal strain values were computed for each pixel within the region of interest, and the average of all pixels computed to determine the state of strain within each image in the sequence. Custom Matlab code was used to sync this strain data with force data collected by the Instron testing device. Modulus was calculated by fitting a linear regression to either the toe or linear region of the resulting stress-strain plot for each sample, and similarly Poisson's ratio was computed from the slope of longitudinal (applied) vs. transverse strain. Dry weights of samples were obtained after lyophilizing

overnight, and after digestion with papain, biochemical analyses were conducted to determine total GAG and collagen content as described in Chapter 3. Each was normalized to dry weight.

Compression testing was performed on cored 4 mm diameter samples from three separate strips, and histologic samples were taken from the remaining tissue. Unconfined compression was applied by first applying a 2 gram creep preload for five minutes. Next, samples were subjected to 10% axial strain applied at 0.05% per second followed by relaxation for 1000 seconds. Although dynamic compressive tests were attempted (additional 1% sinusoidal deformation to equilibrated constructs at 1.0 Hz) in all cases but controls, loads were below the detection limit of the system.

Histologic analyses were performed as described in Chapter 3. Samples from each group (n = 2) embedded in OCT freezing medium and flash frozen in liquid nitrogen. Embedded samples were cryo-sectioned in the plane perpendicular to the fiber direction (i.e. in cross-section) and stained to visualize GAG (Alcian Blue) or collagen (Picrosirius Red). Alcian Blue and Picrosirius Red stains were visualized on an upright Leica DMLP microscope.

4.3 Results

Effects of chondroitinase and collagenase digestions were first examined by histology to confirm removal of GAG and collagen, respectively. Staining of the cross-section of fresh samples revealed abundant accumulation of GAG

(Fresh, Figure 4.2) and collagen (Fresh, Figure 4.3) throughout the sample thickness. In fact, GAG and collagen contents reached as high as 15% and >30% of the dry weight in the PBS group, respectively, indicating that the constructs were indeed mature and contained relatively large amounts of extracellular matrix. Performing the digestion protocol in the absence of any degradative enzyme had no effect on GAG content or distribution (PBS, Figure 4.2). Treatment with chondroitinase resulted in a complete depletion of GAG from the construct (ChABC, Figure 4.2). Similarly, collagenase treatment resulted in a complete removal of GAG from the construct (COL-ASE, Figure 4.2).

No differences in collagen content and distribution were observed between the freshly sectioned samples and those subject to the digestion protocol; ChABC treatment also had no effect on collagen (Figure 4.3). However, treatment with collagenase resulted in a complete removal of collagen from the construct (COL-ASE, Figure 4.3). All histologic findings were confirmed quantitatively by DMMB and OHP assays to determine the amount of GAG and collagen present, respectively (Figure 4.4).

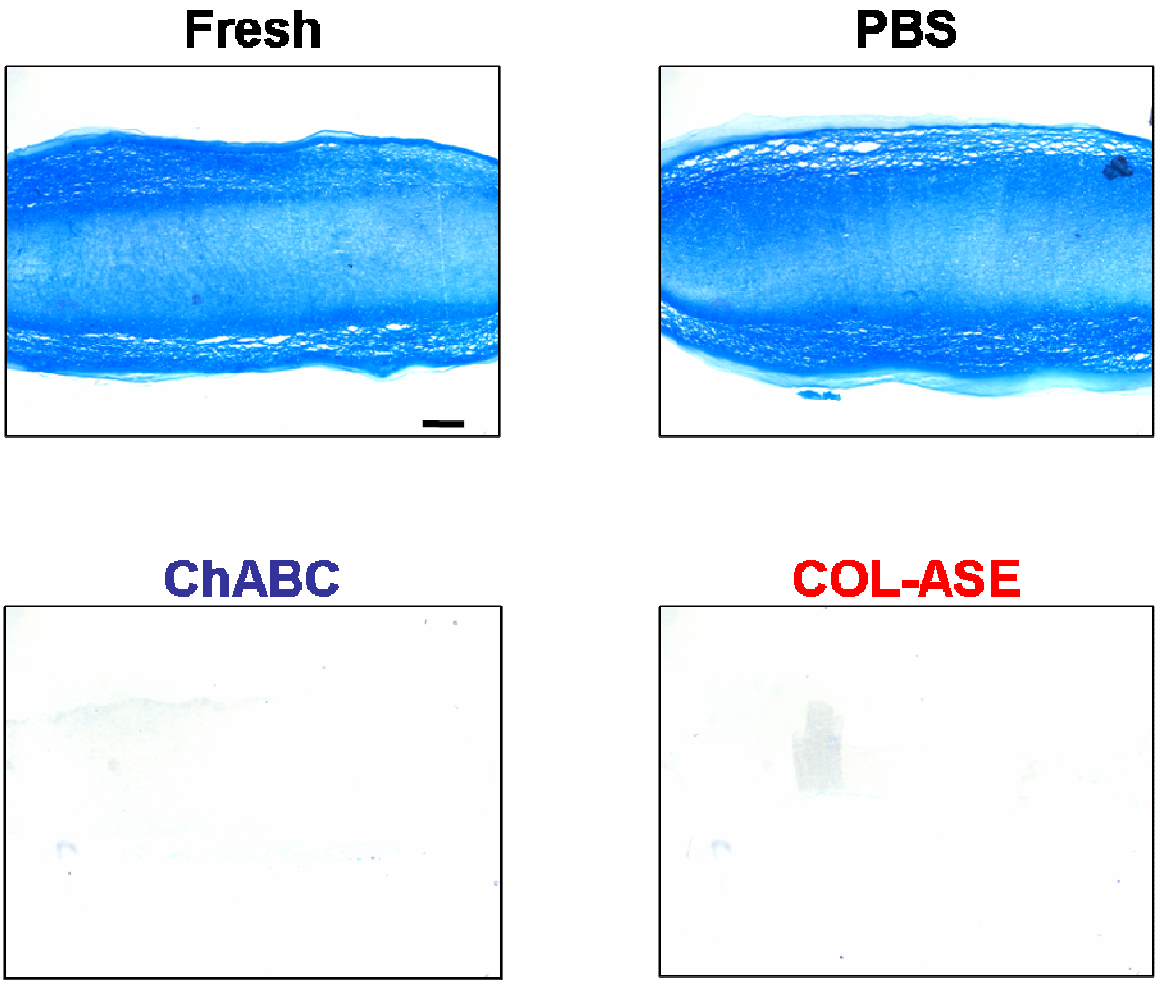

Figure 4.2 Alcian Blue staining of freshly sectioned MSC-seeded electrospun PCL scaffolds after 120 days of culture (Fresh). GAG content is unaltered in the digestion protocol alone (PBS), however is dramatically reduced after chondroitinase ABC treatment (ChABC) and collagenase treatment (COL-ASE). Scale = 250 μm.

Compression testing of the acellular scaffold revealed a soft (~1 kPa peak stress) initial response, followed by very little stress relaxation (< 10%, Figure 4.5). After 120 days of culture and extracellular matrix deposition, fresh and PBS constructs were significantly higher in peak stress and relaxation when compared to SCAF, indicating that extracellular matrix deposition drastically altered the mechanical behavior of constructs relative to the scaffold.

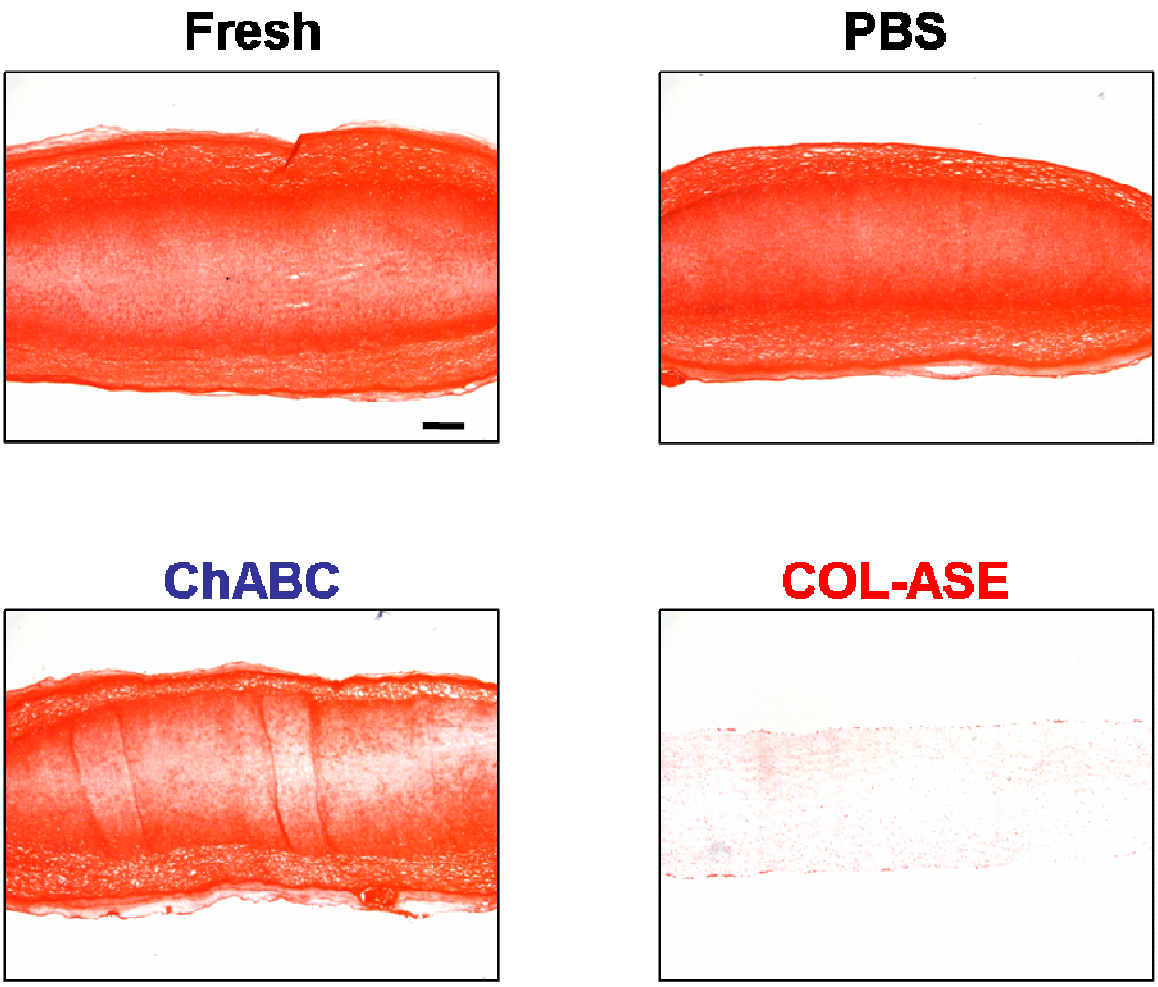

Figure 4.3 Picrosirius Red staining of freshly sectioned MSC-seeded electrospun PCL scaffolds after 120 days of culture (Fresh). Collagen content is unaltered in the digestion protocol alone (PBS) and with chondroitinase treatement (ChABC), however after collagenase treatment (COL-ASE) collagen was depleted. Scale = 250 µm.

No significant difference was observed between the fresh control and the PBS control, indicating that the digestion protocol alone had no effect on compressive properties. Removal of GAG in ChABC constructs resulted in a reduction of compressive peak stress to SCAF levels, while the % stress relaxation was unaffected relative to PBS (Figure 4.5). On the other hand, removal of both GAG and collagen in COL-ASE samples resulted in a return of both peak stress and % stress relaxation to SCAF levels.

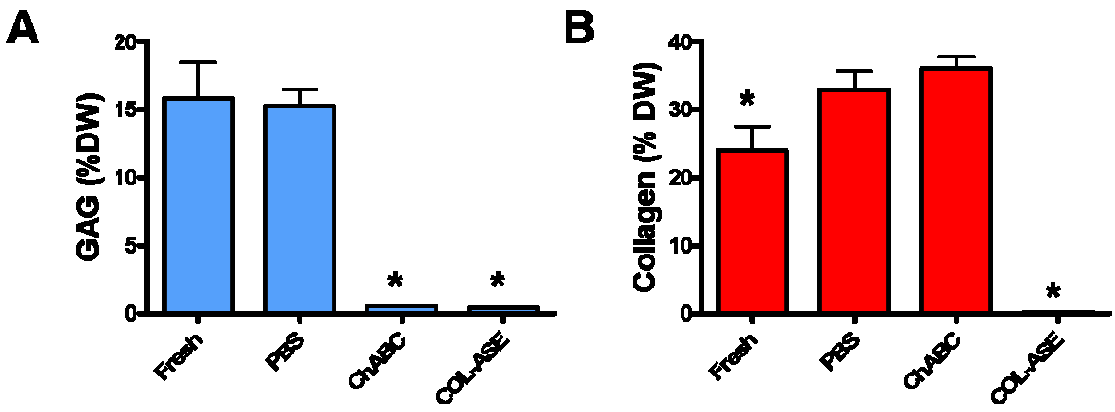

*Figure 4.4 Biochemical analyses to quantify GAG (A) and collagen (B) content confirmed findings of histologic analyses: chondroitinase and collagenase digestion depleted GAG and collagense depleted collagen. * = p < 0.05 compared to PBS.*

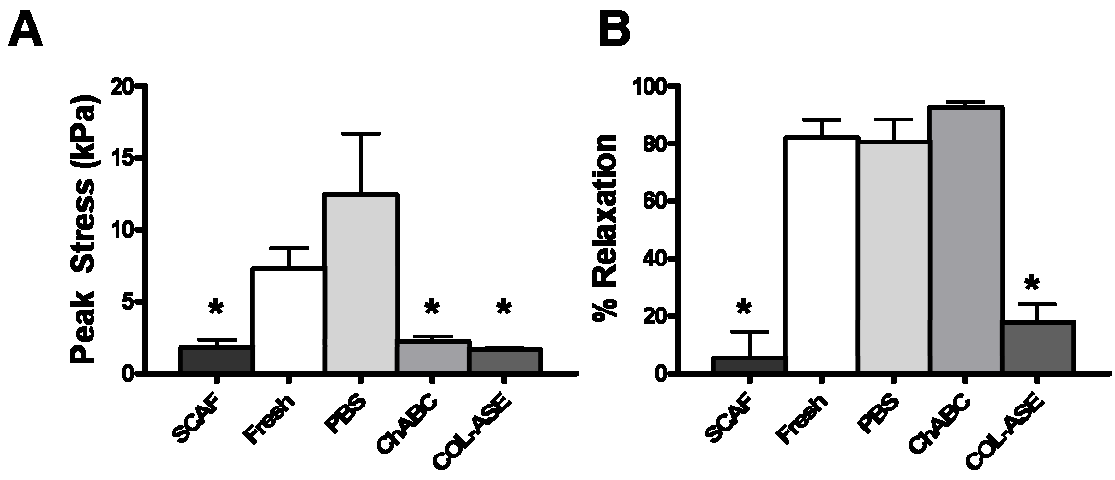

*Figure 4.5 Unconfined compression of constructs revealed changes in peak stress (A) and % stress relaxation (B). * = p < 0.05 compared to PBS.*

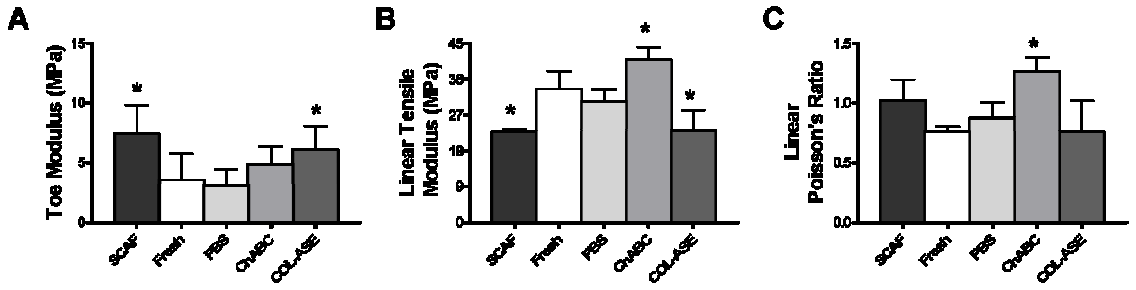

Figure 4.6 Uniaxial tensile testing revealed changes in toe-region modulus (A), linear-region modulus (B), and Poisson's ratio (C). * = $p < 0.05$ compared to PBS.

Tensile testing revealed a significant reduction in toe region modulus and a significant increase in linear region modulus for the mature, fresh constructs compared to SCAF (Figure 4.6). No significant difference was observed between the fresh and the PBS controls, indicating that the digestion protocol alone had no effect on tensile properties. Removal of GAG and collagen with COL-ASE resulted in a return of toe and linear region moduli to SCAF levels (Figure 4.6). Surprisingly, leaving the collagen network intact and removing only the GAGs via ChABC treatment resulted in a significant (>10 MPa) increase in the tensile modulus compared to PBS and fresh samples. ChABC samples also had a significantly higher Poisson's ratio than PBS and fresh controls.

4.4 Discussion

In this study, the methods developed in the previous chapter were applied to generate mature engineered fibrocartilage constructs in order to determine whether the major extracellular components, GAG and collagen, play the same

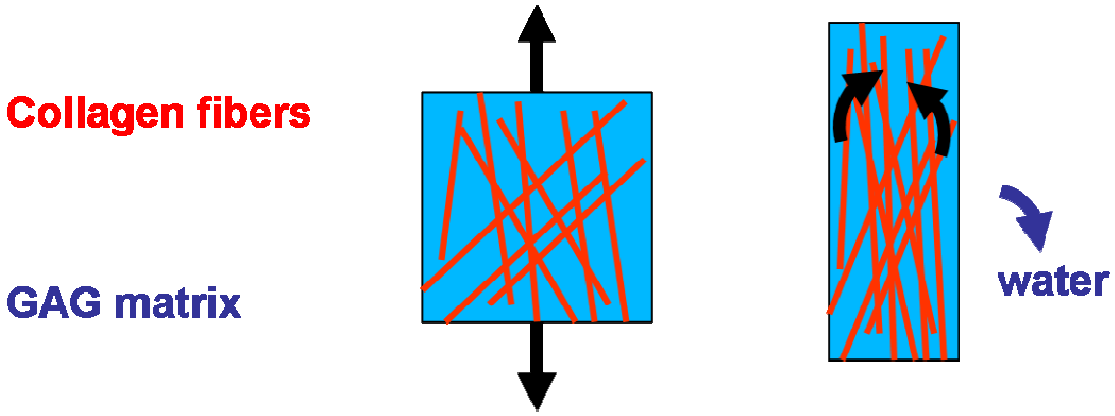

Figure 4.7 Schematic representation of fiber recruitment in a GAG-rich matrix. Somewhat disperse collagen fibers (red) embedded in the GAG matrix (blue) reorient under uniaxial tensile load, compressing the intervening matrix in the process and squeezing water out . GAG depletion may eliminate this resistance to fiber recruitment under load, stiffening the tensile response.

mechanical roles in these engineered tissues as the do in native load-bearing soft tissues. Constructs achieved native annulus fibrosus GAG content (15% in engineered constructs vs. 10 – 20% for native annulus fibrosus) and while considerable collagen was accumulated, total collagen remained slightly below native (30% vs 50 – 70%). MSCs were used in place of the annulus fibrosus cells of the previous chapter in order to maintain the generality of this study, and because in later chapters (Chapters 6 – 8), MSCs will be used exclusively. However, it is likely that the findings of this chapter would be similar if AF cells were used in place of MSCs.

Consistent with the convention for native tissues, GAG plays an important role in the compressive response of engineered fibrocartilage. GAG removal with

chondroitinase or with collagenase (which also removes collagen) resulted in a return of compressive peak stress to scaffold-only values, indicating that GAG and not collagen or other extracellular matrix molecules dictates the compressive response of these engineered tissues. This is consistent with experiments on the intervertebral disc as well as cartilage and meniscus, where GAG removal results in a dramatic reduction in compressive properties. The transient response to compression, indicated by % stress relaxation, was very low for the acellular scaffold, and increased dramatically with extracellular matrix deposition. The acellular scaffold likely experienced little relaxation because hydraulic permeability was so high that water was exuded during the loading phase of the test, and equilibrium reached at or soon after peak stress. Additionally, without GAGs or other molecules to establish osmotic pressure, there was no osmotic restriction to fluid exudation. On the other hand, after extracellular matrix deposition (fresh and PBS), stress relaxation of over 80 % was observed. This is similar to the behavior of hydrated native tissues, and suggests that fluid pressurization occurs during the loading phase, and is subsequently dissipated as fluid slowly leaves the tissue. Because GAG removal did not affect % relaxation, but GAG and collagen removal did, it is expected that collagen is primarily responsible for determining the hydraulic permeability and therefore the transient response of the tissue under compression. This is consistent with the role of collagen observed in cartilage (Park, Nicoll et al. 2008). These results suggest that cells seeded on electrospun, aligned nanofibrous PCL scaffolds

generate a tissue that resists compressive loads by a mechanism that is consistent with load-bearing soft tissues of the musculoskeletal system.

As indicated in Chapter 3, electrospun aligned PCL scaffolds are nonlinear in tension, with distinct toe and linear regions. Matrix deposition differentially affected the tensile response, with a significant increase in the linear region modulus accompanied a reduction in the toe region modulus. The reason for a reduction in toe region modulus remains unclear, however it is interesting to note that with the progressive removal of GAG, then GAG and collagen, toe region modulus progressively increased toward acellular scaffold levels. More importantly, the linear region modulus increased significantly with matrix deposition, and this increase was completely eliminated upon removal of collagen via collagenase treatment. This finding is consistent with the well established notion that collagen resists tensile stresses in load-bearing soft tissues. Perhaps most interesting however, was the unexpected finding that removal of GAG, a molecule conventionally thought to have little to no role in tensile properties, resulted in a dramatic (> 10 MPa) increase in the linear region modulus compared to the untreated mature construct.

While there are many possible mechanisms by which GAG depletion may increase the tensile properties, one we consider here is described in Figure 4.7. If a population of aligned fibers, dispersed about some prevailing direction of alignment, are enmeshed within a GAG-rich isotropic matrix, application of a uniaxial load would result in reorganization of the fibers, rotating them toward the direction of loading. In the process, rotating fibers must compress their

surrounding matrix as the fibers collapse inward toward the loading direction, and consequently water is exuded from the material as it contracts laterally. However, if the GAG-rich matrix is perturbed, for instance via ChABC treatment as was done in the present study, fibers would be free to reorient without impediment from the surrounding matrix. Therefore, it is possible that GAG depletion results in enhanced fiber recruitment, as the matrix is no longer able to resist fiber reorganization after GAG removal. The significant increase in Poisson's ratio with chondroitinase treatment supports this model, as stiffening of the tensile response due to enhanced fiber recruitment would necessitate larger lateral contractions under longitudinal stretch. In other words for a given extension along the loading direction, an increase in the Poisson's ratio may indicate an increase in fiber rotation toward the loading direction, consistent with the proposed model of stiffening (Figure 4.7).

It is unclear whether this interplay between GAG and collagen in the tensile response of these engineered tissues is an aberrant behavior or if it indicates some higher level of similarity with how native load-bearing soft tissues function. The role of GAG in the mechanics of such tissues has been widely investigated using an approach similar to the current one, relying on chondroitinase ABC to degrade and remove GAG from the tissue of interest. While their role in resisting compressive forces is well established, there is no clear consensus regarding what role, if any, GAGs play in the response to tensile forces. This has been examined in a number of load-bearing soft tissues that span a wide range of endogenous GAG contents, from tendon and ligament (

0.1% - 1% dry weight) to articular cartilage (~20% dry weight). In tissues with relatively low GAG content, there are conflicting reports on the effects of GAG removal on tensile properties (Viidik, Danielson et al. 1982; Screen, Chhaya et al. 2006; Lujan, Underwood et al. 2009). Screen et al. observed tensile stiffening with GAG removal in rat tail tendon fascicles, however other reports suggest GAG depletion had no effect on tensile properties. One reason for the lack of consensus on this topic may be that the role of GAGs and how they interact with collagen under load is a tendon-specific phenomenon, such that different observations may be found in different tendons, depending on their composition, organization, and loading environment. Further complicating such studies is the dramatic effect of PBS incubation on tissues. Because GAG loss and tissue swelling often occur, the effect of the enzymatic digestion is often minimal in comparison to the protocol itself (Viidik, Danielson et al. 1982; Screen, Chhaya et al. 2006; Lujan, Underwood et al. 2009). This limitation demonstrates the advantage of studying engineered tissues as simple functional analogs for native ones, as in the present study the digestion protocol in PBS did not have any effect on GAG content or any tensile or compressive properties.

Unlike studies in ligament and tendon, where little GAG is present, investigations in cartilage demonstrate that indeed GAG depletion does result in stiffening of the tensile response in the linear region of the stress-strain curve. This has been demonstrated in both native cartilage (Schmidt, Mow et al. 1990; Asanbaeva, Tam et al. 2008) as well as engineered cartilage constructs (Natoli, Revell et al. 2009). Finally, Ateshian and coauthors recently developed a

constitutive model for articular cartilage that replicated many experimental findings of cartilage mechanics, including tensile stiffening upon GAG depletion (Ateshian, Rajan et al. 2009). The study modeled cartilage as tension-only fibers with dispersed orientations embedded in a proteoglycan ground matrix that was osmotically swollen. Ateshian et al. arrived at a similar explanation to that dicussed in the present study (Figure 4.7), suggesting that GAG-related osmotic swelling of the matrix restricts fiber reorganization under uniaxial load, and reduction in the fixed charge density, and therefore osmotic pressure, allows fibers to reorient and become more effectively recruited. Unlike the present study, however, both theoretical and experimental studies of cartilage suggest that tensile stiffening upon GAG depletion should be accompanied by a reduction in modulus in the toe region, as fibers are rotating without restriction (Schmidt, Mow et al. 1990; Ateshian, Rajan et al. 2009). GAG depletion had no effect on the toe region modulus in the present work; however, this does not discount parallels between the cartilage and engineered fibrocartilage response to GAG depletion. The degree of reduction in toe region modulus upon GAG depletion may be dependent on the degree of dispersion of fiber orientations as well as fiber stiffness. For instance, if in GAG depleted constructs the fibers are highly aligned, then the toe-region response may be dictated by fibers that are already parallel to the loading direction, such that any softening effect due to rotation of the dispersed fibers would be inconsequential. This is not mutually exclusive with the large strain response, where enhanced fiber recruitment would stiffen the tissue additively. Additional work, including the application of a constitutive model

like that presented by Ateshian et al. is necessary to understand this disparity, as well as to confirm the mechanism by which GAG removal stiffens the tensile response of mature MSC-seeded electrospun scaffolds (Figure 4.7).

Because the GAG content achieved in the present study (~15% dry weight) is closer to cartilage (20% dry weight) than tendon and ligament (0.1% - 1% dry weight), it is likely that the effect of GAG depletion on tensile properties is dependent on the amount of GAG initially present. Unfortunately, little has been done to investigate the functional role of GAG in native fibrocartilages like the knee meniscus and annulus fibrosus. Because these tissues contain similar amounts of GAG to the engineered tissues generated in the present study, it is likely that GAG removal in these tissues will also produce a stiffening response in tension. Work is currently underway to test this directly.

Importantly, this study demonstrates that cells on aligned electrospun scaffolds are not only producing and accumulating the correct extracellular molecules – GAG and collagen – but that they are being assembled in such a way that their mechanical functions are conserved with respect to load-bearing soft tissues of the musculoskeletal system. This is a strong indication that aligned electrospun scaffolds direct the formation of functional tissue analogs, and that this approach can be successfully used in subsequent chapters to engineer a fibrocartilage that replicates the form and function of the annulus fibrosus.

These findings may have important implications for MSC biology as well as tissue engineering. While there has been a substantial amount of work done to arrive at a consensus regarding the appropriate environmental conditions and

stimuli for MSC differentiation along chondrogenic, adipogenic, and osteogenic lineages, much less has been done to understand what factors drive MSCs differentiation toward a fibrous or fibrochondrogenic phenotype. The present study demonstrates a culture system that permits fibrochondrogenic extracellular matrix production by MSCs, and while genetic markers that signify differentiation were not investigated in the present work, a powerful downstream output measure, tissue level mechanics, indicates that MSCs on aligned electrospun scaffolds in the presence of TGF-β3 give rise to a fibrocartilage tissue in which mechanical function of its constituents is conserved with respect to native load-bearing soft tissues of the musculoskeletal system.

4.5 Conclusions

In the previous chapter, the mechanics of acellular electrospun nanofibrous PCL scaffolds were shown to replicate many of the functional hallmarks of fibrous soft tissues, including anisotropy and stress-strain nonlinearity. In the present study, we demonstrated that when cells were introduced to these scaffolds and subjected to an extended culture duration, they generated a GAG and collagen rich extracellular matrix. In the resulting fibrocartilage tissue, both GAG and collagen performed functional roles that are consistent with their roles in load-bearing tissues of the musculoskeletal system: GAGs resisted compression and collagen resisted tension. Additionally, we noted a possible role for GAG in restricting collagen recruitment in fibrocartilage

tissues. These data provide strong support for the use of electrospun scaffolds in tissue engineering of the annulus fibrosus and other load-bearing tissues. In the next chapter, focus will be placed on applying these methods to engineer a replacement for a single lamella of annulus fibrosus.

CHAPTER 5: INTEGRATING THEORETICAL AND EXPERIMENTAL METHODS FOR TISSUE ENGINEERING OF A SINGLE LAMELLA OF ANNULUS FIBROSUS

5.1 Introduction

In Chapter 3, electrospun nanofibrous scaffolds were introduced as a promising point of initiation for annulus fibrosus (AF) tissue engineering: nanofibrous scaffolds qualitatively replicated the nonlinear, anisotropic and finite elastic behaviors of native AF, and supported cell attachment, survival and extracellular matrix deposition in short term (4 weeks) culture. We also introduced the concept of using constitutive models as a tool to study evolving tissues, with model parameters serving as metrics of functional growth. In the present work, we build on this foundation, employing a hyperelastic constitutive law to understand the *long-term* (8 weeks) functional growth of AF cell-seeded scaffolds.

It has become increasingly recognized that when evaluating load-bearing tissue engineered constructs such as the AF, it is not sufficient to simply address histological and biochemical outcomes (Butler, Goldstein et al. 2000). It is necessary to evaluate mechanical function of the engineered construct with respect to the native tissue mechanics. Furthermore, complex mechanical behaviors require consideration, including nonlinearity and anisotropy; thus a linear measure of mechanical function such as modulus may not sufficiently assess the

construct function with respect to native tissue benchmarks. Hyperelastic constitutive modeling, which has a long history in the study of the native AF (Wu and Yao 1976; Klisch and Lotz 1999; Eberline, Holzapfel et al. 2001; Sun and Leong 2004; Wagner and Lotz 2004; Caner, Guo et al. 2007; Guerin and Elliott 2007) and other fiber-reinforced tissues, can provide insight into construct material behavior along the entire loading regime. Additionally, the terms of a structurally-based strain energy model have physical significance that can be particularly advantageous in understanding and redirecting the evolution of engineered tissue structure-function relationships.

Structural constitutive models have recently been utilized to study *acellular* electrospun mesh mechanical behavior (Courtney, Sacks et al. 2006; De Vita, Leo et al. 2006). Studies like these are useful to determine application-specific design criteria for tissue engineering scaffold fabrication; however, the models were not used to evaluate cell-mediated changes in engineered tissue mechanics. Due to the amount of micro-structural and micro-mechanical information necessary for such approaches, cell-mediated changes may be difficult to interpret in the context of model inputs, obfuscating the interpretation of model results. The time-dependent functional growth of AF cell-seeded aligned electrospun nanofibrous scaffolds was quantified in Chapter 3 using a linear homogenization model that had been previously applied to native AF (Yin and Elliott 2005). While this approach was limited by a model formulation that did not account for the material nonlinearity, it yielded quantitative measures of AF cell-mediated changes in construct mechanics. Together these studies provide strong evidence for the

power of utilizing hyperelastic constitutive modeling to assess and optimize AF functional tissue engineering.

The objective of the work presented in this chapter was to integrate theoretical and experimental approaches for functional tissue engineering of a single lamella of the AF. Aligned nanofibrous scaffolds were seeded with AF cells, and assayed for functional growth using experimental methods (e.g., mechanical testing, biochemistry, histology). A hyperelastic fiber-reinforced constitutive model was used to characterize time-dependent evolution of the engineered AF. The constitutive model accounted for nonlinearity and anisotropy and provided scalar parameters associated with physical tissue function (e.g., fiber and matrix properties). These parameter values evolved with culture duration, elucidating physical mechanisms of functional growth. The model was validated and then used to predict time-dependent changes in the simulated response of engineered AF constructs to physiologic loading scenarios including biaxial and shear loading.

5.2 Materials and Methods

5.2.1 Scaffold Fabrication

Aligned PCL scaffolds were electrospun as described in Chapters 3 and 4, with some modification. Fibers were collected for 5 – 6 hours on a grounded shaft rotating at 7,500 rpm, yielding an aligned nanofibrous sheet approximately 250 μm thick. To create samples with discrete fiber orientations of 0^o, 30^o, and 90^o, rectangular samples (5 mm × 30 mm) were excised from the nanofibrous sheet

with the long axis of the sample rotated by an angle, φ, with respect to the prevailing fiber direction.

5.2.2 AF Cell Isolation and Maturation of Cell-Laden Constructs

AF cells were isolated from the caudal discs of skeletally mature bovine donors within 12 hours of slaughter as described in Chapter 3. Scaffolds with three fiber orientations ($\varphi = 0^o, 30^o, 90^o$) were sterilized, rehydrated, and coated with 20 μg/mL fibronectin. Second passage AF cells were seeded onto scaffolds at a density of 1×10^6 per construct, and scaffolds were cultured in 6 well plates, in 3 mL of a chemically defined growth medium comprised of Dulbecco's modified eagle's medium, 0.1μM dexamethasone, 40 μg/mL L-Proline, 100 μg/mL Sodium Pyruvate, 1% Insulin, Transferrin, Selenium/Premix, and 1% penicillin, streptomycin and fungizone supplemented with 10 ng/mL Transforming Growth Factor β-3 (Mauck, Yuan et al. 2006).

5.2.3 Mechanical Testing and Biochemistry

After 1 day, 4 and 8 weeks in free swelling culture, intact cell-laden scaffolds from each orientation ($\varphi = 0^o, 30^o, 90^o$) were collected for uniaxial tensile testing followed by biochemical analyses (n = 4 – 5 per φ per time point). Prior to testing, sample thickness was determined at three points along the length of each sample using a custom contact/indentation system (Soslowsky, An et al. 1994). Width and gage length were measured by digital calipers. Samples were lightly airbrushed with black enamel paint to generate texture for strain analysis, and

tested in uniaxial tension as described in Chapter 4. Briefly, samples were placed into customized serrated grips and maintained in a phosphate buffered saline bath during the testing protocol that consisted of a 5 minute preload and 15 cycles of preconditioning, followed by a quasi-static constant elongation test until failure at a rate of 0.1% strain/sec. This protocol has been commonly used for testing native AF in uniaxial tension, and is sufficiently slow to eliminate viscoelastic effects (Elliott and Setton 2001; Guerin and Elliott 2006; Guerin and Elliott 2007). Images were analyzed by texture correlation to determine the local surface deformations, and two-dimensional components of Lagrangian strain (**E**) were calculated as in Chapter 4. Modulus was calculated by fitting a linear regression to the linear region of the resulting stress-strain plot for each sample.

Biochemical assays were performed to determine sulfated glycosaminoglycan (GAG), total collagen, and DNA content as described in the previous chapters. After tensile testing, samples were digested for 16 hours in papain at 60^{o}C. Digested samples were analyzed for GAG content using the 1,9-dimethylmethylene blue dye-binding assay, for orthohydroxyproline (OHP) content (after acid hydrolysis) by reaction with chloramine T and dimethylaminobenzaldehyde and for DNA content using the PicoGreen dsDNA Quantification kit. OHP was converted to collagen content for a 1:10 ratio of OHP:collagen (Hollander, Pidoux et al. 1995; Vunjak-Novakovic, Martin et al. 1999; Mauck, Yuan et al. 2006).

5.2.4 Histology and Actin Staining

Samples for each angle (n = 2 per φ per time point) were fixed overnight in 4% paraformaldehyde at 4^{o}C, embedded in OCT freezing medium and flash frozen in liquid nitrogen. Embedded samples were cryo-sectioned longitudinally to 8 μm thickness perpendicular to the fiber plane and stained for collagen with Picrosirius Red, for cellular nuclei with Haematoxylin and Eosin (H&E), and for GAG with Alcian Blue. Additional 8 week samples for φ = 30^{o} were sectioned in the fiber plane, and stained with Picrosirius Red to visualize collagen orientation (n = 2). Collagen orientation was measured by quantitative polarized light microscopy as described previously (Gimbel, Van Kleunen et al. 2004). Cytoskeletal actin was visualized at 3 days(Li, Mauck et al. 2007). Briefly, filamentous actin was labeled with Alexafluor 488 conjugated phalloidin. Cell nuclei were counterstained with DAPI. The time point of 3 days was selected for optimal visibility, as at earlier time points the cells are sparsely seeded, while at later time points, confluence and abundant extracellular matrix deposition obscured cell borders. Samples were imaged at 20× on a Nikon T30 inverted fluorescent microscope equipped with a CCD camera and the NIS Elements software package.

5.2.5 Constitutive Model

Hyperelastic materials are described by a scalar strain energy density function, W, that can describe material behaviors for finite and nonlinear deformations. Determining the optimal form of W to capture the complex behavior of biological materials is an active area of study (Humphrey and Yin 1987; Bischoff 2006; Gasser, Ogden et al. 2006; Klisch 2006; Limbert and Middleton 2006;

Wagner, Reiser et al. 2006; Guerin and Elliott 2007). Modifications to hyperelastic constitutive models have been developed to account for the anisotropy of fiber-reinforced composites (Spencer 1972) by prescribing special properties along axes of anisotropy, representing fiber populations. A hyperelastic fiber-reinforced constitutive model was formulated to model the tensile behavior of AF cell-seeded scaffolds. The strain energy density function (W) for cell-seeded constructs was decomposed into the sum of a matrix strain energy function (W_m) and a fiber strain energy function (W_f) (Spencer 1972). This approach was used in place of a constrained mixture model in order to eliminate the need to calculate mass fractions. Determination of mass fractions of fibers and extrafibrillar material is not experimentally straightforward for engineered fibrocartilage tissues; an advantage of the theory outlined in Spencer (1972) is that these mass fractions are absorbed into the modulus-type parameters in the model (see below). Throughout the discussion of the model formulation, implementation, and results, we refer to cell-deposited extracellular material as 'extracellular matrix', while the term 'matrix' is reserved for nonfibrillar material such as GAGs, which we assume contribute only to isotropic material behavior. The model ‘fiber’ phase refers to the fibrous extracellular matrix, such as collagen, as well as polymeric nanofibers of the scaffold. Scaffold fibers and newly deposited collagen fibers were assumed to lie along the same direction; this assumption was verified by experimental results (see below). While the material properties of collagen and polymer fibers are not likely to be identical, this modeling approach only requires that they contribute to anisotropy through the same type of nonlinearity and along the same direction.

The W_f used (below) has been employed in a number of studies of native tissue to describe collagen fibers (Eberline, Holzapfel et al. 2001; Wagner and Lotz 2004; Gasser, Ogden et al. 2006; Guerin and Elliott 2007), while successful use of the model to fit day 1 (scaffold-only, minimal extracellular matrix) stress-strain data would support the use of the same W_f to describe electrospun PCL nanofibers.

The matrix phase was described as a Neo-Hookean compressible material (Holzapfel 2000) according to:

$$W_m = \frac{\mu}{2\beta}(I_3^{-\beta} - 1) + \frac{\mu}{2}(I_1 - 3) \tag{5.1}$$

where μ and $\upsilon = \frac{\beta}{1+2\beta}$ are the two scalar material parameters that characterize the matrix mechanics. μ is related to the modulus of matrix, while υ is related to matrix compressibility (the proclivity of a material to change volume during a given deformation). In the small strain approximation, μ and υ reduce to the shear modulus and Poisson's ratio of linear elasticity. The scalars $I_1 = tr\mathbf{C}$ and $I_3 = \det(\mathbf{C})$ are invariants of the Right Cauchy Green Tensor $\mathbf{C} = \mathbf{F}^T\mathbf{F}$, where $\mathbf{F}$ is the deformation gradient tensor (Ogden 1997). The fiber phase was described according to an exponential law commonly used for fibrous soft tissues (Fung 1982; Holzapfel 2000; Eberline, Holzapfel et al. 2001; Guerin and Elliott 2007):

$$W_f = \frac{\gamma}{\xi}(e^{\xi(I_4-1)^2} - 1) \tag{5.2}$$

where γ and ξ are the two scalar material parameters that characterize fiber mechanics. γ is related to the fiber modulus, while ξ represents the degree of stress-strain nonlinearity of the fiber material. While it is convenient to think of γ

as a fiber modulus, this is not a strictly accurate interpretation. γ only identifies the relative contribution of the anisotropic component to the overall constitutive law; it is more of a weighting factor for anisotropy than a fiber modulus. The scalar I_4 is an invariant defined as $I_4 = \mathbf{a} \cdot \mathbf{Ca}$, where **a** is a unit vector along the fiber direction (Spencer 1972). To account for the inability of the fiber phase to resist compressive deformations, I_4 was set to unity for $I_4 < 1$ (Ateshian 2007). From (Eq. 5.1) and (Eq. 5.2), the full constitutive law can be written according to $\mathbf{T} = 2I_3^{-1/2}\mathbf{F}\frac{\partial W}{\partial \mathbf{C}}\mathbf{F}^{\mathbf{T}}$ as follows:

$$\mathbf{T} = I_3^{-1/2}[\mu(\mathbf{FF}^{\mathbf{T}} - I_3^{-\beta}\mathbf{I}) + 2\gamma(I_4 - 1)e^{\xi(I_4-1)^2})\mathbf{Fa}_o \otimes \mathbf{a}_o\mathbf{F}^{\mathbf{T}}] \quad (5.3)$$

Where **T** is the Cauchy stress tensor. Because **T** is a second order tensor, the tensoral equation (Eq. 5.3) is a system of nine equations for the nine components of Cauchy stress. Cauchy stress was chosen because, unlike the 1st Piola Kirchoff stress, Cauchy stress is symmetric. While 2nd Piola Kirchoff stress is symmetric, it does not represent a physical state of the material. In summary, the complete model contains four scalar material parameters: μ and v to describe the matrix phase, and γ and ξ to represent the fiber phase.

In order to apply the model to experimental tensile test data for engineered AF constructs, we adhered to the following coordinate system throughout the study: the loading direction for all experiments was along the x_1 direction, and 2D strains were measured in the fiber-containing plane formed by the x_1 and x_2 axes. φ is the angle formed between the fiber direction **a** and the

loading axis (x_1) (Figure 5.1A). For uniaxial and biaxial loading in the x_1-x_2 plane, the nonzero components of Eq. 5.3 in component form are:

$$T_{11} = I_3^{-1/2}[\mu(\lambda_1^2 - I_3^{-\beta}) + 2\gamma(I_4 - 1)e^{\xi(I_4-1)^2})\lambda_1^2 a_1^2] \quad (5.4a)$$

$$T_{22} = I_3^{-1/2}[\mu(\lambda_2^2 - I_3^{-\beta}) + 2\gamma(I_4 - 1)e^{\xi(I_4-1)^2})\lambda_2^2 a_2^2] \quad (5.4b)$$

$$T_{12} = T_{21} = I_3^{-1/2}[2\gamma(I_4 - 1)e^{\xi(I_4-1)^2}\lambda_1\lambda_2 a_1 a_2] \quad (5.4c)$$

where λ_i are stretch ratios along the directions x_i for i=1,2,3. For uniaxial tension along the x_1 direction, $T_{22} = T_{33} = 0$.

Least squares curve fits of the model stress to full experimental stress-strain curves for φ = 90° samples were performed to yield values for the two matrix parameters, μ and ν, at 1 day, 4 and 8 weeks. For each sample, two-dimensional strains were measured during tensile tests, and extrapolated to three dimensional strains according to a Poisson's ratio ν_{13}, computed as part of the curve fit. These values were used to compute model stresses, which were fit simultaneously to the three normal components of the Cauchy stress: T_{11} was experimentally measured during the tensile test, while a traction free boundary condition was enforced for the transverse stresses ($T_{22} = T_{33} = 0$). This condition ensured uniqueness of the resulting parameter values. For uniaxial tension along φ = 90°, $I_4 = 1$ and the fiber term in (Eq. 5.3) is identically zero, leaving the fiber parameters γ and ξ undetermined while providing best-fit values for matrix parameters μ and ν. Least squares curve fits of the model to full stress-strain curves for φ = 0° samples were next performed to yield values for the two fiber parameters, γ and ξ, at each 1 day, 4 and 8 weeks. For each time point, the corresponding average values of μ and ν (obtained above) were employed. Out of plane strains for φ=0° were assumed

based on transversely isotropic material symmetry (E_{33} = E_{22}). Traction free boundary conditions were unnecessary for these fits, because fibers are aligned along the loading direction, so that requiring transverse stresses to be zero provides no constraint on the values of fiber parameters. The constitutive law used in this study is a simple form used widely in biomechanics applications. For further details on model robustness and parameter sensitivity the reader is directed to related studies referenced here (Guerin and Elliott 2007; O'Connell, Guerin et al. 2009).

Upon calculation of the four material parameters (μ, ν, γ, and ξ) from the $\varphi=0^{o}$ and 90^{o} data sets at each 1 day, 4 weeks and 8 weeks, model validation was carried out by *predicting* the stress-strain behavior of $\varphi=30^{o}$ samples. Because v_{12} varies with φ (Nerurkar, Baker et al. 2006), its value was determined by least squares curve fitting of the traction free boundary conditions for each parameter set and sample-specific 2-D deformations. The resulting 3-D strain data was used with time-point matched material parameter values to compute a model-predicted stress T_{11} as a function of experimentally measured strains. Agreement of the model predicted stress with the corresponding experimental stress was assessed to indicate the suitability of the proposed model as a full quantitative description of engineered AF mechanics during maturation. The contribution of fiber and matrix phases to the uniaxial tensile response at $\varphi = 30^{o}$ was computed by additive decomposition of (Eq. 5.3) into fiber stress ($\mathbf{T}^{f}$) and matrix stress ($\mathbf{T}^{m}$). Fraction of total stress for the fibers was computed as $\frac{T_{11}^{f}}{T_{11}}$. Growth related changes in the

fiber contribution were determined by using the material parameters associated with 1 day and 8 weeks.

5.2.6 Model Simulations

Two simulations to compute stresses under physiological loading of engineered AF mechanics were performed for $\varphi = 30^o$: 1) shear stresses associated with uniaxial and biaxial extension, analogous to AF loading during axial compression, flexion, and extension, and 2) circumferential and shear stresses associated with shear loading, analogous to torsion. First, because stress and strain tensors are not generally co-axial tensors for anisotropic materials, normal deformations that preserve the rectangular shape of a body can generate shear stresses in addition to normal stresses. For $\varphi = 30^o$, the shear stress T_{12} associated with uniaxial ($\lambda_1 > 1$) and equibiaxial ($\lambda_1 = \lambda_2$) extension were computed according to Eq. 5.4c. For the uniaxial case, deformations along the loading axis were prescribed, and transverse strains were computed according to Poisson's ratios either experimentally measured (time point matched v_{12}), or as described above (v_{13}). For the simulation of equibiaxial extension, plane strain was assumed, with equal extension along the x_1 and x_2 axes. Second, the model was used to simulate the shear response of engineered AF constructs and how the response evolved with time in culture. Shear was simulated as an isochoric deformation due to a force on the face perpendicular to x_2 in the direction x_1. The amount of shear (κ) was prescribed, and the resulting nonzero components of **T** were computed according to:

$$T_{11} = I_3^{-1/2}[2\gamma(I_4 - 1)e^{\xi(I_4-1)^2}a_1^2] \quad (5.5a)$$

$$T_{22} = I_3^{-1/2}[\mu\kappa^2 + 2\gamma(I_4 - 1)e^{\xi(I_4-1)^2}(\kappa^2 a_1^2 + 2\kappa a_1 a_2 + a_2^2)] \quad (5.5b)$$

$$T_{12} = I_3^{-1/2}[\mu\kappa + 2\gamma(I_4 - 1)e^{\xi(I_4-1)^2}(\kappa a_1^2 + a_1 a_2)] \quad (5.5c)$$

5.2.7 Statistics

Significance ($p \leq 0.05$) was evaluated by one way ANOVA with a Bonferroni post hoc test for the variable of culture duration (time). Goodness of model fits and predictions are reported in R^2 and Bland Altman limits of agreement (bias ± standard dev), reported in MPa(Bland and Altman 1986). Correlations between model parameters and biochemical measures were determined by linear regression. Correlations were considered significant for $p \leq 0.05$.

5. 3 Results

5.3.1 Experimental results

In this study, scaffolds with prescribed fiber angles ($\varphi = 0^o$, 30^o, 90^o) were seeded with AF cells and cultured over 8 weeks. For $\varphi = 0^o$ and $\varphi = 30^o$, constructs behaved nonlinearly in uniaxial tension and underwent finite elastic deformations (Figure 5.1). New tissue growth was evident from a time-dependent improvement in mechanical behavior and biochemical composition for all fiber

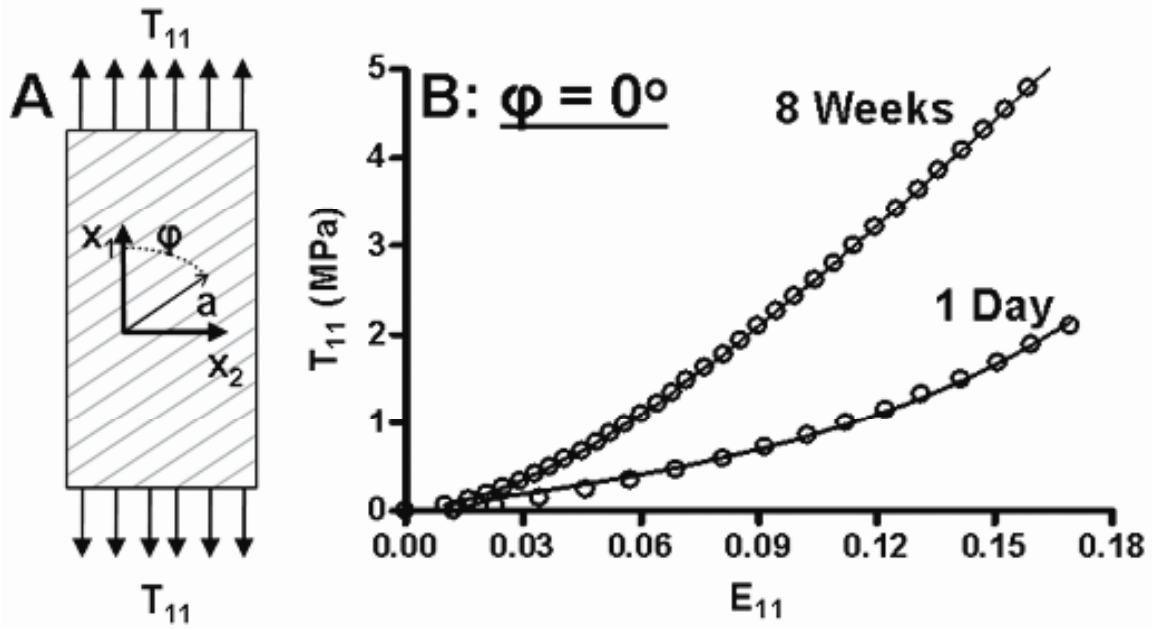

Figure 5.1 Schematic representation (A) of coordinate system for uniaxial tension (T11) with fiber angle (φ) indicated by the unit vector a. Representative curves (B) for engineered AF (φ = 0o) demonstrate a nonlinear response in uniaxial tension. The nonlinearity and modulus increased from 1 day to 8 weeks of culture. The model (solid lines) successfully fit experimental tensile behavior (open circles).

orientations (Figure 5.2). From 1 day to 8 weeks, the linear region modulus for φ = 0^o increased by ~25 MPa (138%, $p < 0.05$, Figure 5.2A), and for φ = 90^o by ~2 MPa (118%, $p < 0.05$, Figure 5.2C). The modulus increase for φ = 30^o was not significant (Figure 5.2B). Collagen and GAG increased by 4 weeks, and continued to increase up to 8 weeks in culture (Figure 5.2D, E). Average DNA content over all φ increased by nearly 5-fold, from 0.49 ± 0.14 μg at 1 day to 1.93 ± 0.74 μg by 8 weeks ($p < 0.05$).

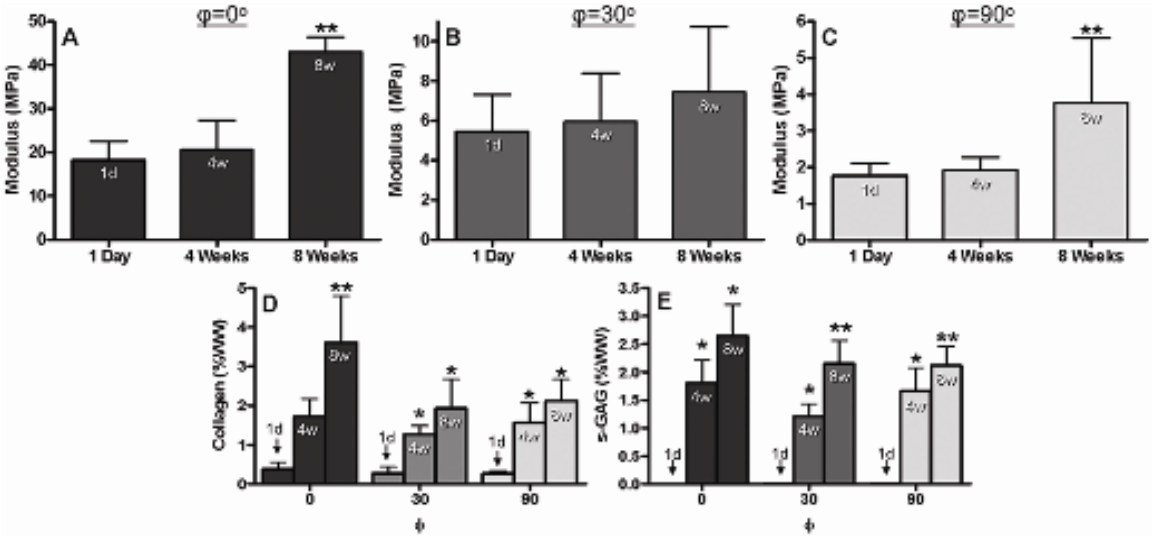

Figure 5.2 Experimentally measured tensile moduli for φ = 0^o (A), φ = 30^o (B), and φ = 90^o (C). Collagen (D) and GAG (E) increased with time for all φ. WW = wet weight. 1d = 1 day, 4w = 4 weeks, and 8w = 8 weeks. * = p < 0.05 compared to day 1, ** = p<0.05 compared to day 1 and 4 weeks. n = 4 –5 per group.

Histologically, infiltration and proliferation of AF cells into the scaffold was observed by 8 weeks, with abundant and relatively uniform deposition of collagen and GAG (Figure 5.3A-C). However, AF cell infiltration was restricted to the outer two-thirds of the scaffold thickness, with a dense border of cells at the periphery (Figure 5.3B). At 4 weeks, infiltration into the scaffold was limited, and collagen and GAG, although readily detected, were less abundant (not shown). These findings agreed with bulk biochemical findings (Figure 5.2D, E). Consistent with the findings of Chapter 3, AF cells were highly aligned with the underlying scaffold fiber direction (Figure 5.3D). Cytoskeletal actin was organized into many prominent stress fibers, also oriented parallel to scaffold fibers. These observations are supported by previous work, in which the maintenance of

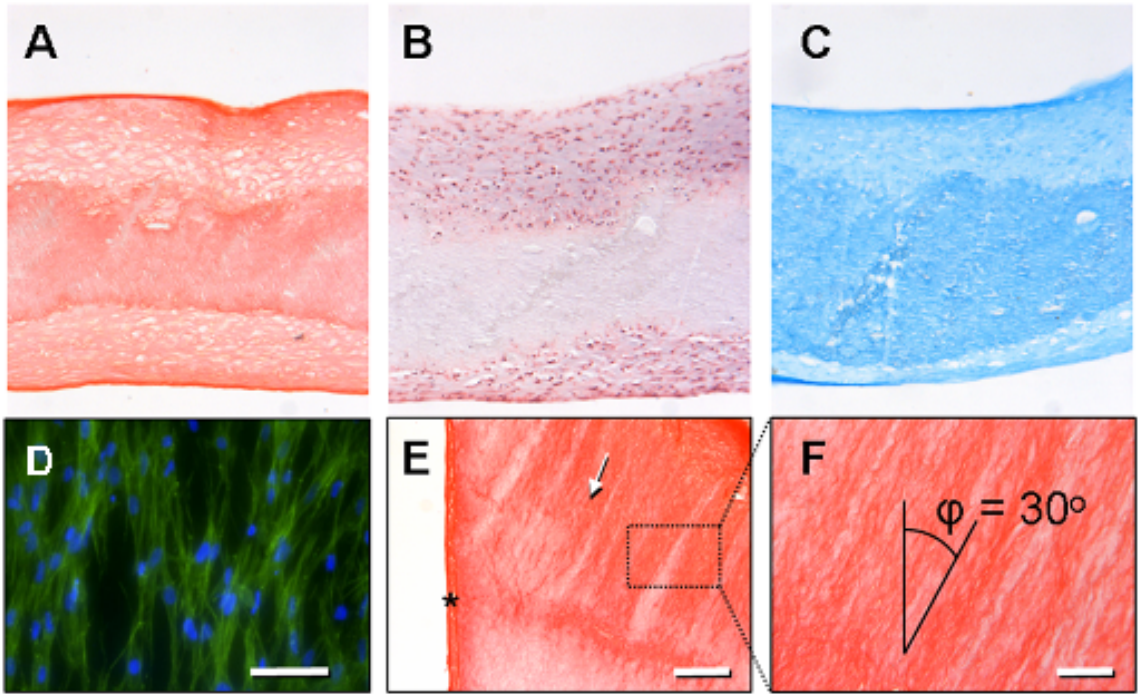

Figure 5.3 Histological sections of a φ = 90o sample at 8 weeks, stained with Picrosirius Red (A), H&E (B), and Alcian Blue (C). Actin (green) stained AF cells with counter-stained nuclei (blue) aligned with nanofibers, viewed in the plane of the scaffold at 3 days (D). Picrosirius Red stained fiber-plane sections for φ = 30o (E, higher magnification in F) revealed oriented collagen in the scaffold mid-substance (white arrow), and a thin disorganized capsule at the periphery (black asterisk). (F) Scale bar = 100 μm (A-C and F), 50 μm (D) and 200 μm (E).

cellular alignment was observed up to 4 weeks after seeding (Li, Mauck et al. 2007). Samples sectioned in-plane with the scaffold fibers revealed newly formed collagen, also organized along the prevailing fiber direction (arrow, Figure 5.3E, F); however, a thin, randomly organized capsule of collagen around the construct perimeter was observed (not shown). The fiber angle of newly formed collagen in the center of the scaffold, measured by quantitative polarized light microscopy at 8 weeks, was 31.1^{o} for $\varphi = 30^{o}$ samples.

5.3.2 Theoretical/model results

The constitutive model had an excellent fit to $\varphi = 90^o$ samples at all time points to yield matrix constants μ and ν (Figure 5.4A,B, and Table 5.1), with an average $R^2 = 0.98$ ($n = 15$). Both matrix constants increased with time, illustrating extra-fibrillar matrix deposition by AF cells. The constitutive model also had an excellent fit to $\varphi = 0^o$ samples (Figure 5.1) to yield fiber parameters γ and ξ (Figure 5.4C, D) with $R^2 = 0.98$ ($n = 13$). γ increased significantly by 8 weeks ($p < 0.05$). ξ increased slightly by 4 weeks, however the change was not significant. Significant correlation was observed between the biochemical measures of collagen and the model fiber parameter γ ($R = 0.81$, Figure 5.5A) and between GAG and the model matrix parameter ν ($R = 0.53$, Figure 5.5B). No correlations were found between matrix parameters and collagen content or between fiber parameters and GAG content ($p > 0.05$).

To validate the model, the measured strains for tensile tests of each $\varphi = 30^o$ sample were input into the model and a prediction of the resulting stress was computed using the four constant values determined above from $\varphi = 0^o$ and $\varphi = 90^o$. These predicted stress-strain curves had excellent agreement with their corresponding experimental curves (Figure 5.6, Table 5.1), with $R^2 = 0.98$ ($n = 13$). Using the average values of parameters μ, ν, γ and ξ for 8 week AF constructs, the uniaxial tensile behavior for $\varphi = 30^o$ was decomposed into contributions from the fiber and matrix phases (Figure 5.7). Fibers provided the predominant stress contribution, with fiber stress increasing with strain.

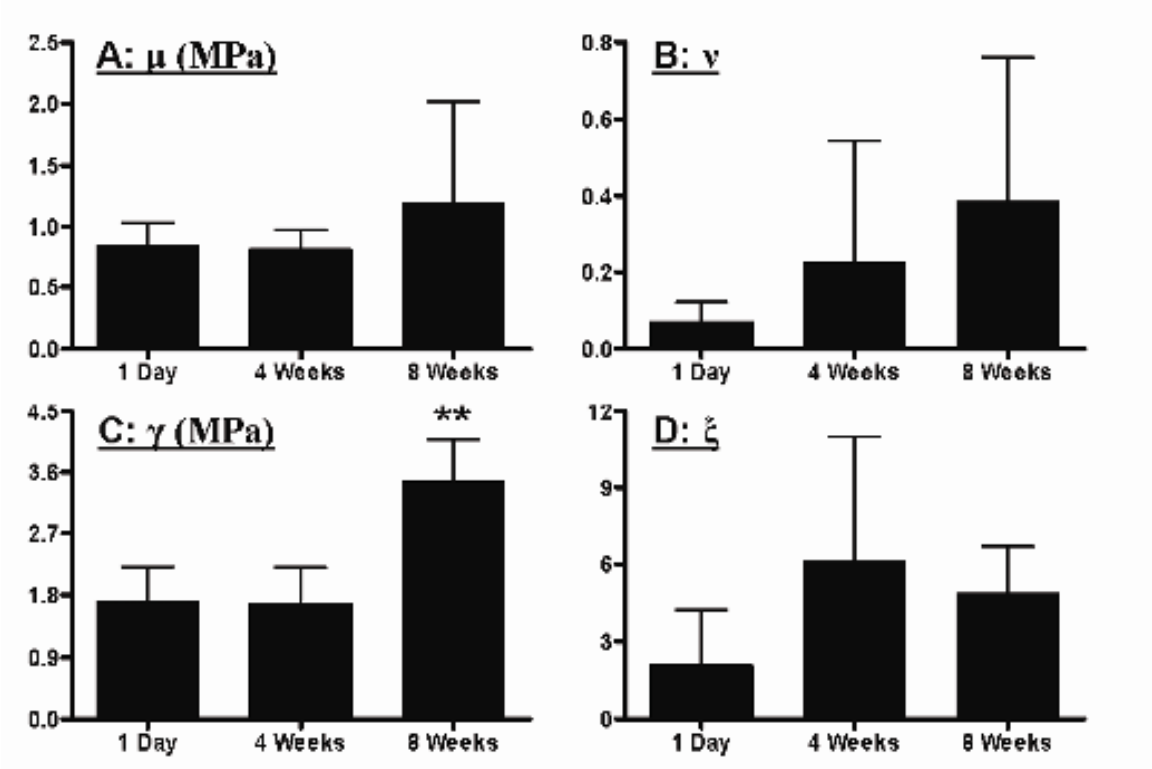

Figure 5.4 The model fit to uniaxial tensile responses for φ = 90o produced matrix parameters μ (A) and v (B). The average values of μ and v were used to fit φ = 0o at each corresponding time-point to yield fiber material parameters γ (C) and ξ (D). ** = p < 0.05 compared to 1 day and 4 weeks. n = 4 – 5 per φ per time point.

Comparison at 1 day and 8 weeks revealed an upward shift in the stress contribution of the fiber phase (inset, Figure 5.7).

Because of the anisotropy of fiber-reinforced materials, normal deformations may generate shear stresses when the deformed configuration is constrained to a rectangular form (as in uniaxial and biaxial tensile testing). The computed magnitude of shear stress (T_{12}) resulting from uniaxial extension (E_{11} = 0.10) varied nonlinearly with fiber angle for 1 day and 8 weeks (Figure 5.8A).

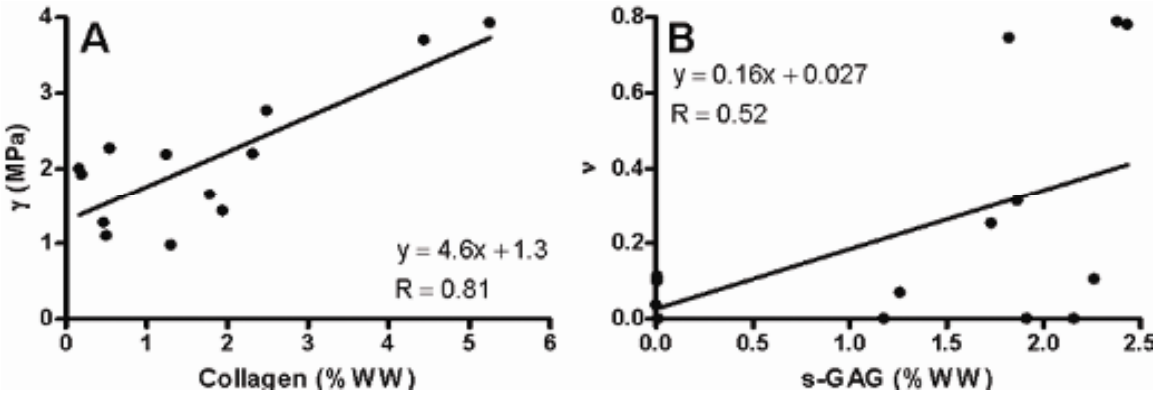

Figure 5.5 Significant correlations were observed between the fiber parameter γ and the collagen content (A) and between the matrix parameter v and the GAG content (B).

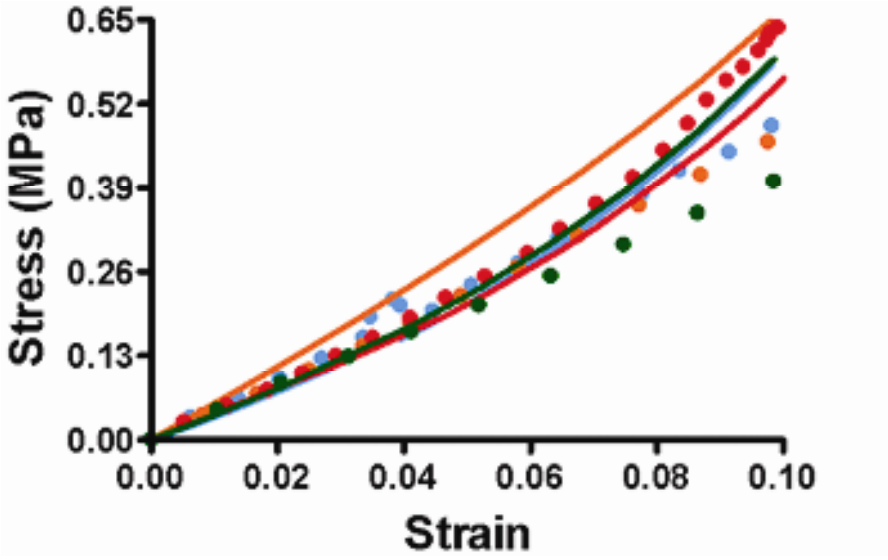

Figure 5.6 For 4 weeks, the model predicted stress-strain behavior at φ = 30^{o} (solid lines) agreed well with the experimentally measured stress (circles). Predicted and experimental curves for each sample are paired by color.

Interestingly, shear stress peaked at approximately $\varphi = 30^o$. Shear stress reduced to zero near $\varphi = 60^o$, implying that, at $E_{11} = 0.1$, fibers were predominantly in compression; however, at much larger strains, fiber reorientation will eventually reestablish tensile (nonzero) fiber stresses. While the magnitude of shear stress increased from 1 day to 8 weeks, the dependence of shear stress on fiber angle was similar. Computing the full stress-strain curve for $\varphi = 30^o$ revealed a time-dependent increase in slope and nonlinearity of the shear stress that accompanied uniaxial extension (Figure 5.8B). Similarly, equibiaxial extension in-plane with the fibers can generate shear stress when the fibers lie oblique to the loading axes. For $\varphi = 30^o$, equibiaxial extension induced a larger and more nonlinear shear stress response than uniaxial tension (Figure 5.8B). Simulating 1 day and 8 week responses illustrated that time-dependent effects were even more pronounced in biaxial tension.

Finally, an isochoric shear deformation was simulated for 1 day, 4 and 8 week AF constructs, with shearing along the x_1 direction for $\varphi = 30^o$ (inset, Figure 5.9A). A considerable increase in the stress response of AF constructs was observed for both normal and shear stresses (Figure 5.9A, B). Normal and shear stresses under shearing were similar in magnitude to uniaxial tensile tests along the fiber direction.

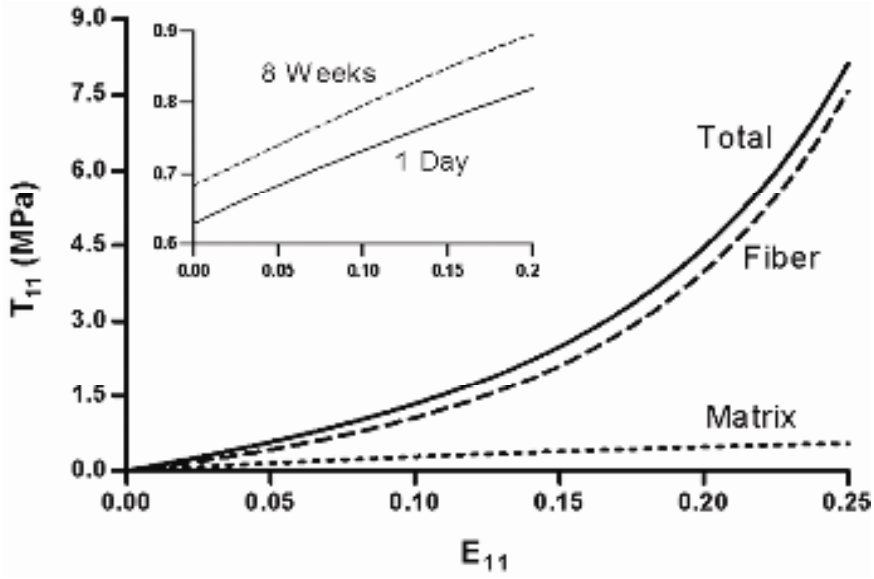

Figure 5.7 Uniaxial stress-strain response for φ = 30o at 8 weeks (Total), decomposed into matrix and fiber stresses. Inset: The fraction of total stress contributed by the fibers was computed at 1 day and 8 weeks.

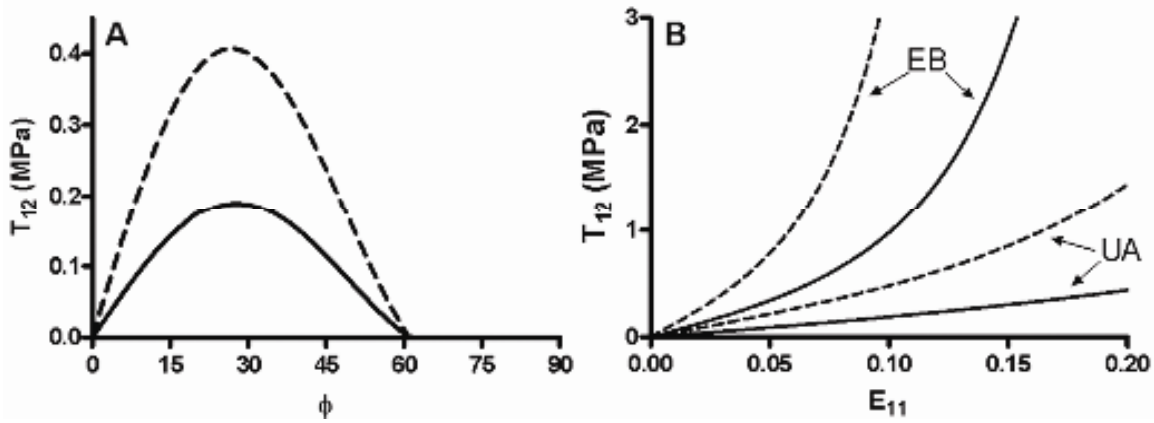

Figure 5.8 The dependence of shear stress T_{12} in uniaxial tension (computed at E_{11} = 0.10) on φ (A). Shear stress T_{12} associated with uniaxial (UA) and equibiaxial (EB) deformations (B). 1 day = solid lines, 8 weeks = dashed lines.

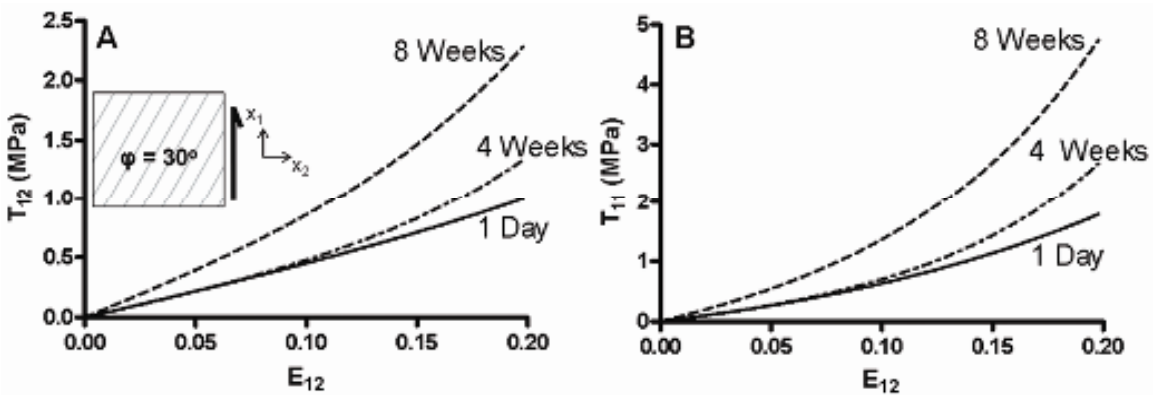

Figure 5.9 Simulation of shear deformation, shown schematically (A, inset) produced both shear (A) and normal (B) stress responses.

	ν_{13}			R^2			BA		
φ	*1 Day*	*4 Weeks*	*8 Weeks*	*1 Day*	*4 Weeks*	*8 Weeks*	*1 Day*	*4 Weeks*	*8 Weeks*
0°	1.10 ± 0.62	0.72 ± 0.29	0.69 ± 0.19	0.97 ± 0.03	0.98 ± 0.02	0.99 ± 0.01	-0.01± 0.05	0.01 ± 0.05	0.03 ± 0.10
30°	< 0.01	< 0.01	1.09 ± 0.78	0.98 ± 0.03	0.99 ± 0.01	0.98 ± 0.03	0.13 ± 0.16	0.02 ± 0.05	0.35 ± 0.2
90°	0.07 ± 0.04	0.20 ± 0.29	0.34 ± 0.34	0.99 ± 0.01	0.99 ± 0.01	0.98 ± 0.01	0.00 ± 0.02	0.00 ± 0.01	0.00 ± 0.01

Table 5.1 Poisson's ratio (ν_{13}) and goodness-of-fit parameters for each time point and orientation. Note that while φ = 0° and φ = 90°are model fits, φ = 30° is in fact a prediction, where model parameters are fixed and stress is simply computer from experimental strains, then compared to experimental stresses.

5.4 Discussion

This study integrated theoretical and experimental approaches for AF tissue engineering utilizing aligned electrospun nanofibrous scaffolds seeded with AF cells. We implemented a hyperelastic fiber-reinforced constitutive model to characterize the evolution of engineered AF constructs with time in culture. The constitutive model was successfully fit to stress-strain responses at each culture time point with nanofibrous scaffold orientations of $\varphi = 0^{o}$ and $\varphi = 90^{o}$, and then was validated by successfully predicting the stress-strain response of $\varphi = 30^{o}$ constructs at each time point.

A key advantage of this approach was that the nonlinear stress-strain behavior of engineered AF constructs was fully described by the model (Figure 5.1B). This is preferable to simply measuring linear modulus (Baker and Mauck 2007; Li, Mauck et al. 2007), as under physiological conditions the AF operates throughout the nonlinear regime of both the 'toe region' (or 'neutral zone') and 'linear region'. Another advantage is that the model material parameters have physical interpretations, representing mechanics of the extrafibrillar matrix (μ and ν) and fibrous extracellular matrix (γ and ξ). For instance, the observation that the linear region moduli increased over 8 weeks (Figure 5.2) simply implies general construct growth. However, the increase in γ with time suggests that AF cells deposited oriented collagen that contributed to construct mechanical function. This is supported by the correlation of the fiber parameter γ with the experimentally measured collagen content (Figure 5.5). Furthermore, although

significance was not achieved, an increase in fiber property ξ with time may suggest that the degree of nonlinearity increased with culture duration. This may represent a shift in load-bearing from the scaffold to the newly deposited collagen fibers, as PCL remains linearly elastic over the culture duration, while collagen increased with time in culture, and confers nonlinearity to most biological tissues (Lanir 1979; Fung 1982). The matrix parameters μ and v also increased with time in culture (although not significantly), indicating that AF cells deposited extrafibrillar extracellular matrix such as GAG, and that this newly deposited matrix also contributed to mechanical function. This is supported by the positive correlation between the model matrix parameter, v, and experimentally measured GAG. In uniaxial tension at $\varphi = 30^{o}$, the total stress response was largely dictated by the fiber phase (Figure 5.7) and the relative fiber contribution increased with construct growth (Figure 5.7 inset), implying that AF cells elaborated fibrous extracellular matrix that improved the tensile load bearing capacity of constructs with an anatomic fiber orientation.

In addition to physical interpretation of model parameters as above, another advantage of the validated constitutive model is the ability to investigate the effect of construct growth for loading configurations encountered under physiologic conditions that cannot be readily measured. Specifically, we considered 1) multi-axial stresses encountered in uniaxial and biaxial extension, and 2) shear loading. Uniaxial tensile testing of $\varphi \neq 0^{o}$ or 90° applies loads oblique to the fiber direction. This generates shear stresses in anisotropic materials because the grips are constrained to one-dimensional motion along the

loading axis, despite a tendency of the material to undergo rotations. In other words, uniaxial loading oblique to the fibers generates reaction stresses in the transverse directions of the crosshead, opposed by shear stresses in the material. Because these shear stresses increase with culture duration, it is likely that newly deposited extracellular matrix enhances fiber-matrix continuity, and thereby encourages fiber reorientation under load. This improved load transfer shields matrix and interfibrillar materials from large strains at low to moderate stresses by allowing the fibrillar components to bear more stress, even when the loading direction does not coincide with the prevailing fiber direction (as is common in the native AF *in vivo*). This shielding effect is a critical requirement in preventing failure of fiber-reinforced soft tissues under physiologic loading, as the formation of tears and fissures in the AF has been attributed, to some extent, to delaminations and debonding between the matrix and fibers (Iatridis and ap Gwynn 2004; Pezowicz, Schechtman et al. 2006). The magnitude of shear stress varied with fiber angle, and, interestingly, was highest near the anatomic fiber angle $\varphi = 30^{o}$ (Figure 5.8A). This result suggests that AF fibers may be optimally oriented to resist large circumferential strains of the disc, while also resisting other complex multi-axial deformations, including those occurring during torsion. In the engineered construct, this phenomenon was present in constructs at 1 Day, and was accentuated by extracellular matrix deposition with time in culture (Figure 5.8A, B). These changes may be indicative of improved load transfer between fibers and matrix in these developing constructs.

Although uniaxial tension is a standard test to evaluate material properties, it does not represent AF physiologic loading: freely contracting boundaries do not occur *in vivo* for the constrained AF. All AF loading, including disc compression and bending, generate AF biaxial loads. Much larger magnitudes of shear stress were observed under equibiaxial extension (Figure 5.8B). Like the uniaxial case, however, the shear stress for a given equibiaxial deformation increased from 1 day to 8 weeks of growth. This suggests that extracellular matrix deposition improved the performance of engineered AF under biaxial deformations. Finally, shear loading of the AF was modeled, representing torsion of the spine. We simulated the effect of a torsional motion of the spine on engineered AF as a shear stress applied 30^o from the fiber direction (Figure 5.9A, inset). The deformation produced nonzero shear and normal components of stress. Interestingly, the normal stresses T_{11} and T_{22} (not shown) were of similar magnitude to the shear stress T_{12}, although slightly larger, demonstrating that fibers resist shear deformations, even when the shearing direction does not coincide with the prevailing fiber direction. This result is in contrast to the notion that shear behavior of fiber-reinforced tissues is driven primarily by the matrix (Weiss, Gardiner et al. 2002). As with uniaxial and biaxial loading, time-dependent growth of constructs revealed an improvement in the shear response of engineered AF with time in culture. These simulations not only provide insight into the physical mechanisms of functional growth of cell-laden constructs, but also indicate that AF cells deposit extracellular matrix on aligned electrospun

scaffolds that improve function over a wide range of mechanical environments that are of direct relevance to the intervertebral disc *in vivo*.

Anisotropic increases in modulus indicate that AF cells preferentially deposit extracellular matrix under the directional guidance of the aligned nanofibrous scaffold. AF cells aligned along the scaffold fibers, with numerous actin stress fibers observed parallel to the fiber direction (Figure 5.3). During embryonic AF development and for various cell types *in vitro*, cellular orientation and actin patterning play an important role in the directional deposition of structurally organized extracellular matrix (Hayes, Benjamin et al. 1999; Hayes, Benjamin et al. 2001; Wang, Jia et al. 2003; Lee, Shin et al. 2005; Canty, Starborg et al. 2006). Similarly in this study, patterned extracellular matrix elaboration was evidenced by quantitative polarized light microscopy of sections in the scaffold fiber-plane, where the collagen fiber direction at 8 weeks closely mirrored the scaffold fiber direction. These results demonstrate that aligned electrospun scaffolds direct organized formation of new collagenous tissue by AF cells, and verify the model assumption that scaffold and collagen fiber orientations are defined by a single direction.

Of the three fiber orientations ($\varphi = 0^o$, 30^o, 90^o), the largest increase in modulus was observed along the fiber direction ($\varphi = 0^o$), where over 8 weeks the modulus increased by approximately 25 MPa to 43 MPa. Despite this large increase, the fiber direction linear modulus remains below that of a single lamella of the AF (80 – 100 MPa) (Skaggs, Weidenbaum et al. 1994; Holzapfel, Schulze-Bauer et al. 2005). This result is in contrast to the results presented in the

previous chapter, where no increase was observed for $\varphi = 0^{o}$. The difference is likely due to modifications to the testing protocol, including the use of serrated grips and optical surface strains to reduce the effects of grip slippage. Additionally, scaffold thickness was reduced from 1 mm to 250 μm to enhance the relative infiltration of AF cells into the scaffold.

5.5 Conclusion

In this study, we provided a framework for the rigorous functional evaluation of engineered AF, with specific application to the mechanics of a single lamella. Although tissue engineering treatments for degenerative disc disease remain beyond the realm of clinical practice, the current work may contribute to the development of annular patches for the treatment of disc herniation. Moreover, development of multilamellar fibrous constructs, when coupled with an engineered nucleus pulposus material (Chapter 8), may eventually lead to fully biologic intervertebral disc replacements.

In conclusion, this study integrated theoretical and experimental approaches for AF functional tissue engineering. We implemented a hyperelastic fiber-reinforced constitutive model to characterize the functional time-dependent evolution of engineered AF constructs. The constitutive model parameters elucidated AF fiber and matrix functional growth. The model was validated and then applied to simulate complex physiologically relevant loading configurations including shear strains in tensile loading, biaxial loading, and shear loading.

Finally, utilizing standard assays, we demonstrated that AF cells seeded on electrospun nanofibrous scaffolds elaborate aligned, organized disc-like extracellular matrix, correlating with measurable changes in mechanical behavior. While in Chapter 3 we determined that electrospun scaffolds are nonlinear and anisotropic, the present study indicates that cells on these scaffolds deposit matrix that enhances both nonlinearity and anisotropy of the construct. Having established here the effectiveness of electrospun nanofibrous scaffolds for engineering single lamellar AF-like tissue, the remaining chapters will focus on extrapolating these results to multi-lamellar AF constructs with opposing fiber orientations.

CHAPTER 6: NANOFIBROUS BIOLOGIC LAMINATES REPLICATE THE FORM AND FUNCTION OF THE ANNULUS FIBROSUS

6.1 Introduction

Successful engineering of load-bearing tissues requires recapitulation of their complex mechanical functions. Given the intimate relationship between function and form, biomimetic materials that replicate anatomic form are of great interest for tissue engineering applications. However, for complex tissues such as the annulus fibrosus, scaffolds have failed to capture their multi-scale structural hierarchy. Consequently, engineered tissues have yet to reach functional equivalence with their native counterparts. In the previous three chapters, we introduced electrospun scaffolds as a method for guiding tissue deposition by AF cells, resulting in measurable changes in mechanical function. In this chapter, we build on the previous work, presenting a novel strategy for annulus fibrosus tissue engineering that replicates the hierarchical, multi-lamellar organization of the AF with anisotropic nanofibrous laminates seeded with mesenchymal stem cells (MSCs). These scaffolds directed the deposition of organized, collagen-rich extracellular matrix that mimicked the angle-ply, multi-lamellar architecture and achieved mechanical parity with native tissue after 10 weeks of *in vitro* culture. Further, we identified a novel role for inter-lamellar

shearing in reinforcing the tensile response of biologic laminates, a mechanism that has not previously been considered for these tissues.

Function of the annulus fibrosus is predicated on a high degree of structural organization over multiple length scales: aligned bundles of collagen fibers reside within each lamella and the direction of alignment alternates from one lamella to the next by 30^{o} above and below the transverse plane (Cassidy, Hiltner et al. 1989). To date, numerous strategies have been proposed to engineer replacement tissues for the annulus fibrosus and the intervertebral disc (Kandel, Roberts et al. 2008). However, these studies have failed to replicate the angle-ply microstructure that is necessary for proper mechanical function of the native tissue. Indeed, these studies have shown, that in the absence of a scaffold that provides the appropriate structural – and perhaps mechanical – cues, cells are unable to spontaneously organize their extracellular matrix into highly specialized architectures like that of the annulus fibrosus. Consequently, no engineered tissue has successfully achieved mechanical properties that are commensurate with the native tissue. Therefore the overarching goal of the present work is to engineer a tissue that achieves functional parity with the annulus fibrosus by developing a strategy that mirrors the natural multi-scale organization of extracellular matrix within this tissue.

A successful strategy for the tissue engineering of load-bearing tissues must rely on the proper selection of biomaterial scaffolds, and their assembly into structures that replicate essential anatomic features of the tissue of interest (Mauck, Baker et al. 2009; Place, George et al. 2009). Therefore, in this study,

we used electrospun nanofibrous scaffolds seeded with MSCs to generate angle-ply multi-lamellar tissues that replicate the anatomic form of the annulus fibrosus. In contrast to scaffolds previously used for annulus fibrosus tissue engineering, which include hydrogels (Chiba, Andersson et al. 1997; Thonar, An et al. 2002) and macroporous synthetic (Wan, Feng et al. 2007; Chou, Reza et al. 2008) and natural (Gruber, Ingram et al. 2003; Chang, Kim et al. 2007) polymers, electrospinning permits the formation of arrays of aligned polymeric nanofibers, serving as a template for the deposition of a unidirectionally organized extracellular matrix by resident cells (Chapters 3 – 5). In the present work, engineered bi-lamellar tissues reached mechanical equivalence with the annulus fibrosus after 10 weeks of *in vitro* culture and revealed a potential role for inter-lamellar shearing as a mechanism of tensile reinforcement for biologic laminates. In addition to advancing the field of annulus fibrosus tissue engineering, these findings provide insight into the relation of form and function in biologic laminates, with implications for other orthopaedic and cardiovascular tissues.

6.2 Materials and Methods

6.2.1 Nanofibrous Scaffold Fabrication

Aligned nanofibrous scaffolds were generated via electrospinning as described in previous chapters and elsewhere, with some modification (Baker and Mauck 2007). Briefly, PCL was dissolved at 143 mg/mL in equal parts tetrahydrofuran and N, N-dimethylformamide, then extruded at 2.5 mL/h via

syringe pump through a spinneret charged to +13 kV. This is in contrast to previous chapters, where the flow rate of PCL was determined by hydrostatic pressure of the PCL itself. The resulting nanofibrous jet was collected on a grounded mandrel (~2.5 inches diameter) rotating at 10 m/s and located 20 cm from the spinneret. Aluminum shields on either side of the spinneret were charged to +9 kV to focus the jet toward the mandrel. Due to the increased diameter of the mandrel, these shields were necessary to overcome the dispersive effects of air flow generated by the mandrel. The spinneret was fanned back and forth to ensure uniform fiber deposition axially along the mandrel (Baker, Gee et al. 2008).

6.2.2 Isolation of bovine MSCs

MSCs were isolated from bone marrow obtained from juvenile (3 – 6 month old) bovine knee joints as described in Chapter 4. Briefly, marrow was plated in basal media, and colony formation observed within 1-2 weeks. Bone debris were removed with subsequent media changes. Cells were filtered at first passage, and expanded to passage 2 as described in previous chapters for AF cells.

6.2.3 Seeding of Nanofibrous Scaffolds with MSCs and bilayer formation

Scaffolds were seeded with passage 2 MSCs as described in Chapter 4. Briefly, scaffolds were sterilized and hydrated, and coated with fibronectin,. 1 x 10^6 cells were applied to the scaffold and samples were transferred to chemically

defined media (DMEM, 0.1μM dexamethasone, 40 μg/mL L-Proline, 100 μg/mL Sodium Pyruvate, 1% Insulin, Transferrin, Selenium/Premix, and 1% penicillin, streptomycin and fungizone supplemented with 10 ng/mL Transforming Growth Factor β3) (Mauck, Yuan et al. 2006). Media was replaced twice weekly for the duration of the study. After two weeks of culture as single layers, bilamellar constructs were formed by layering two scaffolds between pieces of porous polypropelene and wrapping with a foil sleeve. Constructs were returned to culture and external constraints removed two weeks later.

6.2.4 Uniaxial Tensile Testing and Biochemical Analyses

As in Chapter 4, cross-sectional area was measured using a custom laser device that provided accurate, noncontact measurements of thickness and width (Peltz, Perry et al. 2009). Samples (n = 5) were clamped with serrated grips and loaded into an Instron 5542 testing device. Gauge length was determined as the distance between grips. All testing was performed in a PBS bath. The mechanical testing protocol was identical to previous chapters, and consisted of: (1) a nominal tare load of 0.1N applied at 0.1% strain/sec, followed by stress relaxation for 5 minutes, (2) 15 preconditioning cycles to 0.1% strain at 0.05% strain/sec, and (3) a quasi-static elongation at 0.1% strain/sec until failure. Strain was determined as extension normalized to gauge length; stress was computed as the load normalized to initial cross-sectional area. Modulus was computed as the slope of the stress-strain plot, determined by regression to the linear portion of the curve.

For biochemical analyses, samples were digested for 16 hours in papain at 60°C, then analyzed for GAG content using the 1,9-dimethylmethylene blue dye-binding assay, for orthohydroxyproline (OHP) content (after acid hydrolysis) to determine collagen content by reaction with chloramine T and dimethylaminobenzaldehyde, and for DNA content using the PicoGreen dsDNA Quantification kit (see Chapters 3 - 5). Unlike previous chapters, where a ratio of 1:10 was used, OHP content was converted to collagen with a ratio of 1 : 7.14 (OHP:collagen) (Neuman and Logan 1950; Mauck, Yuan et al. 2006).

6.2.5 Histology

Samples (n=3) were cryo-sectioned as described in the previous two chapters. Briefly, samples were embedded in OCT freezing medium and sectioned to 8 μm thick slices by cryotomed. Sections were fixed with 4% paraformaldehyde in PBS and stained for cell nuclei (40,6-diamidino-2-phenylindole, DAPI), glycoasaminoglycans (Alcian Blue) and collagen (Picrosirius Red). DAPI-stained sections were visualized at 20× on a Nikon T30 inverted fluorescent microscope. Alcian Blue and Picrosirius Red stains were visualized on an upright Leica DMLP microscope. Annulus fibrosus from skeletally mature bovine caudal discs were processed identically. Quantitative polarized light microscopy was performed on Picrosirius Red stained sections to quantify collagen alignment as described in Chapter 4 and elsewhere (Thomopoulos, Williams et al. 2003). Briefly, grayscale images were collected (20×) at 10° increments using a green bandpass filter (BP 546 nm) with crossed

analyzer and polarizer coordinately rotated through 90°. This was repeated with the filter replaced by a λ compensator. Custom software was then used to determine collagen fiber orientations for a series of nodes within the central portion of each region of interest. This analysis was performed on sections taken slightly out of the lamination plane in order to obtain sections that simultaneously passed through each lamella as well as the interlamellar space.

6.2.6 Bilayer Lap Testing

Nanofibrous scaffolds of approximately 1 mm thickness were prepared as above and excised along the fiber direction. Two weeks of after seeding with MSCs, samples (n = 5) were placed in apposition with a 20 mm overlap and secured with porous polypropylene and foil and cultured as above. Lap tests were performed by gripping the overhang on either end of the bilayer and extending to failure at 0.2 mm/s. Interface strength was determined from the maximum force normalized to overlap area.

6.2.7 Acellular Bilayers

Aligned nanofibrous scaffolds of approximately 1 mm thickness were excised at 30^{o} from the fiber direction. Agarose was dissolved in PBS at 2, 4, 5, and 6% w/v and melted by autoclaving. Molten agarose (40^{o} C) was applied to the surface of one scaffold before the addition of a second layer of scaffold, and allowed to set at room temperature. This method was used to create bilayers with both Parallel and Opposing fiber orientations for each of the six agarose

concentrations. No significant difference was observed in cross sectional area across all concentrations, indicating controlled, reproducible interface formation for all bilayers. Resulting bilayers (n = 5) were tested in uniaxial tension as described above.

6.2.8 Statistics

Significance was established by $p \leq 0.05$ as determined by two-way ANOVA with a Tukey's post hoc test for independent variables of bilayer orientation (Parallel/Opposing) and culture duration (or agarose concentration). All data are reported as mean ± standard deviation. A complete biologic replicate was completed for all experiments, confirming the obtained results.

6.3 Results

To replicate the structural hierarchy of the annulus fibrosus, bi-lamellar tissue constructs were formed first as single lamellar tissues from aligned nanofibrous scaffolds seeded with MSCs, and then formed into bilayers after two weeks of *in vitro* culture. MSCs were used in place of annulus fibrosus cells (Chapters 3, 5) due to the clinical limitations associated with the latter; specifically, it remains uncertain whether healthy cells can be isolated from degenerate discs, while isolation from healthy discs may result in donor site morbidity. In contrast, MSCs are multipotent and can be readily isolated from

bone marrow aspirate, making them an attractive cell source for engineering a

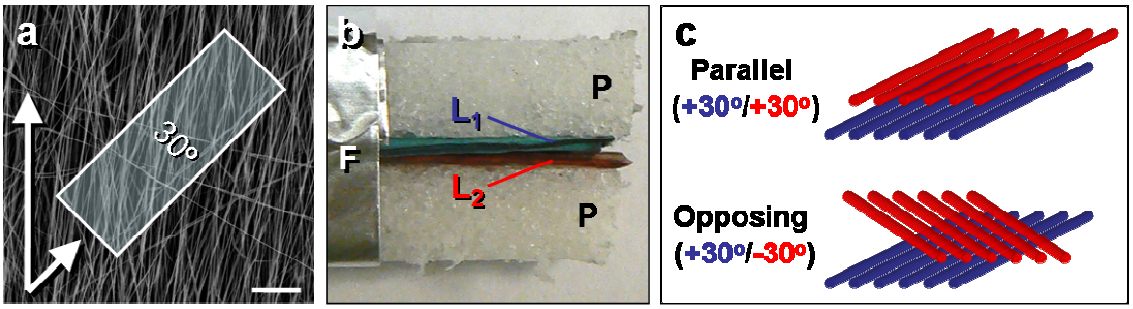

Figure 6.1 Fabrication of bi-lamellar tissue constructs. Scaffolds were excised 30° from the prevailing fiber direction of electrospun nanofibrous mats to replicate the oblique collagen orientation within a single lamella of the annulus fibrosus (A). At 0 weeks, MSC-seeded scaffolds were formed into bilayers between pieces of porous polypropylene and wrapped with a foil sleeve (B). Bilayers were oriented with either Parallel (+30°/+30°) or Opposing (+30°/-30°) fiber alignment relative to the long axis of the scaffold (C). P = porous polypropylene; F = foil; $L_{1/2}$ = lamella 1/2. Scale = 25 μm (a).

broad range of tissues (Caplan 1991; Pittenger, Mackay et al. 1999). Planar sheets of scaffolds were fabricated by electrospinning poly(ε-caprolactone) (PCL) onto a rotating mandrel to instill alignment among the collecting fibers. Mats of ~250 μm thickness were electrospun to match the natural lamellar thickness of the annulus fibrosus (Marchand and Ahmed 1990). PCL was employed due to its slow degradation rate, ability to be readily formed into nanofibers, and its proven potential for *in vivo* application (Li, Chiang et al. 2009). Moreover, we showed in Chapter 3 that aligned electrospun PCL meshes mimic the anisotropy and nonlinearity of fiber-reinforced soft tissues, and undergo finite elastic deformations.

Rectangular scaffolds (5 mm x 30 mm) were excised from the nanofibrous mat with their long axis rotated 30° from the prevailing fiber direction. This produces aligned scaffolds whose fiber angle (Figure 6.1A) reflects the oblique

alignment of collagen fibers within a single lamella of the annulus fibrosus. These single lamellar scaffolds were seeded with bovine MSCs and cultured *in vitro* in a media formulation supportive of fibrocartilagenous differentiation (Chapter 4). After two weeks, lamellae were brought into apposition between pieces of porous polypropylene and wrapped with a foil sleeve (0 weeks, Figure 6.1B). Bilayers were formed with the nanofibers in adjacent lamellae running either parallel at $+30^{o}$ (Parallel) or in opposing directions of $+30^{o}$ and -30^{o} (Opposing,Figure 6.1C). After two additional weeks of culture, the external supports were removed and laminates remained intact.

Biochemical analyses through 10 weeks of *in vitro* culture revealed significant accumulation of sulphated glycosaminoglycans (Figure 6.2A,D) and collagen (Figure 6.2B,E), two of the primary extracellular components of the annulus fibrosus, within both Parallel and Opposing bilayers. In the two weeks preceding bilayer formation, cells began infiltrating through the thickness with a dense cell layer at the scaffold periphery (not shown). After bilayer formation, these outer cell layers fused in the contacting region between two lamellae, forming a thin inter-lamellar space that became more pronounced with culture duration (asterisk, Figure 6.2C-E). Glycosaminoglycans and collagen were distributed throughout each lamella, and within this inter-lamellar space, indicating the successful formation of a biologic interface between the two layers (Figure 6.2C, D). MSCs infiltrated into the scaffold, but remained most densely populated at the surfaces (Figure 6.2E). No differences in cell, glycosaminoglycan or collagen quantity and localization were observed between

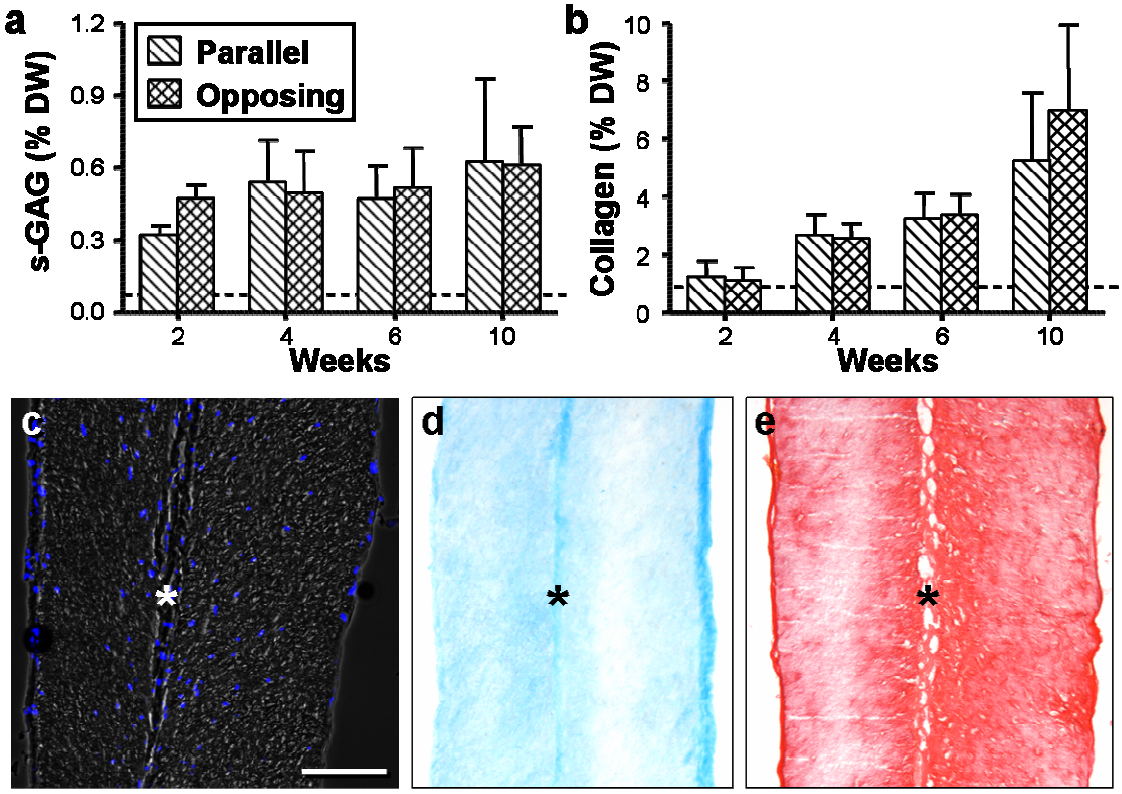

Figure 6.2 Elaboration of extracellular matrix within bilayers seeded with mesenchymal stem cells. Sulphated glycosaminoglycan (GAG, A) and collagen (B) content of Parallel and Opposing bilayers increased with culture duration ($p \leq 0.05$). There were no significant differences between Parallel and Opposing bilayers at any time point. Alcian Blue (C), Picrosirius Red (D), and DAPI (E) staining of Opposing bilayer cross-sections after 10 weeks of in vitro culture. DW = dry weight. Dashed line indicates content at 0 weeks, when bilayers were formed. Error bars (A, B) represent the standard deviation of the mean. * indicates inter-lamellar space. Scale bar = 250 µm (C, D), 200 µm (E).

Parallel and Opposing bilayers, nor were any differences observed compared to single lamella constructs maintained under identical culture conditions (normalized to dry weight, not shown). This indicates that altering the direction of alignment of one lamella relative to the other did not affect cell biosynthesis and that culture in the thicker, two-lamella format did not diminish *in vitro* growth relative to single lamella constructs. Despite abundant deposition of extracellular

matrix molecules, collagen and glycosaminoglycan contents remained less than the native annulus fibrosus. It is possible that some form of mechanical stimulation (Gokorsch, Weber et al. 2005; Neidlinger-Wilke, Wurtz et al. 2005; Reza and Nicoll 2008) or *in vivo* implantation(Mizuno, Roy et al. 2006) may be necessary to generate native tissue composition in a clinically relevant time frame.

We next examined collagen organization in matured constructs. Parallel and Opposing bilayers were visualized obliquely to observe collagen alignment simultaneously across layers (Figure 6.3A). When stained for collagen and viewed by polarized light microscopy, intra-lamellar collagen was highly birefringent in both Parallel (Figure 6.3B) and Opposing (Figure 6.3C) bilayers, indicating that collagen was aligned with the underlying nanofibrous scaffold. Collagen deposited into the inter-lamellar region, however, was disorganized. As indicated by the hue of birefringence, intra-lamellar collagen was co-aligned within Parallel bilayers and oriented along two opposing directions for Opposing bilayers. Additionally, collagen organization within Opposing bilayers compared favorably with similarly prepared sections of annulus fibrosus (Figure 6.3D), indicating successful replication of the multi-scale collagen architecture of the native tissue. Importantly, disorganized inter-lamellar matrix was also observed in the native annulus fibrosus, as has been shown previously (Smith and Fazzalari 2006).

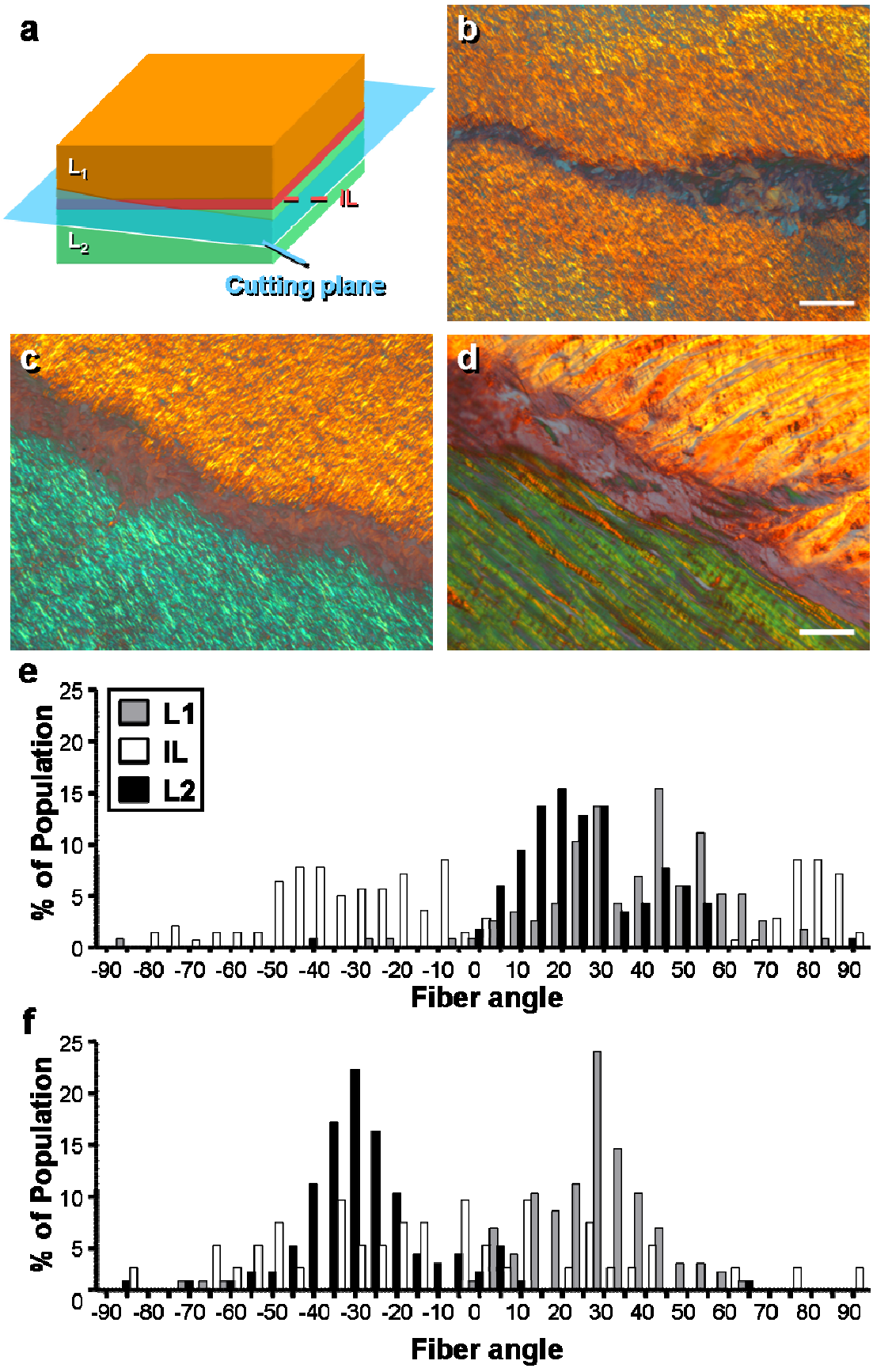
a
L1
IL
L2
Cutting plane
b
c
d
e
% of Population
L1
IL
L2
Fiber angle
f
% of Population
Fiber angle

Figure 6.3 Angle-ply collagen alignment and orientation. Sections were collected obliquely across lamellae (A), stained with Picrosirius Red, and viewed under polarized light microscopy to visualize collagen organization. When viewed under crossed polarizers, birefringent intensity indicates the degree of alignment of the specimen, while the hue of birefringence indicates the direction of alignment. After 10 weeks of in vitro culture, Parallel bilayers contained co-aligned intra-lamellar collagen within each lamella (B). Opposing bilayers contained intra-lamellar collagen aligned along two opposing directions (C), successfully replicating the gross fiber orientation of native bovine annulus fibrosus (D). In engineered bilayers, as well as the native annulus fibrosus, a thin layer of disorganized (nonbirefringent) collagen was observed at the lamellar interface (denoted by *). The distribution of collagen fiber orientations was determined by quantitative polarized light analysis(Thomopoulos, Williams et al. 2003). Prominent peaks in fiber alignment were observed near 30^{o} in both lamellae of Parallel bilayers (E); however in Opposing bilayers two fiber populations were observed, aligned along +30^{o} and -30^{o} (F). Scale bar = 200 μm (B, C), 100 μm (D). L1/2 = Lamella 1/2; IL = Inter-lamellar space.

Quantitative polarized light analysis confirmed co-alignment of intra-lamellar collagen in Parallel bilayers, indicated by overlapping fiber populations (Figure 6.3E) at approximately +30^{o} from the long axis. However, fiber populations within Opposing bilayers demonstrated two distinct peaks in orientation: +30^{o} and -30^{o} from the long axis. For both Parallel and Opposing bilayers, inter-lamellar matrix orientations were widely distributed with no single distinct peak, confirming lack of alignment in this region. Opposing bilayers present the first instance in which an engineered tissue has successfully replicated the angle-ply laminate architecture of the annulus fibrosus. Despite successful replication of major architectural features, it is also apparent from the histologic comparison above that some intra-lamellar characteristics of collagen organization, such as crimp and fibril bundling, were not replicated by the

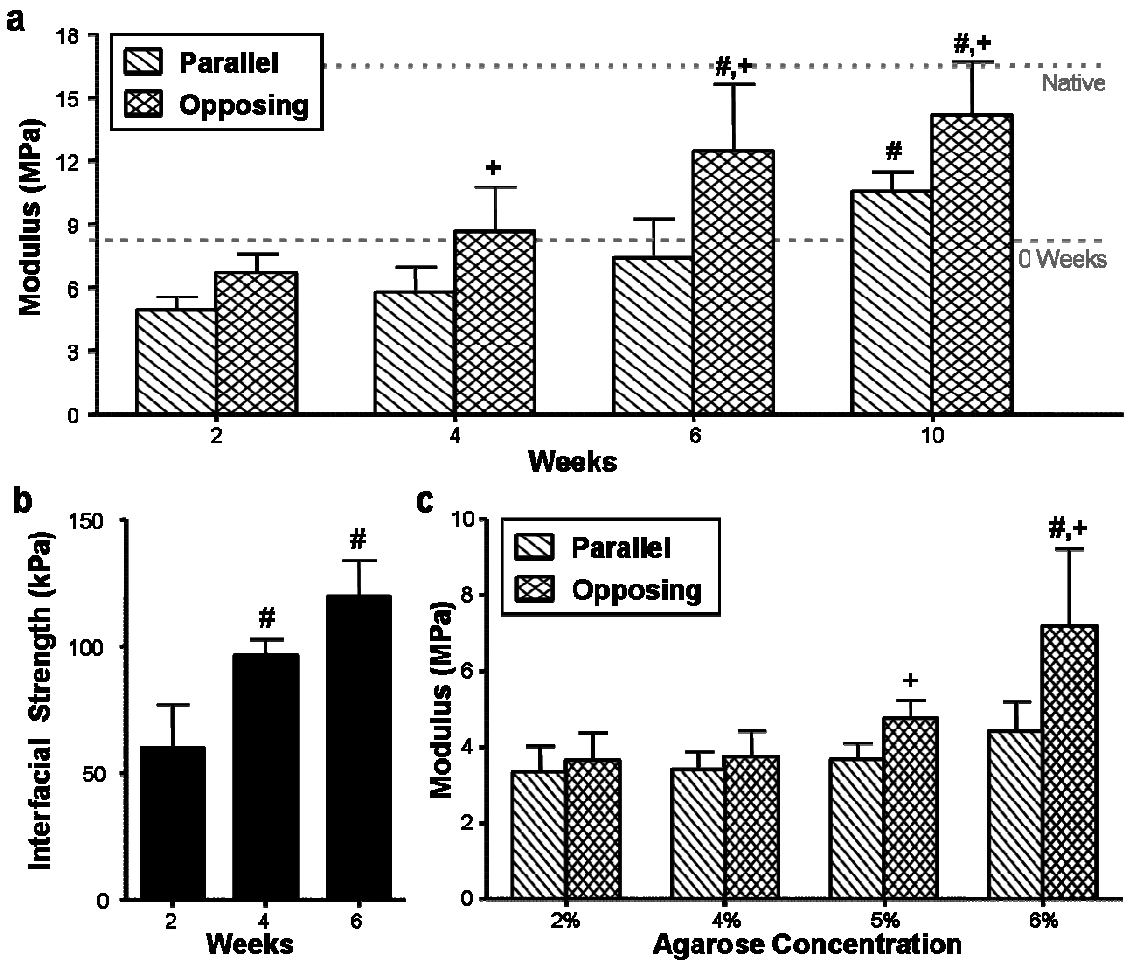

Figure 6.4 Relating inter-lamellar mechanics with the tensile response of biologic laminates. Uniaxial tensile moduli of MSC-seeded Parallel and Opposing bilayers increased with in vitro culture duration, with Opposing bilayers achieving significantly higher moduli than Parallel bilayers from 4 weeks onward (A). # = p ≤ 0.05 compared to single lamellar modulus at 0 weeks. + = p ≤ 0.05 compared to Parallel modulus. Native = circumferential tensile modulus of native human AF (Elliott and Setton 2001). Lap testing of MSC-seeded laminates showed increasing interface strength with in vitro culture duration (B). # = p ≤ 0.05 compared to 2 weeks. To elucidate the role of interface properties on the tensile response of bilayers, uniaxial tensile testing was performed on acellular bilayers formed from nanofibrous scaffolds bonded together by agarose of increasing concentrations (C). Increasing inter-lamellar agarose concentration – and hence inter-lamellar stiffness – significantly increased the tensile modulus of acellular Opposing bilayers, but had no effect on the Parallel bilayer group. # = p ≤ 0.05 compared to orientation-matched 2% agarose. + = p ≤ 0.05 compared to concentration-matched Parallel bilayers. All error bars (A-C) represent standard deviations of the mean.

engineered construct. It is currently not known how MSCs can be induced to replicate these fine features, ubiquitous throughout connective tissues of the body. Nonetheless, an advanced understanding of how collagen crimp and fiber bundling arise during development, and how they can be recreated *in vitro*, will likely play an important role in the future of tissue engineering for load-bearing soft tissues.

We next determined whether replication of anatomic form translates to enhanced mechanical function of these biologic laminates. Because the annulus fibrosus is subjected to large circumferential tensile stresses during *in vivo* compression of the intervertebral disc, a primary objective of this study was to generate an engineered tissue with a uniaxial tensile modulus of similar magnitude to the tensile modulus of the native tissue along its circumferential direction. For both Parallel and Opposing bilayers, tensile moduli increased with culture duration when compared to single lamellar moduli at the time of bilayer formation (0 weeks, Figure 6.4A). In the first few weeks after apposition, a reduction in modulus was observed due to swelling; stiffness steadily increased for both groups for all time points (not shown). Interestingly, Opposing bilayer moduli were significantly greater than Parallel bilayers by as early as 4 weeks, and remained higher through completion of the study at 10 weeks ($p \leq 0.05$). In fact, Opposing (14.2 ± 2.5 MPa) – but not Parallel (10.6 ± 0.9 MPa) – bilayers achieved a tensile modulus by 10 weeks that approximates the circumferential tensile modulus of the annulus fibrosus to within 15% (17.3 MPa) (Elliott and

Setton 2001). This is, to date, the closest an engineered tissue has come to matching the tensile properties of the annulus fibrosus (Table 2.2, Chapter 2).

The disparity in mechanical function between Parallel and Opposing bilayers, despite compositional equivalence, suggests that when the two fiber populations are combined in opposition, the resulting laminate is stiffer than if the same two fiber populations coincide. For this to be true, it is necessary that fiber populations interact across the interface, and do so in an orientation-dependent manner. Because interaction across lamellae requires that they be bonded together, we next sought to determine the role of inter-lamellar matrix in the macroscopic tensile response of biologic laminates. As this stiffening effect was not observed initially, but instead developed with time in culture, it is likely that a sufficiently strong interface must exist for this reinforcement to occur. Therefore, we examined the evolution of interfacial strength over time by performing lap tests on MSC-seeded nanofibrous bilayers. In order to isolate the functional properties of the interface, intra-lamellar deformations were reduced by: (1) using thicker (1 mm) scaffolds and (2) aligning nanofibers parallel to the loading axis in both lamellae. Scaffolds of this size and orientation were two orders of magnitude stiffer than the interface, allowing direct measurement of interfacial properties with minimal intra-lamellar deformation. Indeed, failure occurred consistently at the interface. Interfacial strength increased by nearly 3-fold within the first six weeks after bilayer formation (Figure 6.4B). This suggests that while after 2 weeks of *in vitro* culture, load can be transmitted across the inter-lamellar space, the strength of bonding continues to increase with culture duration. This supports

the potential role for lamellar bonding in explaining the functional disparity between Parallel and Opposing bilayers.

It is well established from studies on fiber-reinforced materials, including electrospun scaffolds (Stella, Liao et al. 2008) and fibrous soft tissues such as the annulus fibrosus (Guerin and Elliott 2006), that fibers re-orient under external forces toward the direction in which loads are applied. Therefore in Opposing bilayers, uniaxial tension induces counter-clockwise fiber rotation in one lamella (L1, Figure 6.5, top) while simultaneously inducing the fibers to rotate clockwise in the adjacent lamella (L2, Figure 6.5). Fiber rotation along two opposing directions would require the movement of one lamella against the other, shearing the inter-lamellar space (IL,Figure 6.5). Therefore, by enhancing the strength of bonding across the two lamellae, the inter-lamellar matrix may resist the local deformations associated with fiber re-orientation, thereby reinforcing the overall tensile response. However, in the case of Parallel bilayers (Figure 6.5, bottom), the fibers within the two lamellae reorient identically, and no shearing of the inter-lamellar space occurs. Because the bonding strength between the two layers increases with culture duration, it is likely that at 2 weeks, no difference was observed between Parallel and Opposing bilayer moduli because the interface was weak and newly formed; however, with increasing culture duration, the disparity in bilayer tensile moduli increased due to improved inter-lamellar bonding, generating a stronger resistance to inter-lamellar shearing.

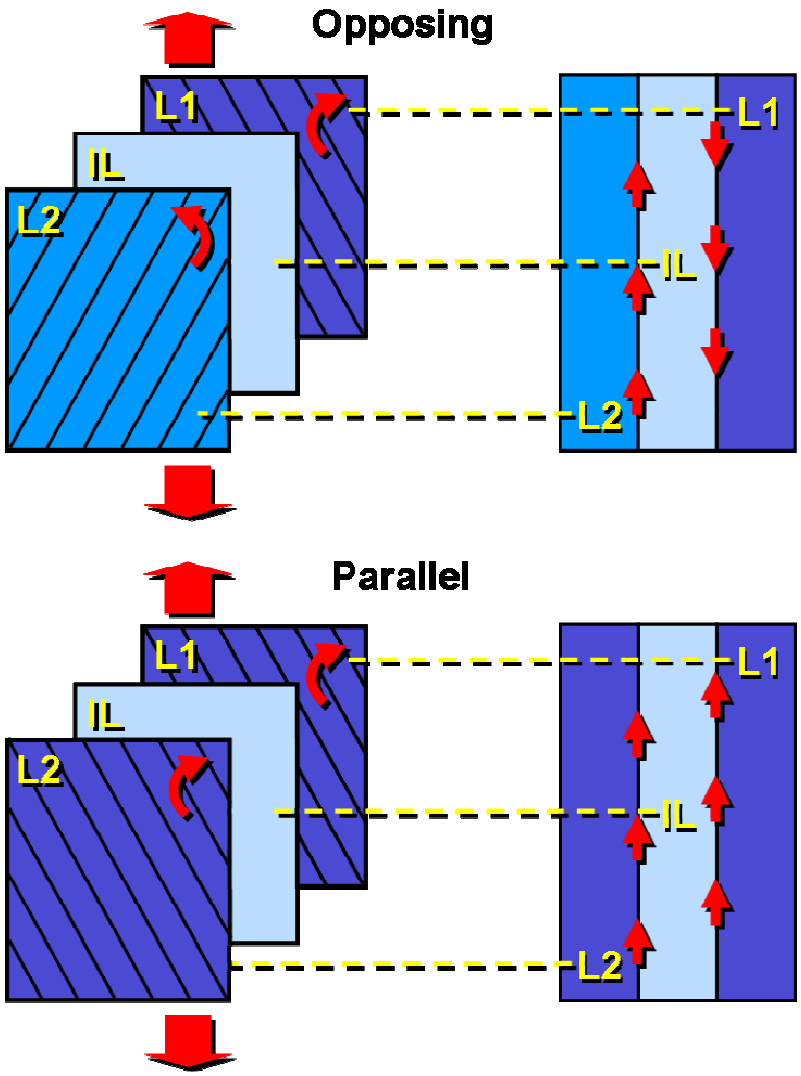

Figure 6.5. A novel mechanism for tensile reinforcement by inter-lamellar shearing of biologic laminates. In Opposing bilayers (top), fibers within each lamella reorient under uniaxial load by rotating (red arrowheads) toward the loading direction. The opposing direction of rotation between lamellae generates shearing of the inter-lamellar matrix. However, in Parallel bilayers (bottom) fibers reorient identically in the two lamellae, and therefore do not shear the inter-lamellar space. L1/2 = Lamellae 1/2; IL = Inter-lamellar space.

While this proposed mechanism is consistent with the stiffening of Opposing bilayers relative to Parallel bilayers, a confirmatory *acellular* study was conducted to isolate the role of inter-lamellar bonding in the mechanical response of biomimetic laminates. This simpler system, which consisted of aligned

electrospun lamellae bonded together by varying concentrations of agarose, permitted the variation of interfacial mechanics without the ambiguity introduced by cell-generated extracellular matrix. The tensile stiffness of agarose is of similar magnitude to the interfacial strength measured above (~100 kPa), and bonding strength can be readily manipulated by altering the gel concentration. Consistent with the proposed mechanism (Figure 6.5), Opposing bilayer modulus increased with increasing agarose concentration ($p \leq 0.05$) and hence inter-lamellar bonding strength, while Parallel bilayers were unchanged (Figure 6.4C). It is notable that while the modulus of agarose alone increases only on the order of a 0.1 MPa with increasing concentration from 2% to 6% (Huang, Yeger-McKeever et al. 2008), the Opposing bilayer modulus increased by 3.5 MPa. Therefore, we conclude that the increase in Opposing bilayer modulus results, not simply from the presence of stiffer inter-lamellar agarose (which would have produced similar changes in Parallel bilayers), but specifically from an increased resistance to shearing as fibers reorient under load. These results confirm the importance of inter-lamellar shearing interactions in reinforcing the tensile response of angle-ply biologic laminates.

6.4 Discussion

Given the structural similarity between Opposing bilayers and the annulus fibrosus (Figure 6.4C, D), it is reasonable to posit that such a mechanism of reinforcement is important for function of the annulus fibrosus as well. While the

structure, composition, and function of its *inter*-lamellar matrix are not well defined, recent work suggests that each is quite complex. Elastin (Smith and Fazzalari 2006), lubricin (Shine and Spector 2008), and collagen type VI (Melrose, Smith et al. 2007) have been detected at lamellar boundaries and microscopy studies suggest that there may be an intricate network of fibrous channels bridging adjacent lamellae (Veres, Robertson et al. 2008). Functionally, however, much less is known about the inter-lamellar matrix of the annulus fibrosus. Recent work suggests that the force required to shear across adjacent lamellae of the annulus is much larger than that required to induce shearing across fibers within a single lamella (Michalek, Buckley et al. 2009). This suggests that bonding across adjacent lamellae, and therefore the proposed mechanism, may be quite important *in vivo*. As a result, the findings of the current work may provide key insight into the relation of form and function in the annulus fibrosus. Because the annulus must simultaneously withstand stresses due to axial loading of the spine as well as torsion, it is possible that the annulus fibrosus is structurally optimized to do so through a combination of collagen fiber stretch and inter-lamellar shearing. This is a unique consequence of its angle-ply organization. Moreover, while inter-lamellar shearing is considered here in the context of the annulus fibrosus and annulus-mimetic engineered tissues, fiber-reinforced laminates are prevalent throughout the body, suggesting that these findings may have implications for other angle-ply laminates, including blood vessels (Rhodin 1980), cornea (Maurice 1957), rotator cuff tendon (Clark and Harryman 1992), urinary bladder wall, diaphragm, and the knee meniscus

(Petersen and Tillmann 1998). To our knowledge, a reinforcement mechanism of the form described here (Figure 6.5) has not previously been proposed or investigated for these or other fiber-reinforced biologic laminates. This finding illustrates how biomimetic materials and engineered tissues can serve as simple analogs for complex tissues, providing key insights into the structure-function relationships of their complex native counterparts.

In the present work, tissue engineered MSC-derived annulus fibrosus bilayers were formed that, after a period of *in vitro* culture, matched native tissue properties and revealed a novel mechanism of reinforcement in angle-ply biologic laminates. Despite this, it should be noted that the base material employed herein (a slow-degrading polyester) was not optimized for tissue formation. Over the last decade, fervent interest in electrospinning for tissue engineering applications has generated an expanding palette of materials for electrospinning, including biologic polymers that themselves can influence the behavior of cells and can be manipulated by cells via natural catabolic mechanisms (Shields, Beckman et al. 2004; McManus, Boland et al. 2007; Zhang, Baughman et al. 2008). These new materials and their combinations (for example composites formed by co- electrospinning multiple polymers simultaneously) can produce scaffolds of a wide range of mechanical, structural, and degradation characteristics. These materials can be tailored to enhance porosity, mechanics, and degradation rates for application-specific properties, and thereby improve tissue formation (Baker, Gee et al. 2008; Baker, Nerurkar et al. 2009). Employing

these methods may further expedite tissue formation based on the angle-ply predicate.

While the tissue generated in this study replicates the form and function of the annulus fibrosus, there remain several formidable challenges that must be addressed as tissue engineering progresses to clinical implementation for the treatment of damaged or degenerate discs. Translation from the present *in vitro* work to an *in vivo* surgical model will ultimately require integration with the surrounding annular tissue. If loads cannot be effectively transmitted across the engineered-native tissue interface, the engineered tissue will do little to protect the disc from further damage, regardless of its functional properties. MSC-seeded nanofibrous scaffolds do integrate with other fibrocartilagenous tissues in vitro (Sheth, Baker et al. 2007) and in vivo (Li, Chiang et al. 2009); however, it remains to be determined whether this will occur for the annulus fibrosus under *in vivo* loading conditions. While in the present work, we matched annulus fibrosus tensile properties, due to the complexity of the intervertebral disc there is no consensus on what other functional measures must be attained, and to what extent, before proceeding to *in vivo* implantation. Because degeneration is thought to initiate from poor nutrient and waste exchange in the largely avascular intervertebral disc, diffusion limited growth may hamper the scaling of the current approach to geometries that are relevant for clinical implementation. Indeed, it is likely that a combination of *in vitro* strategies (such as deformational loading bioreactors to enhance nutrient transfer and tissue deposition) and post-operative measures (such as immobilization to allow integration) will be

necessary to overcome these obstacles. Despite these considerable hurdles, the present study marks a significant advance in our understanding of biologic laminates such as the annulus fibrosus, and provides a rational approach to the generation of hierarchically and functionally equivalent replacement tissues.

6.5 Conclusions

In this chapter, we progressed along the multi-scale hierarchy of the annulus fibrosus from single lamellar tissues that mimic the intra-lamellar collagen organization of the native tissue (Chapters 3 – 5) to bi-lamellar tissues with opposing, angle-ply collagen alignment. The discovery of a novel inter-lamellar shearing mechanism indicates that the constitutive model applied in Chapter 5 to characterize single lamellar mechanics will not be sufficient to characterize the complex mechanics of these bilayers. Modifications to account for this behavior will be investigated in Chapter 7 before proceeding to the application electrospun scaffolds for the formation of whole disc composites with a central nucleus pulposus surrounded by an angle-ply, electrospun annulus fibrosus in Chapter 8.

CHAPTER 7: A HYPERELASTIC MODEL FOR INTER-LAMELLAR SHEARING IN ENGINEERED NANOFIBROUS BIOLOGIC LAMINATES

7.1 Introduction

In the previous chapter, electrospun scaffolds were seeded with mesenchymal stem cells (MSCs) and formed into nanofibrous biologic laminates. MSCs deposited an oriented collagen-rich extracellular matrix, resulting in an engineered tissue that replicated the angle-ply collagen alignment of the native annulus fibrosus (AF). This included opposing +/-30^{o} intra-lamellar collagen within adjacent layers, as well as a thin layer of disorganized collagen forming the interface between the layers. This interface was also observed in sections of native annulus fibrosus and has been noted by others as well (Smith and Fazzalari 2006). In Chapter 6, we determined that this interlamellar material plays an important role in the tensile response of the construct, whereby uniaxial loading in the plane of the fibers (perpendicular to the direction of lamination) results in shearing of the interlamellar space as fibers reorient along opposing directions in two adjacent lamellae (Chapter 6). Consequently, opposing (angle-ply) bilayers reached with 15% of the tensile modulus of native tissue while parallel bilayers, where no interlamellar shearing takes place, failed to achieve parity with native tissue and were significantly lower in modulus than opposing bilayers.

In Chapter 5, a hyperelastic constitutive model was applied and validated for single lamellar AF constructs formed from AF cell-seeded nanofibrous scaffolds. The model made use of the additive decomposition of the strain energy function (W) of the composite into the sum of martrix (W_m) and fiber (W_f) strain energy functions (Spencer 1972; Wagner and Lotz 2004; Guerin and Elliott 2006; Wagner, Reiser et al. 2006; Guerin and Elliott 2007). This model was validated by successfully predicting the stress-response of samples with a 30^o fiber orientation to uniaxial load. While expanding the model used in Chapter 5 from a single fiber population to two opposing fiber populations with identical material properties is a trivial modification (see below), the interlamellar shearing effects observed in Chapter 6 cannot be captured by a fiber/matrix model alone. Therefore the objective of the current chapter is to modify the hyperelastic model introduced in Chapter 5 to account for interlamellar shearing, and to employ this novel model to better understand the role of interlamellar shearing in the mechanical response of biologic laminates, as well as how this role evolves with culture duration for engineered biologic laminates. The model developed here will be an important tool with which to probe the mechanics of native annulus fibrosus in order to determine the role of interlamellar shearing in the mechanical behavior of this complex native tissue.

7.2 Materials and Methods

7.2.1 Engineering MSC-seeded nanofibrous biologic laminates

Oriented nanofibrous mats were electrospun as described in Chapter 6. Rectangular samples (5 x 30 mm^2) approximately 250 μm in thickness were cut from the electrospun mat with the long axis rotated either by 30^o or 90^o with respect to the prevailing fiber direction (see Chapters 3 – 6). As in Chapter 6, samples were cut with angled tips to indicate the direction of the fibers within each scaffold. Scaffolds were sterilized and rehydrated as in previous chapters via 1 hour incubations in sequentially diluted solutions of ethanol (100%, 70%, 50%, 30%, PBS, PBS), then incubated in fibronectin (20 μg/ml) overnight.

MSCs were isolated as in Chapter 6, expanded to passage 2, and seeded onto scaffolds with either 30^o or 90^o fiber orientations as described. Briefly, cells in basal media (DMEM with 10% FBS and 1% PSF) were concentrated to 10^7 cells/mL, then seeded onto scaffolds at a concentration of 500,000 cells per side. Cell seeded scaffolds were maintained in 4 mL of basal media overnight, then switched to chemically defined growth media supplemented with 10 ng/mL TGF-β3 (Chapters 3 – 6). After two weeks of pre-culture, samples were formed into bilayers as described in Chapter 6. Three bilayer orientations were constructed: two as in the previous chapter, opposing (+/- 30^o) and parallel (+/+ 30^o), and one new orientation, transverse (+/+ 90^o). Bilayers were formed by layering two constructs between two pieces of porous polypropylene and wrapping with a foil sleeve, as in Chapter 6. The motivation for selecting these orientations is outlined below in the discussion of the hyperelastic model. Two weeks after bilayer formation, the external constraints were removed as in Chapter 6.

7.2.2 Measuring functional growth of nanofibrous biologic laminates

At 2, 4, and 10 weeks, bilayers from transverse, parallel, and opposing orientations were subject to uniaxial tensile testing followed by biochemical analyses to determine GAG and collagen content as described in the previous chapters (Chapters 3 – 6). Additional samples (n = 2) were processed for histologic examination of GAG and collagen content and localization as in the previous chapters. Briefly, mechanical testing was carried out by first speckle coating samples (n = 5) by airbrushing their surface with black enamel paint (Testors) after measurement of their cross-sectional area using a non-contact laser method (Chapter 4). Samples were then clamped in custom serrated grips and loaded into an Instron 5542 testing system and, after preload and preconditioning, were ramped to failure at 0.1% strain per second. During the ramp, images were captured using a camera with a magnifying lens. Images were taken of the airbrushed surface at 5 seconds per image, corresponding to one image per 0.5% strain. These images were post-processed with Vic-2D image correlation software to compute 2-D Lagrangian strains (**E**) and coupled with the Instron force/stress data using custom Matlab code. Linear region modulus was computed as previously described (Chapters 3 – 6), while the model was applied to stress-strain curves in full as described below.

7.2.3 Formulating a novel hyperelastic term for interlamellar interactions

A constitutive model was formulated, based on the work introduced in Chapter 5, in order to better understand the role of interlamellar shearing interactions in reinforcing the tensile response of biologic laminates. Because the base model (fibers and matrix) was described in detail in Chapter 5, here we will only discuss deviations from the original model. For a summary of the original model, please refer to Chapter 5 for details.

7.2.3.1 Extending from one fiber population to two

Following the theory of strongly anisotropic solids outlined by Spencer (Spencer 1972), the total strain energy of a material can be decomposed into a base, isotropic response due to the extra-fibrillar matrix, and an anisotropic response, that results directly from the fibers. In other words, the fibers are modeled as energetic penalties along defined directions, specified by unit vectors that describe the fiber orientations. In Chapter 5, the fiber direction for a single fiber was defined by the unit vector **a**. In the present chapter, we define a second population of fibers according to a unit vector **b**. In the case of parallel and transverse bilayers, where the orientation of fibers are identical within each layer, **a** = **b**, and we can confirm that for this special case that the model recovers the form of a single fiber population as described in Chapter 5. Additionally, it is important to distinguish between the current/deformed fiber directions, **a** and **b**, and fiber directions in the reference/undeformed configuration, $\mathbf{a}_o$ and $\mathbf{b}_o$. As in Chapter 5, objectivity of the constitutive relations will be satisfied through the use

of invariants to define the strain energy function. The three invariants of the Cauchy Green tensor (**C** = $\mathbf{F}^T\mathbf{F}$) are isotropic invariants, and are therefore useful for defining isotropic behavior of the matrix. As in Chapter 5, the matrix is defined here according to a Neo-Hookean compressible material description, with the following strain energy function (Holzapfel 2000):

$$W_m = \frac{\mu}{2\beta}(I_3^{-\beta} - 1) + \frac{\mu}{2}(I_1 - 3) \tag{7.1}$$

where μ and $\upsilon = \frac{\beta}{1+2\beta}$ are the two scalar material parameters that characterize the matrix mechanics. μ is related to the modulus of matrix, while υ is related to matrix compressibility (the proclivity of a material to change volume during a given deformation).

As introduced in Chapter 5, the anisotropic contribution of a fiber population is incorporated through the use of so-called pseudo-invariants of the Cauchy Green tensor, which also make use of the unit vector representing the fiber direction. For a single fiber population, $\mathbf{a}_o$, the following two invariants are introduced; only I_4 was used in Chapter 5:

$$I_4 = \mathbf{a}_o \cdot \mathbf{C}\mathbf{a}_o \tag{7.2a}$$

$$I_5 = \mathbf{a}_o \cdot \mathbf{C}^2\mathbf{a}_o \tag{7.2b}$$

Similarly, for the second fiber population, $\mathbf{b}_o$, we have two invariants (Eq. 7.3 a, b), along with a third invariant, (Eq. 7.3c) that relates the two fiber populations to one another:

$$I_6 = \mathbf{b}_o \cdot \mathbf{C}\mathbf{b}_o \tag{7.3a}$$

$$I_7 = \mathbf{b}_o \cdot \mathbf{C}^2 \mathbf{b}_o \tag{7.3b}$$

$$I_8 = \mathbf{a}_o \cdot \mathbf{C}\mathbf{b}_o \tag{7.3c}$$

The approach of Spencer is not limited to two fiber populations, but can be expanded to any number of discrete fiber populations, increasing the number pseudo-invariants associated with the composite (Spencer 1972).

In Chapter 5, PCL nanofibers and cell-deposited collagen fibers were modeled using a single fiber strain energy function. This is in contrast to a constrained-mixture approach, which discretizes the contributors to composite anisotropy into distinct types of fibers, requiring mass fractions to scale the relative role of each fiber type in the over-all constitutive relation. While such a model is more detailed in its description, the inability to obtain reliable measures of mass fraction limits the benefits of such an approach. Moreover, the use of a single strain energy function to describe all fibers was specifically validated in Chapter 5, along with the exponential form of fiber strain energy function. Therefore it is assumed that the intralamellar collagen and PCL fibers behave as they did in single lamellar studies, and we use the same form of fiber strain energy function as that validated for this system in Chapter 5:

$$W_f = \sum_{i=4,6} \frac{\gamma_i}{2\xi_i} (e^{\xi_i (I_i - 1)^2} - 1) \tag{7.4}$$

where γ_i and ξ_i are the scalar material parameters that characterize fiber mechanics. For *i = 4* and *i = 6*, these scalars describe the fiber population defined by $\mathbf{a}_o$ and $\mathbf{b}_o$, respectively. γ_i is related to the fiber modulus, while ξ_i represents

the degree of stress-strain nonlinearity of the fiber material (Fung 1982; Holzapfel 2000; Eberline, Holzapfel et al. 2001; Guerin and Elliott 2007). The summation over *i = 4, 6* accounts for contribution of the two fiber populations, while the 2 that appears in the denominator is a correction necessary for Eq. 7.4 to reduce to Eq. 4.2 when $\mathbf{a}_o = \mathbf{b}_o$. Additionally, if we assume that fibers are identical within the two layers, so that the only thing that differs between them is their orientation (as opposed to stiffness), then Eq. 7.4 simplifies to:

$$W_f = \frac{\gamma}{2\xi} \sum_{i=4,6} (e^{\xi(I_i - 1)^2} - 1) \tag{7.5}$$

Note that in 7.5, now the fiber term has only two constants, as in Chapter 5, despite the presence of two distinct fiber populations. As in Chapter 5, to account for the inability of the fiber phase to resist compressive deformations, I_4 and I_6 are set to unity for $I_{4/6} < 1$ (Ateshian 2007). This ensures, for instance, that tensile loading of transverse bilayers would be resisted entirely by the Neo-Hookean matrix, despite compressive strains observed transversely along the fiber direction. However, it is important to note that this restriction on I_4 and I_6 is only enforced for W_f, since as shown below I_4 and I_6 appear in the interlamellar shearing term due to their geometric interpretation as stretch squared along the fiber direction; the requirement that these values be greater than or equal to one is inconsistent with this interpretation for fibers subject to compressive strains.

7.2.3.2 A novel hyperelastic model for interlamellar shearing of biologic laminates

The decomposition of *W*, the total composite strain energy function into fiber and matrix strain energy functions can be interpreted as a base isotropic response, the matrix, with an added energetic cost associated with stretching the material along the direction prescribed by a unit vector representing a fiber direction. Similarly, the role of interlamellar shearing interactions is incorporated here as an additional energetic cost that is associated with changing the relative angle between two fiber populations. In other words the additive decomposition of the total composite strain energy function, *W*, is given by:

$$W = W_m + W_f + W_{\text{int}} \tag{7.6}$$

where W_{int} is the strain energy function that describes the contribution of interlamellar shearing to the response of biologic laminates under uniaxial tension.

To define the energetic cost associated with interlamellar shearing, it is necessary to first identify a kinematic event that describes interlamellar shearing as it was described in the previous chapter. Because interlamellar shearing was assumed to result from fibers reorienting in opposing directions under load, the change in angle between the two fiber populations was chosen as the kinematic variable of choice (Figure 7.1). The angle between two vectors is related to their dot product, and therefore the W_{int} was chosen to follow the form:

$$W_{\text{int}} = W_{\text{int}}(\mathbf{a}\cdot\mathbf{b} - \mathbf{a}_O\cdot\mathbf{b}_O) \tag{7.7}$$

or in other words, the strain energy function is a function of the change in angle between two fiber populations as the fibers reorient under load. While the description in Eq. 7.7 is not necessarily objective, it can be rewritten in

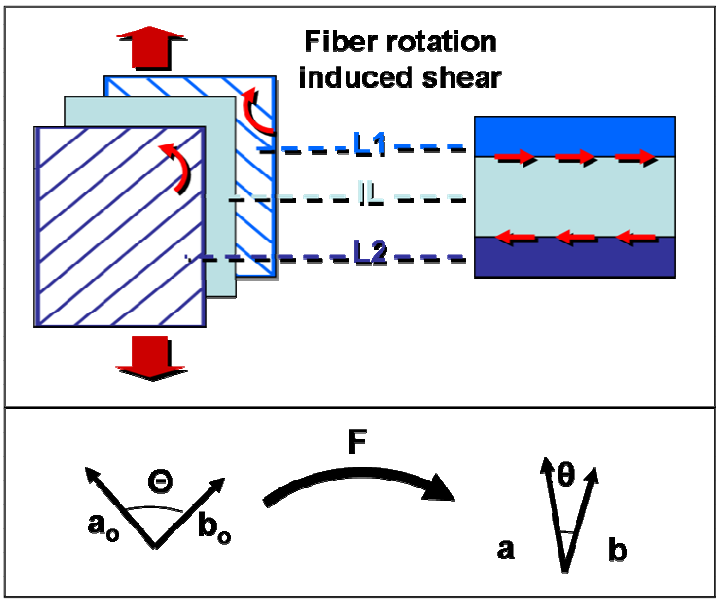

Figure 7.1 Proposed mechanism of interlamellar reinforcement of the tensile response of two opposing fiber populations, shown schematically (top) and mathematically (bottom). a_o, b_o = undeformed fiber directions; a, b = deformed fiber directions. F is the deformation gradient tensor; Θ = undeformed angle between fiber populations; θ = deformed angle between fiber populations.

terms of strain invariants (Eq. 7.2, 7.3) according to the following substitutions in order to confirm that it is:

$$\mathbf{a}\cdot\mathbf{b}-\mathbf{a}_o\cdot\mathbf{b}_o=\left(\frac{\mathbf{F}\mathbf{a}_o}{|\mathbf{F}\mathbf{a}_o|}\right)\cdot\left(\frac{\mathbf{F}\mathbf{b}_o}{|\mathbf{F}\mathbf{b}_o|}\right)-\mathbf{a}_o\cdot\mathbf{b}_o \tag{7.8a}$$

$$\left(\frac{\mathbf{F}\mathbf{a}_o}{|\mathbf{F}\mathbf{a}_o|}\right)\cdot\left(\frac{\mathbf{F}\mathbf{b}_o}{|\mathbf{F}\mathbf{b}_o|}\right)=\left(\frac{\mathbf{F}\mathbf{a}_o\cdot\mathbf{F}\mathbf{b}_o}{(\mathbf{F}\mathbf{a}_o\cdot\mathbf{F}\mathbf{a}_o)^{1/2}(\mathbf{F}\mathbf{b}_o\cdot\mathbf{F}\mathbf{b}_o)^{1/2}}\right)=\left(\frac{\mathbf{a}_o\cdot\mathbf{F}^T\mathbf{F}\mathbf{b}_o}{(\mathbf{a}_o\cdot\mathbf{F}^T\mathbf{F}\mathbf{a}_o)^{1/2}(\mathbf{b}_o\cdot\mathbf{F}^T\mathbf{F}\mathbf{b}_o)^{1/2}}\right) \tag{7.8b}$$

$$\left(\frac{\mathbf{a}_o\cdot\mathbf{F}^T\mathbf{F}\mathbf{b}_o}{(\mathbf{a}_o\cdot\mathbf{F}^T\mathbf{F}\mathbf{a}_o)^{1/2}(\mathbf{b}_o\cdot\mathbf{F}^T\mathbf{F}\mathbf{b}_o)^{1/2}}\right)=\left(\frac{\mathbf{a}_o\cdot\mathbf{C}\mathbf{b}_o}{(\mathbf{a}_o\cdot\mathbf{C}\mathbf{a}_o)^{1/2}(\mathbf{b}_o\cdot\mathbf{C}\mathbf{b}_o)^{1/2}}\right) \tag{7.8c}$$

$$\left(\frac{\mathbf{a}_o \cdot \mathbf{C}\mathbf{b}_o}{(\mathbf{a}_o \cdot \mathbf{C}\mathbf{a}_o)^{1/2}(\mathbf{b}_o \cdot \mathbf{C}\mathbf{b}_o)^{1/2}}\right) = \frac{I_8}{(I_4 I_6)^{1/2}} \tag{7.8d}$$

Therefore, Eq. 7.7 can be rewritten in the following form:

$$W_{\text{int}} = W_{\text{int}}\left(\frac{I_8}{(I_4 I_6)^{1/2}} - \mathbf{a}_o \cdot \mathbf{b}_o\right) \tag{7.9}$$

To arrive at a specific form of W_{int}, linear and nonlinear functions of the expression in Eq. 7.8d were considered. Because experimental results of the previous chapter suggested that interlamellar shearing plays a larger role with increasing strain magnitudes, it was assumed that a linear function of the kinematic measure (Eq. 7.8d), whose slope decreases with increasing stretch for a 30^o ply angle (Figure 7.2), would not sufficiently fit the convex stress-strain curves observed in the present study and previous chapters. Therefore, a nonlinear form was adopted, modeled after W_f such that two parameters could be used to define its role with similar interpretations as the fiber term:

$$W_{\text{int}} = \frac{\kappa}{2\delta}\left(e^{\delta(\mathbf{a}\cdot\mathbf{b}-\mathbf{a}_o\cdot\mathbf{b}_o)^2} - 1\right) = \frac{\kappa}{2\delta}\left(e^{\delta\left(\frac{I_8}{(I_4 I_6)^{1/2}}-\mathbf{a}_o\cdot\mathbf{b}_o\right)} - 1\right) \tag{7.10}$$

where κ and δ are constants defining the strength of the interlamellar interaction and the degree of nonlinearity of its contribution to the stress-strain response as a function of strain. Note that when **F** = **I**, W_{int} = 0, indicating that this particular form of strain energy function is consistent with a stress-free reference configuration. Additional discussion regarding the suitability of W_{int} for this application and interpretation will be given below.

7.2.3.3 Defining the constitutive law of nanofibrous biologic laminates

To arrive at the constitutive law, Eq. 7.1, 7.5, and 7.10 were first substituted into Eq. 7.6 to provide the full strain energy function of composite:

$$W_m = \frac{\mu}{2\beta}(I_3^{-\beta} - 1) + \frac{\mu}{2}(I_1 - 3) + \frac{\gamma}{2\xi}\sum_{i=4,6}(e^{\xi(I_i-1)^2} - 1) + \frac{\kappa}{2\delta}\left(e^{\delta\left(\frac{I_8}{(I_4I_6)^{1/2}} - \mathbf{a}_o\cdot\mathbf{b}_o\right)} - 1\right) \tag{7.11}$$

Next to determine the stress strain relationship, Eq. 7.11 was substituted into the equation for the 1st Piola-Kirchoff stress tensor:

$$\mathbf{t} = 2\mathbf{F}\frac{\partial W}{\partial \mathbf{C}} = 2\mathbf{F}\left(\frac{\partial W}{\partial I_k}\frac{\partial I_k}{\partial \mathbf{C}}\right) \tag{7.12}$$

which can be expanded for the particular case of Eq. 7.11 to:

$$\mathbf{t} = 2\mathbf{F}\left(\frac{\partial W_m}{\partial I_1}\frac{\partial I_1}{\partial \mathbf{C}} + \frac{\partial W_m}{\partial I_3}\frac{\partial I_3}{\partial \mathbf{C}} + \frac{\partial W_f}{\partial I_4}\frac{\partial I_4}{\partial \mathbf{C}} + \frac{\partial W_f}{\partial I_6}\frac{\partial I_6}{\partial \mathbf{C}} + \frac{\partial W_{\text{int}}}{\partial I_4}\frac{\partial I_4}{\partial \mathbf{C}} + \frac{\partial W_{\text{int}}}{\partial I_6}\frac{\partial I_6}{\partial \mathbf{C}} + \frac{\partial W_{\text{int}}}{\partial I_8}\frac{\partial I_8}{\partial \mathbf{C}}\right) \tag{7.13}$$

The resulting constitutive relation for the nanofibrous biologic laminate:

$$\begin{aligned}\mathbf{t} = {} & \mu(\mathbf{F} - I_3^{-\beta}\mathbf{F}^{-T}) + \gamma\left((I_4-1)e^{\xi(I_4-1)^2})\mathbf{F}\mathbf{a}_o\otimes\mathbf{a}_o + (I_6-1)e^{\xi(I_6-1)^2})\mathbf{F}\mathbf{b}_o\otimes\mathbf{b}_o\right) \\ & + \kappa\left(\frac{I_8}{(I_4I_6)^{1/2}} - \mathbf{a}_o\mathbf{b}_o\right)e^{\delta\left(\frac{I_8}{(I_4I_6)^{1/2}} - \mathbf{a}_o\mathbf{b}_o\right)^2}\left(\frac{1}{(I_4I_6)^{1/2}}\mathbf{F}\mathbf{a}_o\otimes\mathbf{b}_o + \mathbf{F}\mathbf{b}_o\otimes\mathbf{a}_o - \frac{I_8}{I_6^{1/2}I_4^{3/2}}\mathbf{F}\mathbf{a}_o\otimes\mathbf{a}_o - \frac{I_8}{I_4^{1/2}I_6^{3/2}}\mathbf{F}\mathbf{b}_o\otimes\mathbf{b}_o\right)\end{aligned} \tag{7.14}$$

1st Piola Kirchoff Stress (**t**) was chosen for simplicity, as the Cauchy stress used in Chapter 5 requires knowledge of the cross-sectional area throughout the deformation. Because the testing system uses one camera and therefore collects only planar information about the deformation, assumptions about the out of plane deformations are necessary. While this introduces some error into the 3D strains used to compute stress, it need not compound these errors by requiring similar assumptions for the determination of cross-sectional area and therefore

stress as well. While the 2nd Piola Kirchoff stress is commonly used in such studies for the native annulus fibrosus (Wagner, Reiser et al. 2006; Guerin and Elliott 2007; O'Connell, Guerin et al. 2009), this measure of stress is not readily interpreted as it refers to a configuration that does not physically exist, and was therefore not used (Holzapfel 2000).

7.2.4 Implementing the modified hyperelastic model to quantify the role of interlamellar shearing

The full stress-strain equation (Eq. 7.14) was applied to experimentally measured stress-strain curves for transverse, parallel, and opposing bilayers in order to generate values for the six material constants: μ, ν, γ, ξ, κ, and δ. This was done by performing least-squares curve fits to the data as described in Chapter 5. Because the model consists of six constants, fitting a single curve would generate non-unique solutions, removing the physical meaning associated with the parameters. Therefore the model was sequentially fit to data sets in order to determine the constants two at a time, using average values of the first pair of in the determination of the next pair, and so on. This was possible because each orientation of bilayer relies on a different combination of mechanisms to resist deformations. For instance, when fibers within each layer are parallel, as is the case for transverse and parallel bilayers, **a** = **b**. Substituting this into Eq. 7.11 or 7.14 demonstrates that under these conditions there is no contribution from interlamellar shearing (W_{int} = 0). This is consistent with the

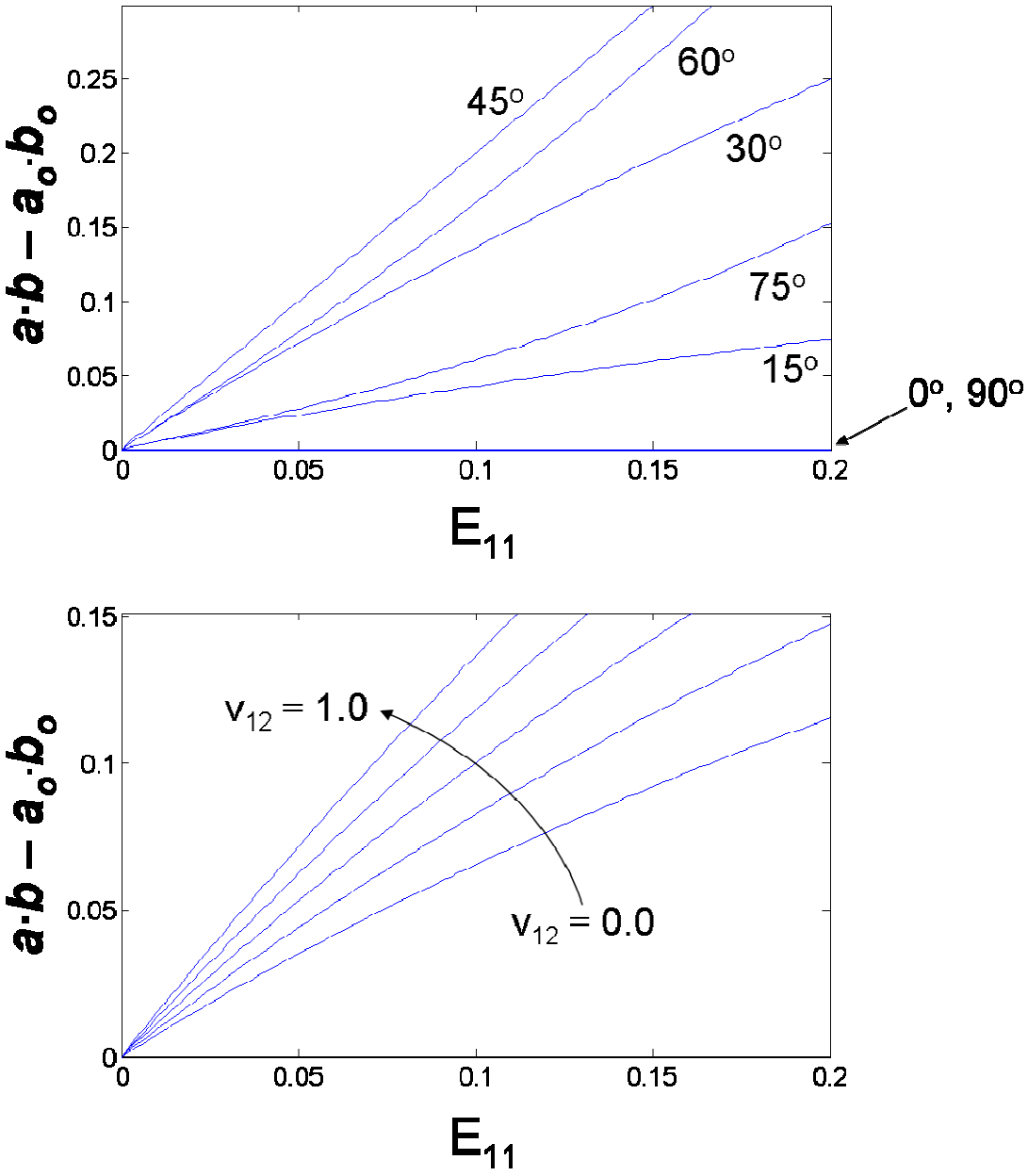

Figure 7.2 The change in angle between two fiber populations was chosen as the kinematic measure to represent interlamellar shearing in the newly proposed model term. This measure, represented by the difference between the dot products of the deformed and undeformed fiber directions, varies with ply angle (A) and Poisson's Ratio (B). Each simulation assumes uniaxial extension along the x_1 direction, bisecting the angle between the two fiber populations.

experimental observations of Chapter 6. Moreover, because fibers are assumed to bear only tensile loads, uniaxial loading transverse to the fiber direction, as is done in transverse bilayers, produces a matrix-only response, as plugging $I_4 = I_6 = 1$ into Eq. 7.5 or 7.14 results in no contribution from the fibers ($W_f = 0$). Therefore fitting stress-strain curves for transverse bilayers would isolate the behavior of the matrix term in the model.

At each time point, fitting the constitutive equation the stress-strain data from transverse bilayers was first performed, and yielded values of matrix parameters μ, and ν. The average values of each constant were computed, and their values plugged into Eq. 7.14. The resulting equation was fit to parallel bilayer data in order to provide unique values of the fiber parameters γ and ξ. Again the values were averaged, and the means substituted into Eq. 7.14 along with the matrix parameter values. Finally the Eq. 7.14 was fit to opposing bilayers, making use of the average values of matrix and fiber constants to determine interlamellar shear interaction parameters κ and δ. Using this tiered curve fitting approach, we generated unique sets of material parameter values at each time point of culture that simultaneously accounted for three special cases of nanofibrous biologic laminates. This process was repeated for each time point, so that the change in each of the six material parameters could be examined as cells deposited extracellular matrix with increasing culture duration.

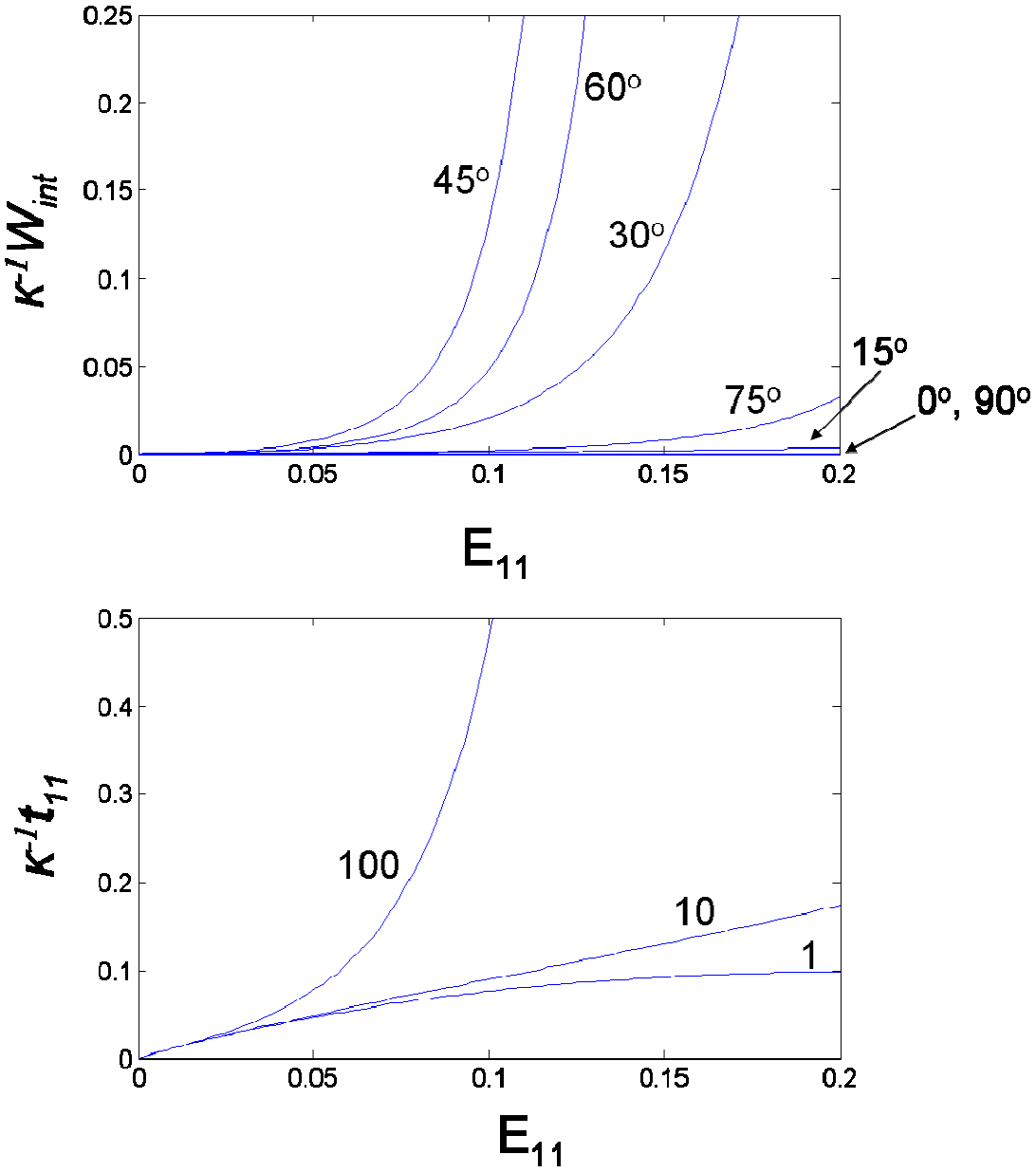

Figure 7.3 A) For the strain energy function chosen to represent interlamellar shearing interactions, strain energy is computed as a function of applied uniaxial tensile strain for a range of fiber ply angles. B) 1st Piola Kirchoff stress associated with interlamellar shearing interactions is shown for three values of nonlinearity parameter δ. For both strain energy and stress, the y-axis is normalized to the modulus-like scalar κ, which is simply a premultiplier of the function that determines its weight in the overall constitutive relation of the composite.

7.2.5 Simulations

To illustrate various features of the model, simple simulations were performed for uniaxial extension of a fiber-reinforced laminate. Extension was along the x_1 direction, and unless stated otherwise the simulations were carried out for the example case of an angle-ply laminate with +/-30^o fiber orientations with respect to the x-axis and a Poisson's ratio v_{12} = 1.0 (based on experimental findings for this orientation of bilayer). Because fibers were restricted to a planar organization with in the x_1-x_2 plane, the Poisson's ratio v_{13} does not affect the interlamellar interaction term and did not need to be stated explicitly in these simulations (see Eq. 7.10).

An additional simulation was carried out using the material parameters obtained from fitting of the model to experimental data; this was done to examine how interlamellar shearing reinforces the tensile response of biologic laminates for a range of deformation magnitudes and ply angles in the specific context of cell-mediated matrix deposition.

7.2.6 Statistics

Significance ($p \leq 0.05$) was evaluated by two way ANOVA with a Tukey's post hoc test for the variables of culture duration (time) and bilayer orientation (transverse, parallel and opposing). Goodness of model fits reported in R^2 and Bland Altman limits of agreement (bias ± standard dev), reported in MPa (Bland and Altman 1986).

7.3 Results

7.3.1 Experimental results

Consistent with findings in the previous chapter, biologic laminates seeded with MSCs accumulated abundant GAG and collagen, two major extracellular components of the intervertebral disc (Figure 7.4). Staining of both GAG and collagen was observed throughout each lamella as well as along the boundaries between layers, including the interlamellar space. This biologic interface was shown in the previous chapter to be the operative structure in interlamellar shearing of nanofibrous biologic laminates. Because samples were viewed in cross-section, no differences in staining were observed between transverse, parallel and opposing bilayers; based on the findings of the previous chapter, sectioning through the fiber planes would have revealed disparate orientations of

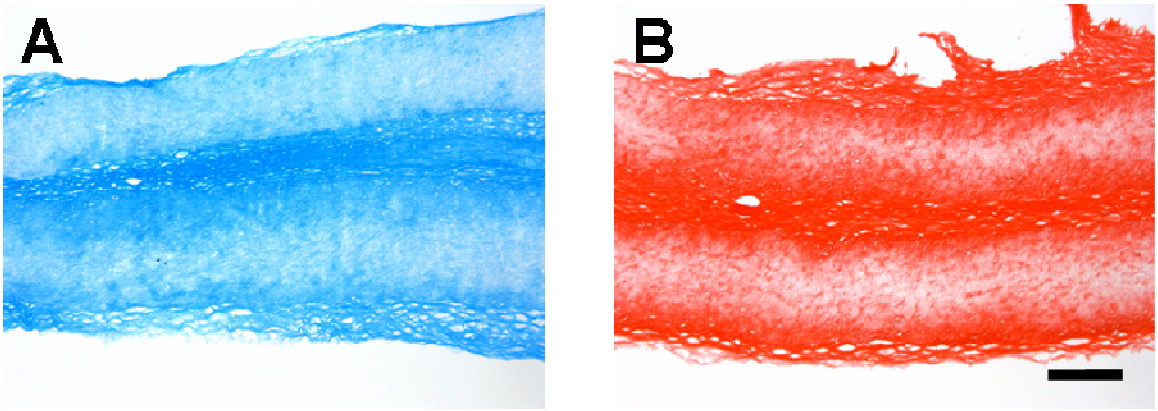

Figure 7.4 Alcian Blue (A) and Picrosirius Red (B) staining of opposing bilayers after 10 weeks of culture demonstrates abundant deposition of GAG and collagen, respectively, within the lamellae and at the lamellar boundaries. No differences in staining were observed between transverse, parallel, and opposing bilayers, consistent with the findings of Chapter 6. Scale = 250 μm.

collagen alignment despite comparable collagen quantities.

Concomitant with matrix deposition, tensile testing of biologic laminates revealed significant increases in tensile modulus for transverse, parallel, and opposing bilayers with culture duration (Figure 7.5). Modulus of the transverse group was similar to the 90^{o} group single lamellar group in Chapter 5, suggesting that the interlamellar matrix contributes little directly to the overall tensile properties of the bilayers. This is consistent with the acellular bilayer experiments in Chapter 6, which showed that weak interlamellar material can contribute strong reinforcement to angle-ply laminates but not to laminates in which fibers run parallel in adjacent lamellae. Increases in tensile modulus of parallel and opposing bilayers were similar in magnitude to the parallel and opposing bilayers in Chapter 6, confirming those findings. Additionally, opposing bilayers were significantly stiffer than parallel bilayers, as in Chapter 6, confirming the motivation for this study: interlamellar shearing reinforces angle-ply biologic laminates.

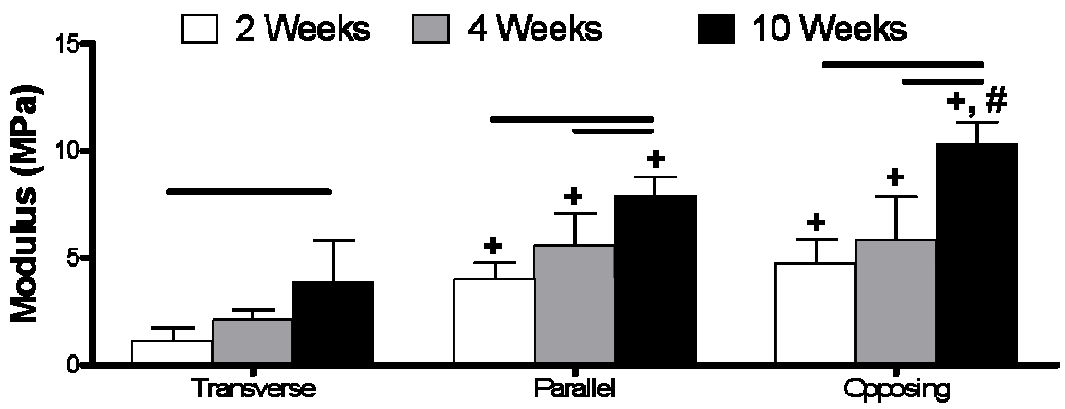

Figure 7.5 Linear region modulus increased with time for transverse, parallel, and opposing bilayers. Significant differences were observed between the three bilayer orientations at each time point. Importantly, opposing bilayers were significantly higher in modulus than parallel bilayers by 10 weeks. p≤0.05 indicated by bars (vs. 2, 4 weeks), + (vs. transverse) and # (vs. = parallel).

7.3.2 Model results

The kinematic measure chosen as the primary deformational variable of the interlamellar shearing term of the model is the change in angle between two fiber populations. To first understand the nature of this kinematic event in the context of uniaxial extension, a simple simulation was carried out in which the change in dot product was computed for a number of ply angles as the laminate is extended along the x_1 direction, which bisects the angle between the two fiber populations (Figure 7.1 and Figure 7.2). The change in ply angle with uniaxial extension depends on initial ply angle (Figure 7.2A). For instance, when the two fiber populations are parallel to one another, or when both fiber populations are parallel or perpendicular to the direction of loading, there is no change in ply angle. This suggests that a strain energy based on this input would vanish when the two fiber populations are parallel to one another. As expected, the degree of

fiber reorientation, and therefore the change in ply angle, is dependent on the Poisson's ratio of the material (Figure 7.2B). An increase in lateral contraction under uniaxial load generates increased fiber rotation, and so greater changes in ply angle. This is consistent with the expectation that interlamellar shearing would be enhanced for angle-ply laminates with large Poisson's ratios.

Next, the strain energy was computed according to Eq. 7.10 for a range of ply angles (Figure 7.3A). Values are normalized to the pre-multiplier κ for simplicity, as this parameter is more important in relating the contribution of interlamellar shearing reinforcement to the total constitutive relation; presently we are concerned only with the behavior of W_{int} and its associated stress-response. As expected from Figure 7.2A, the strain energy is a constant zero for the case where the fiber populations are parallel to one another at 0^o and 90^o, indicating that the chosen form of W_{int} replicates an important feature of the interlamellar shearing mechanism observed in Chapter 6. This is also consistent with the assumption of the present study, that fitting the constitutive law to parallel bilayer data would isolate behaviors associated with matrix and fibers, but not interlamellar shearing reinforcement. The shape of the strain energy curve as well as magnitude of strain energy is strongly influenced by the ply angle (Figure 7.3A). Strain energy and nonlinearity of the curve progressively increased with increasing ply angle up until 45^o, beyond which lower strain energy was observed. Importantly, strain energy curves were not symmetric about the 45^o ply angle; in other words, complimentary angles such as 30^o and 60^o or 15^o and 75^o did not produce identical curves.

Next, stress due to the interlamellar shearing term was computed according to 7.14 with $\mu = \gamma = 0$ in order to isolate and examine only the response of the new model term. Again the stress was normalized to κ (Figure 7.3B). Shape of the stress-strain curve was strongly influenced by the nonlinearity parameter δ for a ply angle of 30^o. Because the ply angle changes progressively less with increasing stretch (Figure 7.2), a competing effect was observed between this kinematic measure and the nonlinearity of the constitutive relation. Specifically, at $\delta = 1$, the stress-strain curve demonstrated decreasing slope with increasing stretch, similar to the curves in Figure 7.2. However, as δ is increased, the stress-strain curve passes through a linear phase before becoming increasingly nonlinear. In this way, modulation of the nonlinearity parameter δ dictates not only the degree of nonlinearity but the general shape of the curve, as the decreasing slope of the kinematic input measure and increasing slope due to the exponential function within which this measure appears to compete.

The full model (Eq. 7.14) was successfully fit to transverse bilayers at each time point to obtain Neo-Hookean material parameters μ and ν (Table 7.1, Figure 7.4A, B). A significant increase in the matrix modulus-like parameter μ was observed with culture duration, indicating an increase in the isotropic response with extracellular matrix deposition (Figure 7.4A). This is consistent with findings in the Chapter 5 for single lamellar constructs. While the average magnitude of ν increased, large sample-to-sample variations resulted in no significant changes with culture duration (Figure 7.4B). This is also consistent with Chapter 5. These parallels between the current results and Chapter 5

suggest that the progression from a single lamella to bilamellar constructs did not greatly affect growth of the isotropic, or matrix component of the composite response, and that the Neo-Hookean material definition for the matrix is still a reasonable assignment.

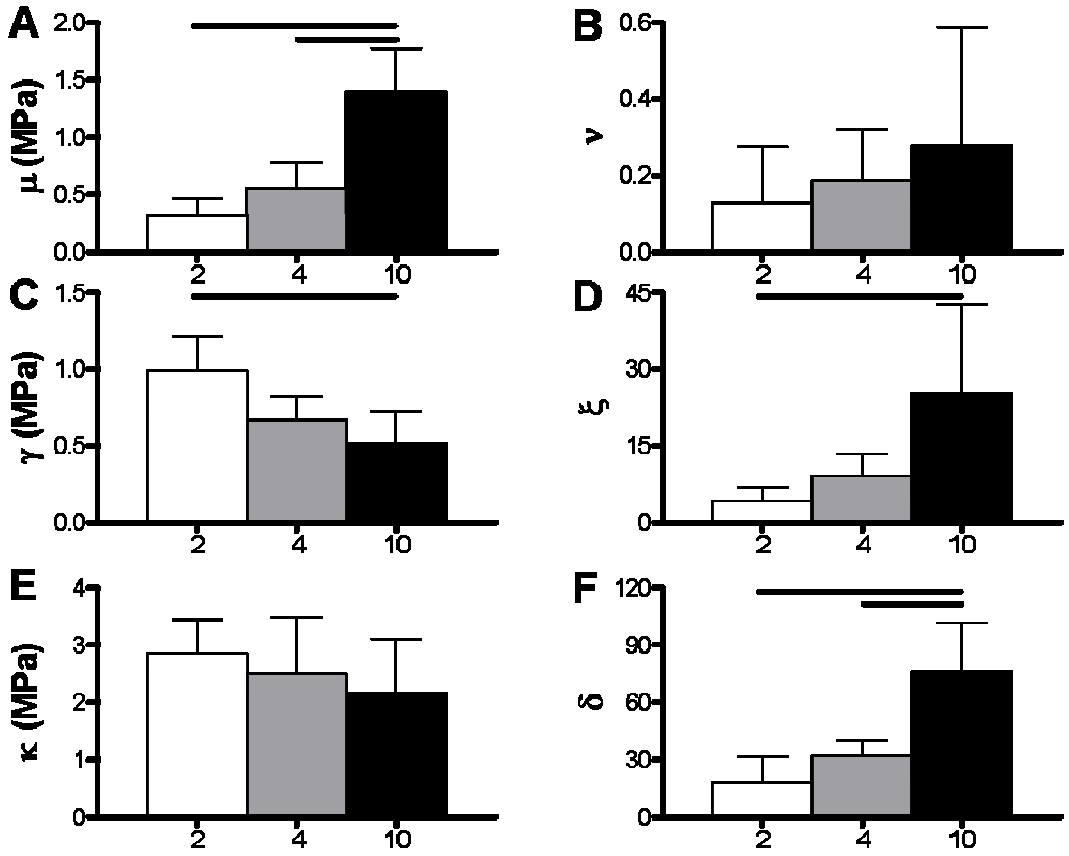

Figure 7.6 Model fits to transverse, parallel, and opposing bilayers resulted in successful fits, generating matrix (A, B), fiber (C, D), and interlamellar interaction (E, F) parameter values at each time point, respectively. Over-bars indicate $p < 0.05$.

Significant changes in both fiber parameters were observed with culture duration (Figure 7.4 C, D). While the fiber nonlinearity parameter ξ increased by nearly 3-fold over 10 weeks (Figure 7.4D), a reduction in the fiber modulus-like term γ was observed (Figure 7.4C). Finally, no significant changes were

observed in the modulus-like term associated with the interlamellar shearing reinforcement (Figure 7.4E). However, the nonlinearity term associated with the interlamellar shearing term increased by 4-fold during the 10 week culture period (Figure 7.4F). Finally, using these average parameter values, the stress-strain curves associated with the interlamellar shearing term were computed for a range of ply angles at each of the time points (Figure 7.5). In each, the stress and modulus were strain-dependent, with largest magnitudes of each seen at the highest stretches. Importantly, the effect of interlamellar shearing was maximized near a ply angle of 45^o – 50^o, with a nonlinear drop-off in stress as the angle deviated from this range. The overall magnitude of interlamellar shearing-induced tensile stress was highest at 10 weeks, indicating that with increased matrix deposition with culture, the effects of interlamellar shearing on tensile behavior were magnified.

	R^2			BA		
	2	**4**	**10**	**2**	**4**	**10**
Transverse	0.93 ± 0.05	0.93 ± 0.06	0.94 ± 0.03	0.002 ± 0.007	0.003 ± 0.013	0.002 ± 0.025
Parallel	0.99 ± 0.0	0.99 ± 0.0	0.98 ± 0.0	0.0011 ± 0.004	0.002 ± 0.007	0.015 ± 0.039
Opposing	0.98 ± 0.03	0.99 ± 0.005	0.98 ± 0.008	0.002 ± 0.009	0.004 ± 0.011	0.01 ± 0.033

Table 7.1 R^2 and Blandt-Altmann (BA) limits of agreement for fits to transverse, parallel, and opposing bilayers at 2, 4 and 10 weeks of culture.

7.4 Discussion

In the present work, a novel hyperelastic model was formulated and applied to data obtained from the mechanics of engineered nanofibrous biologic laminates. The model successfully characterized the contribution of inter-lamellar shearing to uniaxial tension of these materials. The model fit the stress-strain curves of opposing bilayers and produced unique, nonzero values for the inter-lamellar material parameters κ and δ (Figure 7.6, Table 7.1), suggesting that the particular form of the interaction term was able to characterize this reinforcement. Moreover, the model was sensitive enough to resolve functional growth of opposing bilayers through the time-varying values of the material parameters that independently describe changes in matrix, fibers, and interlamellar shearing reinforcement with extracellular matrix deposition by resident cells. Effectively, the material parameters serve as functional metrics of growth, demonstrating quantitatively the physical mechanisms that underlie enhanced tissue function. Matrix material parameters varied with culture duration in a similar fashion to single lamellar constructs (Chapter 5). However, fiber parameters behaved differently in the present work than in the single lamellar case. Specifically, a significant increase was observed in the fiber modulus-like parameter γ in Chapter 5, while in the present study the same parameter significantly

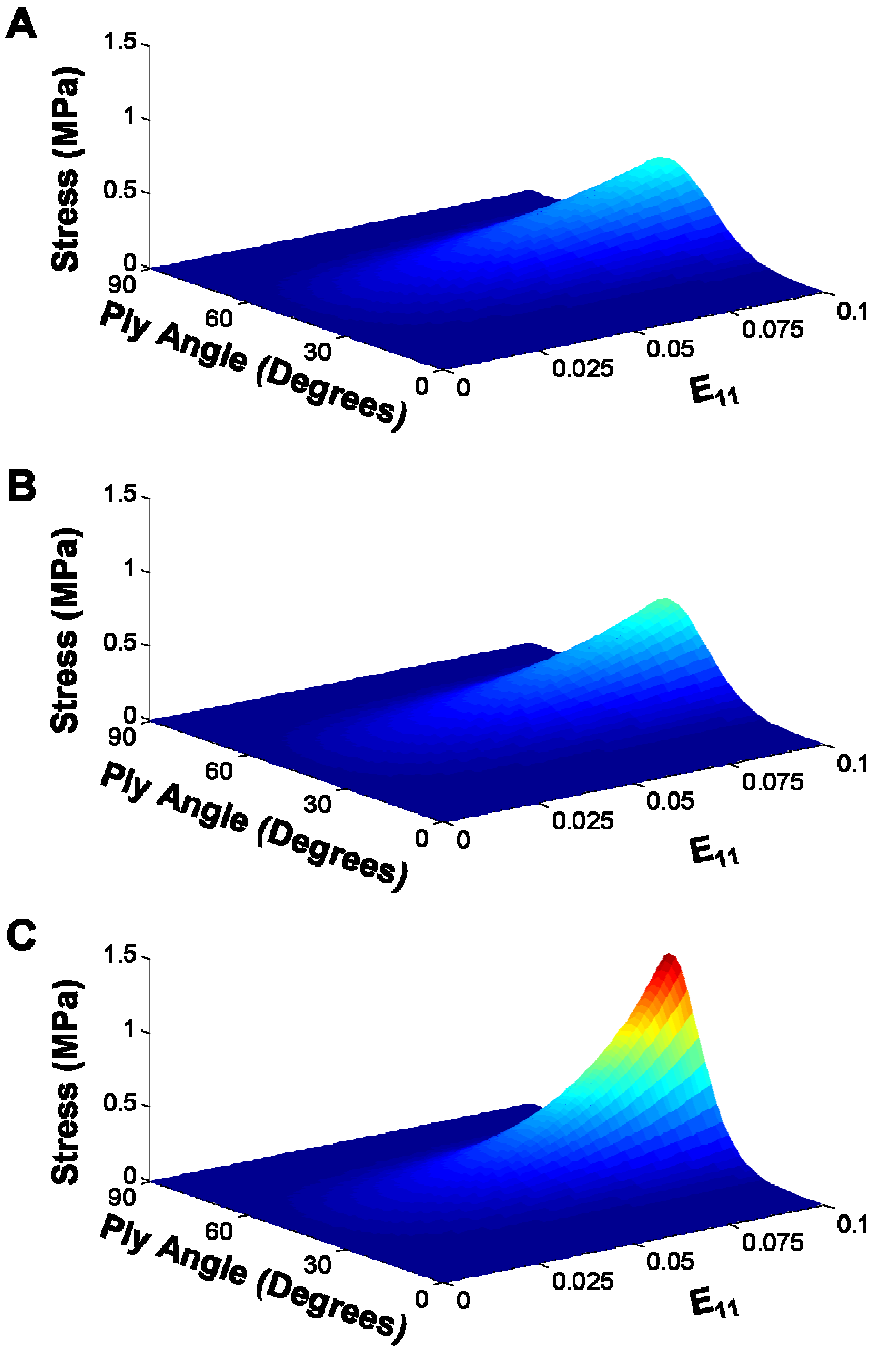

Figure 7.7 Simulation of interlamellar shearing induced tensile stresses (t_{11}) at 2 (A), 4 (B), and 10 (C) weeks. Slope and magnitude of stress-strain increased with culture duration, with maximal contributions in each time point occurring near a ply angle of 45^o – 50^o. It is within this ply angle that the most dramatic increases were seen with culture duration as well.

decreased with culture duration. However, this parameter is closely coupled with the other fiber parameter, ξ, which controls the degree of stress-strain nonlinearity in the fibers. ξ increased by nearly 4-fold in the present study while in the single lamellar work no significant increase was observed. Together these observations suggest that, relative to the single lamellar constructs, in the present work there was a growth-related reduction in the small-strain response, or toe region modulus, while the larger strain response was much stiffer with extracellular matrix deposition. This could point to a difference in the structure-function behavior between single lamellar constructs and parallel bilayers. However, it is more likely that the differences in fiber modulus and nonlinearity between the two studies are a consequence of how the study was carried out: in Chapter 5, fiber parameters were obtained from fitting stress-strain curves obtained from stretching along the fiber direction of a single lamellar construct, while in the present study fiber parameters were obtained from fitting stress-strain curves associated with stretching 30^o from the fiber direction (parallel bilayers). Because in Chapter 5 the fiber-matrix model was validated by successfully predicting the response of 30^o samples from the 0^o and 90^o data, we assumed in the present study that whether fiber parameters were obtained from parallel bilayers with a 30^o or 0^o orientation, the results would be similar. Any error associated with the model prediction would thereby be propagated into the current study. Nonetheless, because the increase in ξ was so large, it is likely that either approach would have preserved this important finding. It is possible that, in the present study, the fiber modulus-like term γ decreased not because

the toe region modulus was reduced, but as a consequence of the exponential form chosen for the fiber strain energy function. In order for an exponential function to fit a stiffer linear region of the curve, the low strain slope would be reduced, meaning not that the constructs had a softer small-strain response, but that the model fit was poorer at small strains in order to achieve a better fit at larger strains. This is a common limitation of the exponential strain energy function used for collagen-rich tissues. Because the slope of an exponential function is also exponential, the fit of an exponential function to biologic tissues that possess a toe region, transition, and linear region, is only valid for moderate strains. At large strains the model would overestimate stress. For this reason, models that rely on other means to generate nonlinearity, such as collagen uncrimping models or fiber dispersion models (Courtney, Sacks et al. 2006; Gasser, Ogden et al. 2006; Ateshian, Rajan et al. 2009; Lake, Miller et al. 2009), are currently under investigation for future work (Chapter 9). Worth noting, however, is the findings of Chapter 4 that even when loaded along the fiber direction, extended culture (120 days) resulted in a significant reduction in the toe-region modulus of MSC-seeded scaffolds. Therefore it remains a possibility extracellular matrix deposition results in a reduced modulus at small strains. More work is needed to elucidate this phenomenon further.

The interlamellar shearing interaction term that was newly proposed and implemented in the present work successfully described the mechanics of angle-ply biologic laminates. While the model successfully fit opposing bilayer data at each time point, the model must next be validated by demonstrating some

predictive capacity of the model. This may be accomplished by testing biologic laminates with other ply angles and predicting the response using the model, or by testing biologic laminates with other testing modalities altogether such as biaxial tension and shear. Nonetheless, the ability to uniquely fit stress-strain curves for opposing bilayers, using matrix and fiber parameters obtained from other ply angles, and the ability to observe changes in the associated parameters with culture, indicates that the present form of interlamellar shearing model is sufficient to characterize the novel reinforcement mechanism first observed in these materials in Chapter 6. In future work, the model will be validated using one or more of these approaches.

Simulations indicated that the extent of tensile reinforcement by inter-lamellar shearing increases with extracellular matrix deposition during culture (denoted by a higher stress peak at 10 weeks compared to 2 or 4 weeks), and depends on the angle-ply alignment of the bilayers, as well as the magnitude of applied stretch (Figure 7.7). The contribution of inter-lamellar shearing is maximized in the range of +/-30^{o} to +/-50^{o}; this range is similar to the anatomic range of ply angles found within the native annulus fibrosus, +/- 30 – 45^{o} (Cassidy, Hiltner et al. 1989; Marchand and Ahmed 1990). Consequently, it is possible that inter-lamellar shearing plays an important role in the ability of the native tissue to withstand loads *in vivo*, and that the annulus fibrosus is structurally optimized to withstand this unique and complex loading environment. For instance, if collagen within the annulus fibrosus were unidirectionally organized along the circumferential direction, shearing stresses associated with

spinal torsion would be poorly supported. The organization of fibers into alternating planes of alignment maximizes the observed interlamellar shearing reinforcement, while a single plane of two interwoven fiber populations would not do so. Similarly, a reduction in the number of lamellae (along with increasing lamellar thickness), as occurs during disc degeneration, would minimize the proposed interlamellar shearing effect, thereby weakening the tensile response. The source of tears and fissues in degenerated intervertebral discs is unknown, however it is possible that structural changes that compromise the optimally functional architecture of the annulus fibrosus predispose the tissue to damage. Finally, while many morphogenetic events during development are known to be strongly influenced by their mechanical environment (Murray, Oster et al. 1983; Murray and Oster 1984; Beloussov 2008; Wozniak and Chen 2009), the biophysical mechanism that drives formation of the unique angle-ply organization of the annulus fibrosus is poorly understood (Peacock 1951; Hayes, Benjamin et al. 1999; Hayes, Benjamin et al. 2001). The findings of the present work may guide future studies to understand the evolving interrelation of form and function during morphogenesis, as well as pathogenesis, of the intervertebral disc and other ordered, load-bearing tissues.

The present work will be particularly important for the comparison of native and engineered tissues, where linear region moduli are insufficient to characterize the large strain, nonlinear mechanics of the native tissue. Moreover, as has been demonstrated elsewhere, a simple fiber and matrix model like the one employed in Chapter 5 is not capable of capturing the uniaxial tensile

properties of native annulus fibrosus (Guerin and Elliott 2007). Modifications like the addition of a term describing the role of interlamellar shearing may be necessary to capture the complex behavior of native annulus fibrosus. While interaction terms have been introduced in the past to describe fiber-matrix interactions (Wagner and Lotz 2004; Guerin and Elliott 2005; Guo, Peng et al. 2006; Wagner, Reiser et al. 2006; Guerin and Elliott 2007), all prior models of the annulus fibrosus have assumed that the two fiber populations that comprise the annulus are interspersed, failing to account for their organization into discrete, alternating planes. However, in the previous chapter, we demonstrated that in nanofibrous biologic laminates, this organization into alternating planes provides an important reinforcement mechanism for resisting tensile stresses. Because these findings suggest that prior models of the annulus fibrosus are limited, in the present chapter a novel constitutive model that accounts for these findings was introduced and successfully applied to nanofibrous biologic laminates. Although the model was applied to engineered tissue constructs, it could readily be extended to the study of native annulus fibrosus tissue; however, the present model may need to be coupled with other terms to provide a robust material definition, as the present study does not discount the role of fiber-matrix interactions or other factors. In future work (see Chapter 9), the model will be used to quantify the role of interlamellar shearing in reinforcing the tensile response of native tissue, and if the present model is deemed appropriate, it will serve as an important tool in the comparison of engineered and native tissue function.

7.5 Conclusions

In the present study, a new hyperelastic model was proposed for biologic laminates to account for the important role of interlamellar shearing in reinforcing the tensile response of these tissues. This approach is distinct from prior models of the annulus, where it is typically assumed that fibers are not in discrete alternating planes, an assumption that may fail to account for interactions between these layers and fiber populations. The model successfully characterized the evolving mechanical function of engineered nanofibrous biologic laminates, and provided new insight into the role of interlamellar shearing and how it depends on ply angle, strain, and culture duration. This work illustrates the value of tissue engineering, not only as a means to eventually replace ailing tissues, but as a tool to instruct the understanding of structure-function relations in native tissues, and as a test-bed for the development of constitutive models to describe them. In future work, the model developed here will be used to determine the importance of inter-lamellar shearing for the function of the native annulus fibrosus.

CHAPTER 8: ENGINEERED DISC-LIKE ANGLE-PLY STRUCTURES FOR INTERVERTEBRAL DISC REPLACEMENT

8.1 Introduction

In the previous chapters, we demonstrated the utility of electrospun nanofibrous scaffolds for engineering fiber-reinforced soft tissues, with emphasis on the annulus fibrosus (AF) of the intervertebral disc. The general framework has been to follow the increasing complexity of the disc (see Chapter 2), from the smallest length scale (intra-lamellar cell and collagen alignment, Chapters 3 – 5) upward. We generated biologic laminates that replicate the angle-ply form of the AF, and arrived within 15% of the tensile modulus of the native tissue (Chapters 6 and 7). Ultimately, however, function of the native AF is macroscopically tied to its interaction with the nucleus pulposus (NP). The disc functions by resisting compressive axial loads through the pressurized, swollen NP, which bulges radially outward against the confining AF under load. The AF also stabilizes more complex motions such as bending and torsion. Therefore, engineered replacements for either the NP or AF must be tested in the context of the whole system, the intact intervertebral disc, to truly gage their success. While the previous chapters have demonstrated that electrospun scaffolds can be used to engineer AF-like tissue, in the present work, we will develop this approach toward integration of an engineered, electrospun AF with a central NP to form a composite disc. Few studies to date, have sought the engineer AF-NP

composites (Mizuno, Roy et al. 2004; Mizuno, Roy et al. 2006; Nesti, Li et al. 2008), and none have yet reported successful recreation of the unique, multi-scale tissue architecture of the disc.

During development, ordered extracellular matrix deposition is preceded by alignment of AF precursor cells, suggesting that cell alignment is an important determinant of matrix organization within the AF (Hayes, Benjamin et al. 1999; Hayes, Benjamin et al. 2001). This implies that for tissue engineering of the disc, structural cues provided either by the scaffold or via mechanical stimulation may be necessary to direct cell alignment and subsequent tissue formation. Topographical guidance directs alignment of AF cells on micro-patterned membranes, and many have reported on the importance of mechanical boundary constraints for directing the alignment of cell-seeded collagen gels (Bowles, Williams et al. ; Barocas and Tranquillo 1997; Costa, Lee et al. 2003). As we have shown in the preceding chapters, electrospinning permits the fabrication of highly aligned arrays of polymeric nanofibers, whose scale and architecture mimic the natural organization of many fiber-reinforced soft tissues such as muscle, tendon, the knee meniscus, and the AF (Mauck, Baker et al. 2009). These scaffolds can be manufactured to possess key mechanical behaviors of fiber-reinforced soft tissues including nonlinearity, anisotropy, and the ability to undergo large elastic deformations (Chapter 3). Moreover, fiber alignment in the scaffold guides alignment of resident cells, as well as the ordered deposition of extracellular matrix (Chapters 4 – 7). Attachment and proliferation on electrospun scaffolds have been observed for bovine and human AF cells and mesenchymal

stem cells (MSCs) (Nesti, Li et al. 2008; Yang, Kandel et al. 2008; Gruber, Hoelscher et al. 2009). In the previous chapters, we have employed aligned nanofibrous scaffolds to engineer single lamellar AF constructs (Chapters 3 - 5), and to fabricate bi-lamellar tissues that replicate the angle-ply fiber organization of the native tissue (Chapters 6 – 7). Although these studies demonstrate the promise of electrospinning for disc tissue engineering, little has been done with electrospinning for AF-NP composite tissue engineering (Nesti, Li et al. 2008). Moreover, of the few studies to engineer whole disc composites, thus far none have successfully replicated the unique multi-scale architecture of the native tissue. As a result, native disc mechanical properties have also not been achieved by an engineered construct. Because the disc functions primarily as a load-bearing tissue, it is imperative that engineered constructs successfully match the native mechanical properties if tissue engineering is to ascend to the stage of clinical implementation.

In the present study, we employed electrospun scaffolds to develop a multi-lamellar cylindrical engineered tissue that replicates the multi-scale architecture of the native AF. We coupled this AF-like structure with a biocompatible hydrogel for the NP, and so created a composite disc-like angle-ply structure (DAPS). Formation and study of these DAPS was carried out in three sequential steps: 1) an *acellular* study, in which we developed the construction algorithm for DAPS formation and performed mechanical testing on these acellular constructs via torsion and unconfined compression; 2) a *short-term* culture study in which DAPS were seeded with bovine AF cells to

demonstrate cell alignment and extracellular matrix deposition in an angle-ply fashion; and 3) a *long-term* culture study with MSCs seeded within each region, to determine the functional maturation of the DAPS via histological, biochemical, and mechanical evaluation. Results from this study provide a foundation from which to build a multi-scale, biologic, anatomically and hierarchically relevant composite DAPS for eventual disc replacement.

8.2 Materials and Methods

8.2.1 Acellular Study: DAPS Fabrication and Mechanical Testing

To generate the AF region of the acellular DAPS, poly(ε-caprolactone) (PCL) fiber mats were electrospun as described previously (Chapters 3 – 7). Briefly, 8 g poly(ε-caprolactone) (PCL, batch # 00702CE) was dissolved at 37^{o}C overnight in 56 mL of equal parts tetrahydrofuran and N, N-dimethylformamide. The PCL solution was extruded at 2.5 mL/h through a spinneret charged to +13 kV, generating a nanofibrous jet that was collected onto a grounded mandrel rotating at 10 m/s to instill alignment in the depositing fibers (Baker, Gee et al. 2008). The fibers were collected for 3 hours to generate a mesh of approximately 250 μm thickness. Rectangular samples (3 mm x 30 mm) were excised from the mesh along the fiber direction.

Strips were laid end-to-end with parallel fiber alignment, and spot welded using a modified soldering iron (Baker, O'Connell et al. 2007) to achieve strips of 150 mm final length. Welds were placed at two near the edges of overlapping

regions. Strips were wrapped concentrically within a custom mold by feeding one end into a slotted core (5 mm diameter), which was then rotated (Figure 8.1A) until an outer diameter of 10 mm was achieved. Molds were machined from PEEK in order to allow for repeated autoclaving of the parts without warping. The free edge was adhered to the outside of the ring using a small drop dissolved PCL to prevent unwrapping upon removal from the cast. Rabbit disc and NP area

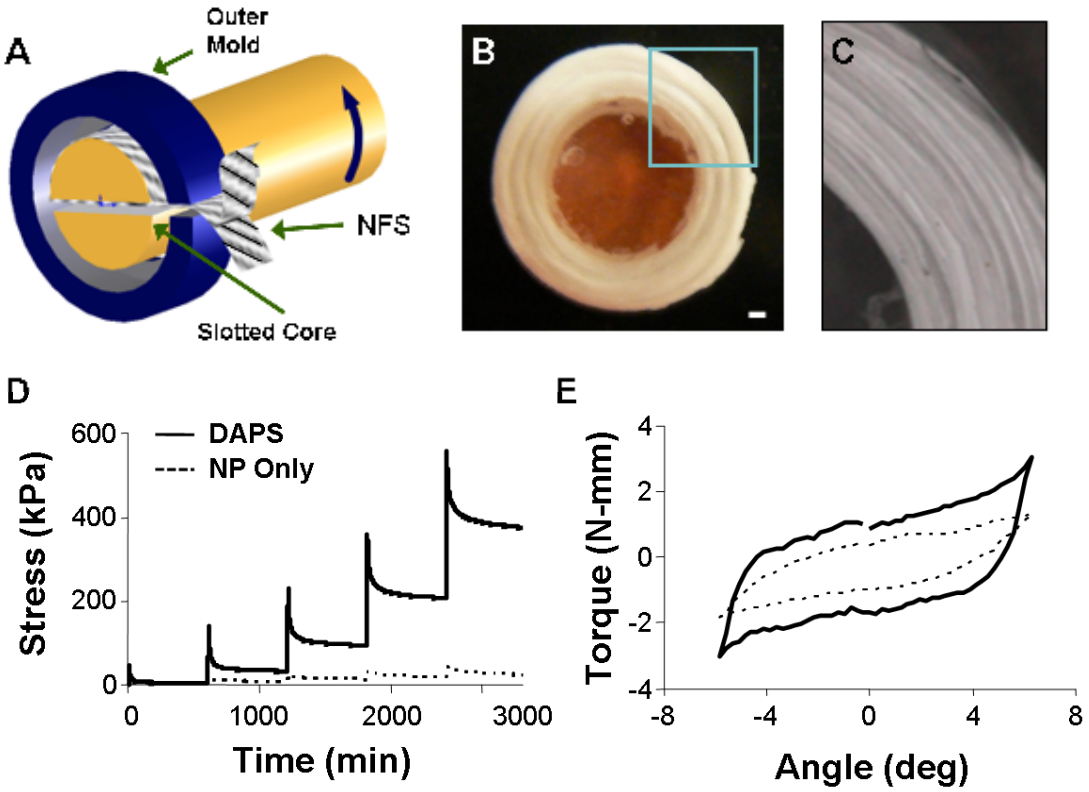

Figure 8.1 A) Schematic showing of fabrication process for formation of engineered disc-like angle-ply structure (DAPS) (NFS: nanofibrous scaffold). B) Gross morphology of DAPS with nanofibrous AF region and agarose NP region, scale bar: 1 mm. C) Close up view of AF region enlarged from box in (B). Representative stress-relaxation (D) and torsion (E) response of DAPS showing the viscoelastic and non-linear behaviors of the composite.

were used to define these geometries (O'Connell, Vresilovic et al. 2007). The core was then removed and the space filled with 5% agarose. To determine the contribution of the NP in the acellular DAPS, a 5% agarose gel was also cast in the shape of the NP region of the DAPS.

Acellular DAPS and agarose-only NP regions were tested in compression and torsion. For compression, 25% total axial strain was applied in 5% increments at 1% per second using an impermeable platen. The load was recorded as constructs relaxed to equilibrium over 10 minutes for each step of compressive deformation. For torsion testing, each construct was first compressed between 120 grit sandpaper-surfaced platens to 25% strain and allowed to relax for 5 minutes to equilibrium. Next, 10 cycles of $\pm$ 6° torsion were applied at 0.05 Hz using a custom-built micro-torsion device (Espinoza Orias, Malhotra et al. 2009). Torque and rotation data were collected and are presented from the 10th cycle. All testing was performed in a phosphate buffered saline (PBS) bath.

8.2.2 Short-term Culture Study: AF Cell Isolation and Analysis of Cell-Seeded DAPS

Outer AF tissue was excised from adult bovine caudal discs and minced before plating on tissue culture plastic in basal media as described in Chapters 3, 5. Adherent cells were collected after two weeks and expanded to passage two in basal medium. A similar construction method to that described above was followed, now using oriented fiber strips that were excised 30^{o} from the fiber

direction as in Chapters 5 – 7. As above, spot welding was necessary to achieve strips of sufficient length. Prior to cell seeding, strips were sterilized through a graded series of EtOH washes (100%, 70%, 50%, 30%, 30 minutes per step), terminating in PBS, and then coated overnight in fibronectin (20 μg/mL). Constructs were seeded at 1.5 x 10^6 cells per side, incubating for 1 hour after each application of cell solution, and pre-cultured in a serum-free, chemically defined growth media containing 10 ng/mL TGF-β3 (Mauck, Yuan et al. 2006) for one week. During this preculture period, every 48 hours strips were separated from one another to prevent the formation of adhesions. After one week, the AF region of the DAPS was formed by coupling two strips with opposing orientations of ±30^o and wrapping as above, such that each rotation increased the lamellar number by 2, with alternating fiber directions between adjacent lamellae (Figure 8.1A).

These AF-only constructs were cultured in six well plates within their molds for 7 days after wrapping in 10 mL of chemically defined medium each (above). Constructs were dehydrated and imaged by SEM (n=2) or cryotomed to 8 or 25 μm thickness (n=2). A subset of samples was sectioned oblique to the transverse axis to visualize in-plane cell and collagen orientations across lamellae interfaces. Sections were stained for cell nuclei (DAPI) and/or filamentous actin (AlexaFluor-phalloidin) or for collagen (Picrosirius Red).

8.2.3 Long-term Study: Analysis of Functional Maturation of MSC-Seeded DAPS

For MSC isolation, bone marrow was isolated from femurs and tibiae of 3-6 month old calves as described in Chapter 4, then plated on tissue culture plastic in basal medium. After initial colony formation, cells were expanded to passage 2 as described above for AF cells.

For long term analysis of DAPS maturation, strips (30^o orientation) were fabricated as above, and seeded with bovine MSCs at -2 weeks and cultured in chemically defined media as above. At 0 weeks, strips were paired into bi-layers with opposing +/-30^o fiber orientations and wrapped concentrically as above (Figure 8.1A). After 1 week to allow for stabilization of the AF region, the central lumen (5 mm diameter) was filled with MSCs encapsulated in 2% agarose at a $20x10^6$ cells/mL as in (Huang, Yeger-McKeever et al. 2008). Fully formed DAPS were cultured an additional two weeks within molds, after which point the molds were removed. This two week period allowed succifient matrix formation for the free outer edge to become adhered to the rest of the construct, so that the AF region would not unravel. Constructs were cultured for an additional 6 weeks after DAPS formation in 8 mL of chemically defined media with 10 ng/mL TGF-β3 per construct, with media changed twice weekly. At 1 week, when agarose encapsulated MSCs were delivered to the central lumen of DAPS, NP-only discs seeded with MSCs were also formed (5 mm diameter and 3 mm thickness). These samples were cultured identically and in parallel to determine the effect of the AF region on NP growth and maturation in the DAPS.

At 1, 3, and 6 weeks after formation, two samples were frozen in OCT freezing medium, cryotomed in the axial plane at 16 μm thickness, and subsequently stained with DAPI for cell nuclei, Alcian Blue for proteoglycans, or Picrosirius Red for collagen. Additional samples were sectioned obliquely, stained with Picrosirius Red, and visualized via polarized light microscopy as in Chapter 6 (Thomopoulos, Williams et al. 2003).

Next, mechanical testing was performed on the full DAPS, followed by biochemical analyses of AF and NP sub-regions (n = 4 per time point). The DAPS were tested in unconfined compression between impermeable platens. Samples were pre-equilibrated for 5 minutes with a creep load of 2 grams, followed by the application of a single 10% axial compressive strain at 0.05% per second, followed by 1000 seconds of relaxation. Equilibrium modulus was derived from the equilibrium stress and the sample geometry, and the percent relaxation from peak to equilibrium stresses. After mechanical testing, the DAPS was separated into AF and NP sub-regions, and these sub-regions assayed for collagen, GAG, and DNA content as in the previous chapters and (Mauck, Yuan et al. 2006). Lapine lumbar AF and NP (n=5) plugs were included in these biochemical analyses to provide native tissue concentrations of these biochemical constituents.

8.2.4 Statistical Analysis:

Significant difference amongst quantitative outcome measures for long-term DAPS cultures was determined by two-way ANOVA with Tukey's post hoc test ($p \leq 0.05$). All results are reported as mean ± standard deviation.

8.3 Results

8.3.1 Acellular Study: DAPS Fabrication and Mechanical Testing

Based on the construction algorithm developed in the acellular study, DAPS were formed that replicated the gross anatomic form of the disc, including a multi-lamellar, angle-ply AF and a gelatinous NP (Figure 8.1B, C). Mechanical testing showed that the DAPS exhibited compressive stress relaxation and nonlinear torsion responses (Figure 8.1D, E), two traits of native disc (Johannessen, Cloyd et al. 2006; Beckstein, Sen et al. 2008; Espinoza Orias, Malhotra et al. 2009). The compressive and shear moduli were each an order of magnitude higher for the DAPS than for the NP-only agarose region. Torsion testing demonstrated nonlinearity that is consistent with physiological disc behavior, with an increasing stiffness at angles greater than 4°. These findings confirm that the AF ring surrounding the NP confers compressive and torsional stiffness to the DAPS, similar to the mechanical interplay between the NP and AF that occurs with loading in the native disc.

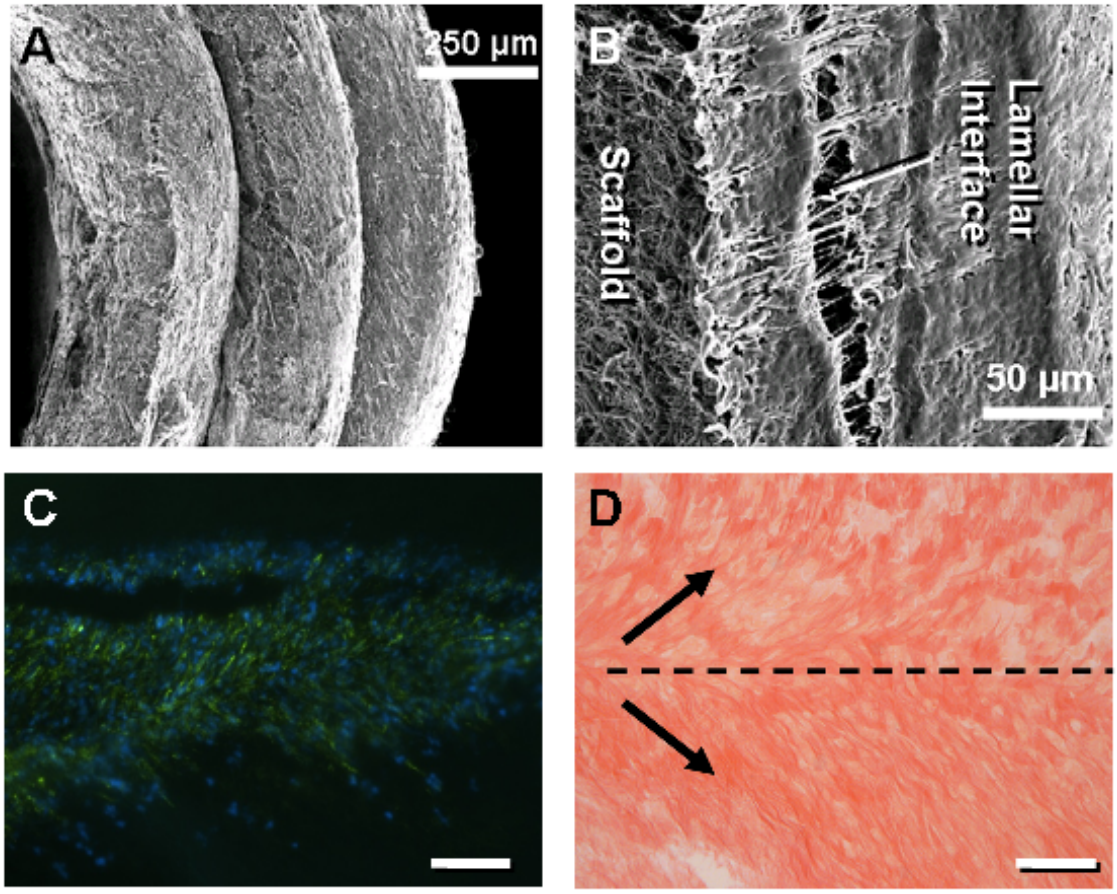

Figure 8.2 (A) SEM of AF region after 1 week of culture. (B) Higher magnification SEM of interface formation between individual lamellae at 1 week time point. Actin (green) and DAPI (blue) staining of cells (C) and Picrosirius Red staining of newly formed collagen (D) organized in alternating directions along interface within sections taken oblique to the axial plane. Scale: 250 µm.

8.3.2 Short-term Culture Study: AF Cell Isolation and Analysis of Cell-Seeded DAPS

In short-term *in vitro* culture with bovine AF cells, AF regions successfully replicated the meso-scale multi-lamellar structure of the native tissue (Figure 8.2A). Over the first week of culture, matrix deposition was evident at the lamellar interfaces when viewed under SEM (Figure 8.2B). At this early time

point of culture, cells colonized the interface, with limited infiltration to intra-lamellar compartments. Oblique histological sections through the interface showed actin staining (indicative of cell alignment and morphology) in opposing directions in adjacent lamellae (Figure 8.2C). Picrosirius Red staining of collagen likewise showed oriented extracellular matrix deposition along these alternating directions in adjacent lamellae (Figure 8.2D).

8.3.3 Long-term Study: Analysis of Functional Maturation of MSC-Seeded DAPS

Next, long-term culture studies were performed with DAPS containing both a multi-lamellar MSC-seeded AF and a gelatinous MSC-seeded NP region. DAPI staining 1 week after formation revealed MSCs distributed homogeneously throughout the NP agarose region and at lamellar boundaries in the AF region (Figure 8.3A). By 6 weeks, DAPS had matured with prominent deposition of extracellular matrix in both the NP and AF regions. Polarized light microscopy of Picrosirius Red-stained oblique sections showed successful replication of native angle-ply collagen architecture, as indicated by the alternating birefringent hues in adjacent lamellae (Figure 8.3B). Staining for GAG (Figure 8.4A, C) and collagen (Figure 8.4B, D) showed accumulation of these molecules in both regions. Notably, staining for both extracellular components appeared to decrease in intensity with progression from the outer AF to the inner AF.

Biochemical analysis confirmed differing extracellular matrix content in the NP and AF regions. At 1 week, DNA content (per wet weight) was higher in the AF region, which had been pre-cultured for 2 weeks prior to the addition of the

NP region (Figure 8.5A, $p < 0.05$). DNA content increased in the NP region with culture, but did not change further in the AF region. At 6 weeks, comparable DNA content was observed in both regions. Similarly, both GAG and collagen content increased in the NP region with culture duration (Figure 8.5 B, C). Both GAG and collagen were higher in the AF region at 1 week, due again to ongoing matrix deposition in this region during the pre-culture period prior to introduction of the gelatinous NP.

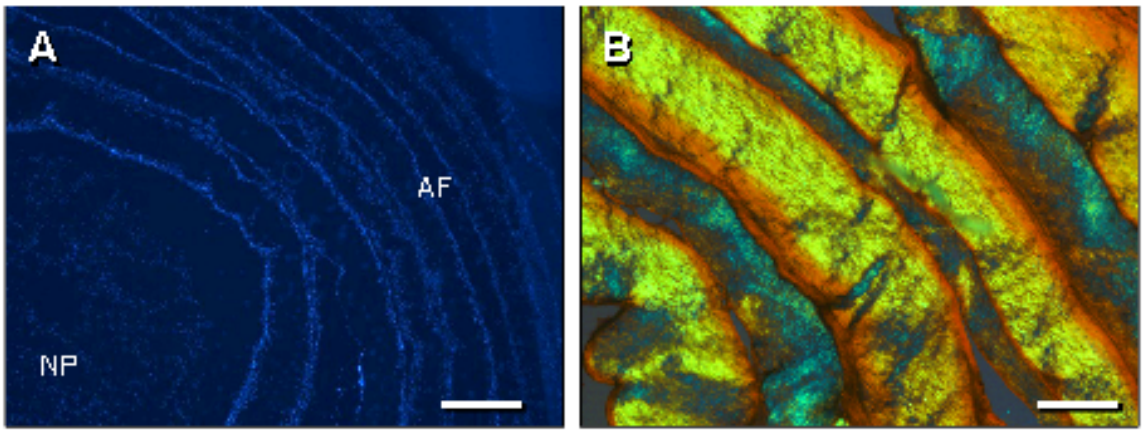

Figure 8.3 (A) DAPI staining of transverse section of DAPS at 1 week, showing homogenous distribution of MSCs in the 'NP' region, and lamellar organization of MSCs in the 'AF' region. Note: separation of NP and AF occurred as an artifact of sectioning. (B) Polarized light image of Picrosirius Red-stained oblique section of 'AF' region at 6 weeks showing birefringent material in opposing orientations with progression through adjacent lamellae. Scale: 500 (A) and 250 (B) μm.

At 6 weeks, GAG content in the NP and AF regions were not different from one another, but both were higher than at 1 week ($p<0.05$). Conversely, collagen content remained higher in the AF region throughout the culture period. By 6 weeks, the DAPS attained DNA contents in both the NP and AF region that were similar to native disc. However, GAG content reached only ~25% of native tissue levels for both NP and AF (~1.2% wet weight, WW for both regions of the DAPS,

~3.8% WW for native AF, ~4.6% WW for native NP). Collagen content, which is 200 times higher in native AF than NP, showed a mixed result; NP collagen content in the DAPS was higher than that measured for native NP (~0.4 vs. ~0.1% WW), while AF collagen in the DAPS was lower than that measured for native AF (~1% vs. 20% WW).

Of note, extracellular matrix in the NP-region of the DAPS was lower when compared to MSC-seeded NP-only constructs cultured in the absence of a confining AF region (0.97 ± 0.09% WW collagen and 2.32 ± 1.1% WW GAG at 6 weeks). This indicates that inclusion of the AF region decreased matrix biosynthesis in the NP-region. Interestingly, DNA content was not significantly different between the NP of DAPS and the NP-only constructs, indicating that extracellular matrix accumulation was reduced despite equivalent cellularity.

Along with extracellular matrix accumulation, DAPS compressive equilibrium modulus and percent stress relaxation increased with time in culture. Specifically, the equilibrium modulus increased over two-fold to 45 kPa by 6 weeks (Figure 8.6A, $p<0.05$). Likewise, the % relaxation increased over this same time course (Figure 6B, $p<0.05$, from ~40% to ~60%). NP-only constructs cultured without an AF region reached 148 kPa and 72 % relaxation over this time course.

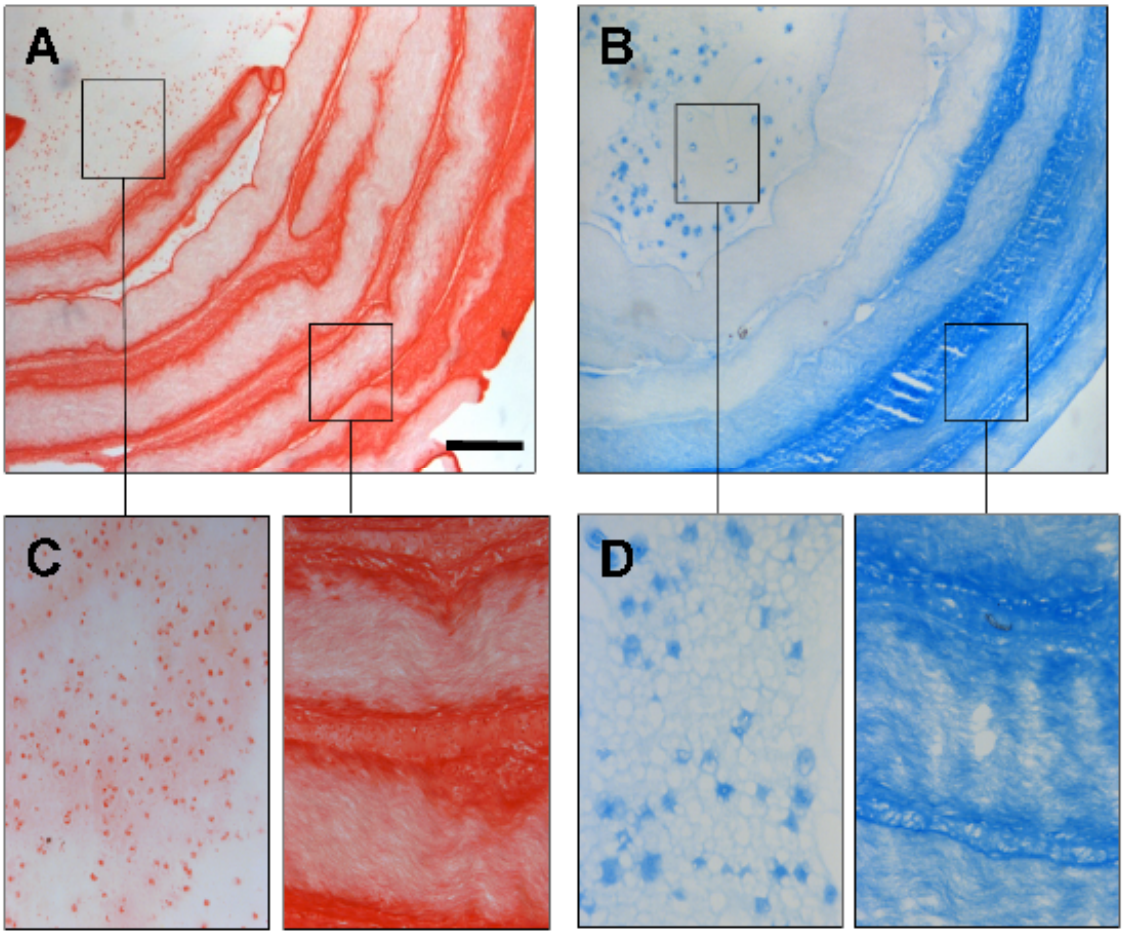

Figure 8.4 Alcian Blue (A) and Picrosirius Red (B) staining of 6 week constructs with magnified images from NP and AF regions shown in (C) and (D) as indicated. Scale = 500 μm (A-B), 125 μm (C-D).

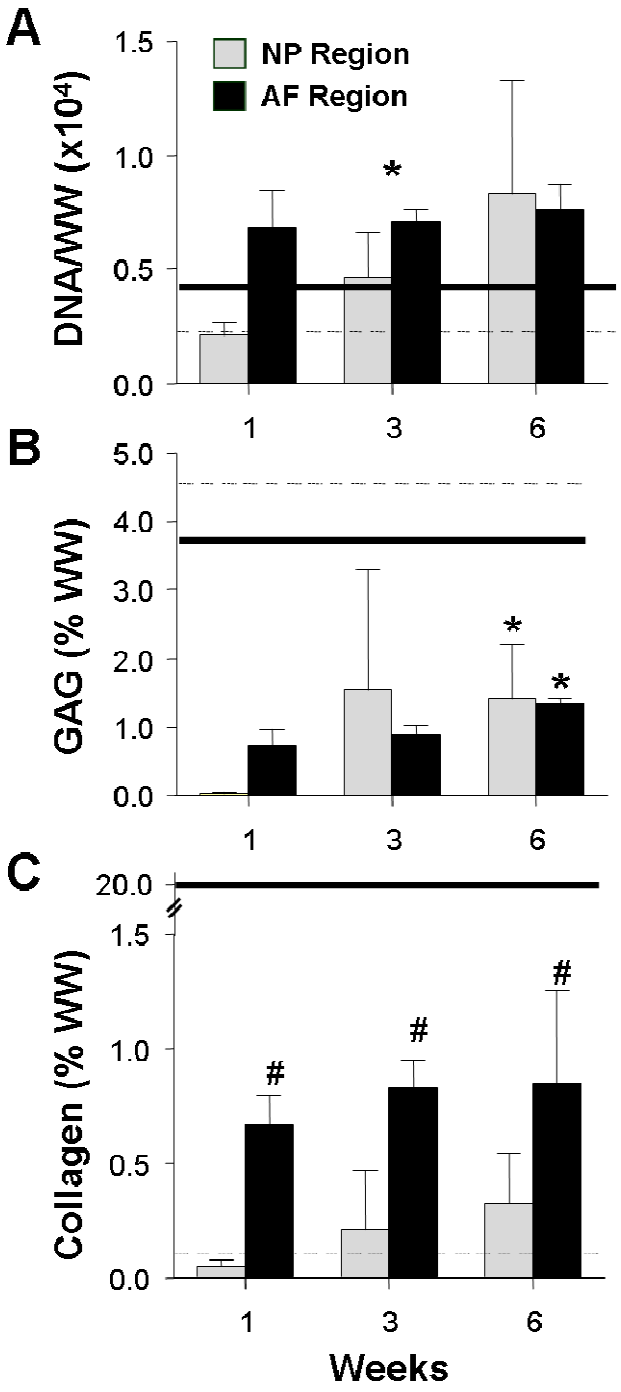

Figure 8.5 DNA (A), GAG (B), and collagen (C) content, reported in % wet weight (% WW) for the 'NP' and 'AF' regions as a function of time in culture. Solid and dashed lines indicate native lapine AF and NP benchmarks, respectively. #indicates p < 0.05 for compared to time-matched 'NP' values; * indicates p < 0.05 for compared to 1 week time point. Results presented as the mean ± SD for 4 samples/group per time point.

8.4 Discussion

In this study, MSC-seeded nanofibrous scaffolds were coupled with an engineered MSC-seeded NP to create a DAPS that replicated the multi-scale anatomic form of the native disc, including a multi-lamellar, angle-ply AF region. These constructs demonstrated improved mechanical properties with extended *in vitro* culture, and qualitatively mirrored several important functional signatures of the native disc. Construct mechanics were assessed using testing modalities and protocols that are commonly used in the study of disc mechanical function. DAPS preserved the multi-scale architectural detail of the AF, such that seeding with both AF cells and MSCs resulted in cell and extracellular matrix alignment at the lamellar interfaces with short-term culture. With long-term *in vitro* culture, these DAPS accrued collagen and GAG within both AF and NP regions, resulting in a two-fold increase in compressive modulus.

Investigation of the mechanics of acellular DAPS constructs demonstrated an improvement in mechanical function when the electrospun AF region was used to reinforce the central agarose NP, indicating that these two regions interact to elicit mechanical responses in compression and torsion that mirror native disc, even prior to extracellular matrix deposition. Such structural measures of the engineered constructs are critical metrics for determining functional equivalence to healthy disc. While strategies that aim to engineer the AF or NP alone may replicate regional properties of the native tissue, and are important to quantify, each of these two disparate tissues must ultimately be

integrated and evaluated in the context of a higher order of structural functionality. While in the present work, cylindrical DAPS were fabricated to approximate disc geometry (most closely replicating caudal discs), the same fabrication procedure can be readily extended to generate more complex geometries seen in the lumbar spine.

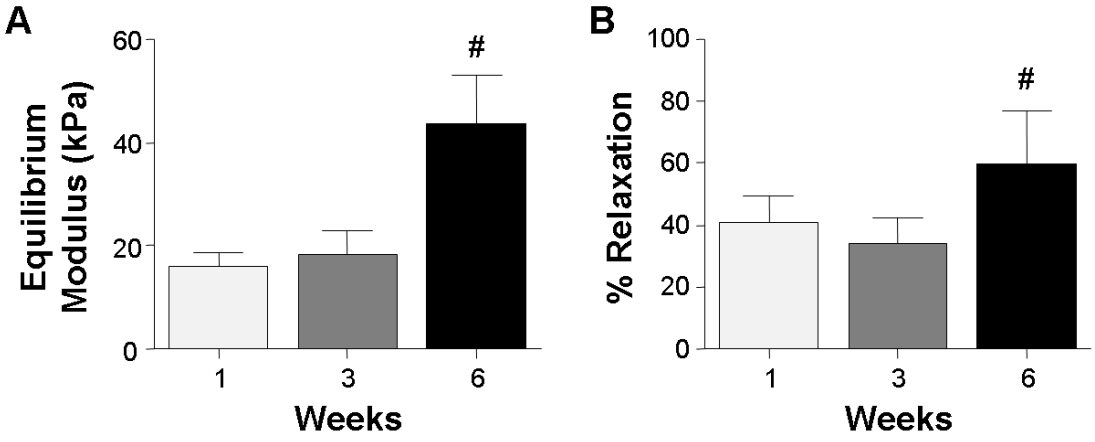

Figure 8.6 Equilibrium modulus (A) and percent stress relaxation (B) measured by unconfined compression for the DAPS as a function of time. # indicates $p \leq 0.05$ compared to the 1 week time point. Results presented as the mean ± SD for 4 samples/group per time point.

In short-term culture of cell-seeded AF regions, resident cells adopted an elongated morphology and were oriented in parallel within each lamella, with the direction of alignment alternating between adjacent lamellae. Both cell shape and organization closely mimicked the behavior of AF precursor cells during development of the embryonic disc (Hayes, Benjamin et al. 1999). Indeed, extracellular matrix deposition was organized along the local direction of cell alignment, resulting in collagen rich lamellae that replicated the angle-ply organization of the native AF. It was demonstrated in Chapters 6 and 7 that this

interaction within and between lamellae have important functional implications in terms of tensile reinforcement. These results further demonstrate that topographic cues present within the DAPS direct ordered growth of the forming tissue. With long-term culture up to 6 weeks, substantial accumulation of collagen and GAG – the two primary components of native disc extracellular matrix – was observed. This matrix accumulation generated measurable changes in mechanical function. Specifically, the compressive modulus more than doubled within 6 weeks of *in vitro* culture.

While relatively few groups have sought to engineer an entire disc (Mizuno, Roy et al. 2004; Mizuno, Roy et al. 2006; Nesti, Li et al. 2008), even fewer studies in disc tissue engineering have considered the mechanical properties of the forming neo-tissue in any context. In one exception, a composite disc was engineered by encapsulating NP cells in an alginate hydrogel surrounded by an AF cell-seeded scaffold of polylactic acid reinforced polyglycolic acid (Mizuno, Roy et al. 2004; Mizuno, Roy et al. 2006). Although biochemical content approached native levels and compressive mechanical properties increased with subcutaneous implantation, tensile properties of the developing AF region and disc-level mechanics were not measured, and the angle-ply architecture of the native AF was not achieved. To our knowledge, the work presented in the current study represents the first whole-disc replacement to replicate this micro-architecture of the disc, and the only study since the foundational work of Mizuno et al. to show enhanced mechanical behavior in an AF-NP composite (Mizuno, Roy et al. 2006).

Although the work presented here and in the preceding chapters demonstrates unique advances in the field of disc tissue engineering, it also highlights several challenges that must be addressed if regenerative medicine is to influence the clinical treatment of disc degeneration and low back pain. First, while biochemical content increased in DAPS, it did not reach native levels (particularly for collagen in the AF) and deposition appeared dependent on radial position. Moreover, extracellular matrix accumulation was severely retarded within the NP of DAPS compared to agarose-only, MSC-seeded cylinders of the same size as the NP region, indicating a prohibitive effect of the surrounding AF region on growth in the NP region. This finding is likely indicative of nutrient limitations in the radial direction in these larger constructs in free swelling culture. Such diffusional challenges have long hindered progress in disc organ culture studies, where the native disc is so large and dense, that under *in vitro* culture conditions, tissue health and matrix biosynthesis cannot be easily sustained under free swelling conditions (Risbud, Izzo et al. 2003). Nutrient and waste exchange is a critical issue that must be considered for any engineered disc replacement that aims to recreate the composition and scale of the native tissue. Moreover, given the nutrient limitations implicit in the native tissue environment, this finding may be exacerbated with *in vivo* implantation, where diffusion through the axial surfaces of the implant would be further reduced by the presence of vertebral bodies. Methods such as dynamic culture in mechanical loading bioreactors or convection-facilitated transport may be required to overcome this limitation *in vitro* (Nerurkar, Sen et al. 2010). For future implantation into the disc

space *in vivo*, it may be necessary to develop techniques that provide for efficient nutrient exchange between the engineered disc and the vascular source that underlies the endplate.

Alternative materials might also be used to enhance DAPS maturation. For instance, in the current construction, while collagen was deposited at the interface of between each pair of lamellae, cellular infiltration (and so matrix formation) was limited to these boundaries. Cellular ingress and distributed extracellular matrix deposition might be improved with the incorporation of sacrificial, water soluble nanofibers within the AF region (Baker, Gee et al. 2008; Baker, Nerurkar et al. 2009). Additionally, while agarose was employed in this study because it is a relatively simple system that has been well characterized, there exist a range of alternative hydrogels that could be used in its place to improve extracellular matrix deposition and functional maturation in the NP region (Erickson, Huang et al. 2009).

In order to compare DAPS mechanics with the native disc, it will be necessary to perform compression testing of the isolated disc. However, excision of the disc from its neighboring vertebrae causes substantial changes in mechanical behavior: the NP depressurizes and collagen fibers of the AF are no longer anchored at their ends. This not only hampers the determination of native tissue benchmarks, but emphasizes the complexity of disc tissue engineering: to properly assess the function of AF and NP constructs, they must first not only be coupled to form an AF-NP composite, but for the most informed approach, the construct must be fabricated with anatomic boundary constraints. While this was

not possible in the present study, future work will address the need to provide either biologic or inert boundaries that permit NP pressurization and anchoring points for the AF along its axial surfaces. As the current technology moves toward *in vivo* application, it will be critically important to develop suitable boundaries for integration with the surrounding vertebrae, as well as the physiologic constraints necessary to appropriately assess functional performance. While these obstacles are considerable, the present work provides a point of initiation, a test-bed in which to begin addressing these challenges for engineered disc replacement.

8.5 Conclusions

In this study, electrospun scaffolds were coupled with a biocompatible hydrogel to form a disc-like angle-ply structure, or DAPS, that replicates the multi-scale architecture of the native intervertebral disc. In addition to distinct NP and AF regions, the AF region consisted of collagenous extracellular matrix that was aligned and organized along alternating planes of +/-30^{o} with respect to the transverse plane. This represents, to date, the first whole disc engineered replacement to mimic these key structural features of the native disc. Moreover, the deposition of this organized matrix resulted in measurable changes in mechanical properties. Consequently, the work presented in this chapter illustrates the ability to translate the work of previous chapters (Chapters 3 – 7) to

a whole disc setting. This is an important step in moving the work of this thesis toward application in an animal model of disc replacement (Chapter 9).

CHAPTER 9: CONCLUSIONS AND FUTURE DIRECTIONS

9.1 Summary

Function of the intervertebral disc is predicated on a high degree of structural organization, spanning a range of length scales. While its function and failure to function during degeneration are certainly complex processes, the disc represents an excellent illustration of how form is intimately tied to function in load bearing tissues of the musculoskeletal system. As such, it is an important tissue to study from both a biomechanics and tissue engineering perspective, a framework within which to develop ways in which cells can be coaxed into forming highly ordered tissues, and investigate how order dictates mechanics in these developing systems.

Electrospinning, while developed nearly a century ago for textile processing, has only recently gained interest among tissue engineers (Mauck, Baker et al. 2009). Although electrospinning has been widely applied for engineering a number of tissues, fewer studies have focused on understanding the mechanical behavior of electrospun scaffolds (Courtney, Sacks et al. 2006; De Vita, Leo et al. 2006; Li, Mauck et al. 2007). Moreover, prior to the work presented here (Chapters 3 – 8), no study had measured the effect of extracellular matrix accumulation on the mechanical properties of cell-seeded electrospun scaffolds. In our characterization of acellular, electrospun PCL scaffolds, we observed that many important mechanical behaviors of fiber-

reinforced soft tissues were replicated, including anisotropy, stress-strain nonlinearity, and the ability to undergo finite elastic deformations (Chapter 3). These are important features for any replacement of load-bearing soft tissues to possess, and we concluded in Chapter 3 that this base material, prior to the deposition of any biologic matrix already satisfies this.

In Chapter 4, we determined that in the presence of TGF-β3, cells on electrospun scaffolds give rise to a functional, GAG and collagen rich fibrocartilage. Moreover, the roles of these two matrix components were found to be consistent with their mechanical roles in native tissues, with GAG directing the response to compression and collagen determining the tensile response of the tissue. Moreover, an interesting interplay between GAG and collagen was observed that suggests a higher level of parallel between the engineered extracellular matrix in these mature constructs and load-bearing soft tissues. Importantly, we confirmed in this study that cells not only deposit the correct matrix compositionally, but the constitutients of the matrix are *organized* in such a way that their mechanical functions are conserved with respect to many load-bearing soft tissues of the musculoskeletal system.

In Chapter 5, we determined that AF cells attach and proliferate on electrospun PCL scaffolds, and that they deposit a collagen-rich extracellular matrix under the directional guidance of the nanofibrous scaffold. Cells aligned and elongated along the nanofiber direction before depositing collagen that was also aligned and parallel to the scaffold fibers. This closely parallels development of annulus fibrosus within the embryo, where cells become elongated and

oriented, prior to the deposition of collagen along the directions of cell alignment (Hayes, Benjamin et al. 1999; Hayes, Benjamin et al. 2001). The deposition of ordered extracellular matrix resulted in a demonstrable increase in uniaxial tensile modulus, achieving the highest modulus obtained by an engineered AF replacement tissue to date. Moreover, by generating a planar arrangement of aligned collagen fibers, we effectively engineered the primary functional unit of the annulus fibrosus, a single lamella. However, the tensile modulus after 8 weeks of culture (45 MPa compared to 18 MPa for the scaffold alone) remained below the range reported for a single lamella of AF tested along the fiber direction (80 – 120 MPa) (Skaggs, Weidenbaum et al. 1994; Holzapfel, Schulze-Bauer et al. 2005). Methods for improving extracellular matrix deposition and mechanical function are described below.

A concept that was first introduced in Chapter 3, then refined in Chapters 5 and 7 is the idea that constitutive models can be used to track and quantify changes in mechanical function of engineered tissues as they mature *in vitro*. In Chapter 3, a five parameter linear homogenization model was used and demonstrated that the two free parameters, describing matrix modulus and fiber-volume fraction, were altered with culture duration. Because this model was limited to small strains and linear elastic behavior, in Chapter 4 a hyperelastic model was used. The formulation was a simplified version of models that have been previously used to study the native annulus fibrosus. Using this model, we were able to characterize the full stress-strain curve of engineered single-lamellar constructs, including the toe, heel, and linear portions of the curve. This

approach indicated significant increases in the parameters associated with fiber properties, and the fiber modulus-like term correlated with experimentally measured collagen content. These studies collectively show the value of constitutive models in characterizing tissue maturation by considering model parameters as metrics of functional growth.

In Chapter 6, the methods developed in Chapter 5 were modified to create angle-ply biologic laminates from electrospun scaffolds seeded with mesenchymal stem cells. These laminates replicated the +/-30^{o} collagen alignment of the native annulus fibrosus, and after 10 weeks of culture arrived at within 15% of the circumferential tensile modulus of the annulus fibrosus (14.3 MPa for the biologic laminate vs. 17 MPa for the native AF). In addition to closely mimicking form and function of the native AF, nanofibrous biologic laminates revealed an important role for inter-lamellar shearing in reinforcing the tensile response of these constructs. These findings yield potential insight into the structure-function relations of native AF, and illustrate the value of tissue engineering as a tool for studying simpler in vitro systems to understand functional behaviors of their complex native counterparts.

Because conventional fiber-matrix models (Chapters 3, 5) cannot capture the effects of interlamellar shearing, in Chapter 7 we introduced a new component to the strain energy function to account this behavior, which was found to play an important role in the response of engineered biologic laminates to uniaxial tension. The strain energy function accounted for interlamellar shearing by assigning an energetic penalty to changes in the angle between two

opposing fiber populations. This model successfully captured the stress-strain behavior of nanofibrous biologic laminates and allowed for an improved understanding of how interlamellar shearing affects tensile properties as a function of microstructure and culture duration and matrix deposition.

Finally in Chapter 9, engineered biologic laminates of the previous chapters were coupled with an engineered NP formed from mesenchymal stem cells encapsulated in agarose. The result was a whole engineered disc that replicated the macroscopic coupling of AF and NP as well as the microscopic organization of the AF into discrete lamellae of alternating fiber alignment. This work represents the first fully engineered intervertebral disc to replicate the multi-scale architecture of the intervertebral disc. Moreover, with culture MSCs deposited an extracellular matrix that resulted in a two-fold increase in compressive properties. However, compressive modulus remained below that of an intact motion segment.

Taken together, this work outlines a tiered approach to disc tissue engineering, that spans from the level of a single lamella (Chapters 3, 4) to multi-lamellar tissues with opposing fiber orientations (Chapters 5, 6) and ultimately a whole intervertebral disc. Further this work sheds new light on how the unique structure of the annulus fibrosus may be optimized to resist a complex loading environment through a combination of fiber stretch and interlamellar shearing. Finally this work indicates an important role for constitutive modeling in understanding the physical mechanisms underlying the improved function of tissues grown *in vitro*.

9.2 Limitations and Future Directions

9.2.1 Enhancing cell infiltration into electrospun scaffolds

While the present work represents a significant step forward in the pursuit of an engineered intervertebral disc replacement, it is not without limitations. One obstacle that has long hampered progress for the use of electrospun scaffolds is the limited ability of cells to infiltrate into nanofibrous scaffolds. Indeed, while over time cells migrated inward from the scaffold periphery, in many cases the central portion of scaffolds was sparsely populated or even devoid of cells and extracellular matrix (e.g. Figure 5.2). There is evidence from some recent work that infiltration can be resolved in one of many ways. For instance, cells can be electro-sprayed into the scaffold during fabrication (Stankus, Guan et al. 2006). However, volatility of the solvents used, the long duration of electrospinning, and sterility are all concerns that make this approach practically limited. Alternatively, composite scaffolds can be electrospun with one slow degrading component, such as PCL, and one rapidly degrading, porogenic component, such as for example polyethylene oxide (PEO). Such scaffolds have been shown to enhance cellular ingress due to the improved porosity that accompanies increased PEO fiber content (Baker, Gee et al. 2008). However, as one might expect, this improvement occurs at the expense of mechanical integrity, as the most dramatic improvement in infiltration occurs at PEO contents so high that cell contractions distort the soft, porous scaffold. Alternatively, we have recently determined that

dynamic culture conditions, which rely on simple agitation of the media to enhance nutrient/waste exchange, dramatically improve cell infiltration into electrospun scaffolds (Nerurkar, Sen et al. 2010). Unfortunately, dynamic culture results in a marked reduction in GAG retention, however removal to free-swelling conditions results in a rapid recovery of GAG content, suggesting that some combination of dynamic and free-swelling culture may overcome the limited cell infiltration that is often associated with electrospun scaffolds.

9.2.2 Enhancing extracellular matrix deposition and functional growth

While extracellular matrix deposition and improved tensile properties were observed for single lamellar constructs (Chapters 3 – 5), tensile properties remained 40 – 80 MPa lower than a single lamella of native AF along its fiber direction. While the culture duration could be extended beyond 8 weeks to resolve this (and in the case of Chapter 4, 120 days), there are other avenues that may expedite tissue deposition, allowing for mechanically viable tissue to be created in a clinically relevant time frame. For instance, improved cell infiltration (above) would result in more uniform matrix deposition, which may improve tensile properties. Moreover, tensile loading bioreactors could be employed to simulate the loading environment of the native disc, and may stimulate an anabolic response from the resident cells. Aligned electrospun scaffolds could also be an important tool in the study of mechano-biology. One could investigate the effects of cyclic tensile loading on cells as a function of fiber orientation, as rotating fiber and hence cell alignment relative to the loading axis would generate

different mechanical stimuli at the cellular level. For instance, aligning nanofibers (cells) along the direction of loading would primarily result in tensile stress among the cells, while rotating the fibers progressively further from the loading direction would result in a shift toward shearing of the cells. This would also be of interest from a disc mechano-biology perspective, as these two examples are simple *in vitro* analogs for the loading seen by AF cells *in vivo* during torsion and axial loading of the spine.

Because loading in the disc is complex, a tensile loading bioreactor is only one of many possible ways to provide mechanical stimulation in a physiologic context. For instance, a shearing bioreactor would also be useful for planar, engineered AF samples. It would be interesting to examine whether cells sense shear differently, and whether shear induces a unique composition of extracellular matrix to be deposited. A second, more ambitious option is to apply forces directly to the whole-disc engineered tissue (Chapter 8). For instance, through the application of combined cyclic compression and torsion, it may be possible to replicate the loading environment of the spine, which would more naturally induce coupled shearing and tension in the annulus region. Because diffusional limitations hindered growth of the engineered whole-disc constructs, it is also possible that, independent of mechanical stimulation, such a bioreactor could improve growth by improving nutrient and waste exchange. Deformational loading results in fluid flow, which permits convective transport, and can enhance nutrient uptake and waste removal compared to simple diffusion (Albro, Chahine et al. 2008).

Another approach to enhance nutrient/waste exchange, cell infiltration, and functional growth would be to implant constructs, whether planar biologic laminates or full engineered discs, in an *in vivo* environment. While subcutaneous implantation would be a good first step, eventually these tissues will need to be implanted within the spine, to determine their ability to withstand the complex loading environment of the disc space. However, implantation within the disc joint raises unique challenges that must be addressed such as how to interface the engineered disc with its surrounding vertebrae, ensuring spine stability and preventing displacement of the new disc from the spinal axis. Additionally, nutrient/waste exchange, which was limited even in free-swelling *in vitro* culture conditions, may be further limited in the disc space, where the axial surfaces are obstructed by endplates or vertebral bodies. It is possible, however, that the *in vivo* environment is better suited to handle diffusional limitations, as these are the conditions under which the disc forms and survives physiologically. Moreover, if vascular invasion can be achieved within the construct, diffusional limitations may be overcome. While the adult disc is largely avascular, blood vessels do penetrate into the outer layers of the AF. Moreover, recent evidence suggests that at later stages of disc morphogenesis that a vascular network permeates the AF region, and later regresses (Smith, Schaer et al. 2010). It may be possible to incorporate angiogenic factors into the electrospun scaffold using methods that have recently been developed for generating nanofibrous scaffolds with drug eluting, microsphere inclusions (Ionescu, Lee et al.).

9.2.3 Improving growth and its assessment in disc-like angle-ply structures

In Chapter 8, functional matrix deposition within engineered whole-disc constructs was assayed by unconfined compression. While this testing modality has been widely used in disc literature to understand native disc mechanics, other testing methods, such as torsion, may provide additional information that will be instructive in comparing native to engineered discs. Additionally, while compression testing is useful for measuring the aggregate effect of nucleus pulposus coupled with annulus fibrosus, ring/tension testing of the annulus alone would directly measure the tensile function of the annular ring. This testing method has been widely used in cardiovascular tissue engineering, and could be performed following compression testing on the same sample.

Other modifications could further enhance the growth of engineered AF and whole-disc constructs as well. PCL was chosen for all electrospinning work in this thesis primarily for its ability to undergo larger elastic deformations than many other commonly used biocompatible, biodegradable polymers (Li, Cooper et al. 2006). However, composite nanofibrous scaffolds have been recently developed, permitting the combination of polymers with a wide range of degradation and mechanical properties (Baker, Nerurkar et al. 2009). We have used a modeling approach similar to that applied in Chapters 5 and 7 to describe these composites, and generated a novel approach for application-specific scaffold design. It is possible that a composite scaffold, consisting of polymers with a range of stiffnesses and degradation rates, may be more amenable to mesenchymal stem cell or AF cell ingress and extracellular matrix deposition. In

the whole-disc constructs, agarose was used for the central nucleus pulposus primarily because it is a well characterized system that is easily implemented. However, the mechanics of agarose, and tissues formed from MSCs seeded in agarose, is quite different than that of the native nucleus pulposus (Mauck, Yuan et al. 2006). It is likely that a different material will be needed as the whole disc engineered constructs move forward. Specifically, it will be important to use a biomaterial that replicates the remarkable swelling behavior of the nucleus pulposus, and its relatively soft equilibrium behavior in unconfined compression (Chapter 2). It is possible that successfully replicating NP behavior would require an almost aqueous scaffold, cultured under external constraints to allow for swelling without tissue dissipation.

9.2.4 Enhancing constitutive models of engineered and native annulus fibrosus

Constitutive models were used widely throughout the work presented here, including a linear homogenization model to first approximate acellular scaffold behavior (Chapter 3), a hyperelastic fiber-reinforced model to describe the large strain behavior of cell-seeded single lamellar constructs (Chapter 5), and finally a modified hyperelastic model to capture the role of interlamellar shearing in the tensile mechanics of biologic laminates (Chapter 7). While these models were useful in furthering our understanding of structure-function relations in engineered tissues and how these relationships compare to native tissue, there are a number of other modeling approaches that may be more suitable in the future. In Chapter 4, for instance, we observed that GAG and collagen in

mature constructs formed from MSC-seeded nanofibrous scaffolds interact mechanically in a hydration and organization dependent fashion. While our current modeling approach cannot accommodate such interactions, a biphasic model that has both solid and fluid phases may be more appropriate. Moreover, such models have recently been modified to account for fiber dispersion (Gasser, Ogden et al. 2006; Ateshian 2007; Ateshian, Rajan et al. 2009). The modeling approach we followed in Chapters 5 and 7, first put forth by AJM Spencer (Spencer 1972), assumes that fibers are uni-directionally aligned along a single direction; while in electrospun scaffolds this is approximately true, there is invariably a level of fiber dispersion about the preferential direction of fiber alignment. Therefore, a model that accounts for fiber dispersion may be instructive for future studies of electrospun scaffolds. Such a model would also address an apparent contradiction regarding the mechanics of electrospun PCL scaffolds: while in the models used here (Chapters 5 and 7), it was assumed that nonlinearity of electrospun aligned scaffolds along their fiber direction was the result of fiber nonlinearity, slabs of cast PCL are linear elastic, suggesting that the nonlinearity may arise from other sources. One likely source, fiber dispersion, could be verified by building dispersion models that use structural information obtained from SEM images as inputs. Finally, homogenization, which was used in a simple application in Chapter 3, is a powerful tool for determining the effective behavior of a wide range of heterogeneous media. Recent advances in the application of homogenization theory for finite elastic deformations make this an appealing avenue for future use in describing the mechanics of engineered

and native annulus fibrosus, as well as many other biologic composites (Lopez-Pamiez and Ponte Castaneda 2004).

9.2.5 Investigating structure-function relations in the native annulus fibrosus

Throughout the present work, investigations into the mechanics of engineered tissues resulted in potential insights into the mechanical behavior of native fiber-reinforced soft tissues. In Chapter 5, we discussed shear stresses generated during uniaxial extension, and how they may play an important role in function of the annulus fibrosus under multi-directional loading *in vivo*. In Chapters 6 and 7, we discovered an important role for interlamellar shearing in reinforcing the tensile response of biologic laminates. Both of these observations can instruct future work on the mechanics of native annulus fibrosus. For instance, to determine whether interlamellar shearing is possible in the native AF, samples many layers thick could be loaded with a portion of superficial layers exempt from the constraints of the grips. This would allow the ungripped layers to be stretched passively by underlying layers of AF. If however load is not transmitted across lamellae, no stretching would be observed in the superficial layers. Coupling experiments like these with the constitutive model developed in Chapter 7 may help address the possibility that interlamellar shearing is an important reinforcement mechanism exploited by the native tissue. Moreover, while the base model of fibers embedded in a matrix was validated in Chapter 5 by successfully predicting the behavior of 30^{o} constructs at each time point, no such validation has been performed to confirm robustness of the interlamellar

interaction term. This will be addressed in future work. It may also be instructive to attach a second load cell to the uniaxial test set-up, as is done for shear testing, so that the shear stresses predicted for uniaxial extension in Chapter 5 could be measured experimentally. This would provide a second, rigorous method for model validation.

9.2.6 Improving methods for testing growth in planar engineered AF constructs

While the focus of Chapters 3 – 7 was on uniaxial tensile properties, the annulus fibrosus is subject to far more complex loading scenarios *in vivo*. Therefore, shear testing and biaxial testing would represent physiologically relevant testing modalities to assay functional evolution of cell-seeded nanofibrous scaffolds for AF tissue engineering. Moreover, due to the water content of the native AF and engineered AF as well, the true behavior of these tissues is viscoelastic. Here the viscoelastic effects were ignored, and accounted for only through the application of quasi-static strains during tensile testing. However because loading rates may be much faster *in vivo*, it will be important to understand the dynamic and time varying properties of these engineered constructs. Particularly upon incorporation of multiple testing modalities, a robust constitutive model will be invaluable for the processing and interpretation of the data generated and incorporating the information from these tests into a single coherent material definition.

9.2.7 Altering biologic variables to enhance functional growth

There are also a number of biologic variables that could be altered to improve tissue growth. TGF-β3 was chosen in the present study as it has been shown that TGF-βs outperform many other growth factors in stimulating matrix production by disc cells (Alini, Li et al. 2003), and TGF-β3 has specifically been shown to out perform the TGF-β1 and TGF-β2 in the chondrogenic differentiation of mesenchymal stem cells as well as in the maintenance of intervertebral discs *in vitro* (Barry, Boynton et al. 2001; Risbud, Izzo et al. 2003). However, there are other growth factors that may be important to consider; GDF-5, for instance, appears to have an important role during morphogenesis of the annulus fibrosus (Iwamoto, Tamamura et al. 2007).

While the cells used in Chapters 3 and 5 were obtained from adult bovine caudal discs, Chapters 4 and 6 – 8 used mesenchymal stem cells. The latter cell type is appealing from a clinical perspective as it may be difficult to obtain healthy AF cells from degenerated discs of patients, while excision of healthy AF tissue may result in donor site morbidity. MSCs on electrospun scaffolds performed approximately equally with AF cells in terms of extracellular matrix deposition and functional growth. However, all MSCs used in the current work were obtained from juvenile bovine bone marrow. This is in many ways, a best case scenario; age and species seem to strongly affect the matrix forming ability of MSCs, with human MSCs performing particularly poorly on electrospun scaffolds. Therefore, moving forward it is unclear what cell source would be most appropriate from a clinical perspective. It is possible that cells can be isolated and expanded from surgical waste generated during microdiscectomy. This may provide a viable and

clinically pertinent human cell source in the future. Alternatively, advances in the field of embryonic stem cell biology, and the recent discovery of human inducible pluripotent (iPS) cells provide further avenues for investigation.

9.3 Conclusion

Despite the vast expanse of variables free for modification in future work, the work presented within this thesis presents a significant step forward in the tissue engineering of the intervertebral disc, as well as the engineering of all load-bearing soft tissues. This work will also bear important findings for the use of electrospun scaffolds for a range of applications, not limited to disc tissue engineering or the broader aims of tissue engineering as a whole. Specifically, by employing electrospun nanofibrous scaffolds, we demonstrated that engineered annulus fibrosus could be formed that replicated the multi-scale organization of the highly ordered native annulus fibrosus, and consequently we developed planar tissues that not only replicated the form of native annulus fibrosus, but matched the circumferential tensile modulus of the tissue as well (Chapters 3 – 7). Ultimately, these biologic laminates were incorporated into a whole-disc composite to replicate the macroscopic features of the native intervertebral disc (Chapter 8). These advances provide a strong footing in the climb toward clinical implementation of a tissue engineering remedy for low back pain and intervertebral disc degeneration.

RELATED PUBLICATIONS

1. **Nerurkar NL**, Mauck RL, Elliott DM. A hyperelastic model to describe interlamellar interactions with application to engineered annulus fibrosus (in preparation).

2. **Nerurkar NL**, Mauck RL, Elliott DM. Selective removal of extracellular matrix components reveals homologous structure-function relationships between engineered and native fibrocartilage (in preparation).

3. Nathan AS, Baker BM, **Nerurkar NL**, Mauck RL. Nuclear deformations on nanofibrous scaffolds (in preparation).

4. **Nerurkar NL**, Sen S, Baker BM, Elliott DM, Mauck RL. Dynamic culture enhances stem cell ingress and extracellular matrix deposition on electrospun nanofibrous scaffolds (submitted).

5. **Nerurkar NL**, Elliott DM, Mauck RL. Functional metrics for intervertebral disc tissue engineering: challenges and opportunities. Journal of Biomechanics (in press).

6. **Nerurkar NL**, Sen S, Huang AH, Elliott DM, Mauck RL. Engineered disc-like angle-ply structures for intervertebral disc replacement. Spine (in press) [****Invited for Special Issue****].

7. **Nerurkar NL**, Baker BM, Sen S, Wible EE, Elliott DM, Mauck RL. Nanofibrous biologic laminates replicate the form and function of the annulus fibrosus. Nature Materials, 8 (12), 2009 [****Cover article****].

8. Mauck RL, Baker BM, **Nerurkar NL**, Burdick JA, Li WJ, Tuan RS, Elliott DM. Engineering on the straight and narrow: the mechanics of nanofibrous assemblies for fiber-reinforced tissue regeneration. Tissue Engineering B: Reviews 2009.

9. Baker BM, **Nerurkar NL**, Burdick JA, Elliott DM, Mauck RL. Fabrication and modeling of multi-polymer nanofibrous scaffolds. Journal of Biomechanical Engineering, 131 (10), 2009 [****Cover article****].

10. **Nerurkar NL**, Mauck RL, Elliott DM. ISSLS prize winner: Integrating theoretical and experimental methods for functional tissue engineering of the annulus fibrosus. Spine, 33 (25), 2008 [****Awarded the 2008 ISSLS Prize in Biomechanics from the International Society for the Study of Lumbar Spine****].

11. **Nerurkar NL**, Elliott DM, Mauck RL. Mechanics of oriented electrospun nanofibrous scaffolds for annulus fibrosus tissue engineering. Journal of Orthopaedic Research, 25(8), 2007 [****Cover article; most referenced paper from JOR in 2008****].

RELATED CONFERENCE ABSTRACTS

1. Elliott DM, **Nerurkar NL**, Huang AH, Kluge JA, Smith LJ, Martin JT, Hebela N, Mauck RL. Disc Tissue Engineering – Can We Make it Stick? 6th World Congress on Biomechanics, Singapore, August 1 – 6, 2010 (submitted).

2. **Nerurkar NL**, Mauck RL, Elliott DM. Modeling inter-lamellar interactions in engineered nanofibrous biologic laminates for annulus fibrosus tissue engineering. Proceedings of the ASME 2010 Summer Bioengineering Conference, Naples, FL, June 16 – 19, 2010 (submitted).

3. **Nerurkar NL**, Sen S, Baker BM, Zachry TL, Elliott DM, Mauck RL. Dynamic culture enhances stem cell ingress and extracellular matrix deposition on electrospun nanofibrous scaffolds. 56th Annual Meeting of the Orthopaedic Research Society, New Orleans, March 6 – 9, 2010.

4. **Nerurkar NL**, Sen S, Huang AH, Elliott DM, Mauck RL. Functional maturation of composites that mimic the hierarchical organization of the intervertebral disc. 56th Annual Meeting of the Orthopaedic Research Society, New Orleans, March 6 – 9, 2010 (podium, selected for Spotlight Session: Tissue Engineering).

5. **Nerurkar NL**, Sen S, Mauck RL, Elliott DM. Selective removal of extracellular matrix components reveals homologous structure-function relationships

between engineered and native fibrocartilage. 56th Annual Meeting of the Orthopaedic Research Society, New Orleans, March 6 – 9, 2010 (podium).

6. Nathan AS, Baker BM, **Nerurkar NL**, Mauck RL. Time-dependent and anisotropic nuclear deformations on aligned nanofibrous scaffolds. 56th Annual Meeting of the Orthopaedic Research Society, New Orleans, March 6 – 9, 2010 (podium).

7. **Nerurkar NL**, Mauck RL, Elliott DM. Alternating Fiber Orientation Enhances the Functional Growth of Nanofibrous Laminates for Annulus Fibrosus Tissue Engineering. BMES 2009 Fall Scientific Meeting, Pittsburgh PA, October 7-10, 2009.

8. Mauck RL, Baker BM, Ionescu LC, **Nerurkar NL**, Burdick JA. Multi-functional and dynamic fibrous scaffolds for tissue engineering and controlled release. Materials Research Society Conference, Boston, MA, November 30 – December 4, 2009 (podium).

9. **Nerurkar NL**, Sen S, Wible EE, Stambough JB, Elliott DM, Mauck RL. Mesenchymal Stem Cell Seeded Nanofibrous Laminates Mimic the Multi-scale Form and Function of the Annulus Fibrosus. Proceedings of the ASME 2009 Summer Bioengineering Conference, Lake Tahoe, CA, June 17 – 21, 2009 (podium).

10. **Nerurkar NL**, Sen S, Mauck RL, Elliott DM. Bilamellar Engineered Constructs Mimic Form and Function of the Native Annulus Fibrosus. Annual Meeting of the International Society for the Study of Lumbar Spine, Miami, FL, May 4-9, 2009 (podium).

11. **Nerurkar NL**, Sen S, Wible EE, Stambough JB, Elliott DM, Mauck RL. MSC-Seeded Nanofibrous Laminates Mimic Multi-Scale Form and Function of the Annulus Fibrosus. 55th Annual Meeting of the Orthopaedic Research Society, Las Vegas, NV, 0209; February 22-25, 2009 (podium).

12. Baker BM, **Nerurkar NL**, Burdick JA, Elliott DM, Mauck RL. Instilling Time-Dependent Behavior in Electrospun, Multi-Polymer Nanofibrous Composites. 55th Annual Meeting of the Orthopaedic Research Society, Las Vegas, NV, 0473; February 22-25, 2009.

13. Baker BM, **Nerurkar NL**, Burdick JA, Mauck RL. The Temporal Behavior of Electrospun, Multi-Polymer Nanofibrous Composites. Proceedings of TERMIS-NA 2008 Conference, San Diego, CA, December 7-11, 2008 (podium).

14. **Nerurkar NL**, Sen S, Wible EE, Stambough JB, Elliott DM, Mauck RL. “MSC-Seeded Nanofibrous Laminates Mimic Multi-Scale Form and Function of the

Annulus Fibrosus." Philadelphia Spine Research Symposium, Philadelphia, PA, November 13, 2008.

15. Baker BM, **Nerurkar NL**, Burdick JA, Elliott DM, Mauck RL. "Fabrication and Modeling of an Electrospun Tri-Polymer Composite for the Engineering of Fibrous Tissues," Proceedings of ASME 2008 Summer Bioengineering Conference, Marco Island, FL, June 25-29, 2008 (podium).

16. **Nerurkar NL**, Nguyen AM, Mauck RL, Elliott DM. Functional evolution of engineered annulus fibrosus using constitutive modeling. 54th Annual Meeting of the Orthopaedic Research Society, San Francisco, CA, 0292; March 2-5, 2008 (podium).

17. **Nerurkar NL**, Orlansky AS, Sen S, Elliott DM, Mauck RL. Multi-scale tissue engineering of the intervertebral disc. 54th Annual Meeting of the Orthopaedic Research Society, San Francisco, CA, 0340; March 2-5, 2008 (podium).

18. Lake SP, **Nerurkar NL**, Mauck RL, Kaldowec JA, Elliott DM, Soslowsky LJ. Development of a Nonlinear Anisotropic Fiber Dispersion Model to Quantify and Predict Mechanics of Normal and Injured Tendon. 54th Annual Meeting of the Orthopaedic Research Society, San Francisco, CA, p. 0824; March 2-5, 2008.

19. **Nerurkar NL**, Elliott DM, Mauck RL. Architecture of nanofibrous scaffolds influences fibrocartilagenous gene expression of annulus fibrosus and mesenchymal stem cells. 6th Combined meeting of the Orthopaedic Research Society, Honolulu, Hawaii, p. 0388; October 20-24, 2007.

20. **Nerurkar NL**, Nguyen AM, Tsing P, Mauck RL, Elliott DM. A hyperelastic fiber-reinforced continuum model to assay functional evolution of tissue engineered annulus fibrosus. 6th Combined meeting of the Orthopaedic Research Society, Honolulu, Hawaii, p. 0389; October 20-24, 2007.

21. **Nerurkar NL**, Nguyen AM, Elliott DM, Mauck RL. Annulus Fibrosus tissue engineering with aligned electrospun nanofibrous scaffolds. 53rd Annual Meeting of the Orthopaedic Research Society, San Diego, CA, p. 0249; February 11-14, 2007 (podium).

22. **Nerurkar NL**, Baker BM, Elliott DM, Mauck RL. Engineering of fiber-reinforced tissues with anisotropic biodegradable nanofibrous scaffolds. 2006 IEEE-EMBS Meeting, New York, NY, Aug 30-Sept 3, 2006 (podium).

REFERENCES

Acaroglu, E. R., J. C. Iatridis, et al. (1995). "Degeneration and aging affect the tensile behavior of human lumbar anulus fibrosus." Spine **20**(24): 2690-701.

Albro, M. B., N. O. Chahine, et al. (2008). "Dynamic loading of deformable porous media can induce active solute transport." J Biomech **41**(15): 3152-7.

Alini, M., W. Li, et al. (2003). "The potential and limitations of a cell-seeded collagen/hyaluronan scaffold to engineer an intervertebral disc-like matrix." Spine **28**(5): 446-453.

Andersson, G. B. (1999). "Epidemiological features of chronic low-back pain." Lancet **354**(9178): 581-5.

Asanbaeva, A., J. Tam, et al. (2008). "Articular cartilage tensile integrity: modulation by matrix depletion is maturation-dependent." Arch Biochem Biophys **474**(1): 175-82.

Ateshian, G. A. (2007). "Anisotropy of fibrous tissues in relation to the distribution of tensed and buckled fibers." J Biomech Eng **129**(2): 240-9.

Ateshian, G. A., V. Rajan, et al. (2009). "Modeling the matrix of articular cartilage using a continuous fiber angular distribution predicts many observed phenomena." J Biomech Eng **131**(6): 061003.

Ateshian, G. A., W. H. Warden, et al. (1997). "Finite deformation biphasic material properties of bovine articular cartilage from confined compression experiments." J Biomech **30**(11-12): 1157-64.

Baer, A. E., J. Y. Wang, et al. (2001). "Collagen gene expression and mechanical properties of intervertebral disc cell-alginate cultures." Journal of Orthopaedic Research **19**(1): 2-10.

Baer, A. E., J. Y. Wang, et al. (2001). "Collagen gene expression and mechanical properties of intervertebral disc cell-alginate cultures." J Orthop Res **19**(1): 2-10.

Baker, B. M., A. O. Gee, et al. (2008). "The potential to improve cell infiltration in composite fiber-aligned electrospun scaffolds by the selective removal of sacrificial fibers." Biomaterials **29**(15): 2348-58.

Baker, B. M. and R. L. Mauck (2007). "The effect of nanofiber alignment on the maturation of engineered meniscus constructs." Biomaterials **28**(11): 1967-77.

Baker, B. M., A. S. Nathan, et al. (2009). "Tissue engineering with meniscus cells derived from surgical debris." Osteoarthritis Cartilage **17**(3): 336-45.

Baker, B. M., N. L. Nerurkar, et al. (2009). "Fabrication and modeling of dynamic multipolymer nanofibrous scaffolds." J Biomech Eng **131**(10): 101012.

Baker, B. M., G. D. O'Connell, et al. (2007). "Multi-Lamellar and Multi-Axial Maturation of Cell-Seeded Fiber-Reinforced Tissue Engineered Constructs." Proceedings of ASME 2007 Summer Bioengineering Conference, Keystone, CO, June 20-24.

Ballyns, J. J., D. Cohen, et al. (2009). "An Optical Method for Evaluation of Geometric Fidelity for Anatomically Shaped Tissue Engineered Constructs." Tissue Eng Part C Methods.

Barocas, V. H. and R. T. Tranquillo (1997). "An anisotropic biphasic theory of tissue-equivalent mechanics: the interplay among cell traction, fibrillar network deformation, fibril alignment, and cell contact guidance." J Biomech Eng **119**(2): 137-45.

Barry, F., R. E. Boynton, et al. (2001). "Chondrogenic differentiation of mesenchymal stem cells from bone marrow: differentiation-dependent gene expression of matrix components." Exp Cell Res **268**(2): 189-200.

Beloussov, L. V. (2008). "Mechanically based generative laws of morphogenesis." Phys Biol **5**(1): 15009.

Best, B. A., F. Guilak, et al. (1994). "Compressive mechanical properties of the human anulus fibrosus and their relationship to biochemical composition." Spine **19**(2): 212-21.

Bland, J. M. and D. G. Altman (1986). "Statistical methods for assessing agreement between two methods of clinical measurement." Lancet **i**: 307-310.

Bowles, R. D., R. M. Williams, et al. "Self-Assembly of Aligned Tissue-Engineered Annulus Fibrosus and Intervertebral Disc Composite Via Collagen Gel Contraction." Tissue Eng Part A.

Bron, J. L., G. H. Koenderink, et al. (2009). "Rheological characterization of the nucleus pulposus and dense collagen scaffolds intended for functional replacement." J Orthop Res **27**(5): 620-6.

Bruehlmann, S. B., J. R. Matyas, et al. (2004). "ISSLS prize winner: Collagen fibril sliding governs cell mechanics in the anulus fibrosus: an in situ confocal microscopy study of bovine discs." Spine **29**(23): 2612-20.

Buma, P., N. N. Ramrattan, et al. (2004). "Tissue engineering of the meniscus." Biomaterials **25**(9): 1523-32.

Butler, D. L., S. A. Goldstein, et al. (2000). "Functional tissue engineering: the role of biomechanics." J Biomech Eng **122**(6): 570-5.

Caplan, A. I. (1991). "Mesenchymal stem cells." J Orthop Res **9**(5): 641-50.

Cassidy, J. J., A. Hiltner, et al. (1989). "Hierarchical structure of the intervertebral disc." Connect Tissue Res **23**(1): 75-88.

Cassidy, J. J., A. Hiltner, et al. (1989). "Hierarchical structure of the intervertebral disc." Connective Tissue Research **23**: 75-88.

Chiba, K., G. B. J. Andersson, et al. (1997). "Metabolism of the extracellular matrix formed by intervertebral disc cells cultured in alginate." Spine **22**(24): 2885-2893.

Chou, A. I., S. O. Akintoye, et al. (2009). "Photo-crosslinked alginate hydrogels support enhanced matrix accumulation by nucleus pulposus cells in vivo." Osteoarthritis Cartilage.

Clark, J. M. and D. T. Harryman, 2nd (1992). "Tendons, ligaments, and capsule of the rotator cuff. Gross and microscopic anatomy." J Bone Joint Surg Am **74**(5): 713-25.

Cloyd, J. M., N. R. Malhotra, et al. (2007). "Material properties in unconfined compression of human nucleus pulposus, injectable hyaluronic acid-based hydrogels and tissue engineering scaffolds." Eur Spine J **16**(11): 1892-8.

Cooper, J. A., Jr., J. S. Sahota, et al. (2007). "Biomimetic tissue-engineered anterior cruciate ligament replacement." Proc Natl Acad Sci U S A **104**(9): 3049-54.

Costa, K. D., E. J. Lee, et al. (2003). "Creating alignment and anisotropy in engineered heart tissue: role of boundary conditions in a model three-dimensional culture system." Tissue Eng **9**(4): 567-77.

Costi, J. J., I. A. Stokes, et al. (2008). "Frequency-dependent behavior of the intervertebral disc in response to each of six degree of freedom dynamic loading: solid phase and fluid phase contributions." Spine **33**(16): 1731-8.

Courtney, T., M. S. Sacks, et al. (2006). "Design and analysis of tissue engineering scaffolds that mimic soft tissue mechanical anisotropy." Biomaterials **27**(19): 3631-8.

Deyo, R. and Y. Tsui-Wu (1987). "Descriptive epidemiology of low back pain and its related medical care in the United States." Spine **12**: 264-268.

Deyo, R. A., D. T. Gray, et al. (2005). "United States trends in lumbar fusion surgery for degenerative conditions." Spine (Phila Pa 1976) **30**(12): 1441-5; discussion 1446-7.

Di Martino, A., A. R. Vaccaro, et al. (2005). "Nucleus pulposus replacement: basic science and indications for clinical use." Spine (Phila Pa 1976) **30**(16 Suppl): S16-22.

Ebara, S., J. C. Iatridis, et al. (1996). "Tensile properties of nondegenerate human lumbar anulus fibrosus." Spine **21**(4): 452-61.

Elliott, D. M. and L. A. Setton (2001). "Anisotropic and inhomogeneous tensile behavior of the human anulus fibrosus: experimental measurement and material model predictions." J Biomech Eng **123**: 256-263.

Erickson, I. E., A. H. Huang, et al. (2009). "Differential Maturation and Structure-Function Relationships in MSC- and Chondrocyte-Seeded Hydrogels." Tissue Eng Part A.

Espinoza Orias, A. A., N. R. Malhotra, et al. (2009). "Rat disc torsional mechanics: effect of lumbar and caudal levels and axial compression load." Spine J **9**(3): 204-9.

Frymoyer, J. (1988). "Back pain and sciatica." N Eng J Med **318**: 291-300.

Fujita, Y., N. A. Duncan, et al. (1997). "Radial tensile properties of the lumbar anulus fibrosus are site and degeneration dependent." Journal of Orthopaedic Research **15**: 814-819.

Fujita, Y., D. R. Wagner, et al. (2000). "Anisotropic shear behavior of the annulus fibrosus: effect of harvest site and tissue prestrain." Med Eng Phys **22**(5): 349-57.

Fung, Y. C. (1982). "Biomechanics: Mechanical Properties of Livign Tissues (2nd Ed.)." 568.

Gasser, T. C., R. W. Ogden, et al. (2006). "Hyperelastic modelling of arterial layers with distributed collagen fibre orientations." J R Soc Interface **3**(6): 15-35.

Gimbel, J. A., J. P. Van Kleunen, et al. (2004). "Supraspinatus tendon organizational and mechanical properties in a chronic rotator cuff tear animal model." J Biomech **37**: 739-49.

Gokorsch, S., C. Weber, et al. (2005). "A stimulation unit for the application of mechanical strain on tissue engineered anulus fibrosus cells: A new system to induce extracellular matrix synthesis by anulus fibrosus cells-dependent on cyclic mechanical strain." International Journal of Artificial Organs **28**(12): 1242-1250.

Gruber, H. E., G. L. Hoelscher, et al. (2006). "Three-dimensional culture of human disc cells within agarose or a collagen sponge: assessment of proteoglycan production." Biomaterials **27**(3): 371-6.

Gruber, H. E., K. Leslie, et al. (2004). "Cell-based tissue engineering for the intervertebral disc: in vitro studies of human disc cell gene expression and matrix production within selected cell carriers." Spine J **4**(1): 44-55.

Guerin, H. and D. Elliott (2006). "Quantifying the contributions of structure to annulus fibrosus mechanical function using a nonlinear, anisotropic, hyperelastic model. ." Journal of Orthopaedic Research, accepted.

Guerin, H. A. and D. M. Elliott (2005). "The role of fiber-matrix interactions in a nonlinear fiber-reinforced strain energy model of tendon." J Biomech Eng **127**(2): 345-50.

Guerin, H. A. and D. M. Elliott (2006). "Degeneration affects the fiber reorientation of human annulus fibrosus under tensile load." J Biomech **39**(8): 1410-8.

Guerin, H. A. and D. M. Elliott (2006). Structure and properties of soft tissue in the spine. Spine Technology Handbook, Academic Press**:** 35-62.

Guerin, H. L. and D. M. Elliott (2007). "Quantifying the contributions of structure to annulus fibrosus mechanical function using a nonlinear, anisotropic, hyperelastic model." J Orthop Res **25**(4): 508-16.

Guo, z. Y., X. Q. Peng, et al. (2006). "A composites-based hyperelastic constitutive model for soft tissue with application to the human annulus fibrosus." Journal of the Mechanics and Physics of Solids **54**: 1952-1971.

Hayes, A. J., M. Benjamin, et al. (1999). "Role of actin stress fibres in the development of the intervertebral disc: cytoskeletal control of extracellular matrix assembly." Dev Dyn **215**(3): 179-89.

Hayes, A. J., M. Benjamin, et al. (2001). "Extracellular matrix in development of the intervertebral disc." Matrix Biol **20**(2): 107-21.

Hickey, D. S. and D. W. Hukins (1980). "X-ray diffraction studies of the arrangement of collagenous fibres in human fetal intervertebral disc." J Anat **131**(Pt 1): 81-90.

Hirsch, C. and J. Galante (1967). "Laboratory conditions for tensile tests in annulus fibrosus from human intervertebral discs." Acta Orthop Scand **38**(2): 148-62.

Holzapfel, G. A. (2000). "Nonlinear Solid Mechanics: A Continuum Approach for Engineering." 455.

Holzapfel, G. A., C. A. Schulze-Bauer, et al. (2005). "Single lamellar mechanics of the human lumbar anulus fibrosus." Biomech Model Mechanobiol **3**(3): 125-40.

Iatridis, J. C. and I. ap Gwynn (2004). "Mechanisms for mechanical damage in the intervertebral disc annulus fibrosus." J Biomech **37**(8): 1165-75.

Iatridis, J. C., S. Kumar, et al. (1999). "Shear mechanical properties of human lumbar annulus fibrosus." J Orthop Res **17**(5): 732-7.

Iatridis, J. C., L. A. Setton, et al. (1998). "Degeneration affects the anisotropic and nonlinear behaviors of human anulus fibrosus in compression." J Biomech **31**(6): 535-44.

Iatridis, J. C., L. A. Setton, et al. (1997). "The viscoelastic behavior of the non-degenerate human lumbar nucleus pulposus in shear." J Biomech **30**(10): 1005-13.

Iatridis, J. C., M. Weidenbaum, et al. (1996). "Is the nucleus pulposus a solid or a fluid? Mechanical behaviors of the nucleus pulposus of the human intervertebral disc." Spine **21**(10): 1174-84.

Ionescu, L. C., G. C. Lee, et al. "An anisotropic nanofiber/microsphere composite with controlled release of biomolecules for fibrous tissue engineering." Biomaterials **31**(14): 4113-4120.

Iwamoto, M., Y. Tamamura, et al. (2007). "Transcription factor ERG and joint and articular cartilage formation during mouse limb and spine skeletogenesis." Dev Biol **305**(1): 40-51.

Jacobs, N. T., J. Morelli, et al. (2010). "Annulus Fibrosus Shear Mechanical Properties and the Contributions of Glycosaminoglycans and Elastic Fibers to Shear are Anisotropic." Transactions of the 56th Annual Meeting of the Orthopaedic Research Society, New Orleans, LA **in review**.

Johannessen, W. and D. M. Elliott (2005). "Effects of degeneration on the biphasic material properties of human nucleus pulposus in confined compression." Spine (Phila Pa 1976) **30**(24): E724-9.

Juncosa-Melvin, N., K. S. Matlin, et al. (2007). "Mechanical stimulation increases collagen type I and collagen type III gene expression of stem cell-collagen sponge constructs for patellar tendon repair." Tissue Eng **13**(6): 1219-26.

Kandel, R. A., S. Roberts, et al. (2008). "Tissue Engineering and the Intervertebral Disc: the Challenges." Eur Spine J **17**: S480-491.

Kasra, M., M. Parnianpour, et al. (2004). "Effect of strain rate on tensile properties of sheep disc anulus fibrosus." Technol Health Care **12**(4): 333-42.

Lake, S. P., K. S. Miller, et al. (2009). "Effect of fiber distribution and realignment on the nonlinear and inhomogeneous mechanical properties of human supraspinatus tendon under longitudinal tensile Loading." J Orthop Res.

Lanir, Y. (1979). "A structural theory for the homogeneous biaxial stress-strain relationships in flat collagenous tissues." J Biomech **12**(6): 423-36.

Levin, D. A., J. J. Hale, et al. (2007). "Adjacent segment degeneration following spinal fusion for degenerative disc disease." Bull NYU Hosp Jt Dis **65**(1): 29-36.

Lewis, N. T., M. A. Hussain, et al. (2008). "Investigation of nano-mechanical properties of annulus fibrosus using atomic force microscopy." Micron **39**(7): 1008-19.

Li, W. J., J. A. Cooper, Jr., et al. (2006). "Fabrication and characterization of six electrospun poly(alpha-hydroxy ester)-based fibrous scaffolds for tissue engineering applications." Acta Biomater **2**(4): 377-85.

Li, W. J., R. L. Mauck, et al. (2006). "Engineering controllable anisotropy in electrospun biodegradable nanofibrous scaffolds for musculoskeletal tissue engineering." J Biomech: in press.

Li, W. J., R. L. Mauck, et al. (2007). "Engineering controllable anisotropy in electrospun biodegradable nanofibrous scaffolds for musculoskeletal tissue engineering." J Biomech **40**(8): 1686-93.

Lopez-Pamiez, O. and P. Ponte Castaneda (2004). "Second-Order Homogenization Estimates Incorporating Field Fluctuations in Finite Elasticity." Mathematics and Mechanics of Solids **9**(3): 243-270.

Lujan, T. J., C. J. Underwood, et al. (2009). "Contribution of glycosaminoglycans to viscoelastic tensile behavior of human ligament." J Appl Physiol **106**(2): 423-31.

Luo, X., R. Pietrobon, et al. (2004). "Estimates and patterns of direct health care expenditures among individuals with back pain in the United States." Spine **29**(1): 79-86.

Marchand, F. and A. M. Ahmed (1990). "Investigation of the laminate structure of lumbar disc annulus fibrosus." Spine **15**(5): 402-410.

Mauck, R. L., B. M. Baker, et al. (2009). "Engineering on the Straight and Narrow: The Mechanics of Nanofibrous Assemblies for Fiber-Reinforced Tissue Regeneration." Tissue Eng Part B Rev.

Mauck, R. L., M. A. Soltz, et al. (2000). "Functional tissue engineering of articular cartilage through dynamic loading of chondrocyte-seeded agarose gels." J Biomech Eng **122**(3): 252-60.

Mauck, R. L., X. Yuan, et al. (2006). "Chondrogenic differentiation and functional maturation of bovine mesenchymal stem cells in long-term agarose culture." Osteoarthritis Cartilage **14**(2): 179-89.

Maurice, D. M. (1957). "The structure and transparency of the cornea." J Physiol **136**(2): 263-86.

Michalek, A. J., M. R. Buckley, et al. (2009). "Elastic fibers govern local strains in the annulus fibrosus under dynamic transverse shear." Transactions of the 55th Annual Meeting of the Orthopaedic Research Society **34**: 1727.

Mizuno, H., A. K. Roy, et al. (2004). "Tissue-engineered composites of anulus fibrosus and nucleus pulposus for intervertebral disc replacement." Spine **29**(12): 1290-7; discussion 1297-8.

Mizuno, H., A. K. Roy, et al. (2006). "Biomechanical and biochemical characterization of composite tissue-engineered intervertebral discs." Biomaterials **27**(3): 362-70.

Moffat, K. L., A. S. Kwei, et al. (2009). "Novel nanofiber-based scaffold for rotator cuff repair and augmentation." Tissue Eng Part A **15**(1): 115-26.

Moutos, F. T., L. E. Freed, et al. (2007). "A biomimetic three-dimensional woven composite scaffold for functional tissue engineering of cartilage." Nat Mater **6**(2): 162-7.

Murray, J. D. and G. F. Oster (1984). "Generation of biological pattern and form." IMA J Math Appl Med Biol **1**(1): 51-75.

Murray, J. D., G. F. Oster, et al. (1983). "A mechanical model for mesenchymal morphogenesis." J Math Biol **17**(1): 125-9.

Natoli, R. M., C. M. Revell, et al. (2009). "Chondroitinase ABC treatment results in greater tensile properties of self-assembled tissue-engineered articular cartilage." Tissue Eng Part A **15**(10): 3119-28.

Nerurkar, N., B. Baker, et al. (2006). "Engineering of fiber-reinforced tissue with anisotropic biodegradable nanofibrous scaffolds." Transactions of IEEE Engineering in Medicine and Biology Society.

Nerurkar, N. L., S. Sen, et al. (2010). "Dynamic culture enhances stem cell ingress and extracellular matrix deposition on electrospun nanofibrous scaffolds. ." Transactions of the 56th Annual Meeting of the Orthopaedic Research Society, New Orleans, LA.

Nesti, L. J., W. J. Li, et al. (2008). "Intervertebral disc tissue engineering using a novel hyaluronic acid-nanofibrous scaffold (HANFS) amalgam." Tissue Eng Part A **14**(9): 1527-37.

Nirmalanandhan, V. S., M. Rao, et al. (2007). "Effect of length of the engineered tendon construct on its structure-function relationships in culture." J Biomech **40**(11): 2523-9.

Nishida, K., J. D. Kang, et al. (1998). "Adenovirus-mediated gene transfer to nucleus pulposus cells. Implications for the treatment of intervertebral disc degeneration." Spine **23**(22): 2437-42; discussion 2443.

O'Connell, G. D., H. L. Guerin, et al. (2009). "Theoretical and experimental evaluation of human annulus fibrosus degeneration: the effect on structure-function relationships." Journal of Biomechanical Engineering **in press**.

O'Connell, G. D., S. Sen, et al. (2007). "Biaxial Mechanics of Native and Engineered Fiber-Reinforced Musculoskeletal Tissues." Proceedings of ASME 2007 Summer Bioengineering Conference, Keystone, CO, June 20-24.

O'Connell, G. D., S. Sen, et al. (2010). "Biaxial Mechanics are Inhomogeneous and Altered with Degeneration in the Human Annulus Fibrosus " Transactions of the 56rd Annual Meeting of the Orthopaedic Research Society, New Orleans, LA.

O'Connell, G. D., E. J. Vresilovic, et al. (2007). "Comparison of animals used in disc research to human lumbar disc geometry." Spine **32**(3): 328-33.

O'Halloran, D. M. and A. S. Pandit (2007). "Tissue-engineering approach to regenerating the intervertebral disc." Tissue Eng **13**(8): 1927-54.

Ogden, R. W. (1997). "Non-Linear Elastic Deformations."

Park, S., S. B. Nicoll, et al. (2008). "Cartilage mechanical response under dynamic compression at physiological stress levels following collagenase digestion." Ann Biomed Eng **36**(3): 425-34.

Peacock, A. (1951). "Observations on the prenatal development of the intervertebral disc in man." J Anat **85**(3): 260-74.

Peltz, C. D., S. M. Perry, et al. (2009). "Mechanical properties of the long-head of the biceps tendon are altered in the presence of rotator cuff tears in a rat model." J Orthop Res **27**(3): 416-20.

Perie, D., D. Korda, et al. (2005). "Confined compression experiments on bovine nucleus pulposus and annulus fibrosus: sensitivity of the experiment in the determination of compressive modulus and hydraulic permeability." J Biomech **38**(11): 2164-71.

Petersen, W. and B. Tillmann (1998). "Collagenous fibril texture of the human knee joint menisci." Anat Embryol (Berl) **197**(4): 317-24.

Pittenger, M. F., A. M. Mackay, et al. (1999). "Multilineage potential of adult human mesenchymal stem cells." Science **284**: 143-147.

Reza, A. T. and S. B. Nicoll (2009). "Characterization of novel photocrosslinked carboxymethylcellulose hydrogels for encapsulation of nucleus pulposus cells." Acta Biomater.

Reza, A. T. and S. B. Nicoll (2009). "Serum-free, chemically defined medium with TGF-ß3 enhances functional properties of nucleus pulposus cell-laden carboxymethylcellulose hydrogel constructs." Biotechnology and Bioengineering **(in press)**.

Rhodin, J. (1980). Architecture of the vessel wall. Handbook of Physiology. R. Berne. Baltimore, Waverly Press.

Richardson, S. M., A. Mobasheri, et al. (2007). "Intervertebral disc biology, degeneration and novel tissue engineering and regenerative medicine therapies." Histol Histopathol **22**(9): 1033-41.

Risbud, M. V., M. W. Izzo, et al. (2003). "An organ culture system for the study of the nucleus pulposus: description of the system and evaluation of the cells." Spine **28**(24): 2652-8; discussion 2658-9.

Sacks, M. S. and W. Sun (2003). "Multiaxial mechanical behavior of biological materials." Annu Rev Biomed Eng **5**: 251-84.

Sato, M., T. Asazuma, et al. (2003). "An atelocollagen honeycomb-shaped scaffold with a membrane seal (ACHMS-scaffold) for the culture of annulus fibrosus cells from an intervertebral disc." Journal of Biomedical Materials Research Part A **64A**(2): 249-256.

Schmidt, M. B., V. C. Mow, et al. (1990). "Effects of proteoglycan extraction on the tensile behavior of articular cartilage." J Orthop Res **8**(3): 353-63.

Screen, H. R., V. H. Chhaya, et al. (2006). "The influence of swelling and matrix degradation on the microstructural integrity of tendon." Acta Biomater **2**(5): 505-13.

Seguin, C. A., M. D. Grynpas, et al. (2004). "Tissue engineered nucleus pulposus tissue formed on a porous calcium polyphosphate substrate." Spine (Phila Pa 1976) **29**(12): 1299-306; discussion 1306-7.

Shao, X. and C. J. Hunter (2007). "Developing an alginate/chitosan hybrid fiber scaffold for annulus fibrosus cells." J Biomed Mater Res A **82**(3): 701-10.

Sheth, N. P., B. M. Baker, et al. (2007). "Biologic integration of fiber-aligned nanofibrous scaffolds with native meniscus." Transactions of the 53rd Annual Meeting of the Orthopaedic Research Society, San Diego, CA,.

Shine, K. M. and M. Spector (2008). "The presence and distribution of lubricin in the caprine intervertebral disc." J Orthop Res **26**(10): 1398-406.

Skaggs, D. L., M. Weidenbaum, et al. (1994). "Regional variation in tensile properties and biochemical composition of the human lumbar anulus fibrosus." Spine **19**(12): 1310-9.

Smith, L. J. and N. L. Fazzalari (2006). "Regional variations in the density and arrangement of elastic fibres in the anulus fibrosus of the human lumbar disc." J Anat **209**(3): 359-67.

Smith, L. J., J. T. Martin, et al. (2009). "Altered lumbar spine structure, biochemistry, and biomechanical properties in a canine model of mucopolysaccharidosis type VII." J Orthop Res **28**(5): 616-622.

Smith, L. J., T. P. Schaer, et al. (2010). "Developmental Origins of the Annulus Fibrosus Lamellar Cross Bridge Network." Transactions of the 56th Annual Meeting of the Orthopaedic Research Society, New Orleans, LA.

Soslowsky, L. J., C. H. An, et al. (1994). "Geometric and mechanical properties of the coracoacromial ligament and their relationship to rotator cuff disease." Clin Orthop Relat Res(304): 10-7.

Spencer, A. J. M. (1972). Deformations of Fibre-reinforced Materials. London, Oxford University Press.

Spilker, R. L. (1980). "Mechanical behavior of a simple model of an intervertebral disk under compressive loading." J Biomech **13**(10): 895-901.

Stankus, J. J., J. Guan, et al. (2006). "Microintegrating smooth muscle cells into a biodegradable, elastomeric fiber matrix." Biomaterials **27**(5): 735-44.

Stella, J. A., J. Liao, et al. (2008). "Tissue-to-cellular level deformation coupling in cell micro-integrated elastomeric scaffolds." Biomaterials **29**(22): 3228-36.

Tan, E. P., S. Y. Ng, et al. (2005). "Tensile testing of a single ultrafine polymeric fiber." Biomaterials **26**(13): 1453-6.

Thomopoulos, S., G. R. Williams, et al. (2003). "Variation of biomechanical, structural, and compositional properties along the tendon to bone insertion site." J Orthop Res **21**: 413-19.

Trout, J. J., J. A. Buckwalter, et al. (1982). "Ultrastructure of the human intervertebral disc. I. Changes in notochordal cells with age." Tissue Cell **14**(2): 359-69.

Veres, S. P., P. A. Robertson, et al. (2008). "ISSLS prize winner: Microstructure and mechanical disruption of the lumbar disc annulus: part II: how the annulus fails under hydrostatic pressure." Spine **33**(25): 2711-20.

Viidik, A., C. C. Danielson, et al. (1982). "On fundamental and phenomenological models, structure and mechanical properties of collagen, elastin and glycosaminoglycan complexes." Biorheology **19**(3): 437-51.

Wagner, D. R. and J. C. Lotz (2004). "Theoretical model and experimental results for the nonlinear elastic behavior of human annulus fibrosus." J Orthop Res **22**(4): 901-9.

Wagner, D. R., K. M. Reiser, et al. (2006). "Glycation increases human annulus fibrosus stiffness in both experimental measurements and theoretical predictions." J Biomech **39**(6): 1021-9.

Wan, Y., G. Feng, et al. (2008). "Biphasic scaffold for annulus fibrosus tissue regeneration." Biomaterials **29**(6): 643-52.

Wang, J. H., F. Jia, et al. (2003). "Cell orientation determines the alignment of cell-produced collagenous matrix." J Biomech **36**(1): 97-102.

Wang, J. Y., A. E. Baer, et al. (2001). "Intervertebral disc cells exhibit differences in gene expression in alginate and monolayer culture." Spine **26**(16): 1747-51; discussion 1752.

Weiss, J. A., J. C. Gardiner, et al. (2002). "Ligament material behavior is nonlinear, viscoelastic and rate-independent under shear loading." J Biomech **35**(7): 943-50.

Wood, M. L., G. E. Lester, et al. (1998). "Collagen fiber sliding during ligament growth and contracture." J Orthop Res **16**(4): 438-40.

Wozniak, M. A. and C. S. Chen (2009). "Mechanotransduction in development: a growing role for contractility." Nat Rev Mol Cell Biol **10**(1): 34-43.

Wu, H. C. and R. F. Yao (1976). "Mechanical behavior of the human annulus fibrosus." Journal of Biomechanics **9**: 1-7.

Yang, X. and X. Li (2009). "Nucleus pulposus tissue engineering: a brief review." Eur Spine J.

Yin, L. and D. M. Elliott (2005). "A homogenization model of the annulus fibrosus." J Biomech **38**(8): 1674-84.

Yoder, J. H., H. B. Henninger, et al. (2009). "Annulus fibrosus shear properties are consistent with motion segment mechanics when fibers are loaded." ASME Summer Bioengineering Conference: 206833.